Geochemical Soil Atlas of Switzerland

Distribution of 20 elements in the topsoil

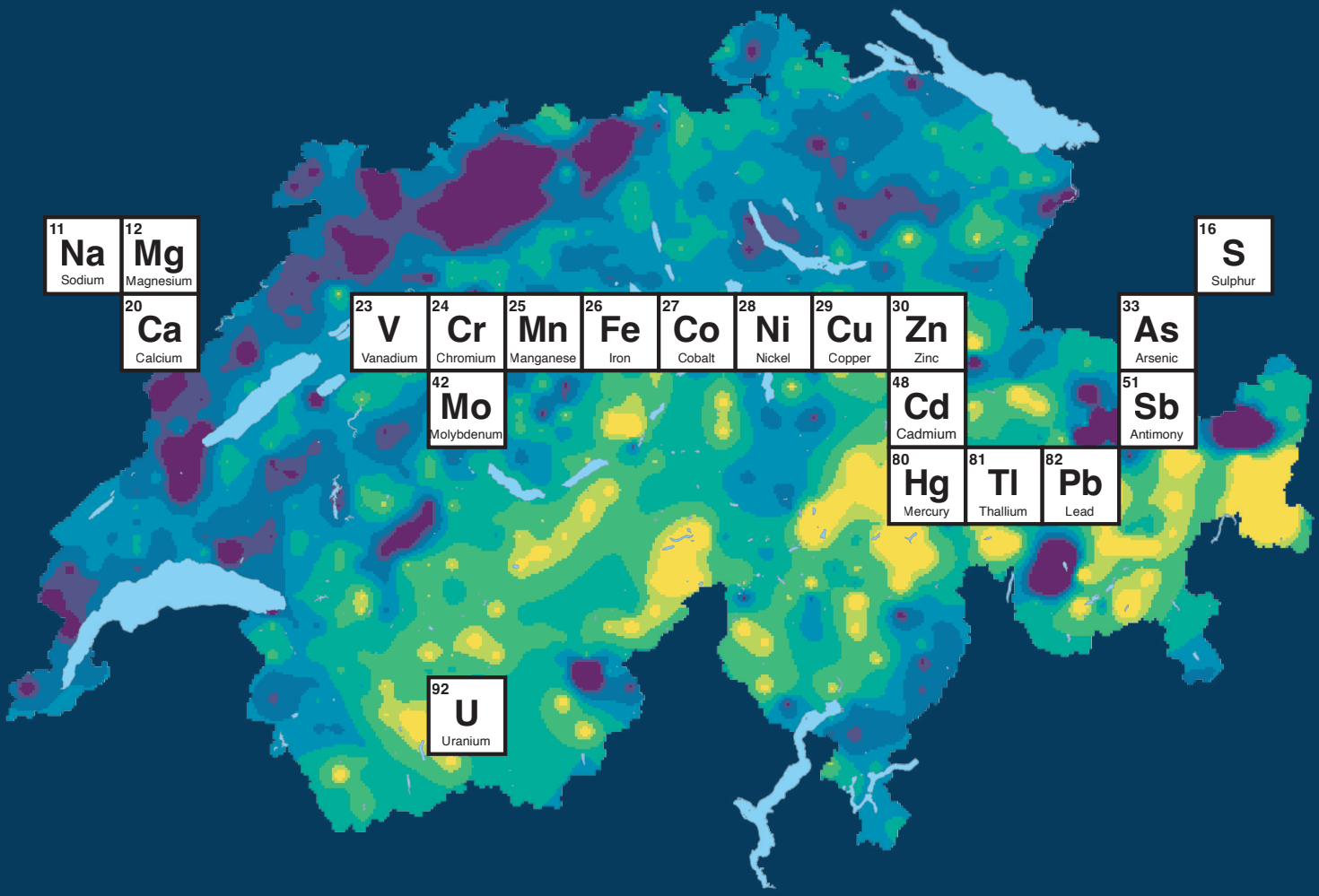

Agroscope good food, healthy environment

ETH Zürich

eawag aquatic research

Schweizerische Eidgenossenschaft
Confédération suisse
Confederazione Svizzera
Confederaziun svizra

Swiss Confederation

Agroscope

Federal Office for the Environment FOEN

Imprint

Publishers	Agroscope, 8046 Zurich, Switzerland, www.agroscope.ch Agroscope is the Swiss Confederation's centre of excellence for research in the agriculture and food sector, and is affiliated with the Federal Office for Agriculture (FOAG). Federal Office for the Environment (FOEN), 3003 Berne, Switzerland, www.bafu.admin.ch The FOEN is an office of the Federal Department of the Environment, Transport, Energy and Communications (DETEC).
Authors	Jolanda E. Reusser[1,2], Maja B. Siegenthaler[1,3], Lenny H. E. Winkel[2,3], Daniel Wächter[1], Ruben Kretzschmar[2], Reto G. Meuli[1] [1]Soil Quality and Soil Use, Agroscope, 8046 Zurich [2]Institute of Biogeochemistry and Pollutant Dynamics IBP, ETH Zurich, 8092 Zurich [3]Department of Water Resources and Drinking Water, Swiss Federal Institute of Aquatic Science and Technology Eawag, 8600 Dübendorf
Information	Jolanda E. Reusser
FOEN support	Alice Badin
Title image	Jolanda E. Reusser
Translation	Translation Service Agroscope, Carol Finch
Layout	Valmedia AG, 3930 Visp, www.valmedia.ch
Download	www.agroscope.ch/geochemicalsoilatlas
Language versions	This publication is also available in German, French and Italian. The original language is German.
Copyright	© Agroscope, FOEN 2023
DOI	https://doi.org/10.34776/gca23-e

Table of contents

1 Introduction

1.1 Elements

There are 118 known chemical elements (Figure 1), with the main elements oxygen (O), silicon (Si), aluminium (Al), iron (Fe), calcium (Ca), magnesium (Mg), sodium (Na) and potassium (K) making up 98.4 % of the mass of the Earth's crust (Amelung *et al.*, 2018a). Some of these, e.g. calcium and magnesium, are considered essential because they are fundamental constituents of plants, humans and animals. However, other elements such as copper (Cu) and zinc (Zn), while still essential, can be harmful at high concentrations. Even at lower concentrations, these elements can be toxic for plants and soil organisms, which tend to be more susceptible than humans. In addition to the essential elements, there are beneficial elements which can promote growth in many plants, for example. Cobalt (Co) – a component of vitamin B_{12} – is a beneficial element essential only for certain living organisms (Amelung *et al.*, 2018b; Schulin *et al.*, 2010). Other elements such as arsenic (As), lead (Pb), cadmium (Cd), mercury (Hg) and uranium (U) are toxic even at low concentrations.

Humans obtain most essential and toxic elements through their diet, with soils being the main source of elements in food and fodder. The extent to which elements accumulate in plants depends on a variety of factors such as plant species, chemical and physical soil properties and the chemical form of the element, i.e. its speciation. Besides the availability of elements, their total concentration in the soil also determines plant uptake. The concentration of trace elements in the soil is generally below 100 mg/kg (Hooda, 2010).

A large proportion of the root biomass is located in the topsoil, which on arable land usually corresponds to the plough layer of around 0 to 20 cm. Since elements (with some exceptions) are taken up by the roots, this uppermost layer of soil plays a vital role in the absorption of essential and toxic elements by plants. Furthermore, humans and grazing animals such as sheep most frequently come into contact with this soil layer (children's playgrounds, sports pitches, farmland, gardens, etc.). Therefore, the Geochemical Soil Atlas of Switzerland focuses on the topsoil.

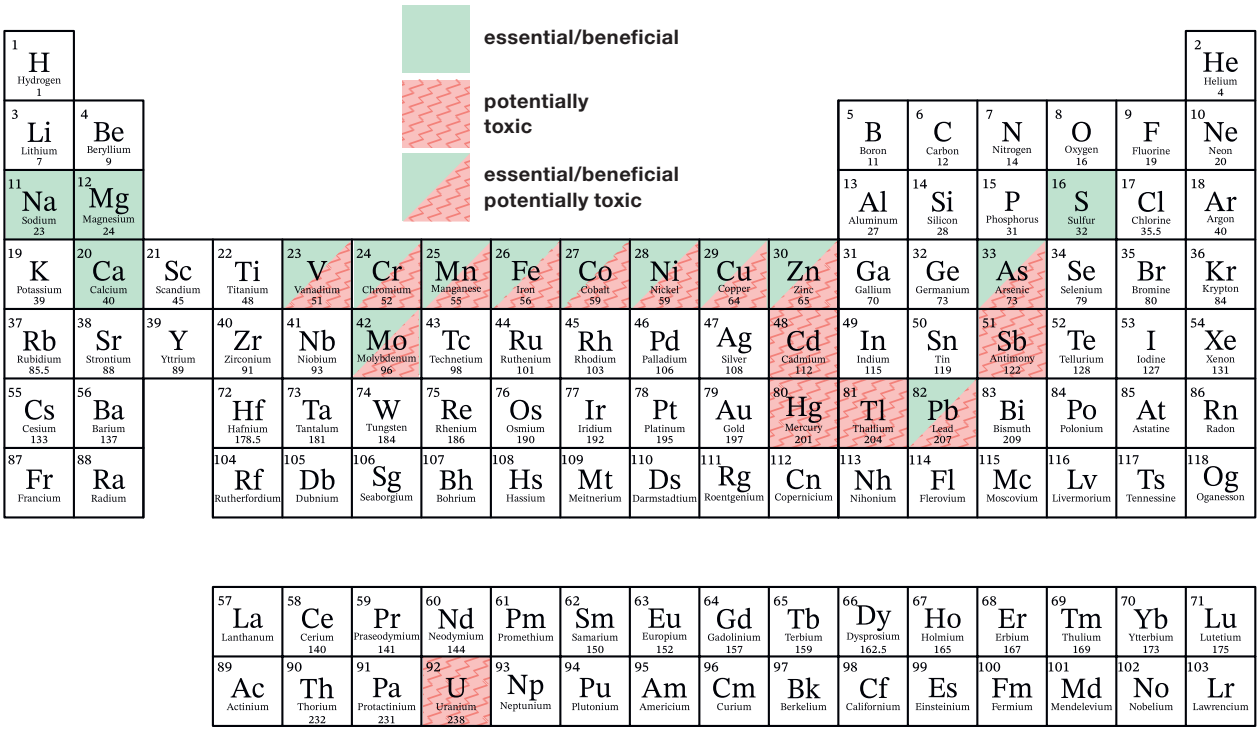

Figure 1 | Periodic table of elements highlighting those in the Geochemical Soil Atlas. Adapted from © 2022 Nagwa.

1.2 Sources and sinks of elements in the soil

The concentration of elements in the soil is shaped by various biotic, chemical and physical processes as well as various inputs and outputs. The following factors can affect element concentrations in soil (Figure 2):

Sources/inputs

- Geogenic sources and other natural sources such as biogenic emissions, atmospheric deposition of dust and sand, volcanic emissions, etc.
- Anthropogenic sources such as direct input to the soil (fertilisers, pesticides, legacy contamination, etc.), input via surface run-off, seepage/groundwater (e.g. irrigation), atmospheric wet and dry deposition of anthropogenic emissions over both short and long distances (industry, traffic, urban emissions, etc.).

Sinks/outputs

- Leaching with displacement to deeper soil layers / into groundwater, which depends on the elements' speciation in the soil as well as hydrological processes and other factors.
- Plant uptake with subsequent harvesting or consumption by animals, i.e. removal of plant material from its original site. The extent to which plants absorb an element depends largely on plant-specific factors as well as on soil properties (e.g. pH) and the speciation of the element. Other factors include the concentration and speciation of other elements.
- Volatilisation due to the formation of volatile chemical compounds (e.g. antimony, arsenic, mercury and sulphur). This sink is largely dependent on biological and chemical soil processes.
- Displacement due to erosion (e.g. surface run-off).
- Displacement by soil organisms (e.g. earthworms).

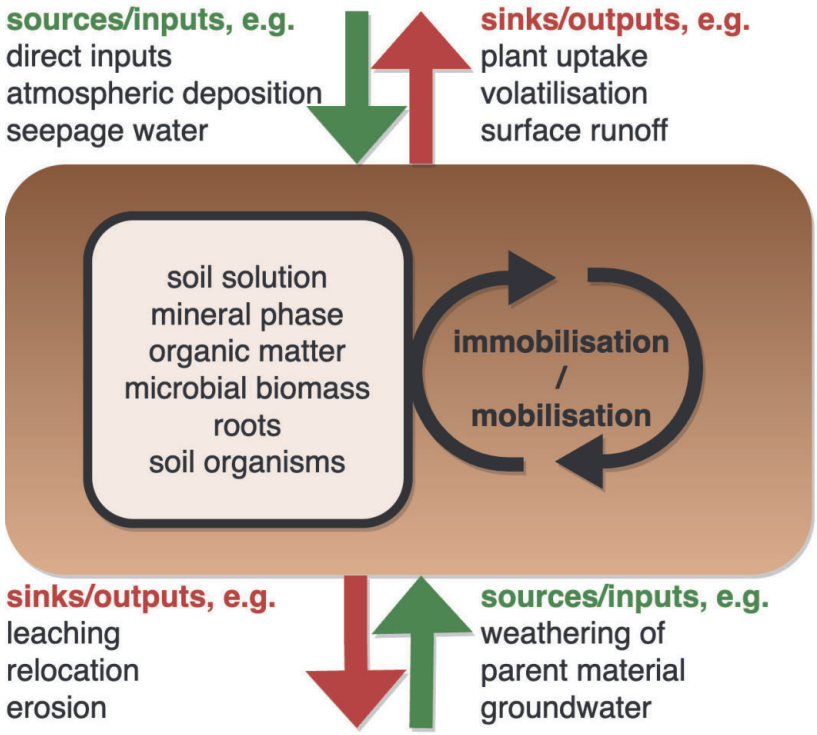

Figure 2 | Diagram of topsoil showing sources/inputs and sinks/outputs of elements, and soil constituents influencing the retention of elements through processes such as sorption, incorporation, chemical precipitation, etc. The origin of these sources/inputs may be geogenic (e.g. parent material), biogenic (e.g. plant residues, excrement) or anthropogenic (e.g. fertilisers, pesticides, legacy contamination).

Immobilisation/mobilisation

Factors affecting the retention of elements in the soil include sorption to the mineral phase, precipitation, and sorption to and/or incorporation into soil organic matter (including plant and microbial biomass). These factors are strongly dependent on biological, chemical and physical soil processes, and on the oxidation state and speciation of the elements.

1.3 Geochemical atlases

Geochemistry aims to quantify the chemical composition of the Earth and identify and evaluate factors influencing the distribution of individual elements (Goldschmidt & Muir, 1954; Reimann *et al.*, 2014). This information is crucial to understanding the behaviour of elements in the environment, and how they are distributed between and circulate within the three compartments – atmosphere, hydrosphere and pedosphere.

Geochemical soil atlases depicting the spatial distribution of element concentrations in soil are consulted in order to localise and evaluate potentially contaminated areas (toxic elements/toxic concentration levels) or areas with deficits (essential/beneficial elements). Examples of such atlases include the Advanced Soil Geochemical Atlas of England and Wales (Rawlins *et al.*, 2012) and the geochemical and mineralogical maps for the soils of the United States of America (Smith *et al.*, 2014). In Europe, the geochemical composition of topsoil has been documented in the 'Geochemical Mapping of Agricultural and Grazing Land Soil, GEMAS' project (Reimann *et al.*, 2014). The GEMAS atlas includes maps showing the spatial distribution of element concentrations at 17 arable sites and 17 grassland sites across Switzerland. This resolution is sufficient to depict Switzerland at European scale, but not to infer detailed information about the spatial distribution of element concentrations within Switzerland.

1.4 Aim of the Geochemical Soil Atlas of Switzerland

This project aims to compile a Geochemical Soil Atlas of Switzerland depicting the status quo and spatial distribution of element concentrations in Switzerland's topsoils. The cantonal environmental protection agencies' working group on 'Intervention levels and risk assessment' (AGIR), the Swiss Federal Office for the Environment (FOEN) as contracting authority, and the contractor jointly selected 20 elements for inclusion in the atlas: antimony (Sb), arsenic (As), lead (Pb), cadmium (Cd), calcium (Ca), chromium (Cr), cobalt (Co), iron (Fe), copper (Cu), magnesium (Mg), manganese (Mn), molybdenum (Mo), sodium (Na), nickel (Ni), mercury (Hg), sulphur (S), thallium (Tl), uranium (U), vanadium (V) and zinc (Zn). The following soil properties were also recorded: pH, total carbon, total nitrogen, organic carbon, soil texture, calcium carbonate content and humus content.

The Geochemical Atlas is the first evaluation of soil analyses to cover the whole of Switzerland with a resolution of around one sampling site per 35 km^2. As such, it provides an important basis for implementing soil-related measures. The information obtained also enables further targeted regional or in-depth national investigations. The findings of the Geochemical Soil Atlas represent a snapshot of element concentrations in Switzerland's topsoil. The interpolated maps serve to highlight regions with high or low concentrations. However, it is not possible to infer any plot-level information or reliable conclusions about the geology, bioavailability, percentage distribution of geogenic and anthropogenic sources, or soil contamination.

2 Underlying data

The Geochemical Soil Atlas of Switzerland is based on data from three datasets. Each dataset is derived from topsoil samples (0–20 cm) which were dried and sieved (< 2 mm). The soil samples from BDM (Biodiversity Monitoring Switzerland) and NABO (the National Soil Monitoring Network) were digested with aqua regia to determine the element concentrations. The UB dataset compiled and harmonised by Stanisic *et al.* (2021) of the University of Bern contains measured values which were analysed by other chemical extraction methods in addition to aqua regia digestion. Figure 3 shows the spatial distribution of the sampling sites. The three datasets are described in detail in the following sections.

2.1 BDM dataset

Biodiversity Monitoring Switzerland (BDM) is one of the national programmes for long-term monitoring of biodiversity in Switzerland (BAFU, 2020). The 'Species diversity in habitats' sampling network is one of BDM's three national networks and includes regular surveys of vascular plants, mosses and molluscs on around 1450 sampling sites. Primary land use (forest, settlement, arable land, grassland, alpine pastures and mountainous areas) and habitat type are also recorded in accordance with Delarze *et al.* (2008). During field surveys for this BDM programme (indicator Z9), soil samples for the BDM dataset were collected at 1238 sites in Switzerland between 2011 and 2015 at a depth of 0–20 cm (Meuli *et al.*, 2017). No soil samples could be taken from the remaining sites in the BDM sampling network due to a lack of soil formation or sealing of the ground (roads, glaciers, lakes, etc.). The dataset was reduced to 1082 sites following the exclusion process (Chapter 3.1).

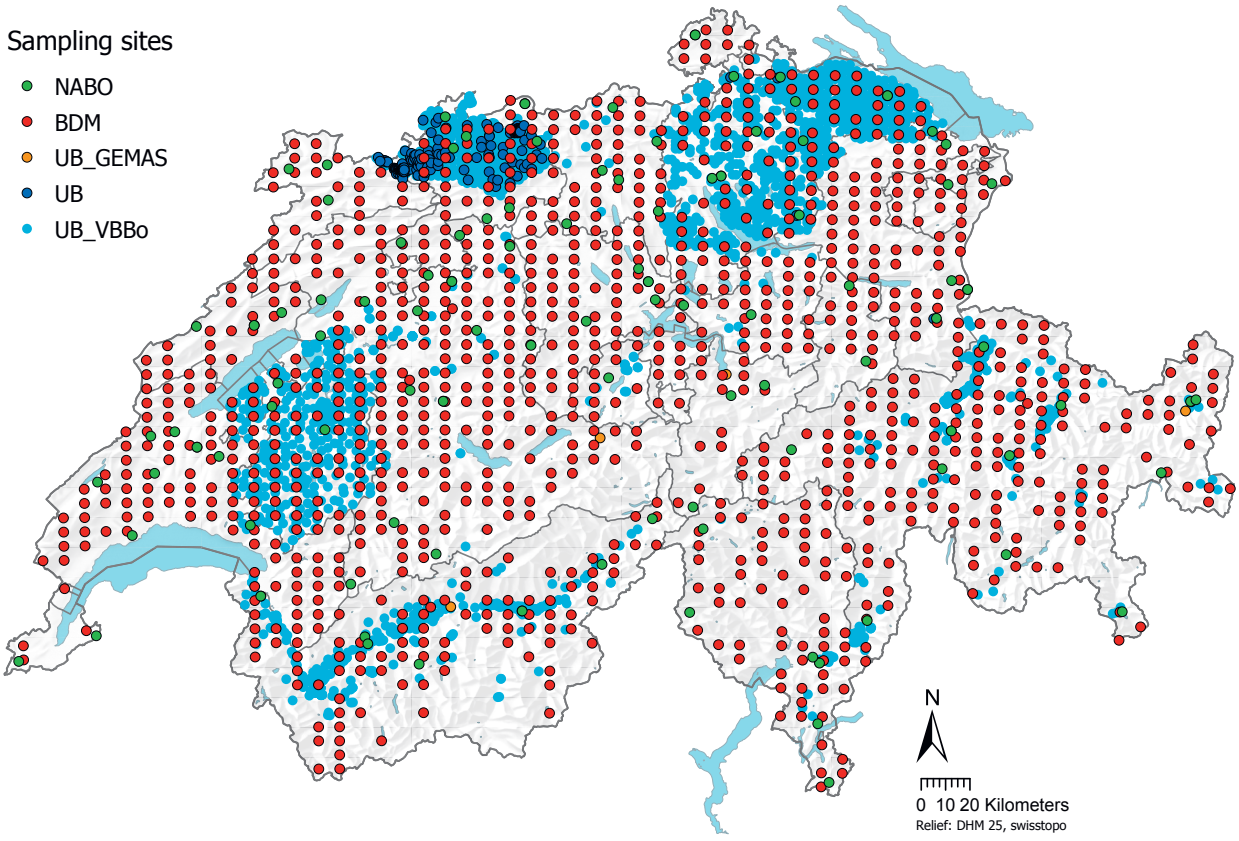

Figure 3 | Distribution of sampling sites of Biodiversity Monitoring Switzerland (BDM, red, 1082 sites) and the National Soil Monitoring Network (NABO, green, 102 sites) and distribution of sites compiled by Stanisic *et al.* (2021) from the University of Bern (UB) based on the digestion method (Chapter 3.1). Dark blue indicates UB sites where soil samples were digested with aqua regia (279 sites), pale blue UB sites where samples were analysed using the 2-M nitric acid extraction process in accordance with the Ordinance on Soil Pollution (VBBo) (3030 sites), and orange the European geochemical soil atlas sites (GEMAS, 17 sites).

2.1.1 Sampling

Sampling was conducted on a 6 km × 4 km grid covering the whole of Switzerland. Since the soil samples were taken from BDM-Z9 indicator sampling sites which were not to be disturbed, two inner circles for recording plants and molluscs and an outer circle with a radius of 3 to 3.5 m for topsoil sampling were marked out on each site. On the outer circle, four topsoil samples aligned with the four cardinal points were collected using a Humax impact probe. The inside of the probe was lined with a plastic sleeve with a 4.8 cm diameter. Where stones, roots or other obstacles impeded the sampling process, the sampling site was moved clockwise within the outer circle by max. 2 m. The litter layer was removed before sampling. The effective sampling depth was checked by inserting a ruler in the borehole. The precise position of the sampling site, sampling depth, land use (Figure 4) and other remarks were logged for each site.

2.1.2 Sample preparation and laboratory analysis

The soil samples were shipped by post in refrigerated transport, then weighed, dried at 40 °C for 48 h and sieved (< 2 mm). The soil samples were placed in plastic containers and stored in Agroscope's soil sample archive together with the sieving residues (gravel, stones and roots). The gravimetric water content, volumetric weight and bulk density of the soil were calculated as per Schwab and Gubler (2016). The per cent proportion of sand, silt and clay as well as the humus content were determined for at least one sample per site following the Agroscope KOF reference method (2020a). From each sample, an aliquot of 10 g was suspended in 25 ml of 0.01 M $CaCl_2$ solution for two hours. Subsequently, the pH was measured in the suspension using a Mettler-Toledo meter in the calibration range of pH 4 to 7. In addition, 0.5 g of a milled subset (< 0.45 mm) of each sample was packed in tinfoil and combusted in a TruSpec CN (Leco) Dry Combustion Analyser at 950 °C to analyse the total carbon and nitrogen content. In soils with pH < 6.5, the measured total carbon was considered equal to the organic carbon content. In soils with pH > 6.5, the total carbonate content was determined initially using hydrochloric acid according to the Agroscope $CaCO_3$ reference method (2020b). The carbonate content was subtracted from the total carbon content to calculate the organic carbon content in these soils (Gubler *et al.*, 2018).

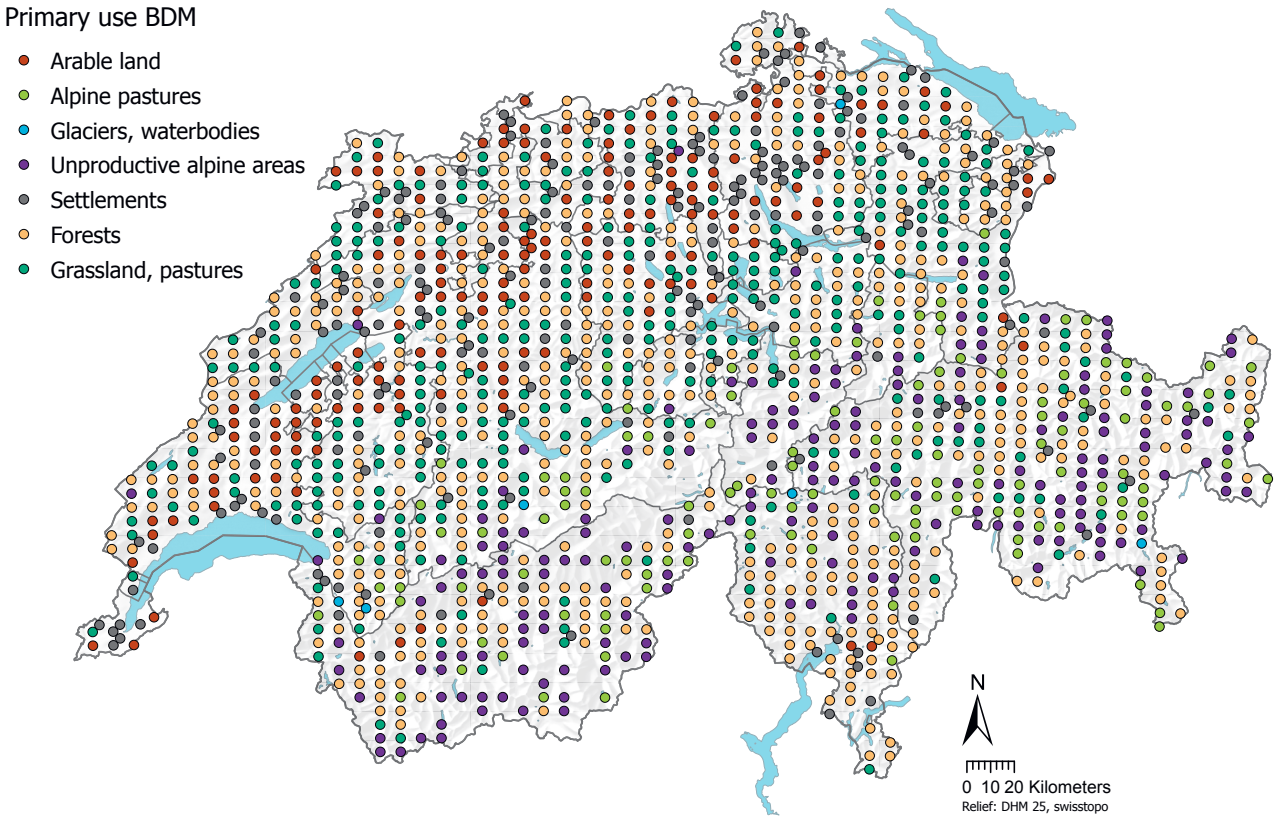

Figure 4 | Land-use types recorded at the BDM-Z9 indicator sites where soil samples were collected (sampling period 2011–2015).

A subset of the samples was sent to the Bureau Veritas Minerals laboratory in Vancouver (Canada) to determine the element concentrations in aqua regia digests. This is the same laboratory that performed the laboratory analyses for the European geochemical soil atlas (Reimann *et al.*, 2014). The samples were dried at 60 °C and milled. For each sample, 15 g of the milled soil was digested with 300 ml of HNO_3:HCl:H_2O (1:1:1) aqua regia (AR) solution (without H_2O_2) and analysed using inductively coupled plasma mass spectrometry (Single Quadrupole ICP-MS) (AQ251 and AQ251-EXT analysis programme from the Bureau Veritas Minerals laboratory, catalogue 2018). The laboratory analysed 5129 samples in total (including reference materials and blanks) in 21 batches between December 2019 and February 2020. For quality control purposes, three different reference materials and 10 NABO reference soils were analysed in replicates. Quality control of the laboratory data showed that the spread of measured values is low overall (good precision) and the measured element concentrations in the standards concur with the certified values (good accuracy).

2.1.3 Limits of detection

The limits of detection (LOD) for the AQ251-EXT analysis programme are summarised in Table 1. The data are based on the Bureau Veritas Minerals laboratory's 2018 catalogue. Table 1 also indicates the median value of all measurements per element. Less than 1 % of measured values were below the LOD. Sulphur was the exception, where around 18 % of all measured values fell short of the LOD. Since sulphur is a nutrient, both high and low concentrations are of interest. Thus, the samples below the LOD were remeasured at the Swiss Federal Institute of Aquatic Science and Technology Eawag using a Triple Quadrupole ICP-MS/MS. With this analytical method, a new LOD of 3.6 ppm was reached, around 56 times lower than that determined by the Bureau Veritas Minerals laboratory. None of the remeasured samples fell below the Eawag LOD. The remeasurement method is described in Chapter 2.1.4.

2.1.4 Remeasurement of sulphur concentrations

The soil samples used to remeasure sulphur concentrations were dried (40 °C for 48 h), sieved (< 2 mm) and milled in a vibrating mill at 25 Hz for 4 min. The digestions were carried out by Agroscope's Environmental Analytics Working Group. A modified aqua regia solution (HNO_3:HCl:H_2O 1:1:1) was used for the digestions, as at the Bureau Veritas Minerals laboratory. For quality control purposes, blank samples and three reference soils from the Wageningen Evaluating Programmes for Analytical Laboratories (WEPAL) were also included. In each case, 1 g of soil was digested in 20 ml of modified aqua regia for 90 min at 120 °C on a heated block. The cooled digests were diluted to 50 ml with H_2O and filtered first with a filter paper and then with a syringe filter (0.45 µm). The ICP-MS/MS measurements were performed by Eawag's Environmental Inorganic Geochemistry Group on a Triple Quadrupole ICP-MS/MS 8900 (Agilent Technologies) linked to an automatic in-line dilution system (ESI prepFAST Autodilution System, Elemental Scientific Inc.). Sulphur (^{32}S and ^{34}S) was measured in H_2 mode (5.5 ml/min H_2) and in O_2 mode (1 ml/min H_2 and 30 % O_2) with three repetitions. Quality checks (QCs) for sulphur from multi-element standards in an original acid matrix were used for quality control purposes. The sulphur concentrations in the digests were corrected by the internal standard and the blank samples. ^{32}S in O_2 mode was selected for further data analysis.

Remeasuring sulphur on a Triple Quadrupole ICP-MS/MS allowed sulphur concentrations in soil samples previously below the LOD (200 ppm) to be quantified. The following results suggest that the Eawag measurement data are of high quality: i) the blank samples were only slightly above the background values obtained by ICP-MS/MS, indicating no contamination with sulphur; ii) the recovery rate for the measured standards (QC and individual standards) was between 88 % and 102 %, and between 69 % and 100 % for the reference soils; iii) the measured values obtained by the Eawag for the reference soils exhibit lower coefficients of variation than the original measured values.

Sulphur concentrations in a total of 500 soil samples were determined by the Bureau Veritas Minerals laboratory and the Eawag. Comparison of the datasets with linear regression forced through the point of origin gave a recovery rate of 80 % for sulphur. Only 10 % of the samples which were below the LOD at the Bureau Veritas Minerals laboratory exceeded the original LOD of 200 ppm at the Eawag. Thus, it was possible to combine the data measured at Eawag with those from the Bureau Veritas Minerals laboratory.

Table 1 | Limit of detection (LOD) based on the AQ251 programme, 2018 catalogue of the Bureau Veritas Minerals laboratory in Vancouver (Canada). Median of all measured values (without blanks and reference materials). The number of measured values below the LOD also excludes blanks. The per cent proportion of measured values below the LOD is indicated in brackets. Values in ppm correspond to mg/kg.

Element	Limit of detection	Median of all measured values	Number of samples below LOD Number (%)
As	0.1 ppm	8.0 ppm	1 (0)
Ca	0.01 %	0.45 %	2 (0)
Cd	0.01 ppm	0.23 ppm	6 (0)
Co	0.1 ppm	8.7 ppm	0 (0)
Cr	0.5 ppm	31.1 ppm	0 (0)
Cu	0.01 ppm	18.40 ppm	0 (0)
Fe	0.01 %	2.19 %	2 (0)
Hg	5 ppb	65 ppb	15 (0)
Mg	0.01 %	0.42 %	3 (0)
Mn	1 ppm	664 ppm	0 (0)
Mo	0.01 ppm	0.81 ppm	0 (0)
Na	0.001 %	0.008 %	1 (0)
Ni	0.1 ppm	28.0 ppm	0 (0)
Pb	0.01 ppm	23.99 ppm	0 (0)
S	0.02 % / 3.6 ppm[1]	0.04 %	1051 (18) / 0 (0)
Sb	0.02 ppm	0.38 ppm	0 (0)
Tl	0.02 ppm	0.15 ppm	6 (0)
U	0.1 ppm	0.7 ppm	14 (0)
V	1 ppm	32 ppm	3 (0)
Zn	0.1 ppm	64.3 ppm	0 (0)

[1] The LOD of 3.6 ppm refers to soil samples remeasured at the Eawag.

2.1.5 Analysis of total mercury concentrations

Elemental mercury is volatile and can outgas from soil samples in certain circumstances. A subset of the BDM dataset was remeasured to investigate whether mercury losses occurred due to volatilisation during aqua regia digestion. The total mercury concentration in 224 individual samples was analysed by the Institute of Biogeochemistry and Pollutant Dynamics' Soil Chemistry Group at ETH Zurich using a Direct Mercury Analyser (DMA). Samples for the subset were selected on the basis of being spread across Switzerland and as representative as possible of the humus concentration range. Dr Sylvain Bouchet performed the quality assurance based on analytical replications of 24 samples (two replications) and four reference materials (three replications).

Total mercury concentrations measured with the DMA correlated strongly with mercury concentrations determined by aqua regia digestion (forced through the point of origin, correlation coefficient $R^2 = 0.98$). Furthermore, the gradient of 1 indicates that possible mercury losses due to volatilisation during aqua regia digestion can be disregarded. Based on these findings, it can be assumed that mercury concentrations in the aqua regia digests approximate the total concentrations in the soil samples. However, the volatilisation of elemental mercury during sample preparation when samples are dried at 40 °C cannot be ruled out (MacSween *et al.*, 2020).

2.2 NABO dataset

The National Soil Monitoring Network NABO has been monitoring the quality of Swiss soils since the 1980s (Gubler *et al.*, 2022). Physical, chemical and biological soil properties are routinely analysed at around 100 sampling sites spread across Switzerland. The data obtained enable temporal trends in soil quality to be derived and evaluated. Element concentrations in aqua regia digests of composite samples from 104 NABO long-term monitoring sites were analysed from 2008 to 2017. Following the exclusion process (Chapter 3.1), 102 sites in total were included in the Geochemical Soil Atlas.

2.2.1 Sampling

On each site, a 10 m × 10 m area was divided into a 2 m × 2 m grid. A composite sample was collected from each grid square by inserting a core sampler (internal diameter 2.5 cm) to a depth of up to 20 cm. The 25 individual samples were combined in a plastic bag (LDPE) to obtain a single composite sample. These samples were shipped and stored in refrigerated containers pending sample preparation.

2.2.2 Sample preparation and laboratory analysis

The soil samples were dried (40 °C for 48 h) and sieved (< 2 mm), as for the BDM samples. The NABO samples were sent with the BDM samples to the Bureau Veritas Minerals laboratory in Vancouver (Canada), where they were milled, digested with aqua regia and then analysed by ICP-MS (see Chapters 2.1.2 and 2.1.4).

2.2.3 Limits of detection

The LODs for the element concentrations correspond to the LODs listed in Table 1.

2.3 UB dataset

At the request of the FOEN, Lucija Stanisic, Dr Juliet Blum and Dr Moritz Bigalke from the Institute of Geography at the University of Bern compiled and homogenised existing data on geogenic soil contamination in one dataset. The data were obtained from the National Soil Information System NABODAT, the cantons, the Swiss Federal Institute for Forest, Snow and Landscape Research WSL as well as 41 academic publications and reports and two engineering consultancy studies. The dataset comprises a total of 152 212 data points for 65 elements, measured at 4760 sites at different depths using different digestion and analysis methods. Sampling took place between 1989 and 2017. In addition, the complete dataset contains the results of the soil sampling campaign carried out for the European geochemical soil atlas (GEMAS; Chapter 1.3). Further information about the complete dataset can be found in the *Zusammenfassender Bericht über bestehende Studien und Untersuchungen zu geogenen Schadstoffgehalten in Böden und Gesteinen der Schweiz* (in German) (Stanisic *et al.*, 2021). For reasons of comparability, data points from the complete dataset which met the criteria listed in Chapters 2.3.1 to 2.3.4 were included in the Geochemical Soil Atlas. The selected data points are hereafter referred to as the UB dataset.

2.3.1 Sampling

Only samples collected in the topsoil from a depth of 0 cm to 18–22 cm were selected. These samples comprise both composite and individual samples collected from different soil layers and varying areal extents.

2.3.2 Sample preparation and laboratory analysis

Samples that had been sieved to 2 mm and subsequently digested with aqua regia were included. To guarantee that the measurement data were comparable with the BDM dataset, we selected only those aqua regia digests that had been analysed using ICP-MS.

In addition to heavy metals, the 20 elements covered by the Geochemical Soil Atlas of Switzerland include non-metals such as sulphur and other elements also considered nutrients such as calcium, magnesium and sodium. Since these elements were not included in the original UB dataset, they were subsequently obtained from NABODAT and added to the UB dataset.

Information about the parent material (e.g. limestone, conglomerate, clay) is available for 322 data points (5 % of the revised dataset). pH values are also available for 3332 data points. The humus content of the revised dataset comprises 30 data points and the C_{org} content 595 data points.

2.3.3 Limits of detection

Since the measurement data in the UB dataset were sourced from a wide variety of sampling campaigns, the analysis methods and analytical instruments used are not standardised. Hence it is not possible to specify a standard LOD per element for the UB dataset. Furthermore, measurement data below the LOD were rarely reported.

2.3.4 Conversion of VBBo values to aqua regia

In addition to the measurement data analysed by aqua regia digestion, the UB dataset also includes 47 667 data points analysed by extraction with 2 M nitric acid following the Ordinance on Soil Pollution (VBBo). According to Stanisic *et al.* (2021), the concentrations measured by the VBBo extraction method correlate with the concentrations measured by aqua regia digestion for certain elements. The regression parameters and transfer functions are listed in Table 4 in the report by Stanisic *et al.* (2021). For cadmium, cobalt, copper and lead, both the correlation coefficient and the recovery rate between the two methods are sufficiently high (≥ 0.8) to justify conversion to aqua regia concentrations. The concentrations of these four elements were converted using the following functions (Stanisic *et al.*, 2021):

- **Cd** $[Cd]_{KW} = ([Cd]_{VBBo} - 0.267) / 0.920$
- **Co** $[Co]_{KW} = ([Co]_{VBBo} + 0.17) / 0.795$
- **Cu** $[Cu]_{KW} = ([Cu]_{VBBo} + 1.25) / 0.854$
- **Pb** $[Pb]_{KW} = ([Pb]_{VBBo} - 0.217) / 0.884$

where $[element]_{KW}$ denotes the concentration measured by aqua regia digestion (mg/kg) and $[element]_{VBBo}$ the concentration measured by the VBBo method with 2 M nitric acid (mg/kg). Since the linear regression of Stanisic *et al.* (2021) was not drawn through the point of origin, the conversion resulted in some negative values. These converted values were excluded from the dataset.

Converting the VBBo concentrations to aqua regia concentrations added a total of 3030 sites to the UB dataset (279 sites): 2790 additional sites with Cd readings, 1827 with Co readings, 2848 with Cu readings and 3003 with Pb readings. As Figure 3 shows, these locations are concentrated in the cantons of Basel-Landschaft, Freiburg, Valais and Zurich.

2.4 Comparability of datasets

Before merging the BDM, NABO and UB datasets, it was necessary to verify their comparability. Element concentrations in the UB dataset were found to be significantly higher than those in the BDM and NABO datasets. These differences stem partly from the spatial aggregation of the UB sampling sites in the canton of Basel-Landschaft (Figure 3) and partly from the choice of sampling sites: in Basel-Landschaft, samples were deliberately taken from sites with suspected high geogenic contamination, so this dataset is biased in favour of higher concentrations compared with random sampling. For this reason, the UB dataset was evaluated separately.

2.5 Supplementary data

For the multivariate data analysis, the element concentrations were correlated not only with the measured soil properties, but with the following supplementary data as well:

- The Swiss DHM25 digital elevation model with a resolution of 25 m, derived from the elevation data of the 1 : 25 000 map of Switzerland (LK25), Swiss Federal Office of Topography swisstopo (Wabern)
- Annual precipitation and temperature, climate normals 1981–2010, Swiss Federal Office of Meteorology and Climatology MeteoSwiss (Zurich Airport)
- 25 lithological and petrographic main groups (Figure 5), classified according to formation, mineralogical composition, grain size and crystallinity, simplified map of the near-surface mineral raw materials of Switzerland (as of 2022), 1 : 500 000, Swiss Federal Office of Topography swisstopo (Wabern), Georesources Switzerland Group (Zurich)
- Modelled deposition data on lead, mercury, cadmium, nitrogen and sulphur oxides for the year 2015, the Norwegian Meteorological Institute (MET, Norway), Meteorological Synthesizing Centre-East (MSC-E, Russia)

Since the modelled deposition data are not available in the same resolution (1 degree longitude × 1 degree latitude) for all sampling years (2011–2015), we used the modelled data from 2015 as proxies. MET Norway has modelled wet and dry depositions of oxidised sulphur as well as reduced and oxidised nitrogen based on European emissions data from 2015. MSC-E Russia has modelled depositions of cadmium, lead and mercury based on European emissions data from 2015. All modelled emissions data from publicly available text files were drawn on the grid of the European Monitoring and Evaluation Programme (EMEP) and extracted for Switzerland. To estimate how the atmospheric deposition of these elements has changed during the sampling period, we compared the moss analyses from individual surveys conducted by the National Air Pollution Monitoring Network (NABEL) from 1990 to 2015 (BAFU, 2018). We found that no significant changes in concentrations of lead, mercury and cadmium were recorded in the moss samples between 2010 and 2015.

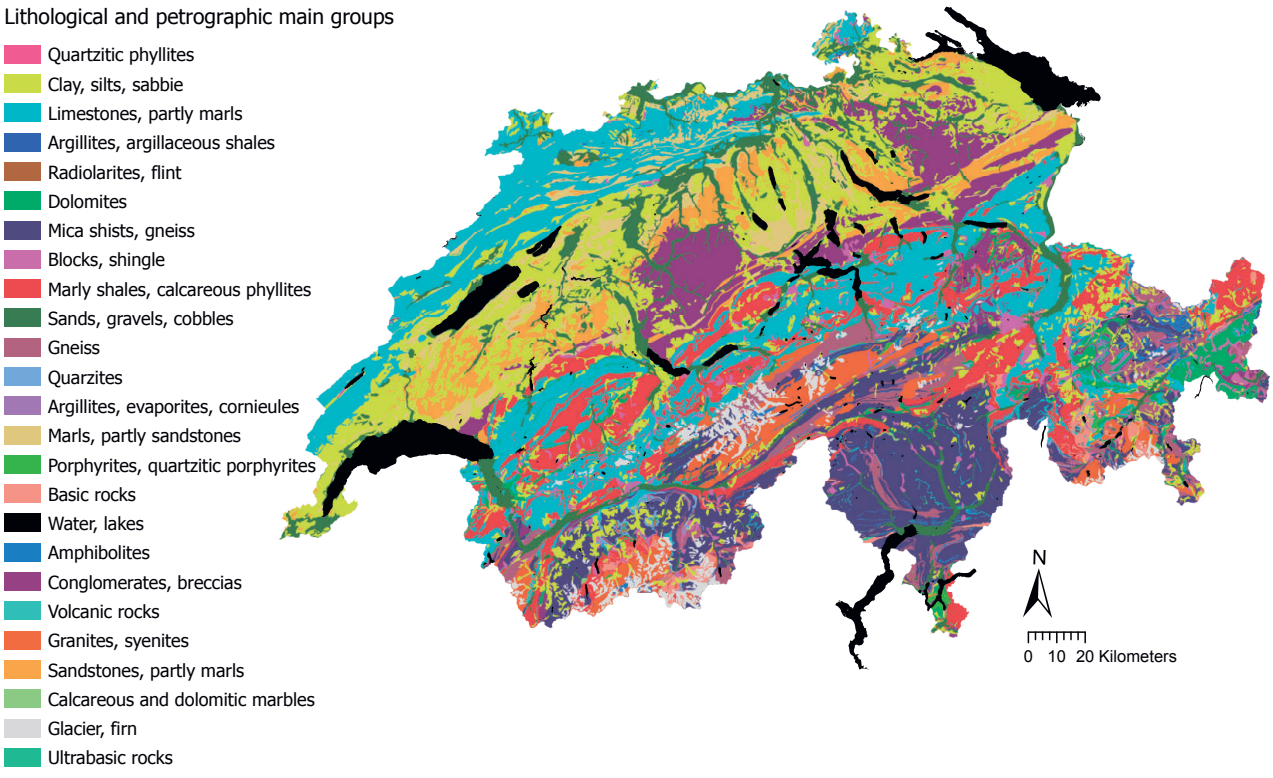

Figure 5 | Lithological and petrographic main groups of the simplified map of the near-surface mineral raw materials of Switzerland (GK500, 2022), Swiss Federal Office of Topography swisstopo (Wabern), Georesources Switzerland Group (Zurich). The map has been adapted.

3 Methodology

3.1 Exclusion process

The multi-stage process used to exclude sites with a potential anthropogenic overprint of element concentrations (BDM and NABO datasets) is illustrated in Figure 6. According to Stanisic *et al.* (2021), the UB dataset contains only measured values for element concentrations assumed to be of primary geogenic origin. In total, 25 BDM, 2 NABO and 70 UB sampling sites were completely excluded.

Since it is not possible to entirely distinguish between anthropogenic and natural sources – both of which influence the samples in varying proportions – it was decided to exclude samples with element concentrations clearly and predominantly influenced by anthropogenic sources. These known or assumed anthropogenic overprints of element concentrations include direct inputs carried over short distances, but not inputs from atmospheric deposition carried over long distances. Sampling sites located within the perimeter of vineyards were not excluded. While it is known that the use of pesticides containing copper in vineyards can result in an accumulation of copper in the topsoil, exclusion of these sites would logically require the exclusion of all other sites with (semi-)diffuse inputs of elements to the soil; for example, fertilised arable land, urban parks, gardens, etc. Yet all direct and/or indirect inputs for all 20 elements are by no means fully known and quantifiable. To avoid distorting the data (bias) through selective exclusion, these sites were included in the data analysis.

The outlier analysis of the BDM dataset is based on an assessment of the variability between individual samples within one site. The coefficient of variation (CV) of the individual samples was used to assess the variability of element concentrations. Sites with a CV greater than 95 % of all CVs were identified as possible outliers. The individual measurements from these sites were then compared with the median for the site. Individual measurements greater than two times the median or smaller than 0.1 times the median were excluded. If the individual measurements for three or more elements deviated from the median for the site in this way, all measured values for the individual sample were compared with the remaining individual samples from the site. If the remaining measurements (element concentrations and soil properties) for the individual sample displayed anomalies compared with the other individual samples from the site, the entire individual sample was excluded. This was the case for forest sites where some individual samples contained significantly higher amounts of humus combined with significantly lower proportions of dry matter. Here it was assumed that – compared with the other individual samples from the sampling site – the litter layer/organic layer disproportionately influenced the measured element concentrations and thus the individual sample was not representative of the site.

The cumulative distribution function was calculated for each element (Chapter 4). No clear inflections can be detected in the upper ranges of this cumulative distribution, which would indicate 'anthropogenically influenced' samples according to Matschullat *et al.* (2000).

In total, 25 BDM, 2 NABO and 70 UB sampling sites were completely excluded from the dataset. The exclusion process for the BDM dataset additionally led to the exclusion of a further 40 individual samples and 333 individual measurements.

3.2 Measured values below the limit of detection

A bias is created in favour of higher values if values below the limit of detection (LOD) are not included in the analysis. In this case, areas with particularly low soil concentrations and thus exhibiting potential deficits are not representatively captured. To avoid this, values below the LOD are shown in a 'smaller than ...' category when presenting the spatial distribution on maps. For the statistical analysis and interpolations, 0.5 times the LOD was assigned to measured values below the LOD unless otherwise indicated, analogous to the method used in the geochemical atlas of England and Wales (Rawlins *et al.*, 2012) and the European geochemical soil atlas (Reimann *et al.*, 2014).

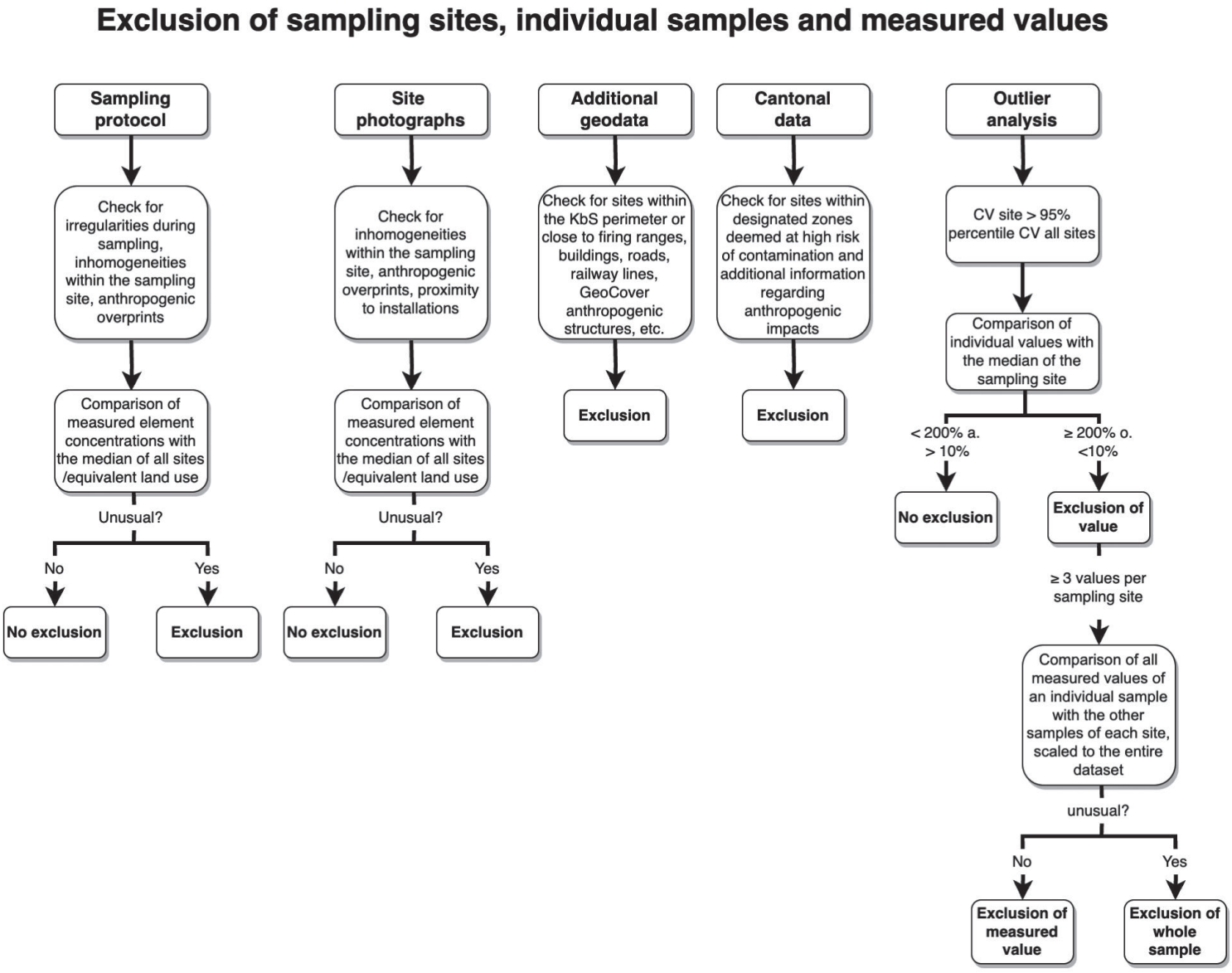

Figure 6 | **Schematic representation of the exclusion process (KbS: register of contaminated sites, CV: coefficient of variation).**

3.3 Univariate data analysis

The median of the element concentrations was used for the univariate data analysis as a robust measure per site.

The results of the univariate data analysis include the median, the mean absolute deviation from the median (MAD) and the 5 %, 25 %, 75 % and 95 % percentiles of the data distribution for each element or soil parameter. The Tukey Inner Fence (TIF) value, used as a possible limit for outliers of geochemical soil data, is also indicated (Jarva *et al.*, 2010; Reimann *et al.*, 2018; Tukey, 1977). This enables the detection of anomalies and detailed investigation of areas which have concentration values above the TIF value. The TIF value is calculated based on a symmetrical data distribution only, which is why the concentration values are log-transformed beforehand (Reimann *et al.*, 2018):

$$TIF = 75\,\%\text{-}Quantil + 1.5 \times IQR$$

where IQR is the interquartile range, i.e. the concentration range between the 25 % and 75 % percentile. The results of the descriptive statistical analysis are summarised in table form.

The concentration distribution of each element is visualised by four diagrams that provide additional information, e.g. on the most frequently occurring concentration values or the approximation of the log-transformed measurement data to a normal distribution. The four diagrams comprise:

A) Box plot, n = total number of sites, n a. S. = sites lying outside the axis range or whisker. The green data points were randomly distributed on the × axis to simplify visualisation. The upper and lower whisker line correspond to 1.5 times the interquartile range. The box incorporates 25 % to 75 % of the data. The central line in the box marks the median. The orange square marks the arithmetic mean of the data.
B) Histogram showing the number of sites per interval. The number of intervals corresponds to the root of the total number of sites. The data were log-transformed to improve visualisation of the distribution. The median is marked with a blue line and the arithmetic mean with an orange line.
C) Quantile-quantile plot of the log-transformed data (blue points) compared with the quantiles of the normal distribution (x axis). The black dashed line represents the theoretical normal distribution.
D) Empirical distribution function in respect of the cumulative distribution function of the log-transformed data.

These diagrams were chosen to visualise the concentration distributions of geochemical soil data, similar to the European geochemical soil atlas. More information can be found in Reimann *et al.* (2011) and Reimann *et al.* (2014).

Since we are interested in the spatial distribution of the concentration values, a point data map was created for each element in addition to the diagrams. To highlight areas with exceptionally low and high concentration values, a standardised method was used to group the concentrations on the point data maps according to the data distribution:

- < LOD, with LOD indicated
- LOD – 5 %
- 5 % – 10 %
- 10 % – 25 %
- 25 % – 50 %
- 50 % – 75 %
- 75 % – 90 %
- 90 % – 95 %
- 95 % – 100 %

The respective concentration ranges in each percentile are indicated in the point data maps. The nine classes are colour-coded in the same way for all elements. The point data maps represent the medians. The relief was derived from the DHM25 digital elevation model of Switzerland (Swiss Federal Office of Topography swisstopo, Wabern).

The point data maps were created with ArcGIS Pro, Version 2.8.3 (© ESRI Inc.). The univariate and multivariate data analysis and creation of diagrams was conducted in R, Version 4.1.3 (R Core Team, 2022) using RStudio, Version 2022.2.1.461 (RStudio Team, 2022). The graphics were created with the *ggplot2* package, Version 3.3.5 (Wickham, 2016).

3.4 Multivariate data analysis

In the multivariate data analysis, the element concentrations were shown in relation to other parameters representing specific factors and processes. These data analyses can provide additional information about possible relationships between elements and factors influencing the concentrations. The focus lies on the potential impact of lithology, land use, soil processes and diffuse atmospheric inputs. The modelled deposition data indicate a potential source of atmospheric deposition. Temperature and precipitation may serve as proxies for erosion processes and indirect effects of vegetation. The total organic carbon (TOC) and total nitrogen (TN) concentrations are representative of soil organic matter (sorption and/or biochemical incorporation). The concentrations of the main elements iron, aluminium, potassium, sodium and magnesium are representative of the mineralogy and/or secondary sorption processes to oxides. Possible sorption processes may be indicated by the clay content. However, the aim of the Geochemical Soil Atlas is not to identify specific sources of element concentrations in the soil but to create an overview of the distribution of elements in Switzerland's topsoil.

The concentrations of each element were compared with the land-use types surveyed for the BDM-Z9 programme and the 25 lithological and petrographic main groups in the simplified map of near-surface mineral raw materials of Switzerland using box plots and a significance test.

3.4.1 Significance test

A Wilcoxon rank sum test (*p*-adjustment following Benjamini and Hochberg, 1995) was performed to determine whether significant differences exist between the element concentrations of land-use types and lithological main groups. This test reduces the influence of extreme values on the results by comparing the respective rank in the data distribution of the concentration values rather than the absolute values (Reimann *et al.*, 2011). The number of sites per group was also taken into account in the data analysis to increase the weighting of groups with many sites compared to groups with only a few sites. The significance was indicated by letters, with the same letter denoting 'no statistically significant differences between these groups. The letters themselves do not indicate any hierarchy with regard to sorting of the data.

The significance tests were performed with the *multcompView,* Version 0.1-8 (Graves *et al.*, 2019), *robustbase,* Version 0.92-7 (Mächler *et al.*, 2016) and *MASS,* Version 7.3-45 (Venables & Ripley, 2002) R packages.

3.4.2 Correlations

Spearman's rank correlation coefficient R^2 was calculated to assess the correlations between element concentrations and soil properties as well as a selection of additional geodata. Since the element concentrations and soil properties have different distributions which do not follow a perfect normal distribution, analysing the rank is preferable to comparing the absolute value of two variables. The *psych* R package, Version 2.2.5 (Revelle, 2022) was used to calculate the significance levels of the correlations.

3.4.3 Factor analysis

As with the principal component analysis (PCA), factor analysis aims to reduce dimensionality, i.e. to extract components from a dataset that have a major impact on variability (Reimann *et al.*, 2011). Reimann *et al.* (2011) recommend the use of factor analysis for evaluating geochemical data since this method excludes the part of the variability which is unique to certain variables, increasing the interpretability of the dataset's overall variability. Reimann *et al.* (2011) also recommend a varimax rotation according to Kaiser (1958) to facilitate separation of the main geochemical processes. The influence of outliers on the results was reduced by scaling the log-transformed concentrations with the minimum covariance determinant (MCD) of the robust covariance matrix. Since with factor analysis, unlike with PCA, the number of factors must be determined at the start, a PCA was performed in advance. The result indicated that 10 components accounted for more than 70 % of the variance of the overall dataset. Factor analysis was then performed with the *stats* R package, Version 4.1.3 (R Core Team, 2022), which is based on the maximum likelihood method. Graphics for the interpretation were created with the factor loadings of individual variables. The factor loading indicates the extent to which a variable is associated with a factor. With factor analysis, strong spatial correlations between variables can overlay correlations due to geochemical processes – as with bivariate correlations. In this case, it is not possible to identify causality (Reimann *et al.*, 2011).

3.5 Spatial interpolations

Surface data can be modelled from point data using geostatic interpolation methods. The resulting surface maps can be used to visually represent regions with different concentration ranges. These interpolations are subject to inherent uncertainties as local variability is lost and extreme values are smoothed out (Reimann *et al.*, 2011). As a result, no plot-level information can be derived from surface maps.

Sampling, analysis and data evaluation for the Geochemical Soil Atlas of Switzerland are based on the European geochemical soil atlas (Reimann *et al.*, 2014). As with the European atlas, the concentration data were interpolated using the ordinary Kriging method. The advantage of this method is not only that a statistically optimised estimated value can be calculated for each point at which a concentration value is to be interpolated, but the quality of the estimate can be quantified by indicating the uncertainty (Cressie, 1993; Reimann *et al.*, 2011). The Kriging interpolation assumes that concentrations on neighbouring sites are more similar than concentrations on more distant sites. In theory, this variance remains more or less unchanged beyond a certain distance. The semivariogram depicting site similarity (variance) as a function of distance serves as the basis for the Kriging interpolation.

The final modelling of the semivariogram was performed according to Malone *et al.* (2017) in R with the *sp,* Version 1.5-1 (Bivand *et al.*, 2013; Pebesma & Bivand, 2005) and *geostat,* Version 2.1-0 (Gräler *et al.*, 2016; Pebesma, 2004) R packages. The BDM, NABO and GEMAS sites (at individual sample level) were used for the interpolations to avoid spatial bias wherever possible. The point pairs were divided into distance intervals of 2 km to create the final semivariogram. The maximum distance at which no further significant increase in the variance of the concentrations is assumed was set between 30 km (Co) and 150 km (Na) based on the previously created semivariograms. The robust variogram estimation proposed by Cressie (1993) was applied. The element concentrations were log-transformed in advance (natural logarithm). An optimised model was performed for the midpoints of a 1 km × 1 km grid for the Kriging interpolation. Since the logarithmic data follow a normal distribution, the logarithmic concentrations and variances were back-transformed following Laurent (1963).

To better visualise and delineate regions with high and low concentrations, the interpolated concentrations were divided into eight concentration ranges corresponding to the 5 %, 10 %, 25 %, 50 %, 75 %, 90 % and 95 % percentiles, analogous to the point data. Since the Kriging interpolations smooth out extreme values, the measured minimum and maximum values are indicated for the concentration ranges of the lowest and highest class. In addition, the coefficient of variation as a percentage is indicated as the relative measure of dispersion of the interpolated concentrations. For the visualisation, the coefficients of variation per grid cell were divided into five classes corresponding to the Jenks Natural Breaks algorithm (De Smith *et al.*, 2018).

The interpolations were validated using the leave-one-out method, whereby one data point is excluded from interpolation and its interpolated value is then computed from the other points (Lado *et al.*, 2008; Pebesma & Bivand, 2005). For cadmium, cobalt, copper and lead, the sites with concentration values measured using the VBBo method with subsequent conversion, as described in Chapter 2.3.4, were compared with the interpolated values. The results of the validation can be found in the annex.

In addition to the ordinary Kriging method, the universal Kriging method was used to interpolate the element concentrations with regard to the lithological and petrographic main groups (Chapter 2.5), the parameters elevation, slope and exposure of the digital elevation model (Chapter 2.5), and the total organic carbon and pH modelled for the whole of Switzerland by Descombes *et al.* (2020). As with Lado *et al.* (2008), the universal Kriging method does not significantly improve the prediction of element concentrations in comparison with the ordinary Kriging method. The results of the universal Kriging interpolation and the comparison with the ordinary Kriging method for cadmium, cobalt, copper and lead can be found in the annex.

4 Element concentrations in Swiss topsoils

The descriptive statistics of the consolidated data set are presented in Table 2. The results for each element are summarised in Chapters 4.1 to 4.20. In summary, the measured element concentrations in Swiss topsoils follow a multimodal, right-skewed, log-normal distribution which is typical of geochemical data (Chapters 4.1 to 4.20). This distribution consists of a variety of underlying distributions depicting various soil processes (Reimann *et al.*, 2011).

Where available and useful, the typical element concentrations of soil-forming rocks in Switzerland are listed based on the publication by Tuchschmid (1995). This comparison can be used to further interpret the measured concentration ranges, although no direct correlation can be derived between concentrations in source rocks and those in topsoils.

Furthermore, the measured concentrations were compared with the tolerance values defined by Eikmann & Kloke (1993), which are based on element concentrations measured in aqua regia digests. Neither short- nor long-term adverse effects on 'normal' quality of life are anticipated at these concentrations (Eikmann & Kloke, 1993). If values exceed the tolerance values, restricted use of the soil based on the location and the protected asset is recommended (Herklotz *et al.*, 1996). These threshold values relate to the usage and the object of protection, i.e. tolerance values will differ for children's playgrounds, domestic gardens and allotments, sports grounds and football pitches, parks and recreational areas, industrial and commercial areas, agricultural land for fruit and vegetable cultivation and non-agricultural ecosystems. Since these usages were not differentiated in the Geochemical Soil Atlas, the measured concentrations are compared with tolerance values for agricultural land. The presented threshold values are not mandatory for Switzerland, but rather provide a helpful reference for interpreting the measured concentrations. A direct comparison with the VBBo thresholds (Swiss Ordinance on Soil Pollution) is not recommended, since conversion of the measured concentrations would be worthwhile only for a very small number of elements, if at all (Stanisic *et al.*, 2021). The threshold values according to Eikmann & Kloke (1993) and their comparison with the VBBo limit values are listed in Annex 8 of the BUWAL 'Manual on risk assessment and measures for polluted soils' (Mailänder & Hämmann, 2005).

The element descriptions in Chapters 4.1 to 4.20 cover a range of topics, starting with geological occurrence in the Earth's crust and moving on to technical uses and potential anthropogenic sources. Since accumulation in the soil depends not only on element sources, but also on various soil processes affecting mobilisation and immobilisation, the next section outlines the prevalent chemical forms of individual elements and their behaviour in the soil. A further section discusses the spatial distribution of elements in Swiss topsoils and compares the concentrations across the different land uses of the BDM dataset. The final section considers the measured element concentrations in the context of existing reference and threshold values.

Table 2 | Medians, percentiles, maxima, minima, mean absolute deviations from the median (MAD) and Tukey Inner Fence values (TIF) of the element concentrations measured in the sieved (< 2 mm) topsoil (0–20 cm). The results of the consolidated dataset comprising the BDM, NABO and GEMAS sampling sites are listed. The n column lists the number of sites included in the analysis. The median and the number of sites n in the UB dataset are listed separately. The median of all individual samples per site was included in the data analysis. 0.5 times the limit of detection (LOD) was assigned to measured values below the LOD (Chapter 3.2). These values are indicated by *.

	Unit	BDM, NABO, GEMAS													UB	
		n	Median	5 %	10 %	25 %	75 %	90 %	95 %	Min	Max	MAD	TIF	n ≥ TIF	n	Median
As	mg/kg	1 201	7.9	2.7	3.6	5.5	12.1	21.9	35.2	0.6	317.4	4.4	40.0	48	275	40.0
Ca	g/kg	1 201	4.2	0.7	1.0	2.0	14.0	67.9	100.9	0.2	247.0	4.4	259.3	0	222	33.0
Cd	mg/kg	1 201	0.24	0.07	0.10	0.16	0.36	0.62	1.04	0.02	5.28	0.14	1.23	43	1 510	0.24
Co	mg/kg	1 201	8.6	2.6	3.9	6.4	11.8	14.9	17.9	0.4	134.2	3.8	29.6	14	2 102	9.8
Cr	mg/kg	1 201	30.3	9.8	13.8	22.9	40.1	52.1	62.8	2.5	1 661.4	12.5	93.2	25	275	81.0
Cu	mg/kg	1 201	18.1	5.8	7.7	11.9	25.7	35.0	40.8	1.7	371.1	9.9	81.2	5	3 123	21.3
Fe	g/kg	1 201	21.8	11.4	13.7	17.5	27.8	33.7	38.3	1.8	142.9	7.3	55.9	10	222	29.0
Hg	mg/kg	1 201	0.066	0.027	0.033	0.046	0.097	0.140	0.180	0.003	2.830	0.035	0.302	13	275	0.050
Mg	g/kg	1 201	4.2	1.4	2.0	3.1	6.2	9.7	14.8	0.2	191.0	2.1	17.2	49	222	5.3
Mn	mg/kg	1 201	655	145	226	403	856	1 139	1 390	18	3 609	337	2 651	8	222	895
Mo	mg/kg	1 201	0.81	0.39	0.47	0.61	1.16	1.78	2.51	0.08	260.99	0.36	3.08	42	275	0.50
Na	mg/kg	1 201	80	40	50	65	115	160	195	20	3 215	30	271	14	222	360
Ni	mg/kg	1 201	27.3	6.2	10.2	19.1	37.5	49.8	63.9	1.1	1 754.8	13.4	103.2	16	275	39.0
Pb	mg/kg	1 201	24.2	13.1	15.0	18.7	30.6	41.3	52.4	1.9	800.8	8.6	63.8	28	3 278	26.1
S	mg/kg	1 201	350	129	160	232	500	700	900	65	4 800	222	1 582	9	10	390
Sb	mg/kg	1 201	0.38	0.18	0.21	0.29	0.50	0.74	0.95	0.05	6.76	0.16	1.16	37	275	0.50
Tl	mg/kg	1 201	0.15	0.07	0.09	0.11	0.21	0.31	0.38	0.01*	1.45	0.07	0.55	14	275	0.59
U	mg/kg	1 201	0.7	0.3	0.4	0.5	1.0	1.6	2.0	0.1	63.6	0.3	2.8	25	270	1.3
V	mg/kg	1 201	32	12	16	23	44	61	75	2	394	16	117	11	275	92
Zn	mg/kg	1 201	64	27	35	48	83	106	128	5	398	25	187	9	275	93

4.1 Antimony (Sb)

Antimony is a non-essential metalloid which occurs naturally in minerals together with sulphur, gold, lead and arsenic (Arai, 2010). Stibnite (Sb_2S_3), the main ore mineral of antimony, can form in the presence of sulphur (Christie & Brathwaite, 2011). In Switzerland, antimony mineralisations are documented in the Vorderrhein and Hinterrhein Valleys in the canton of Grisons (GB), the Murg Valley (Murgtal) in the canton of St Gallen (SG) and the Malcantone region in Southern Ticino (FGS, 2023b; Jost *et al.*, 2014). Antimony was once mined on Monte Pellegrino in the latter region. Sampling sites assigned to the granite/syenite lithological group in the Geochemical Soil Atlas have significantly lower antimony concentrations than other sites, such as those assigned to the dolomite or limestone group (Figure 8).

Antimony is a constituent of some lead-containing alloys which are used to increase the hardness of ammunition, for example. This explains why increased antimony concentrations of anthropogenic origin are detected in soil, particularly in the bullet traps of shooting ranges (Scheinost *et al.*, 2006). Antimony is also used in batteries, piping, soldering agents, semiconductors and cabling, as a catalyst for polymerisation of plastics, as a flame retardant for plastics and clothing, and in pharmaceuticals (Arai, 2010). According to Mathys *et al.* (2007), the greatest point emissions of antimony in Switzerland are expected to be found on shooting ranges, while road traffic (specifically brake pad wear) may be the primary source of diffuse emissions.

Antimony's solubility and mobility in soil are strongly dependent on pH and redox conditions (Arai, 2010). Under oxic conditions, i.e. in the presence of oxygen, antimony is relatively immobile, since Sb(III) and Sb(V) are bound to soil components such as iron (hydr)oxides, clay minerals and soil organic matter (Arai, 2010).

Measured antimony concentrations in Swiss topsoils follow a unimodal, right-skewed, log-normal distribution (Figure 7). Because the distribution is skewed to the right, the arithmetic mean is substantially higher than the median (A) as it is strongly influenced by extreme values. Similarly, the upper percentiles deviate significantly from the normal distribution (C).

High antimony concentrations are mostly found in topsoil in Southern Ticino and the eastern Central Alps (Figure 9). In total, 37 sites are classified as geochemical outliers based on the TIF method. In contrast, particularly low antimony levels were measured in the Upper Valais.

The top 2 cm of agricultural soils is estimated to contain 28 t of antimony in total (Mathys *et al.*, 2007). No significant differences in antimony concentrations were found between the different land-use types at the BDM sites (Figure 8).

Since the biogeochemical behaviour of antimony is very similar to that of arsenic (Arai, 2010), it is generally thought to exhibit a similar toxicity (Mathys *et al.*, 2007). The Sb(III) oxidation state appears to be more toxic and more soluble than Sb(V) (Johnson *et al.*, 2005; Jost *et al.*, 2014). The tolerance and trigger value of antimony in aqua regia soil digests is 2 mg/kg for children's playgrounds and sports grounds (Lühr *et al.*, 1996). Three sites exceed the toxicity value for sports grounds (5 mg/kg). For agricultural land and fruit and vegetable cultivation, the toxicity value of 25 mg/kg is significantly higher than the maximum measured value of 6.76 mg/kg.

Element	Symbol	Atomic number	Median	5 %	95 %
Antimony	Sb	51	0.38 mg/kg	0.18 mg/kg	0.95 mg/kg

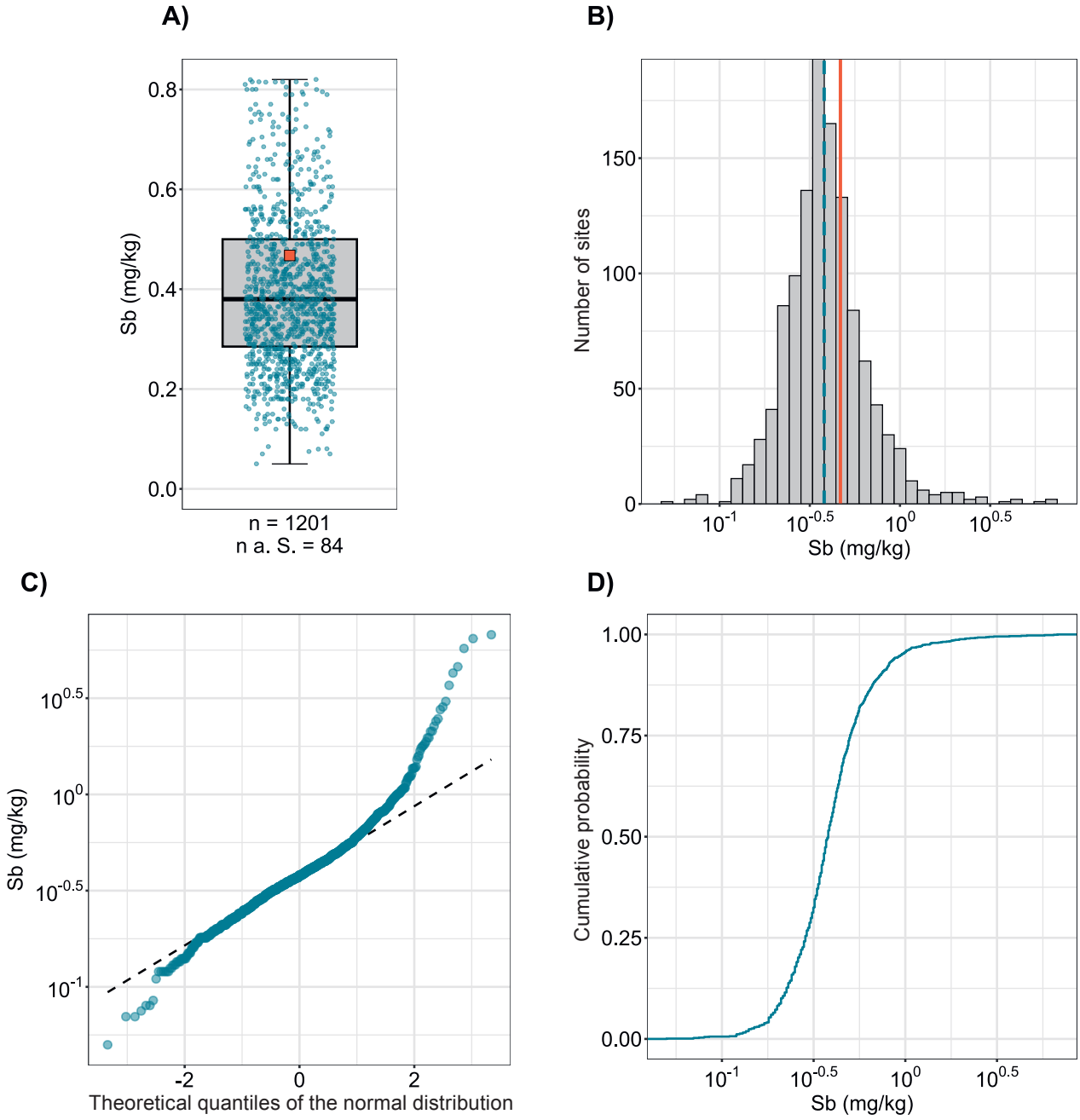

Figure 7 | Distribution of antimony concentrations (mg/kg soil). The allocated value is the median of individual samples per site. The dataset presented comprises the BDM, NABO and GEMAS sampling sites. n = total number of sites, n a. S. = sites lying outside the axis range or whisker.

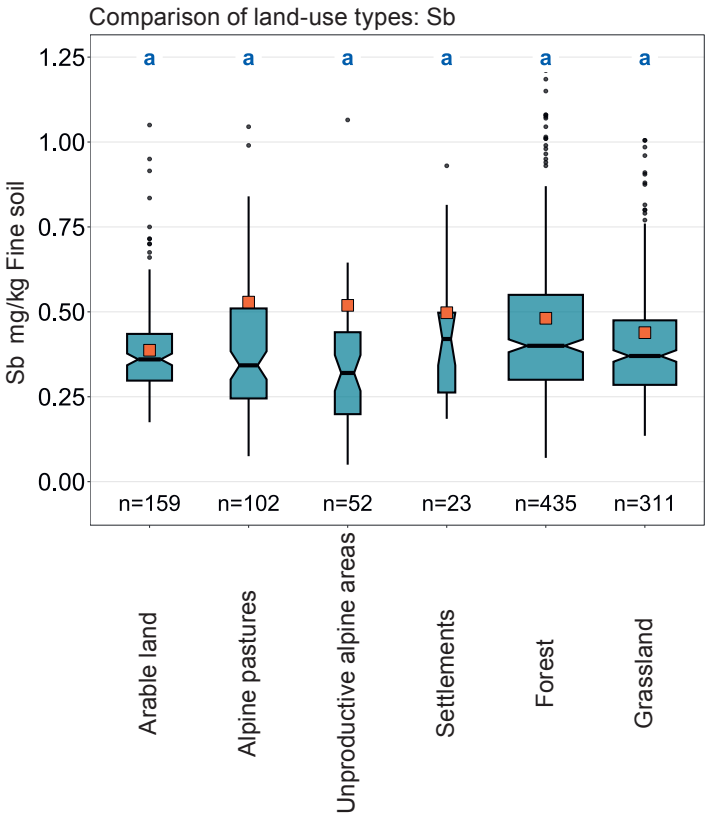

Figure 8 | Comparison of antimony concentrations (mg/kg soil) in relation to the Z9 land-use types of the BDM sampling sites (top) and the lithological and petrographic groups in the simplified map of near-surface mineral raw materials of Switzerland (1 : 500 000, swisstopo, bottom). The median of all individual samples per site was included in the data analysis (BDM, NABO and GEMAS datasets). The number of sites per group is indicated beneath the boxes. Letters in blue: significant differences between groups ($p < 0.001$) based on a Wilcoxon rank sum test with P-adjustment using the Benjamini and Hochberg method. Not all outliers are shown. Orange square: arithmetic mean of the data.

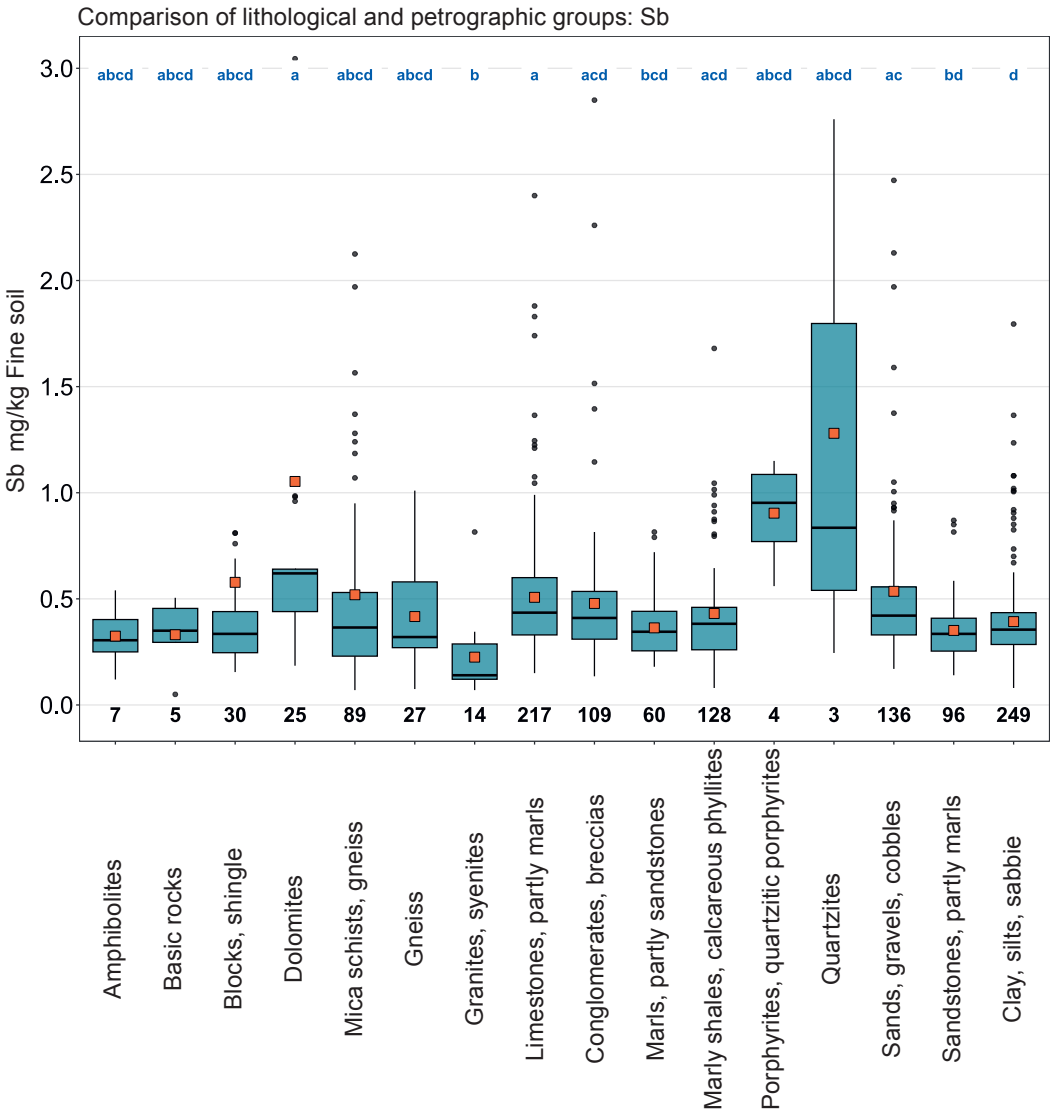

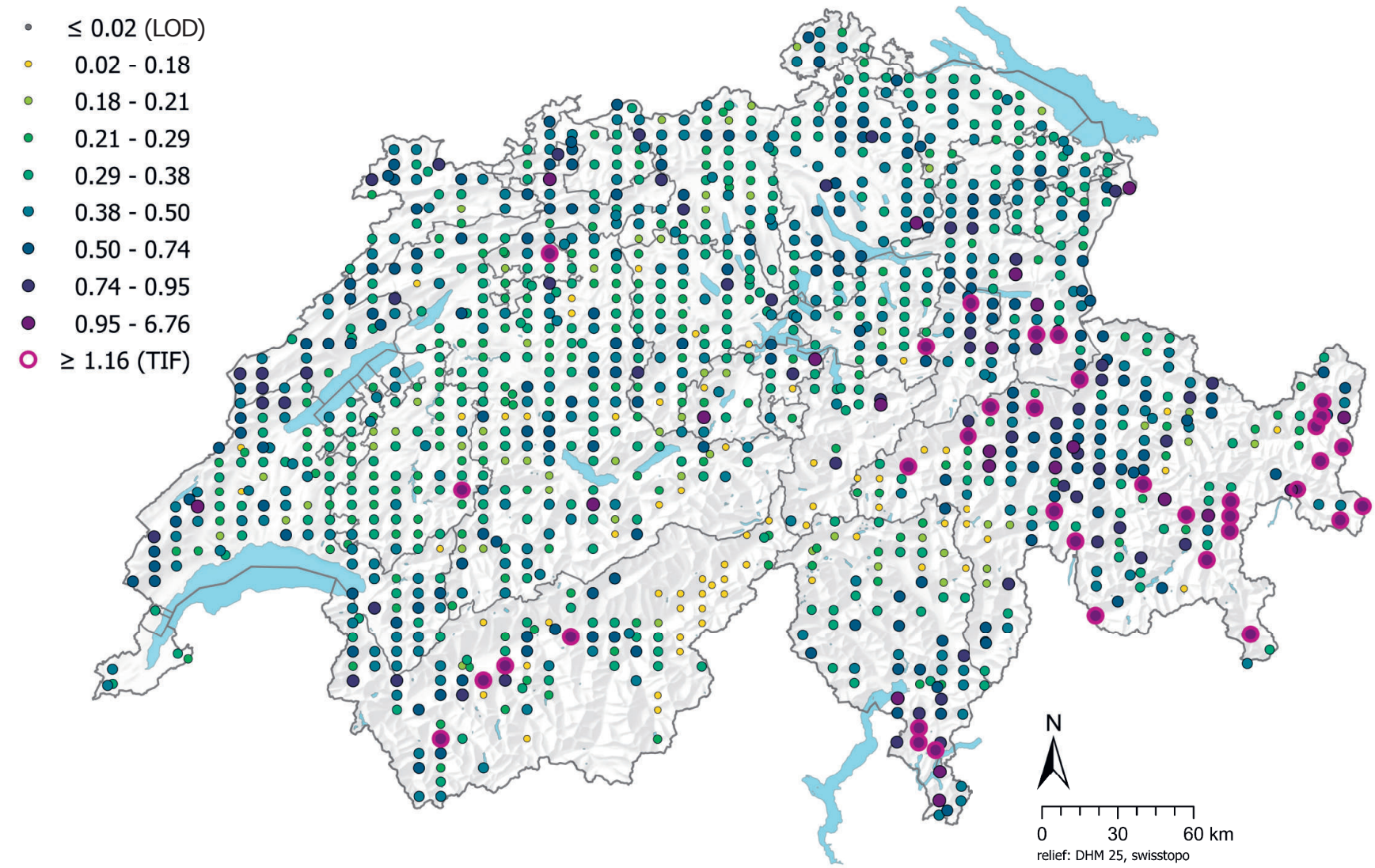

Figure 9 | Spatial distribution of antimony concentrations (mg/kg soil) measured at the BDM, NABO and GEMAS sites. The data points show the median of several individual samples per site. 0.5 times the limit of detection (LOD) was assigned to measured values below the LOD. The classes correspond to the 5 %, 10 %, 25 %, 50 %, 75 %, 90 % and 95 % percentiles. TIF: Tukey Inner Fence, outlier as per Reimann *et al.* (2018). LOD: limit of detection

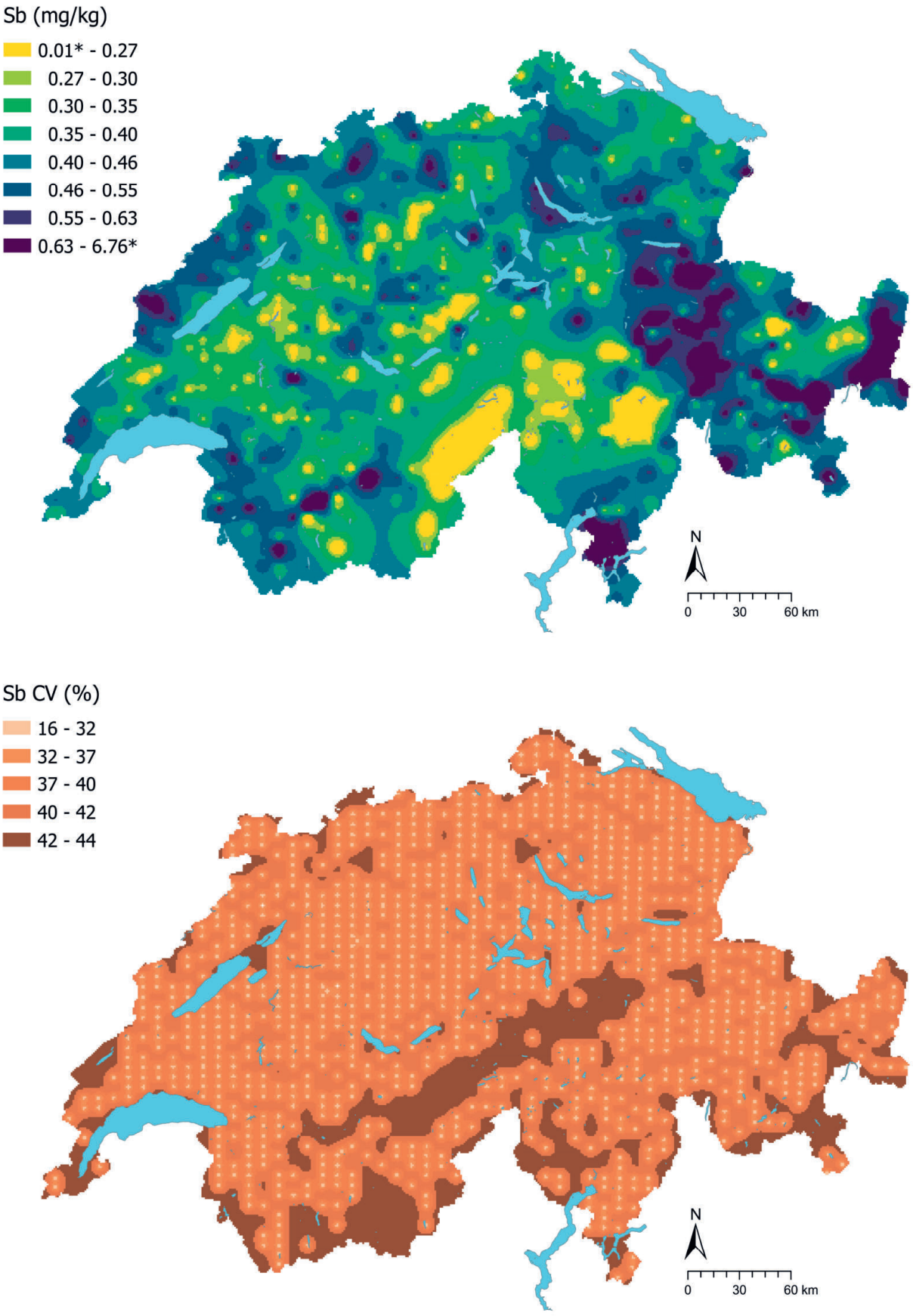

Figure 10 | Interpolated antimony concentrations (mg/kg soil) at the BDM, NABO and GEMAS sites (top) and coefficient of variation (%) of the interpolated concentrations (bottom). The concentrations were divided into eight classes corresponding to the 5 %, 10 %, 25 %, 50 %, 75 %, 90 % and 95 % percentiles. The coefficients of variation were divided into five classes corresponding to the Jenks Natural Breaks algorithm. The interpolation was performed using the ordinary Kriging method (1 km × 1 km grid). In the classes of interpolated values, * denotes the minimum and maximum value of the point data calculated from the limit of detection.

4.2 Arsenic (As)

Like antimony, the metalloid arsenic is in group 15 of the periodic table. The average arsenic concentration in the Earth's crust is 2 to 5 mg/kg (Tamaki & Frankenberger, 1992). The main ore of arsenic is arsenopyrite (FeAsS), which is documented to occur in Switzerland mainly in the cantons of Valais, Grisons and Ticino (Pfeifer *et al.*, 2010). Clay-rich rocks, sedimentary iron ores, coal, and peat and bog deposits can contain high concentrations of arsenic (NEROS, 2019). In the Jura, elevated arsenic concentrations are reported to occur in iron-bearing limestone and clay (Pfeifer *et al.*, 2010). High concentrations of arsenic measured in the topsoil at certain sites in the Jura may be caused by these geogenic origins (Figure 13).

In addition to weathering of arsenic-bearing rocks and displacement due to hydrothermal processes (Pfeifer *et al.*, 2010), anthropogenic inputs can lead to arsenic accumulation in the soil. Sources include smelting of arsenic ores, coal combustion, and agricultural inputs from fertilisers, insecticides, herbicides and fungicides, animal feed, wood preservatives, antibacterial treatments and deworming products (Arai, 2010; Sheppard *et al.*, 2009).

As with antimony, the mobility of arsenic within the soil is largely determined by the prevailing redox conditions. How strongly arsenic is bound in the soil depends on the presence of iron and aluminium oxides, clay minerals, and on the soil calcium content (Arai, 2010). Furthermore, the sorption of arsenic in the soil is determined by pH; the adsorption of the oxyanion arsenate at oxide surfaces, e.g. iron oxide, decreases with increasing pH (Amelung *et al.*, 2018c). However, the correlation analysis does not indicate a correlation between arsenic concentrations and pH, although a weak correlation with iron concentrations was found (Chapter 6.1). The previously mentioned bio-geochemical similarity between arsenic and antimony is also evident in the tight clustering of these two elements in the factor analysis (Chapter 6.2).

The measured arsenic concentrations in topsoil follow a unimodal, right-skewed, log-normal distribution typical of geochemical elements (Figure 11). With regard to the spatial distribution, high values were frequently measured in the eastern Jura and in the Engadin. Most of the 48 sites whose concentrations exceed the TIF value and are thus classified as outliers are located in these areas. Significant accumulations of arsenic in soil are known to occur in former ore mining areas, for example in the Buus (BL) or Malcantone region (TI) (AUE & Schmutz, 2016; NEROS, 2019). In this dataset too, concentrations measured in these regions are elevated. Arsenic concentrations in topsoils on the south side of the Alps and in the western Swiss Plateau are low in comparison with other regions (Figure 13). Arsenic concentrations measured in arable land were not higher than those in other land-use types. However, arsenic concentrations in the topsoils of grasslands were significantly higher than in forests (Figure 12).

Arsenic, particularly in its inorganic form, can pose a threat to human, animal, and plant health, even at low levels. Chronic toxicity, which results from long-term exposure, is more severe than acute toxicity (NEROS, 2019; Tamaki & Frankenberger, 1992). According to the threshold values defined by Eikmann *et al.* (1993) for potentially harmful substances, the trigger value of arsenic for gardens and agricultural land is 40 mg/kg, analogous to the TIF threshold. The toxicity value of 80 mg/kg, defined by Mailänder & Hämmann (2005) as the remediation value in accordance with the VBBo, is exceeded at 17 sites.

Element	Symbol	Atomic number	Median	5 %	95 %
Arsenic	As	33	7.9 mg/kg	2.7 mg/kg	35.2 mg/kg

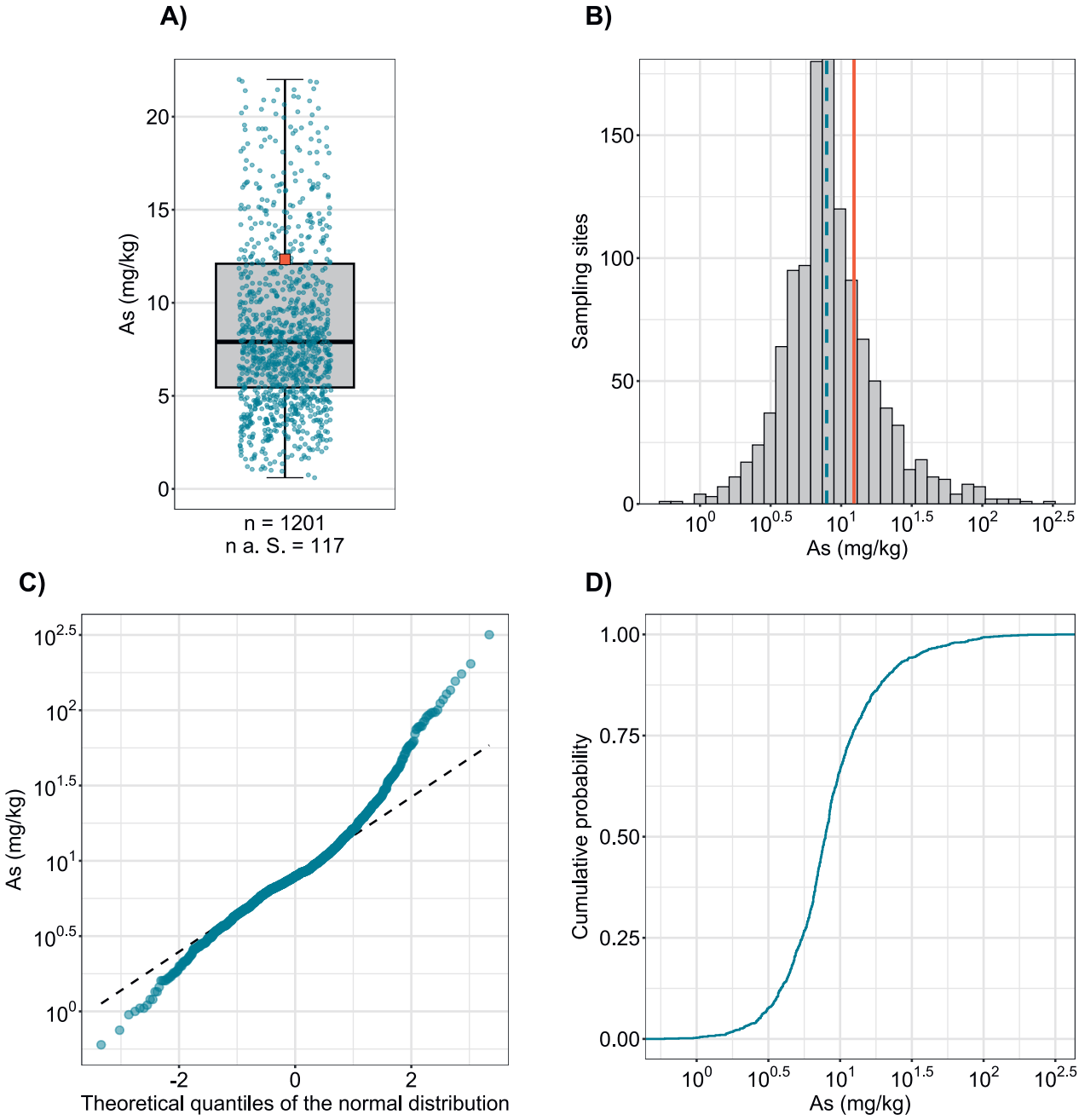

Figure 11 | **Distribution of arsenic concentrations (mg/kg soil). The allocated value is the median of individual samples per site. Measured values below the limit of detection were disregarded. The dataset presented comprises the BDM, NABO and GEMAS sampling sites. n = total number of sites, n a. S. = sites lying outside the axis range or whisker.**

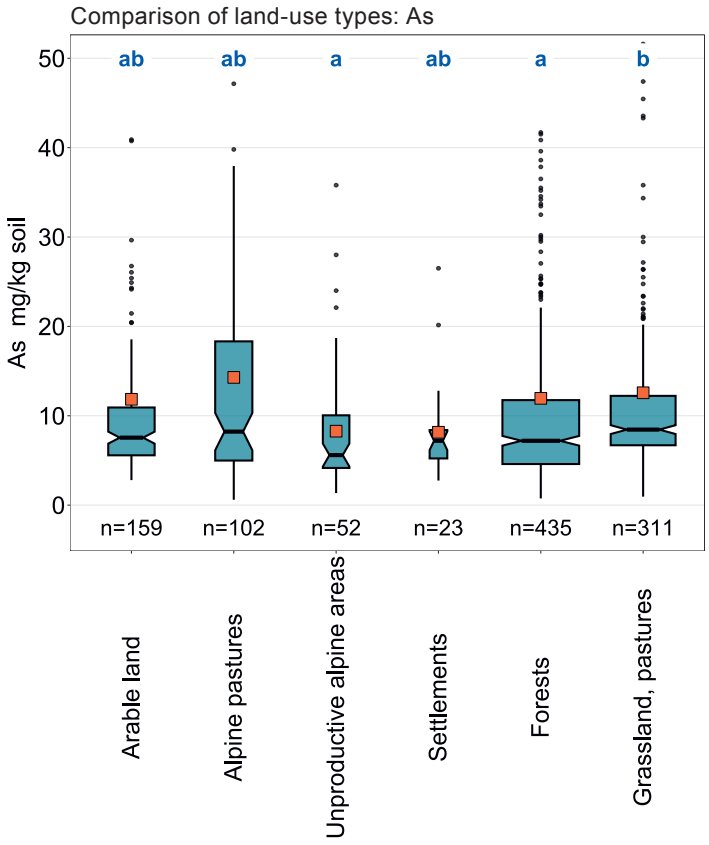

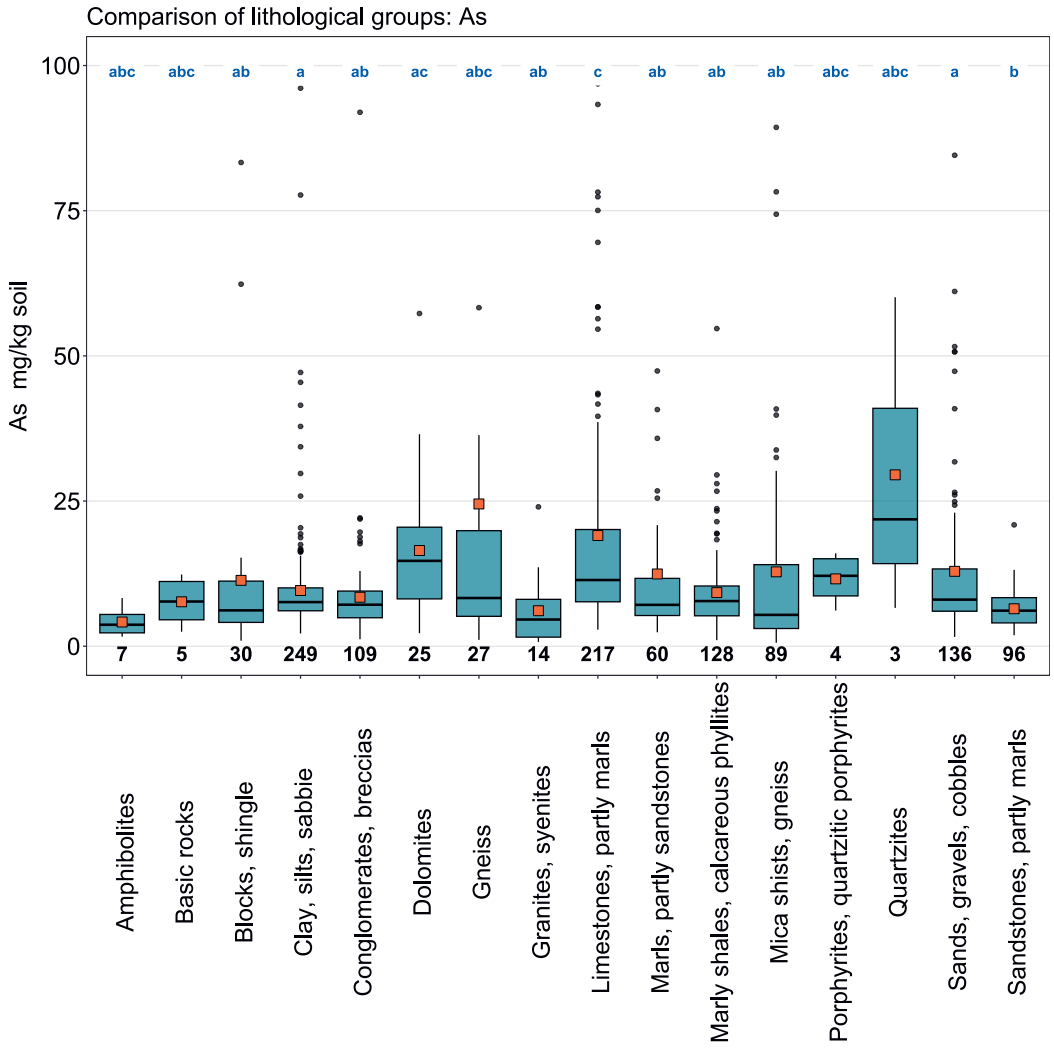

Figure 12 | Comparison of arsenic concentrations (mg/kg soil) in relation to the Z9 land-use types of the BDM sampling sites (top) and the lithological and petrographic groups in the simplified map of near-surface mineral raw materials of Switzerland (1 : 500 000, swisstopo, bottom). The median of all individual samples per site was included in the data analysis (BDM, NABO and GEMAS datasets). The number of sites per group is indicated beneath the boxes. Letters in blue: significant differences between groups ($p < 0.001$) based on a Wilcoxon rank sum test with P-adjustment using the Benjamini and Hochberg method. Not all outliers are shown. Orange square: arithmetic mean of the data.

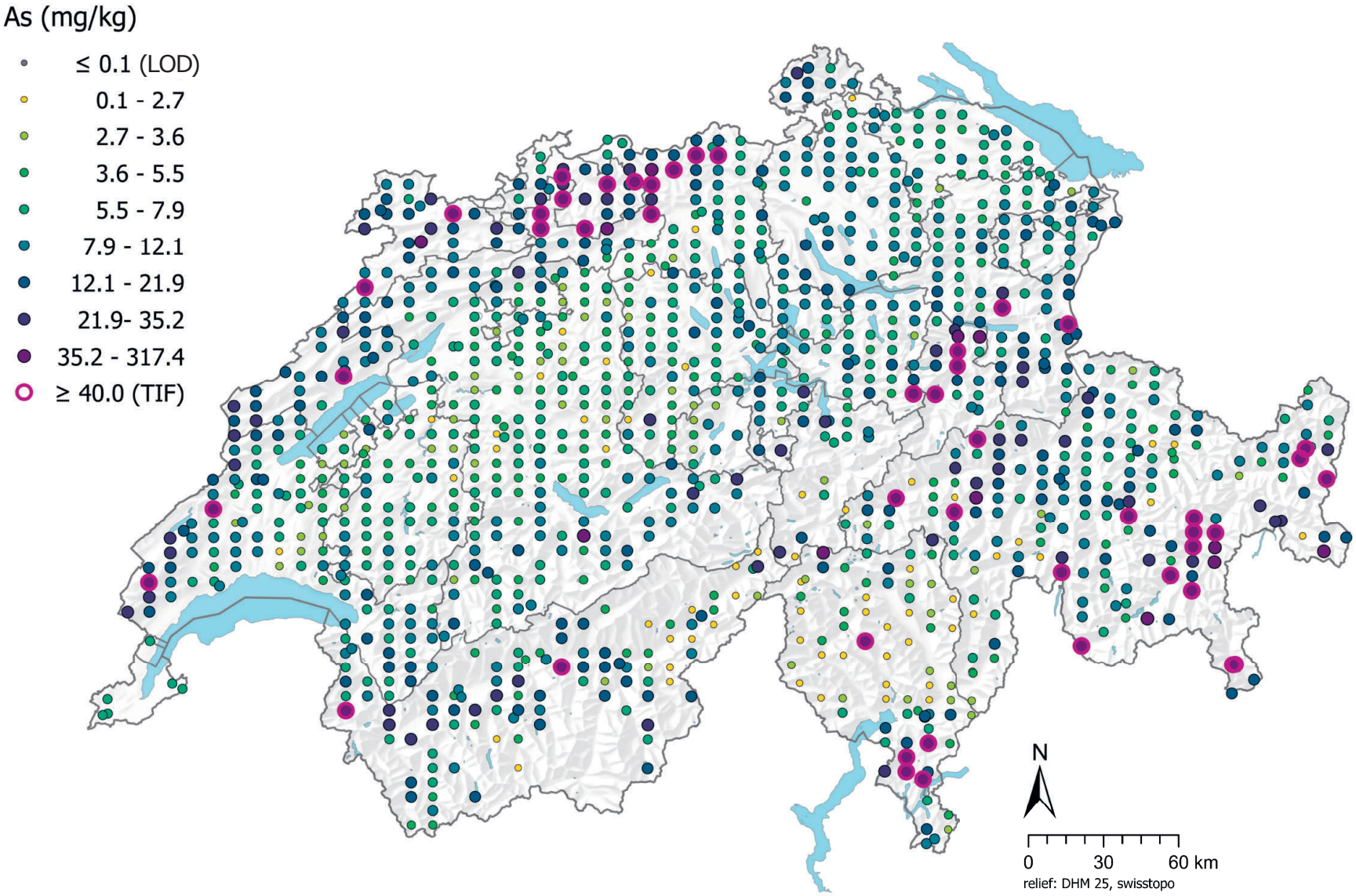

Figure 13 | **Spatial distribution of arsenic concentrations (mg/kg soil) measured at the BDM, NABO and GEMAS sites. The data points show the median of several individual samples per site. 0.5 times the limit of detection (LOD) was assigned to measured values below the LOD. The classes correspond to the 5 %, 10 %, 25 %, 50 %, 75 %, 90 % and 95 % percentiles. TIF: Tukey Inner Fence, outlier as per Reimann *et al.* (2018). LOD: limit of detection**

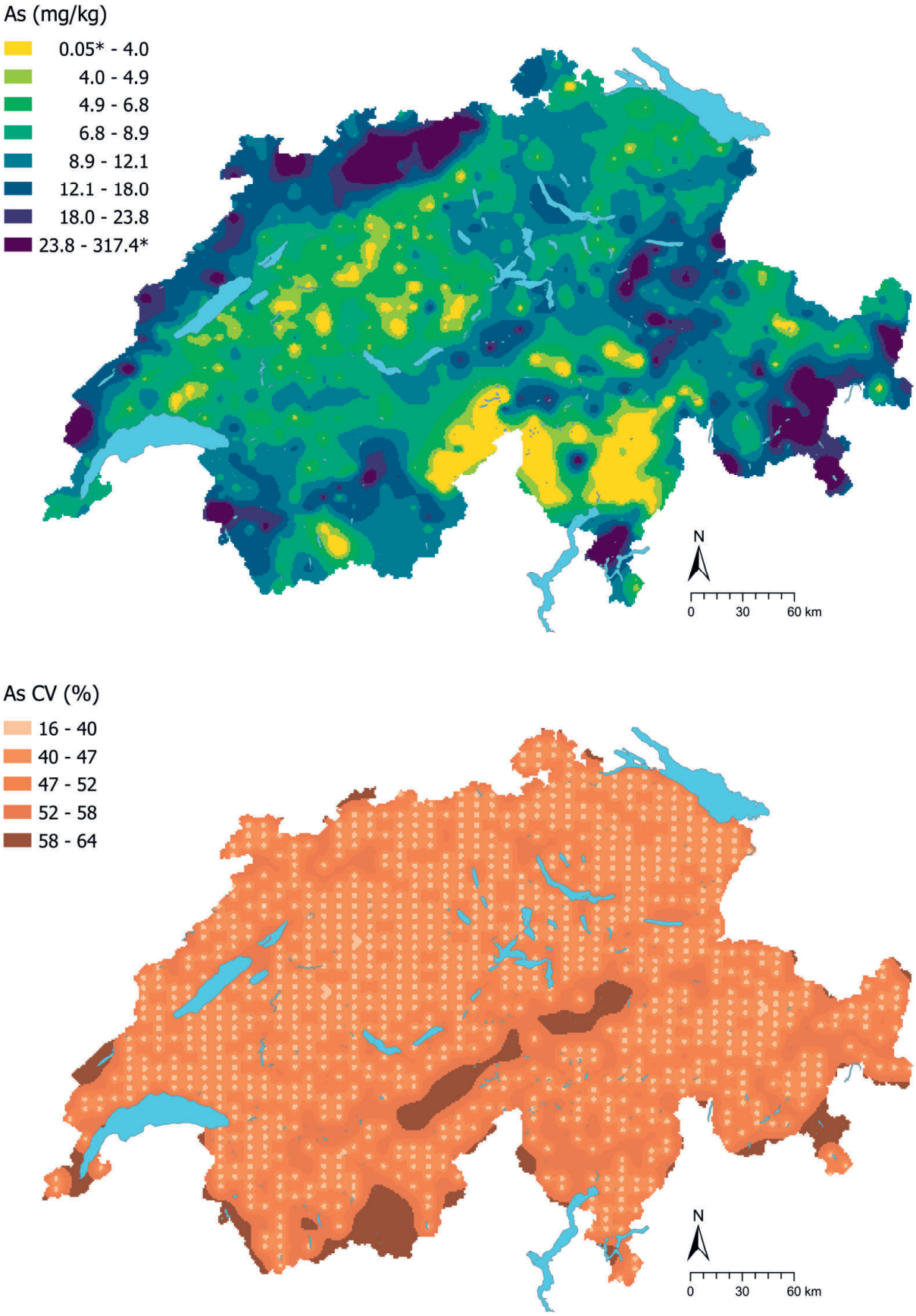

Figure 14 | Interpolated arsenic concentrations (mg/kg soil) at the BDM, NABO and GEMAS sites (top) and coefficient of variation (%) of the interpolated concentrations (bottom). The concentrations were divided into eight classes corresponding to the 5 %, 10 %, 25 %, 50 %, 75 %, 90 % and 95 % percentiles. The coefficients of variation were divided into five classes corresponding to the Jenks Natural Breaks algorithm. The interpolation was performed using the ordinary Kriging method (1 km × 1 km grid). In the classes of interpolated values, * denotes the minimum and maximum value of the point data calculated from the limit of detection.

4.3 Lead (Pb)

Lead, which is considered a heavy metal due to its high density, is in group 14 of the periodic table. The main mineral of lead is the sulphide galena (PbS), also known as lead glance (Hough, 2010). Traces of lead also occur in minerals such as feldspar, mica and magnetite (Reimann *et al.*, 2014). High levels of lead are likely to be present in granitic and sedimentary rocks containing high concentrations of clay minerals, sulphides and organic carbon, as well as in sandstone rich in feldspar and mica (Tuchschmid, 1995). Although carbonate rocks contain comparatively low lead concentrations according to Tuchschmid (1995), topsoil samples belonging to the limestone group display statistically significant high levels of lead. (Figure 16). The median lead concentration is 24 mg/kg (Table 2), which is higher than typical concentrations (50 % of the measurement data, 6.8–22.9 mg/kg) recorded by Tuchschmid (1995) in the various geochemical facies and lithofacies of soil-forming rocks in Switzerland.

Lead has been in use for over 5500 years due to its relatively low melting point of 327.5 °C, which makes it easy to extract and process. The element was initially used in pipework, as a pigment and in glass production, and nowadays mostly in batteries (Reimann *et al.*, 2014). Lead was added to petrol before this practice was banned in 2000, thus the element is regarded as the main pollutant in soils adjacent to roads (AGIR, 2020). Sampling sites along roads were excluded and no correlations were found between lead concentrations and proxies for atmospheric deposition at the remaining sites (Chapter 6.1). In contrast, lead concentrations correlated weakly with cadmium and mercury concentrations ($R^2 = 0.57$ and $R^2 = 0.59$ respectively), which could indicate similar sources. Sites where the measured lead concentrations exceeded the TIF value occur mainly on the south side of the Alps and in the western Jura, as well as at certain sites in the Alps (Figure 17). Lead concentrations in the topsoils of the western Swiss Plateau and the Valais are comparatively low.

Forest and grassland exhibit significantly higher lead concentrations than arable land (Figure 16). In the European geochemical atlas, higher lead concentrations were also recorded for grassland sites than for arable sites (median: 18 mg/kg as against 16 mg/kg) – possibly because samples from the grassland sites contain higher total organic carbon (TOC) levels (Reimann *et al.*, 2014). However, the data from the Geochemical Soil Atlas of Switzerland correlate only weakly with the TOC ($R^2 = 0.47$, Chapter 3.4.2). At the NABO sampling sites, a general decrease in lead concentrations in all land-use types surveyed was observed between 1985 and 2009 (Gubler *et al.*, 2015). The authors attribute this decrease to reduced airborne emissions following the ban on lead in petrol on the one hand, and a mixing of soil layers resulting in a dilution of lead concentrations on the other.

Lead is highly toxic to humans and aquatic organisms (Reimann *et al.*, 2014). The tolerance value defined by Eikmann *et al.* (1993) for agricultural land is 500 mg/kg. One site exceeds this value. In most cases, only a small portion of the total lead concentration in soil is bioavailable since the majority is not present in solution, but is adsorbed or precipitated (Hough, 2010).

Element	Symbol	Atomic number	Median	5 %	95 %
Lead	Pb	82	24.2 mg/kg	13.1 mg/kg	52.4 mg/kg

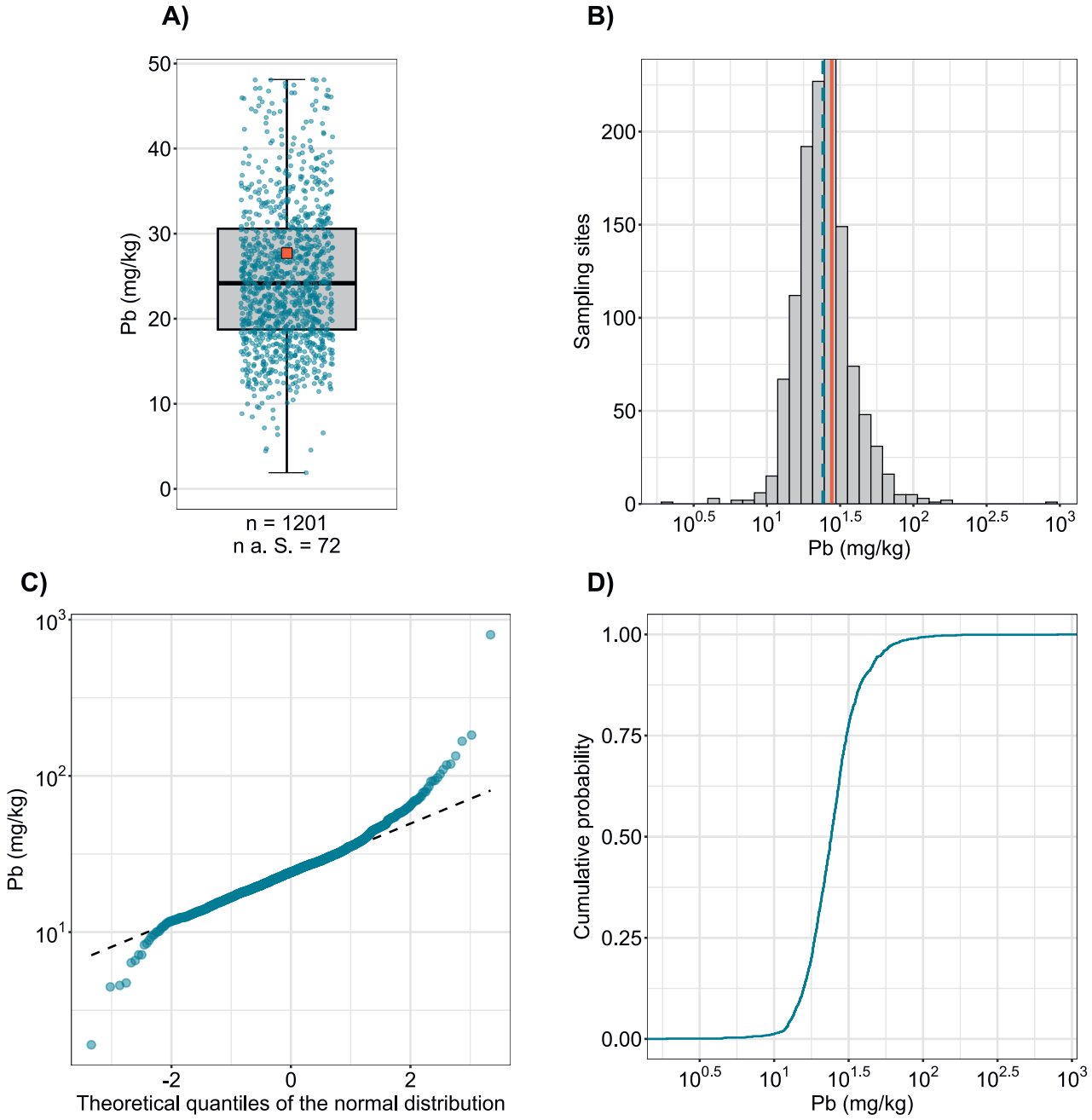

Figure 15 | Distribution of lead concentrations (mg/kg soil). The allocated value is the median of individual samples per site. The dataset presented comprises the BDM, NABO and GEMAS sampling sites. n = total number of sites, n a. S. = sites lying outside the axis range or whisker.

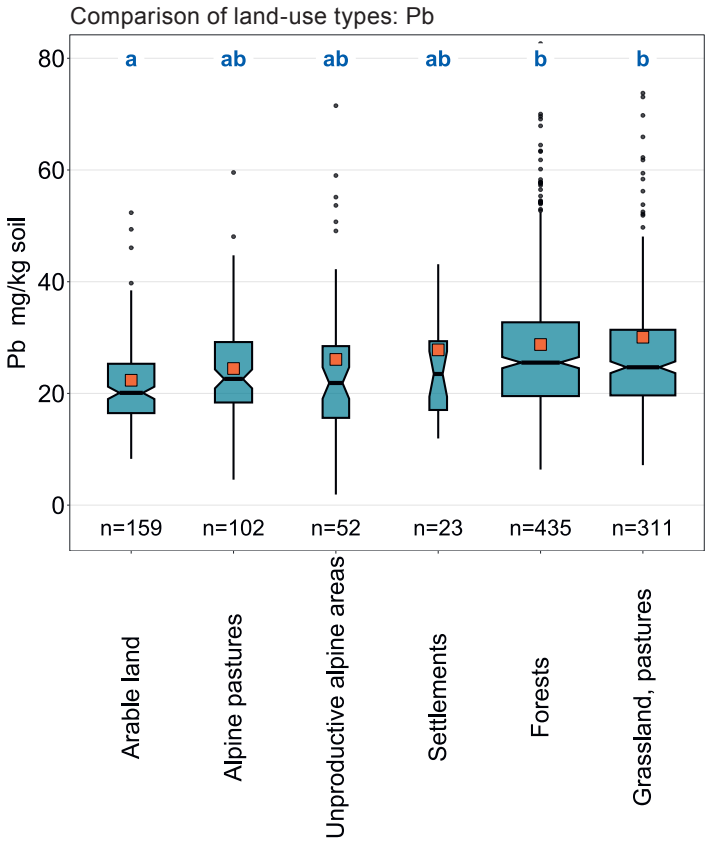

Figure 16 | **Comparison of lead concentrations (mg/kg soil) in relation to the Z9 land-use types of the BDM sampling sites (top) and the lithological and petrographic groups in the simplified map of near-surface mineral raw materials of Switzerland (1 : 500 000, swisstopo, bottom). The median of all individual samples per site was included in the data analysis (BDM, NABO and GEMAS datasets). The number of sites per group is indicated beneath the boxes. Letters in blue: significant differences between groups ($p < 0.001$) based on a Wilcoxon rank sum test with P-adjustment using the Benjamini and Hochberg method. Not all outliers are shown. Orange square: arithmetic mean of the data.**

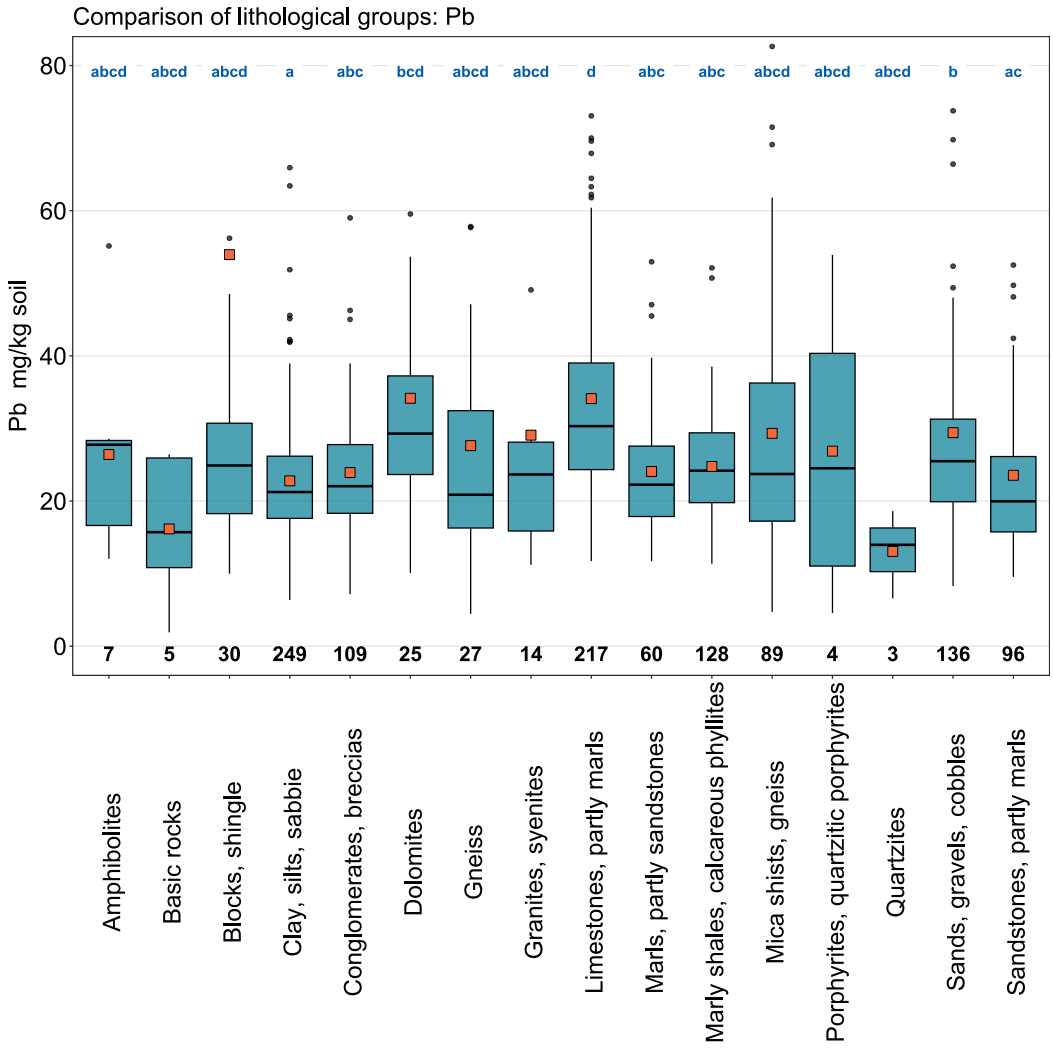

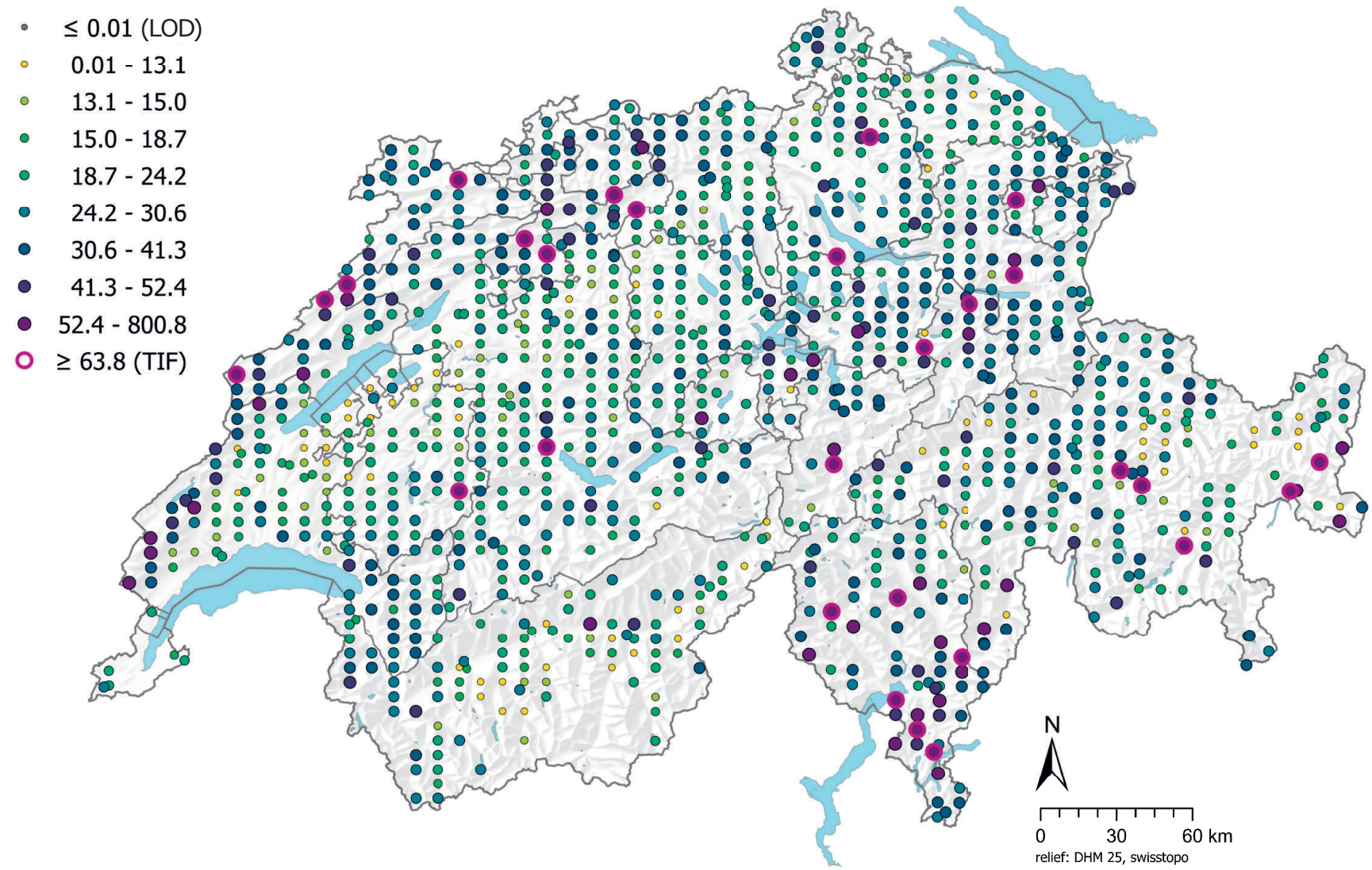

Figure 17 | **Spatial distribution of lead concentrations (mg/kg soil) measured at the BDM, NABO and GEMAS sites. The data points show the median of several individual samples per site. The classes correspond to the 5 %, 10 %, 25 %, 50 %, 75 %, 90 % and 95 % percentiles. TIF: Tukey Inner Fence, outlier as per Reimann *et al.* (2018). LOD: limit of detection**

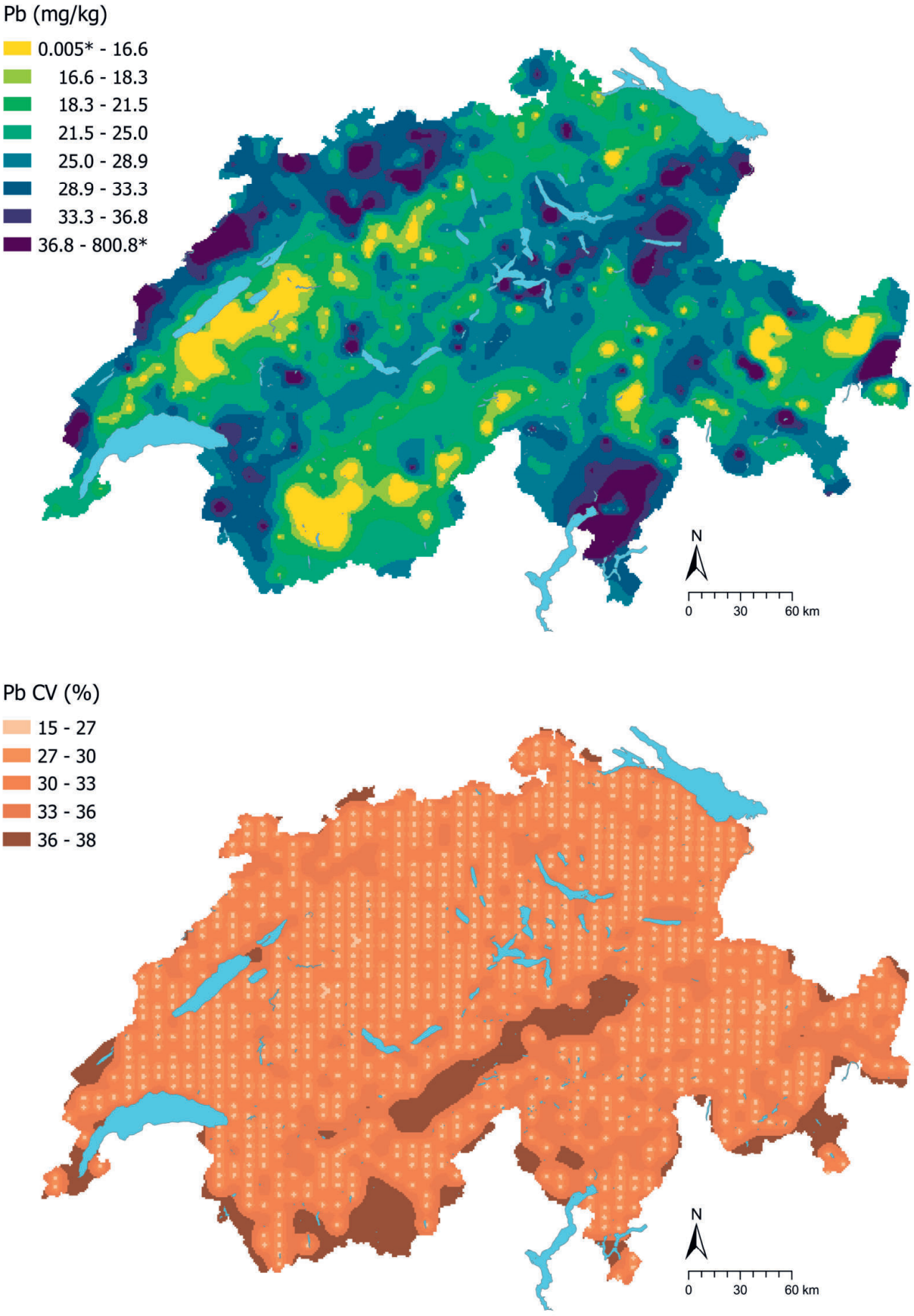

Figure 18 | Interpolated lead concentrations (mg/kg soil) at the BDM, NABO and GEMAS sites (top) and coefficient of variation (%) of the interpolated concentrations (bottom). The concentrations were divided into eight classes corresponding to the 5 %, 10 %, 25 %, 50 %, 75 %, 90 % and 95 % percentiles. The coefficients of variation were divided into five classes corresponding to the Jenks Natural Breaks algorithm. The interpolation was performed using the ordinary Kriging method (1 km × 1 km grid). In the classes of interpolated values, * denotes the minimum and maximum value of the point data calculated from the limit of detection.

4.4 Cadmium (Cd)

Cadmium is a metal in group 12 of the periodic table. Although its main minerals (e.g. greenockite) are rare, traces of cadmium can be found in iron-magnesium silicates (e.g. amphibole and biotite), iron oxides (magnetite) and zinc ore minerals (sphalerite) (Tuchschmid, 1995). The geochemical properties and mineralogical occurrence of cadmium are very closely related to those of zinc (Tuchschmid, 1995). These two elements share similar characteristics in the soil and in plant uptake (Chaney, 2010; Khan *et al.*, 2014). These similarities are reflected in the (albeit weak) correlation between the measured cadmium and zinc concentrations (R^2 = 0.65, Chapter 6.1).

Cadmium can be mobile in the soil, especially under oxidising conditions and at a pH below 8. However, the Cd^{2+} ion tends to adsorb to clay minerals and soil organic matter or form complexes with iron and manganese hydroxides (Reimann *et al.*, 2014). Cadmium concentrations in topsoil samples belonging to the limestone group are significantly higher than those in the other groups (Figure 20). This could be due to the geogenic presence of cadmium in limestone (mineralised limestone; Tuchschmid, 1995) or to the increased weathering rate of limestone compared with silicate, which can lead to cadmium accumulation in the soil (Quezada-Hinojosa *et al.*, 2015). Furthermore, cadmium can precipitate with carbonates at pH levels above 8 (Reimann *et al.*, 2014). Limestone weathering can also cause an accumulation of clay minerals, which in turn immobilise released Cd ions through sorption processes. The slightly negative correlation of cadmium concentrations with sand content and at the same time slightly positive correlation with clay content may indicate the sorption of cadmium to clay minerals (R^2 = 0.55, Chapter 6.1). Cadmium is thought to accumulate in soil not only through weathering processes but also through fertiliser application and atmospheric inputs (e.g. coal combustion) (Imseng *et al.*, 2018; Keller & Schulin, 2003; Wiggenhauser *et al.*, 2019). Cadmium concentrations were significantly higher in grassland samples than in other land-use types (Figure 20). However, the study by Bigalke *et al.* (2017) found no significant differences in cadmium concentrations between arable and grassland sites. The authors attributed this to the fact that cadmium accumulation on arable sites caused by the use of mineral phosphate fertilisers is masked by other inputs (farmyard manure, sewage sludge ash and atmospheric deposition) and by the output associated with harvesting and land management.

With a median of 0.24 mg/kg (Table 2), cadmium concentrations in the topsoil are slightly above typical concentrations for soil-forming rocks (0.06–0.23 mg/kg) and above typical, hypothetical concentrations for decarbonised soil overlying limestone (0.3–0.7 mg/kg; Tuchschmid, 1995). In a Europe-wide comparison, the median cadmium concentration in Swiss topsoils is slightly higher than the medians for arable (0.18 mg/kg) and grassland sites (0.20 mg/kg) documented by Reimann *et al.* (2014). Regarding the spatial distribution, cadmium levels are higher in topsoils in the Jura region than in 95 % of the remaining sites and exceed concentrations of 1 mg/kg (Figure 21). These results suggest that cadmium accumulates in topsoils in the Jura presumably due to limestone weathering processes. Cadmium concentrations in the Swiss Plateau are comparatively low.

The tolerance value defined by Eikmann *et al.* (1993) for agricultural land is 2 mg/kg. This value is exceeded at 12 sites.

Element	Symbol	Atomic number	Median	5 %	95 %
Cadmium	Cd	48	0.24 mg/kg	0.07 mg/kg	1.04 mg/kg

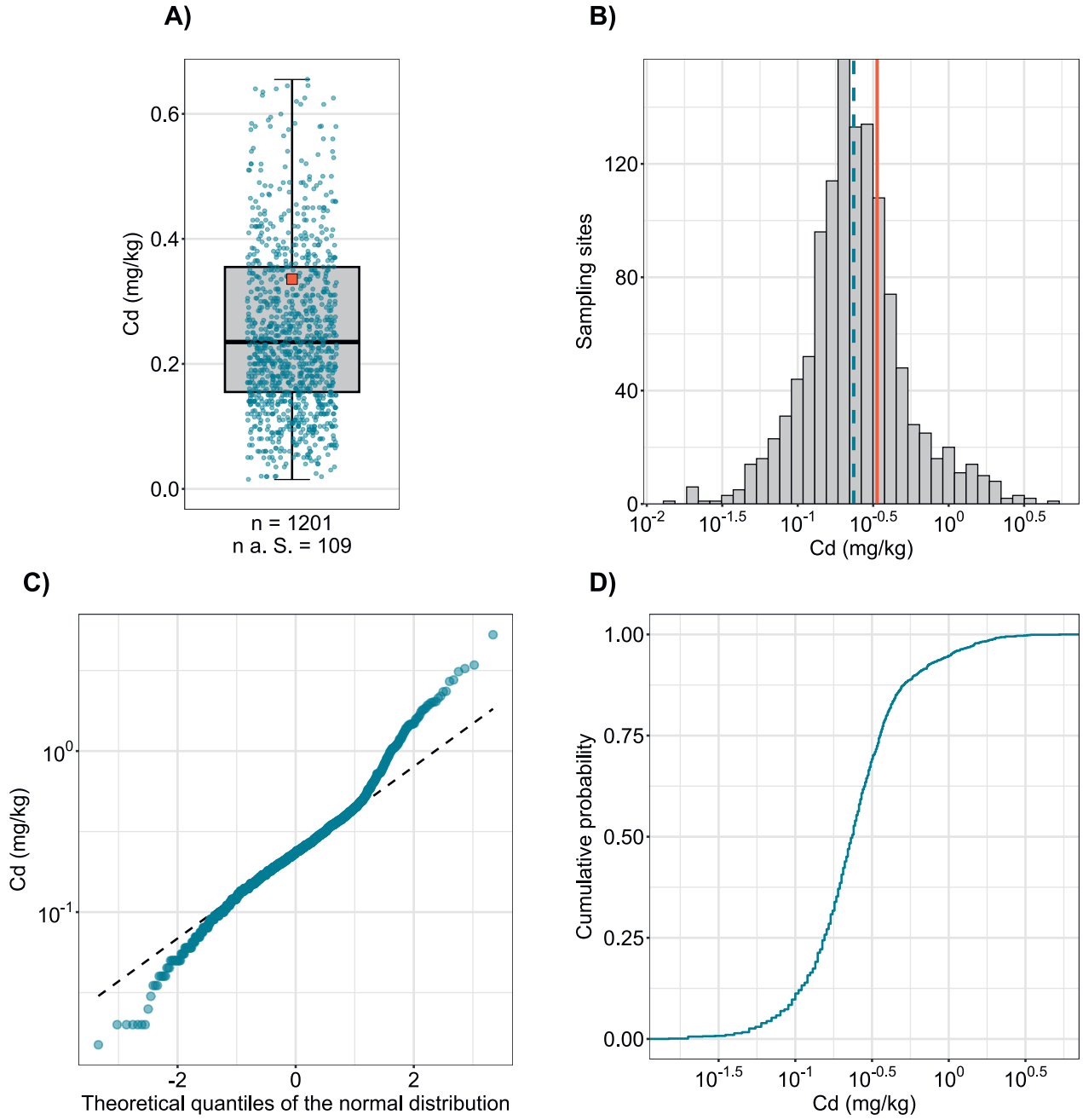

Figure 19 | **Distribution of cadmium concentrations (mg/kg soil). The allocated value is the median of individual samples per site. Measured values below the limit of detection were disregarded. The dataset presented comprises the BDM, NABO and GEMAS sampling sites. n = total number of sites, n a. S. = sites lying outside the axis range or whisker.**

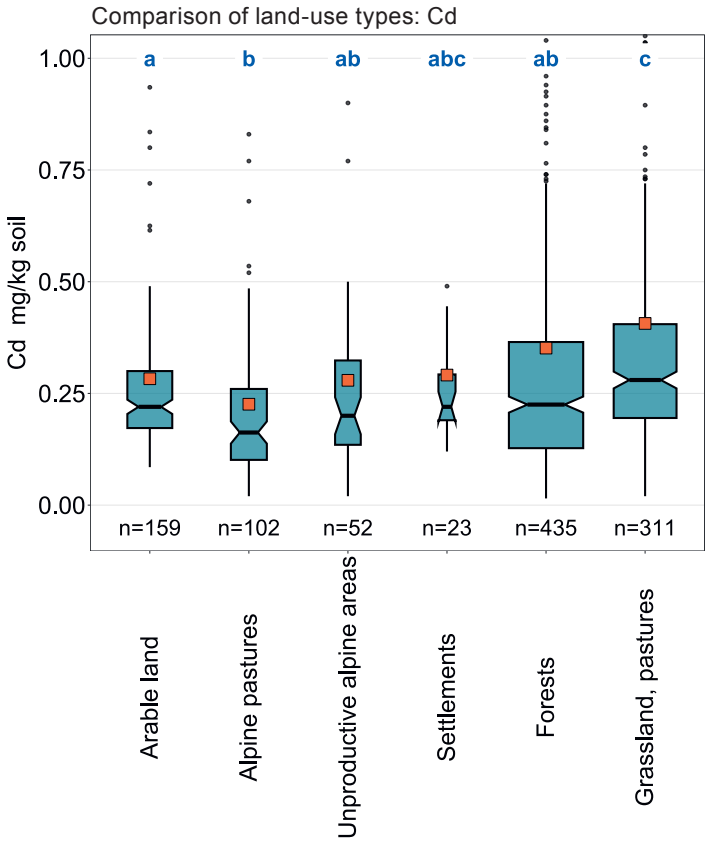

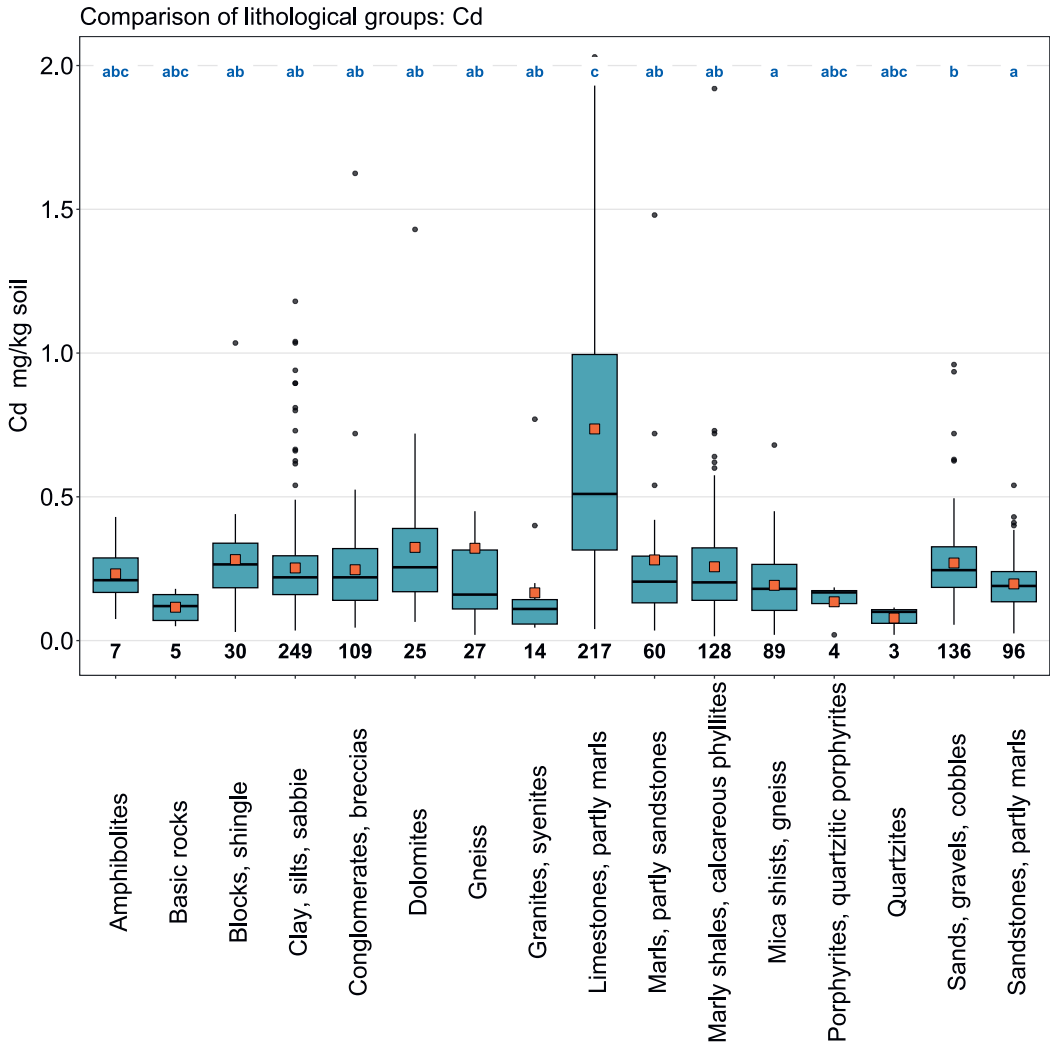

Figure 20 | **Comparison of cadmium concentrations (mg/kg soil) in relation to the Z9 land-use types of the BDM sampling sites (top) and the lithological and petrographic groups in the simplified map of near-surface mineral raw materials of Switzerland (1 : 500 000, swisstopo, bottom). The median of all individual samples per site was included in the data analysis (BDM, NABO and GEMAS datasets). The number of sites per group is indicated beneath the boxes. Letters in blue: significant differences between groups ($p < 0.001$) based on a Wilcoxon rank sum test with P-adjustment using the Benjamini and Hochberg method. Not all outliers are shown. Orange square: arithmetic mean of the data.**

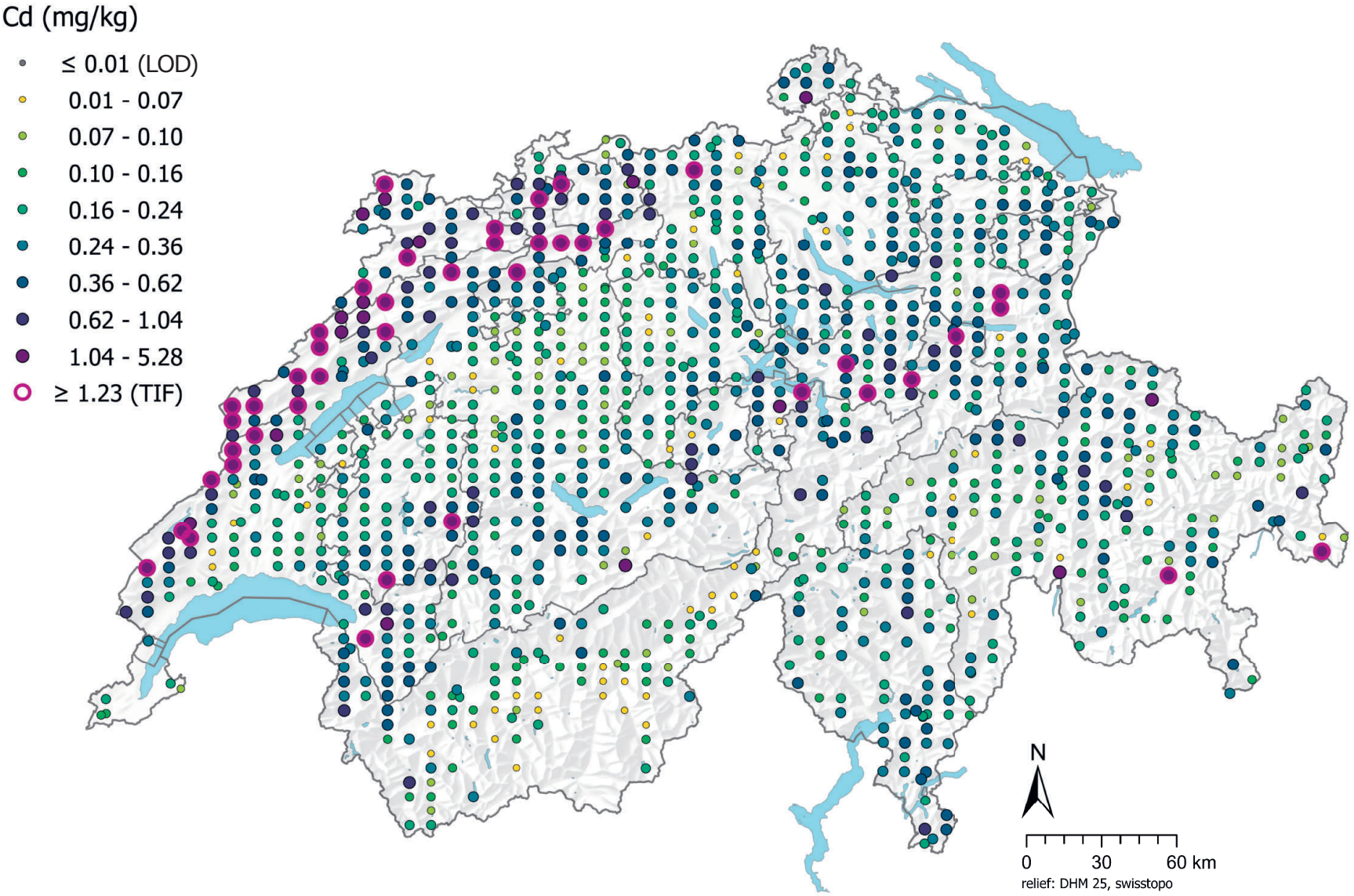

Figure 21 | **Spatial distribution of cadmium concentrations (mg/kg soil) measured at the BDM, NABO and GEMAS sites. The data points show the median of several individual samples per site. 0.5 times the limit of detection (LOD) was assigned to measured values below the LOD. The classes correspond to the 5 %, 10 %, 25 %, 50 %, 75 %, 90 % and 95 % percentiles. TIF: Tukey Inner Fence, outlier as per Reimann *et al.* (2018). LOD: limit of detection**

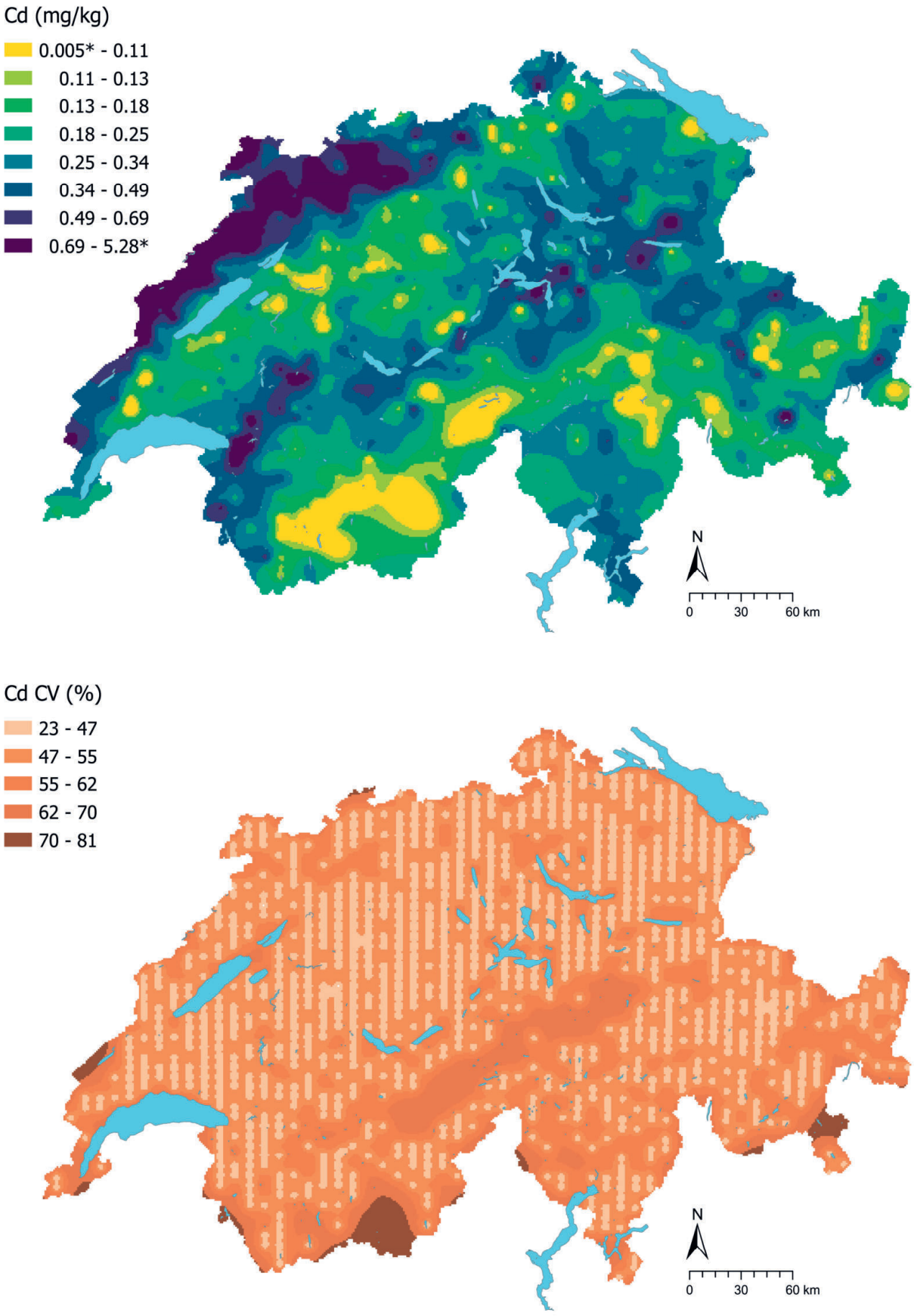

Figure 22 | Interpolated cadmium concentrations (mg/kg soil) at the BDM, NABO and GEMAS sites (top) and coefficient of variation (%) of the interpolated concentrations (bottom). The concentrations were divided into eight classes corresponding to the 5 %, 10 %, 25 %, 50 %, 75 %, 90 % and 95 % percentiles. The coefficients of variation were divided into five classes corresponding to the Jenks Natural Breaks algorithm. The interpolation was performed using the ordinary Kriging method (1 km × 1 km grid). In the classes of interpolated values, * denotes the minimum and maximum value of the point data calculated from the limit of detection.

4.5 Calcium (Ca)

Calcium is an essential alkaline earth metal in group 2 of the periodic table, making up 3.4 % by mass of the geosphere (Earth's crust + atmosphere + hydrosphere) (Fluck & Heumann, 2017). Calcium is the fifth most abundant element in the Earth's crust and a major component of minerals such as calcite ($CaCO_3$), gypsum ($CaSO_4$) and dolomite ($CaMg[CO_3]_2$), which tend to weather more rapidly than other minerals (Reimann *et al.*, 2014). The widespread occurrence of calcium in carbonate rocks is also reflected in its high concentrations in topsoils overlying limestone and dolomite (Figure 24). The heterogeneous group of sand, gravel and pebbles, which represents a mixture of all possible rocks and minerals, also contains high levels of calcium.

The pH-dependent weathering of calcium carbonates and other calcium-bearing minerals releases mainly Ca^{2+} ions, which are bound in the soil in an exchangeable form (Amelung *et al.*, 2018b). Accordingly, calcium concentrations correlate strongly with measured calcium carbonate levels and pH ($R^2 > 0.9$, Chapter 3.4.2), which is also apparent from the grouping of these three parameters in the factor analysis (Chapter 3.4.3). Ca^{2+} performs two important functions in the soil: it helps to stabilise soil aggregates by binding to clay minerals and in soil solution it influences the concentrations of trace elements (Amelung *et al.*, 2018b; Reimann *et al.*, 2014). Calcium concentrations correlate weakly with cadmium concentrations ($R^2 = 0.54$, Chapter 6.1). This is possibly due to limestone weathering processes and the resulting co-accumulation of cadmium and calcium in the soil on the one hand, and to exchange between Ca^{2+} and Cd^{2+} cations at the sorption surfaces in the soil or precipitation of carbonates on the other. As a component of calcium carbonate, calcium also plays an important role in the soil buffering mechanism. Thus, farmers spread lime on their land to counter soil acidification. Calcium is also essential for plant growth and influences cold tolerance, stress tolerance, root distribution and leaf shape (Amelung *et al.*, 2018b). In humans, calcium is integral to bone formation and the functioning of the nervous system (Reimann *et al.*, 2014). However, in addition to pH, it is the calcium concentration in the soil solution rather than the total content that is key to the assessment of calcium deficiencies in the soil (Amelung *et al.*, 2018).

The measured calcium concentrations have a bimodal distribution, which could indicate that two different main processes regulate its depletion and accumulation in the topsoil (Figure 23). One distribution may describe the natural distribution of element concentrations based on the calcareous parent material and soil-forming processes, while a second distribution may represent overlying anthropogenic influences, for example the application of lime and fertiliser to arable soils (Amelung *et al.*, 2018b). Furthermore, settlement areas have significantly higher calcium concentrations than other land-use types, suggesting anthropogenic influences (Figure 24). In contrast, calcium concentrations at forest sites and alpine pastures tend to be low, possibly indicating soil acidification in some places.

Comparatively high calcium concentrations recorded in the eastern Swiss Plateau, the Jura and the Randen Mountains (Schaffhausen, SH) were attributed to the carbonate-bearing parent material in these areas (Figure 25). Low concentrations were recorded in the southern Alps. The values measured for the geochemical atlas lie within the typical range for soils (1–12 g/kg; Amelung *et al.*, 2018).

Element	Symbol	Atomic number	Median	5 %	95 %
Calcium	Ca	20	4.2 g/kg	0.7 g/kg	100.9 g/kg

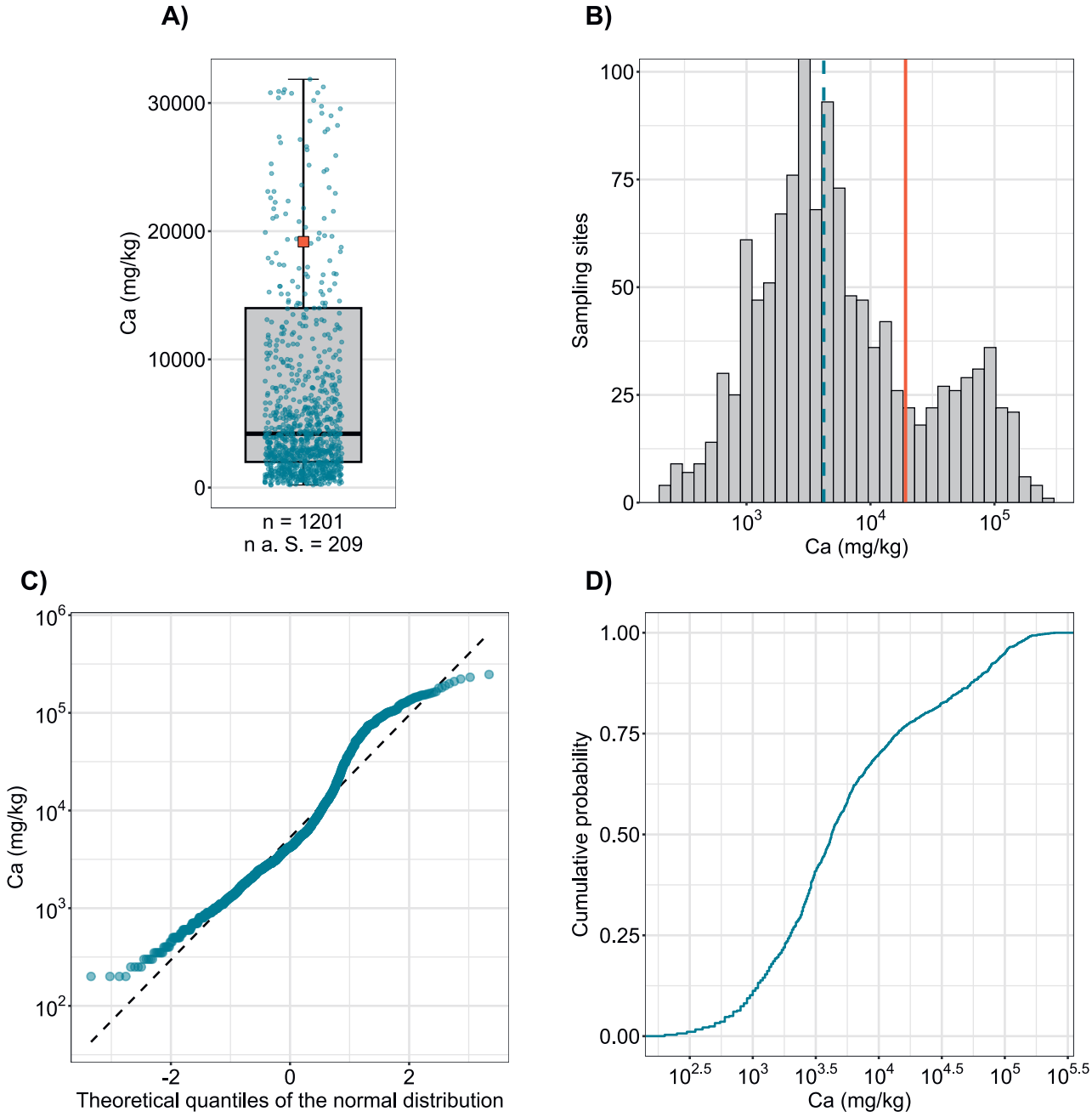

Figure 23 | Distribution of calcium concentrations (mg/kg soil). The allocated value is the median of individual samples per site. Measured values below the limit of detection were disregarded. The dataset presented comprises the BDM, NABO and GEMAS sampling sites. n = total number of sites, n a. S. = sites lying outside the axis range or whisker.

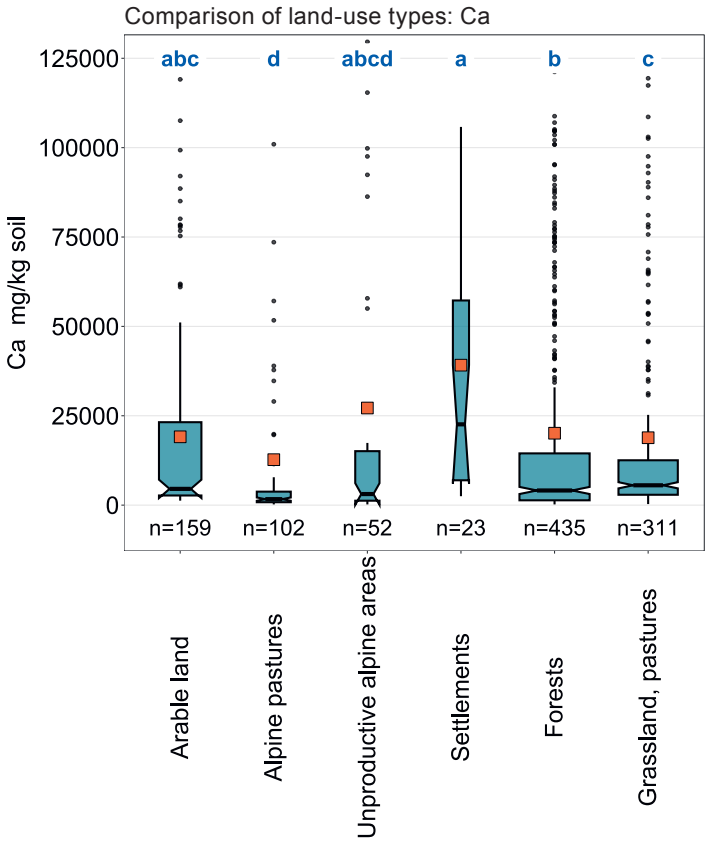

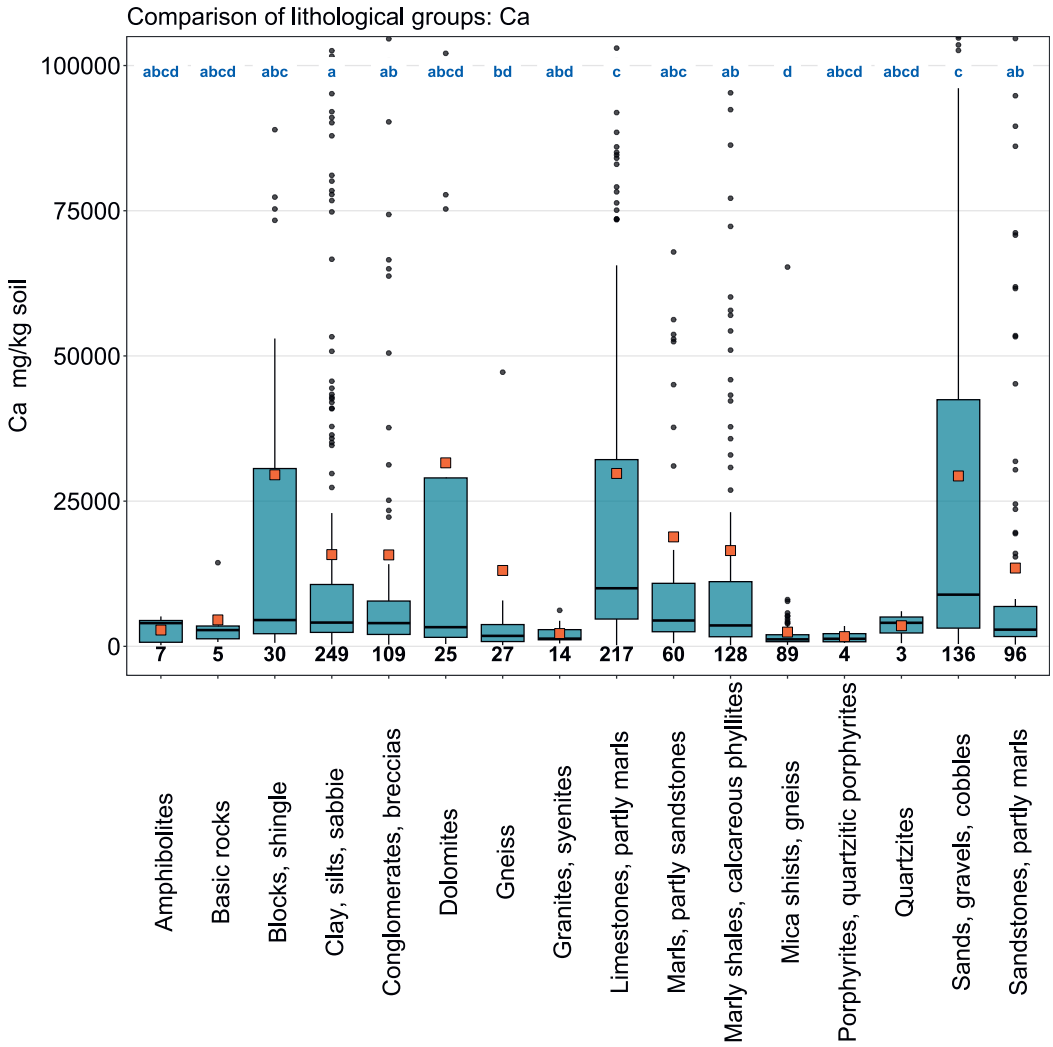

Figure 24 | **Comparison of calcium concentrations (mg/kg soil) in relation to the Z9 land-use types of the BDM sampling sites (top) and the lithological and petrographic groups in the simplified map of near-surface mineral raw materials of Switzerland (1 : 500 000, swisstopo, bottom). The median of all individual samples per site was included in the data analysis (BDM, NABO and GEMAS datasets). The number of sites per group is indicated beneath the boxes. Letters in blue: significant differences between groups ($p < 0.001$) based on a Wilcoxon rank sum test with P-adjustment using the Benjamini and Hochberg method. Not all outliers are shown. Orange square: arithmetic mean of the data.**

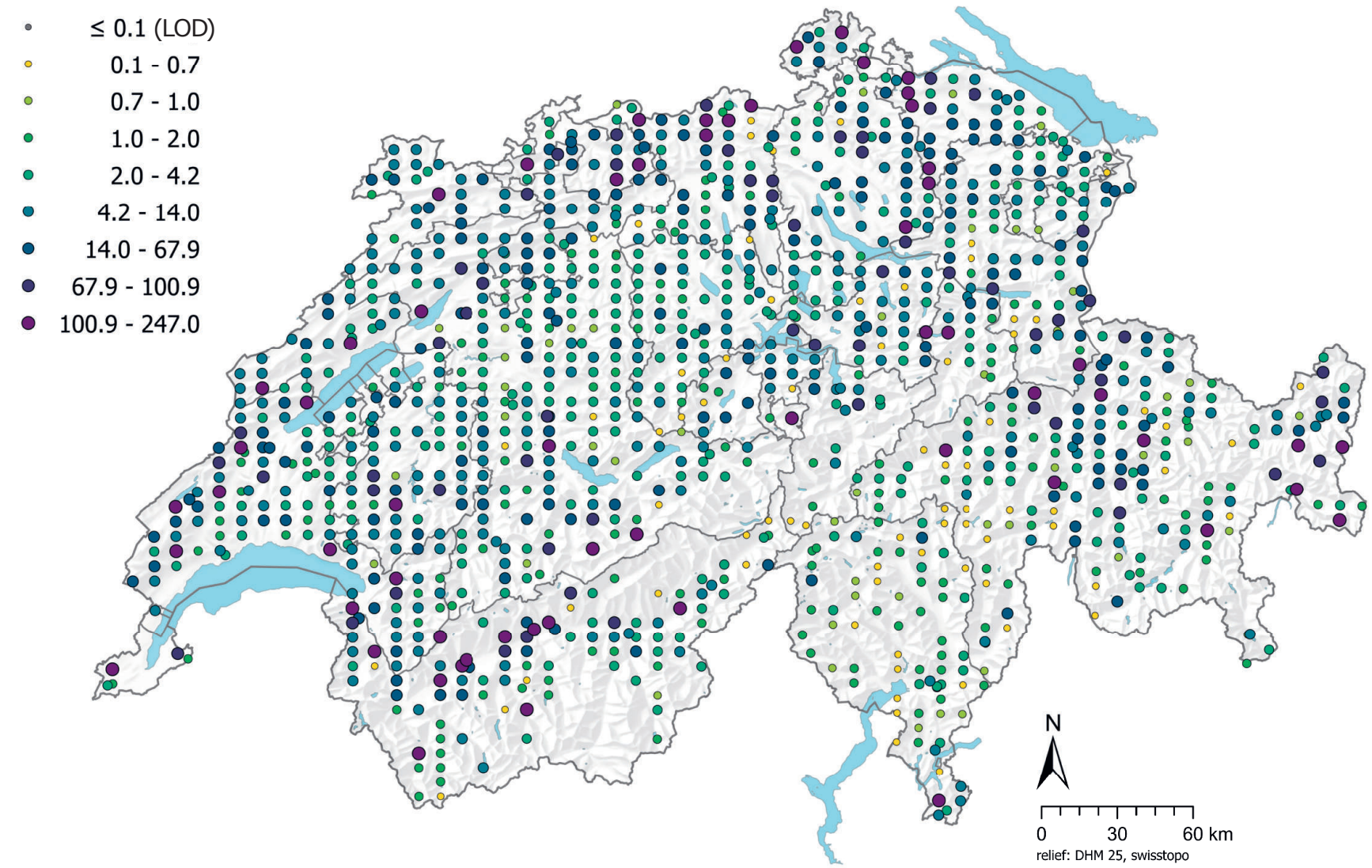

Figure 25 | Spatial distribution of calcium concentrations (mg/kg soil) measured at the BDM, NABO and GEMAS sites. The data points show the median of several individual samples per site. 0.5 times the limit of detection (LOD) was assigned to measured values below the LOD. The classes correspond to the 5 %, 10 %, 25 %, 50 %, 75 %, 90 % and 95 % percentiles. TIF: Tukey Inner Fence, outlier as per Reimann *et al.* (2018). LOD: limit of detection

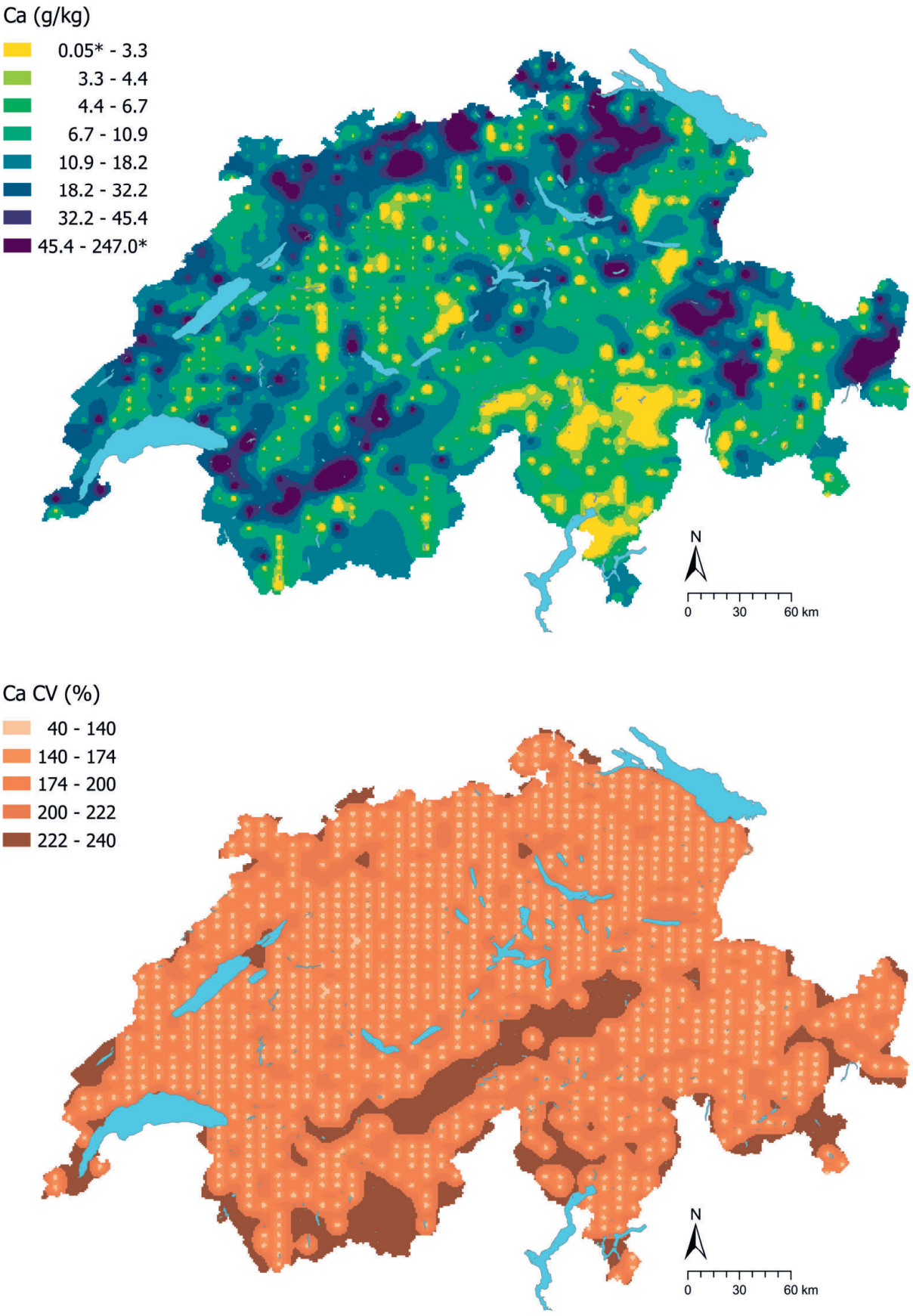

Figure 26 | Interpolated calcium concentrations (mg/kg soil) at the BDM, NABO and GEMAS sites (top) and coefficient of variation (%) of the interpolated concentrations (bottom). The concentrations were divided into eight classes corresponding to the 5 %, 10 %, 25 %, 50 %, 75 %, 90 % and 95 % percentiles. The coefficients of variation were divided into five classes corresponding to the Jenks Natural Breaks algorithm. The interpolation was performed using the ordinary Kriging method (1 km × 1 km grid). In the classes of interpolated values, * denotes the minimum and maximum value of the point data calculated from the limit of detection.

4.6 Chromium (Cr)

Chromium is a group 6 metal and is essential in the Cr(III) oxidation state for some living organisms, including humans. However, it can be toxic even at low concentrations. The Cr(VI) form in particular is highly carcinogenic (Ma & Hooda, 2010; Zayed & Terry, 2003). According to Tuchschmid (1995), chromium occurs exclusively in iron- and aluminium-bearing silicates (e.g. pyroxene, amphibole and biotite) and oxides (e.g. magnetite), with basic and ultrabasic rocks containing the highest concentrations. Similarly, the highest chromium concentrations were measured in the topsoil of sites with underlying basic rocks (Figure 28). However, these differences in concentration are not statistically significant due to the low number of sites in this group. Tuchschmid (1995) documented chromium concentrations exceeding 75 mg/kg in over 25 % of the rock samples investigated, especially in ultrabasic to basic magnetites and metamorphites and in pelitic sedimentary rocks and sediments. According to Tuchschmid (1995), rocks containing high levels of chromium can be found throughout Switzerland. Furthermore, the geogenic occurrence of chromium is strongly associated with cobalt and nickel concentrations since all three elements are closely related to iron and magnesium levels in the rocks. In fact, measured chromium concentrations correlate with these elements (nickel: $R^2 = 0.72$) and with vanadium concentrations ($R^2 = 0.77$, Chapter 6.1). This could be because both elements are associated with the precipitation of iron oxides in soil (Amelung *et al.*, 2018a), or because both elements occur mainly in mafic minerals (Chapter 6.1.).

Chromium is used predominantly for steel production, electroplating and in wood preservatives (Reimann *et al.*, 2014). Chromium enters the environment and soil through point sources (e.g. contamination from electroplating plants) and diffusely through atmospheric deposition, sewage sludge, mineral fertilisers, farmyard manure (e.g. poultry manure) and lime (Ma & Hooda, 2010; Nicholson *et al.*, 2003).

Under alkaline soil conditions (pH above 5), Cr(III) is mainly precipitated as poorly soluble chromium hydroxide or is adsorbed to surfaces, limiting its bioavailability (Ma & Hooda, 2010). In contrast, Cr(VI) is strongly water-soluble and mobile, although in soil it can rapidly be reduced to Cr(III), depending on pH and redox conditions (Reimann *et al.*, 2014).

In this dataset, high chromium concentrations were measured in the Jura and the western Swiss Plateau (Figure 29). Topsoils in the canton of Grisons have a particularly heterogeneous chromium distribution with individual hotspots which can be classified as outliers based on the TIF method.

Significantly higher chromium concentrations were measured in soils at arable and grassland sites than at other land-use types (Figure 28). From 1985 to 2009 virtually no changes in chromium concentrations were reported in the topsoils of the NABO sampling network (Gubler *et al.*, 2015). The authors concluded that chromium concentrations in the soil, together with those of nickel and cobalt, are determined by geological conditions rather than by atmospheric and agricultural inputs. Nevertheless, historic anthropogenic inputs cannot be ruled out.

The tolerance value of 200 mg Cr/kg (Eikmann *et al.*, 1993) for agricultural land is exceeded at nine sites. However, since only total concentrations were analysed in the digests, it is not known whether chromium is present in the soil in the form of essential Cr(III) or toxic Cr(VI).

Element	Symbol	Atomic number	Median	5 %	95 %
Chromium	Cr	24	30.3 mg/kg	9.8 mg/kg	62.8 mg/kg

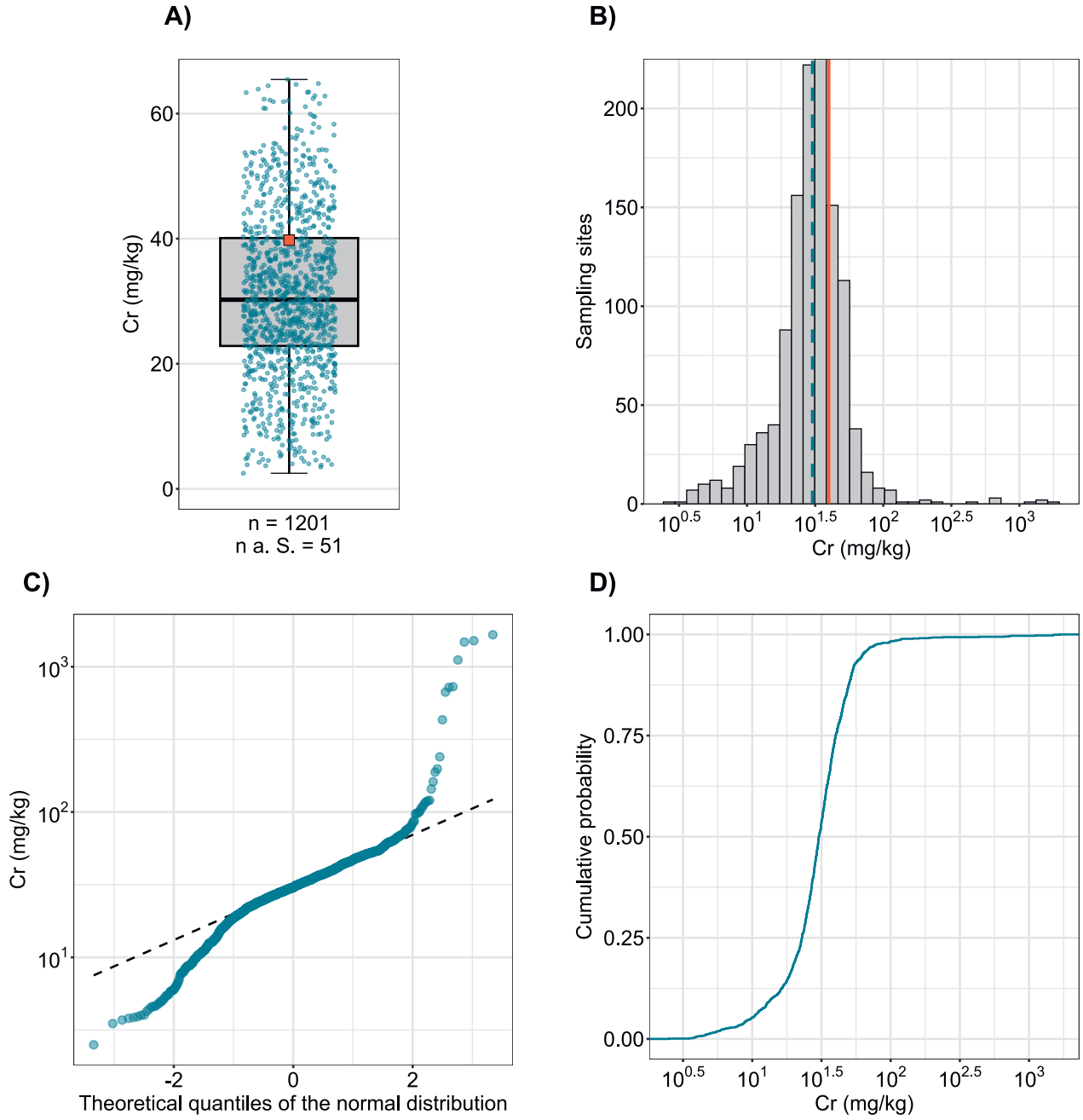

Figure 27 | **Distribution of chromium concentrations (mg/kg soil). The allocated value is the median of individual samples per site. The dataset presented comprises the BDM, NABO and GEMAS sampling sites. n = total number of sites, n a. S. = sites lying outside the axis range or whisker.**

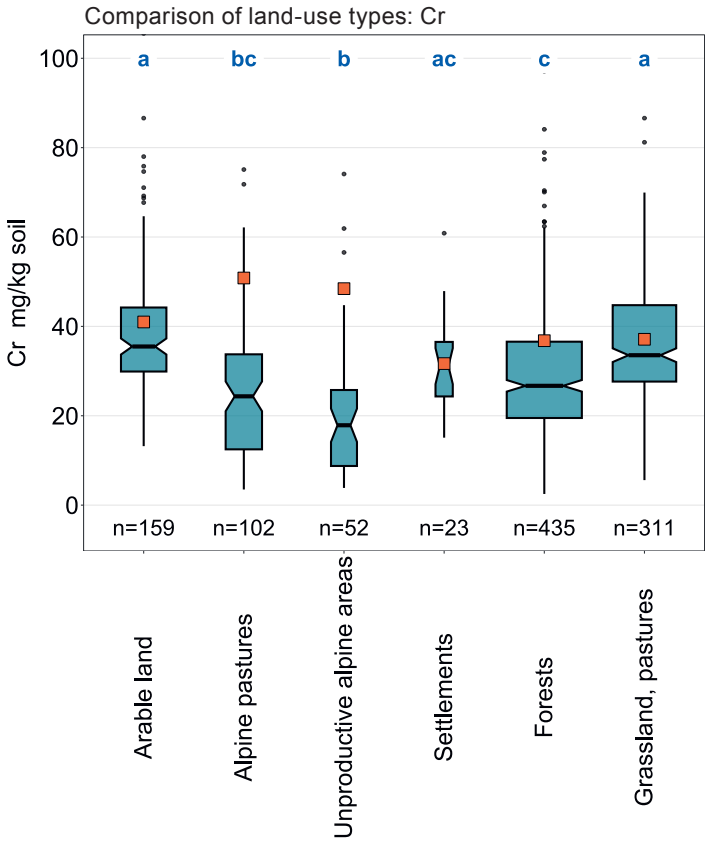

Figure 28 | **Comparison of chromium concentrations (mg/kg soil) in relation to the Z9 land-use types of the BDM sampling sites (top) and the lithological and petrographic groups in the simplified map of near-surface mineral raw materials of Switzerland (1 : 500 000, swisstopo, bottom). The median of all individual samples per site was included in the data analysis (BDM, NABO and GEMAS datasets). The number of sites per group is indicated beneath the boxes. Letters in blue: significant differences between groups ($p < 0.001$) based on a Wilcoxon rank sum test with P-adjustment using the Benjamini and Hochberg method. Not all outliers are shown. Orange square: Arithmetic mean of the data.**

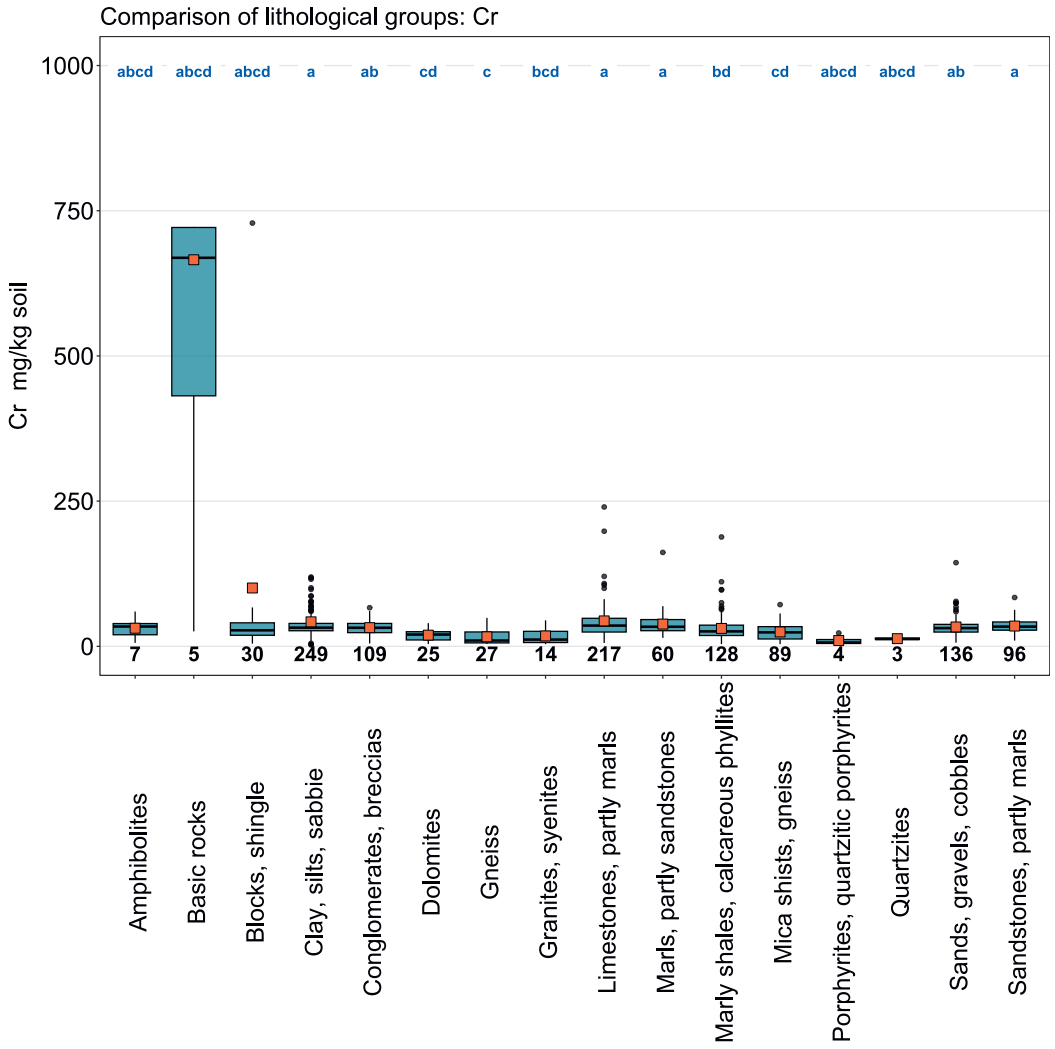

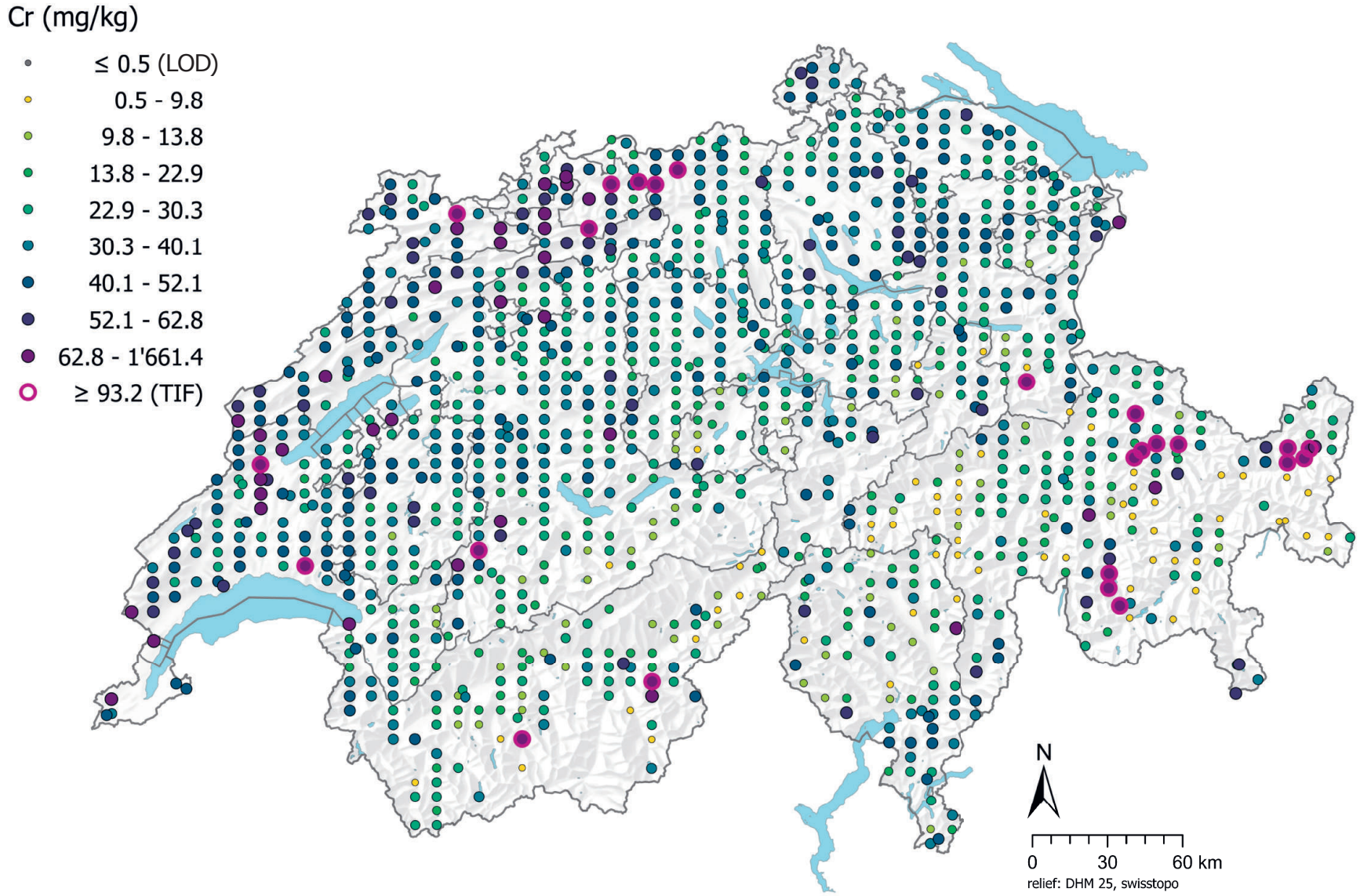

Figure 29 | **Spatial distribution of chromium concentrations (mg/kg soil) measured at the BDM, NABO and GEMAS sites. The data points show the median of several individual samples per site. The classes correspond to the 5 %, 10 %, 25 %, 50 %, 75 %, 90 % and 95 % percentiles. TIF: Tukey Inner Fence, outlier as per Reimann *et al.* (2018). LOD: limit of detection**

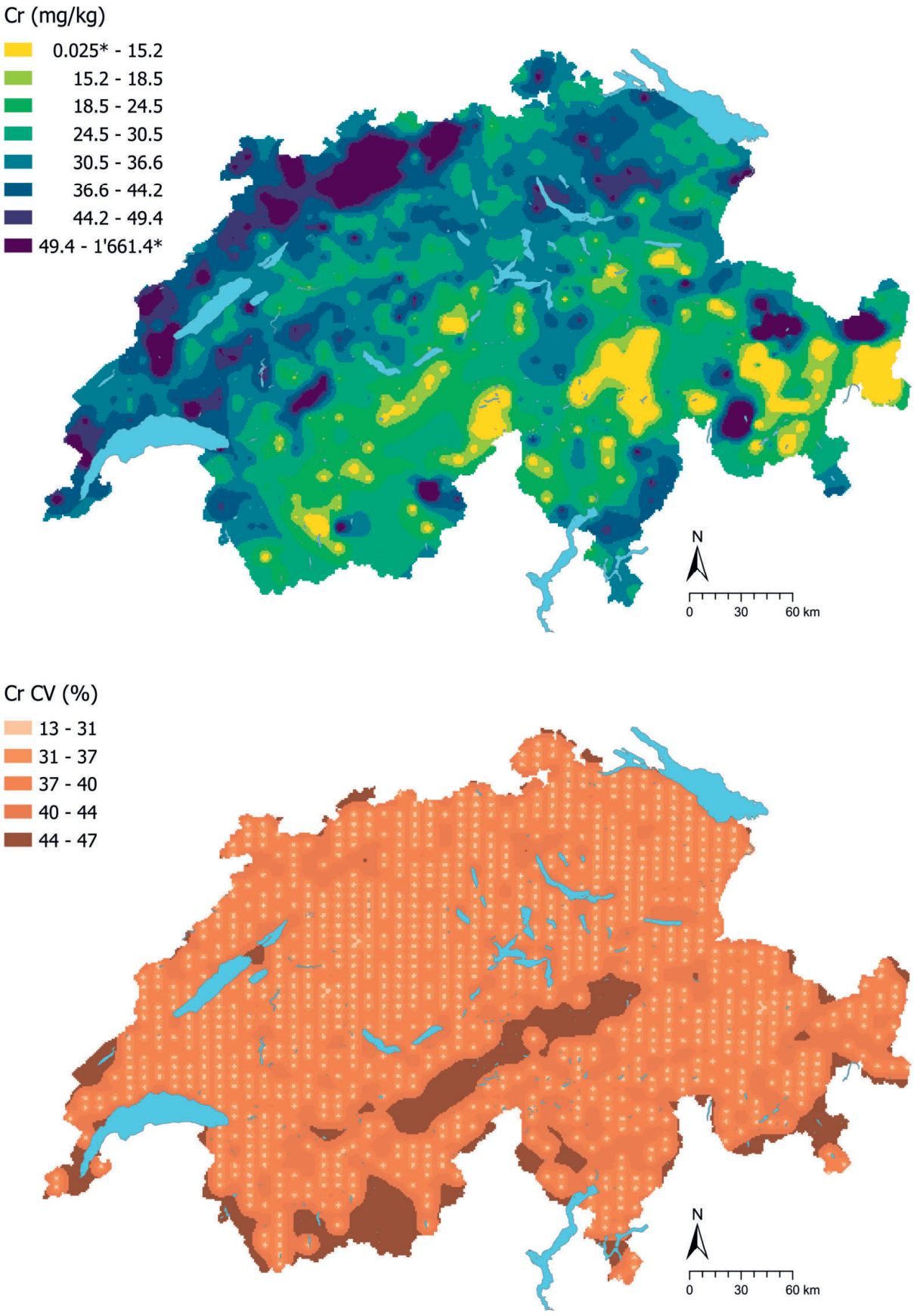

Figure 30 | Interpolated chromium concentrations (mg/kg soil) at the BDM, NABO and GEMAS sites (top) and coefficient of variation (%) of the interpolated concentrations (bottom). The concentrations were divided into eight classes corresponding to the 5 %, 10 %, 25 %, 50 %, 75 %, 90 % and 95 % percentiles. The coefficients of variation were divided into five classes corresponding to the Jenks Natural Breaks algorithm. The interpolation was performed using the ordinary Kriging method (1 km × 1 km grid). In the classes of interpolated values, * denotes the minimum and maximum value of the point data calculated from the limit of detection.

4.7 Cobalt (Co)

Cobalt is a metal in group 9 of the periodic table. Its main minerals, smaltite ([Co, Fe, Ni]As_2) and cobaltite (CoAsS), are very rare (Reimann *et al.*, 2014). Because of the siderophilic characteristics of cobalt, it commonly forms minerals containing arsenic, sulphur and/or selenium (Kabata-Pendias, 2011). Cobalt predominantly occurs in iron- and magnesium-rich rocks – mainly iron-rich silicates, e.g. olivine, pyroxene and biotite – and in oxides, e.g. magnetite (Tuchschmid, 1995). Thus basic and ultrabasic rocks in the Alps and their metamorphites, e.g. serpentinite, and the bole clays in the Jura Mountains can contain extremely high concentrations (Tuchschmid, 1995). Like chromium, cobalt is very closely related to nickel in geochemical terms, which may be reflected in their positive correlation in the topsoil samples and grouping in the factor analysis (Chapter 3.4.2 and 3.4.3), and also in the clearly – although not significantly – elevated concentrations at sites assigned to the basic rock group (Figure 32).

Cobalt's main use is in batteries: together with lithium and graphite, it is a key component of electric vehicle batteries (Gulley, 2022). This is one reason why global mining of cobalt has increased almost tenfold since 1995 (22 100 million tonnes). The Democratic Republic of Congo produces around 70 % of the world's cobalt (Gulley, 2022; Ma & Hooda, 2010). Cobalt is also used in alloys, in the synthesis of chemical compounds, in fertilisers and in pharmaceuticals (Kabata-Pendias, 2011). Cobalt emissions are produced during copper and nickel smelting and refining, coal combustion and steel processing (Reimann *et al.*, 2014).

As pH rises, the Co(II) form of cobalt becomes increasingly immobile in soil due to increased sorption to soil components (Amelung *et al.*, 2018b; Ma & Hooda, 2010). According to Ma & Hooda (2010), up to 79 % of cobalt in soil is associated with iron and manganese oxyhydroxides, since Co(II) oxidises to the less soluble Co(III) at their surfaces and is subsequently incorporated or precipitated. Cobalt concentrations measured in the topsoil samples correlate strongly with iron concentrations (R^2 = 0.84, Chapter 6.1), which can be attributed to the geogenic origin of cobalt in iron-bearing rocks on the one hand and its association with iron oxyhydroxides in the soil on the other.

Cobalt concentrations in the soil are typically between 5 and 15 mg/kg (Amelung *et al.*, 2018b; Ma & Hooda, 2010), with concentrations measured in Swiss topsoils being within this range (Figure 31). Sites with comparatively high cobalt concentrations occur sporadically in Grisons and the Jura (Figure 33). Sites with chromium and nickel concentrations defined as TIF outliers are located in these areas as well (Figure 29 and Figure 61), which could indicate a predominantly geogenic origin. Grassland sites exhibit significantly higher cobalt concentrations than forest sites (Figure 32), possibly due to the higher pH of grassland compared with forest sites, which causes an increase in the sorption of cobalt to oxides.

As a major constituent of vitamin B_{12}, cobalt is an essential element for humans and animals (Amelung *et al.*, 2018b). However, high cobalt concentrations can be toxic to both plants and humans (Ma & Hooda, 2010). The tolerance value for cobalt on agricultural land is 200 mg/kg (Lühr *et al.*, 1996). None of the sampling sites exceed this value.

Element	Symbol	Atomic number	Median	5 %	95 %
Cobalt	Co	27	8.6 mg/kg	2.6 mg/kg	17.9 mg/kg

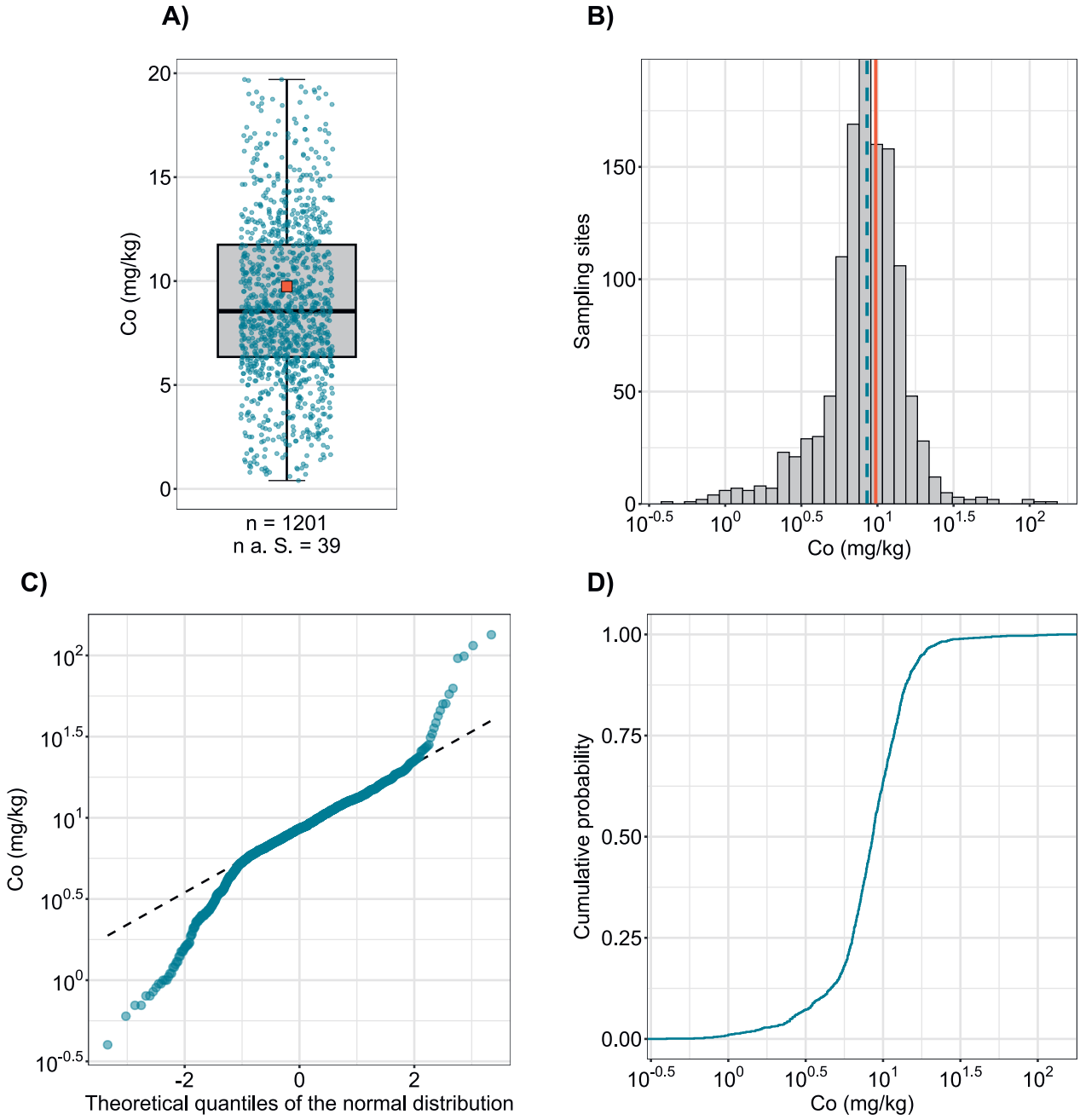

Figure 31 | **Distribution of cobalt concentrations (mg/kg soil). Measured values below the limit of detection were disregarded. The dataset presented comprises the BDM, NABO and GEMAS sampling sites. n = total number of sites, n a. S. = sites lying outside the axis range or whisker.**

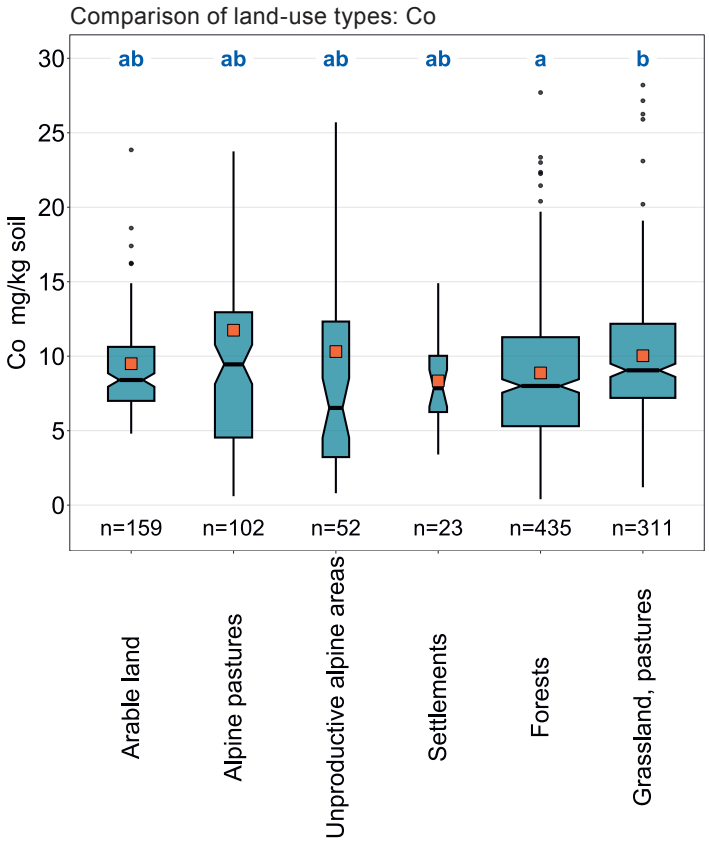

Figure 32 | **Comparison of cobalt concentrations (mg/kg soil) in relation to the Z9 land-use types of the BDM sampling sites (top) and the lithological and petrographic groups in the simplified map of near-surface mineral raw materials of Switzerland (1 : 500 000, swisstopo, bottom). The median of all individual samples per site was included in the data analysis (BDM, NABO and GEMAS datasets). The number of sites per group is indicated beneath the boxes. Letters in blue: significant differences between groups ($p < 0.001$) based on a Wilcoxon rank sum test with P-adjustment using the Benjamini and Hochberg method. Not all outliers are shown. Orange square: arithmetic mean of the data.**

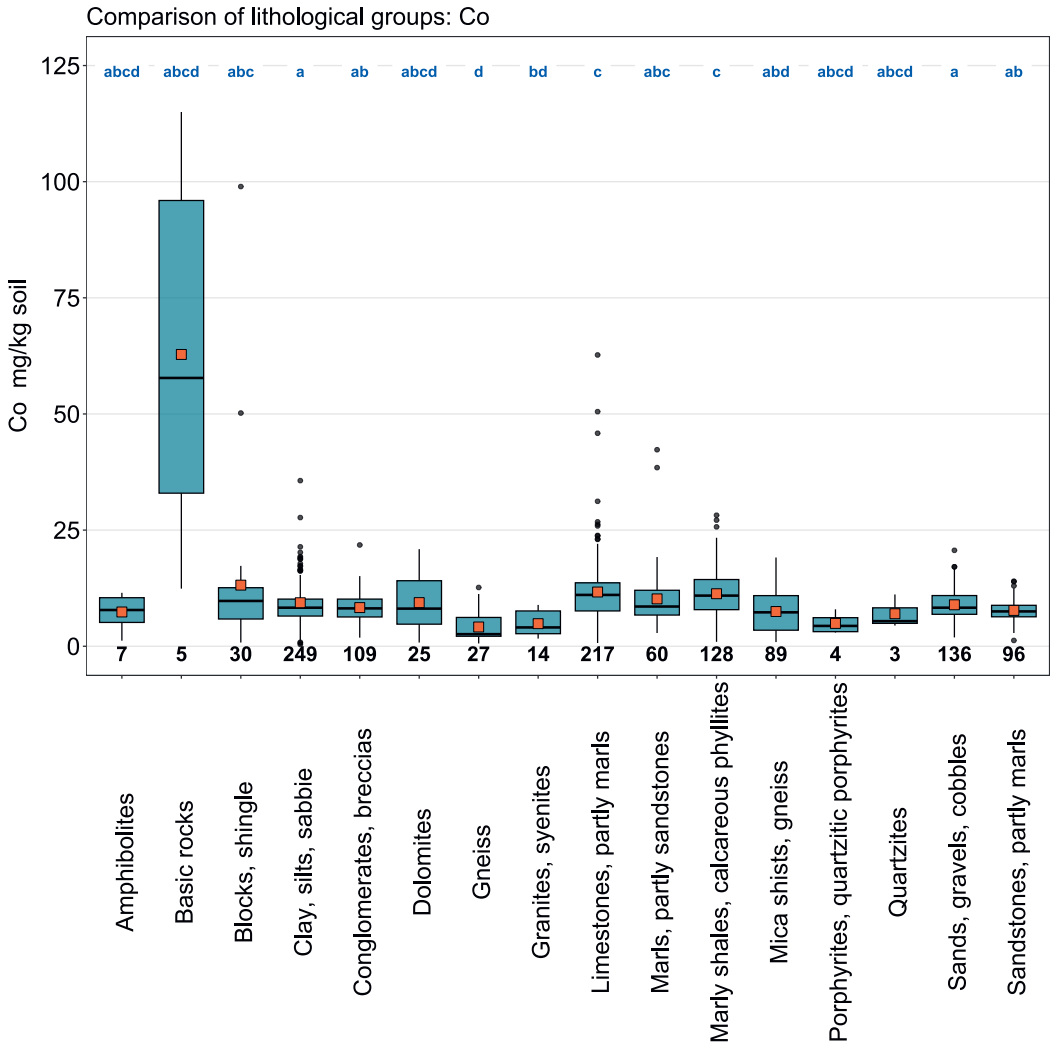

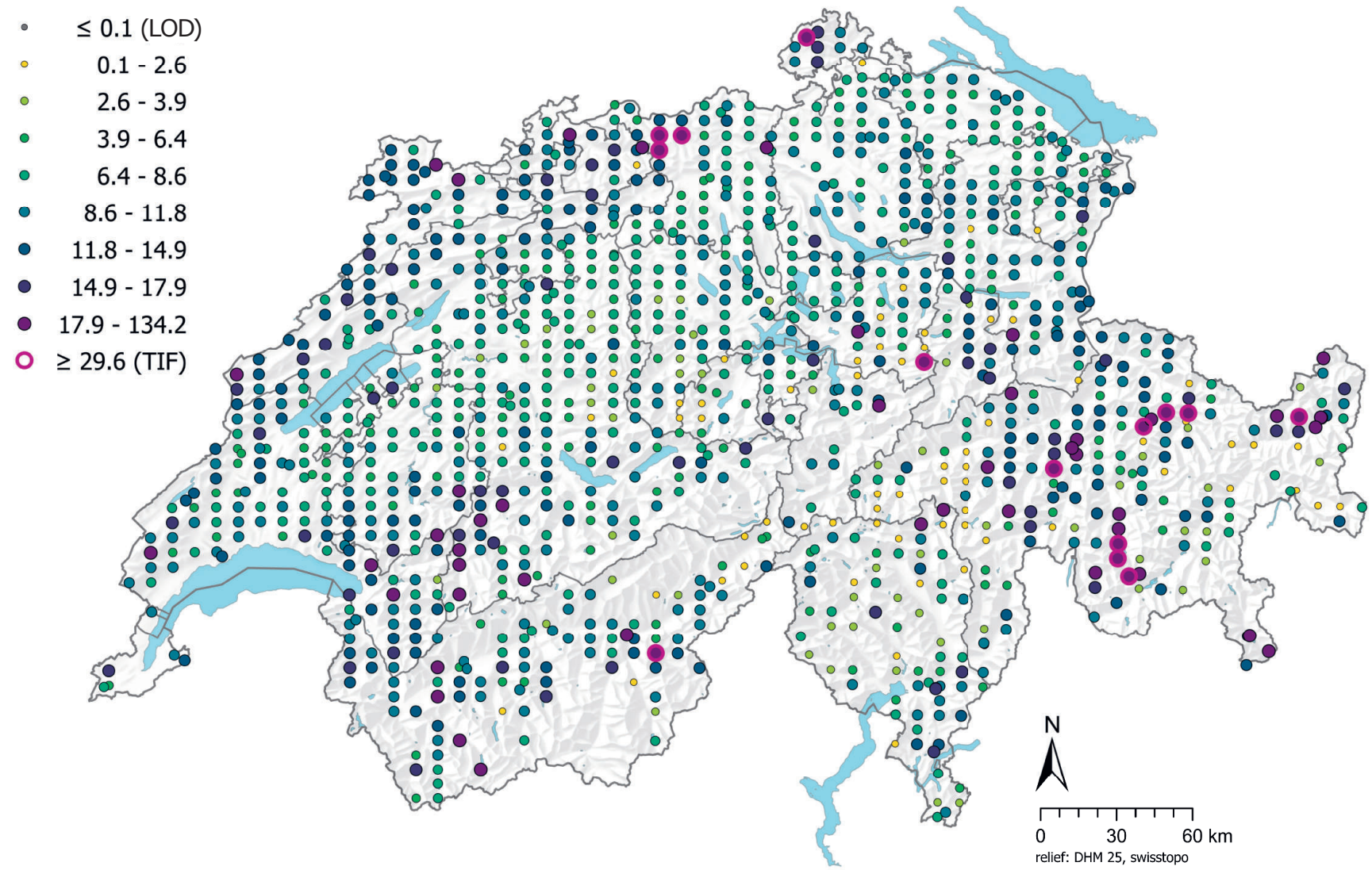

Figure 33 | **Spatial distribution of cobalt concentrations (mg/kg soil) measured at the BDM, NABO and GEMAS sites. The data points show the median of several individual samples per site. The classes correspond to the 5 %, 10 %, 25 %, 50 %, 75 %, 90 % and 95 % percentiles. TIF: Tukey Inner Fence, outlier as per Reimann *et al.* (2018). LOD: limit of detection**

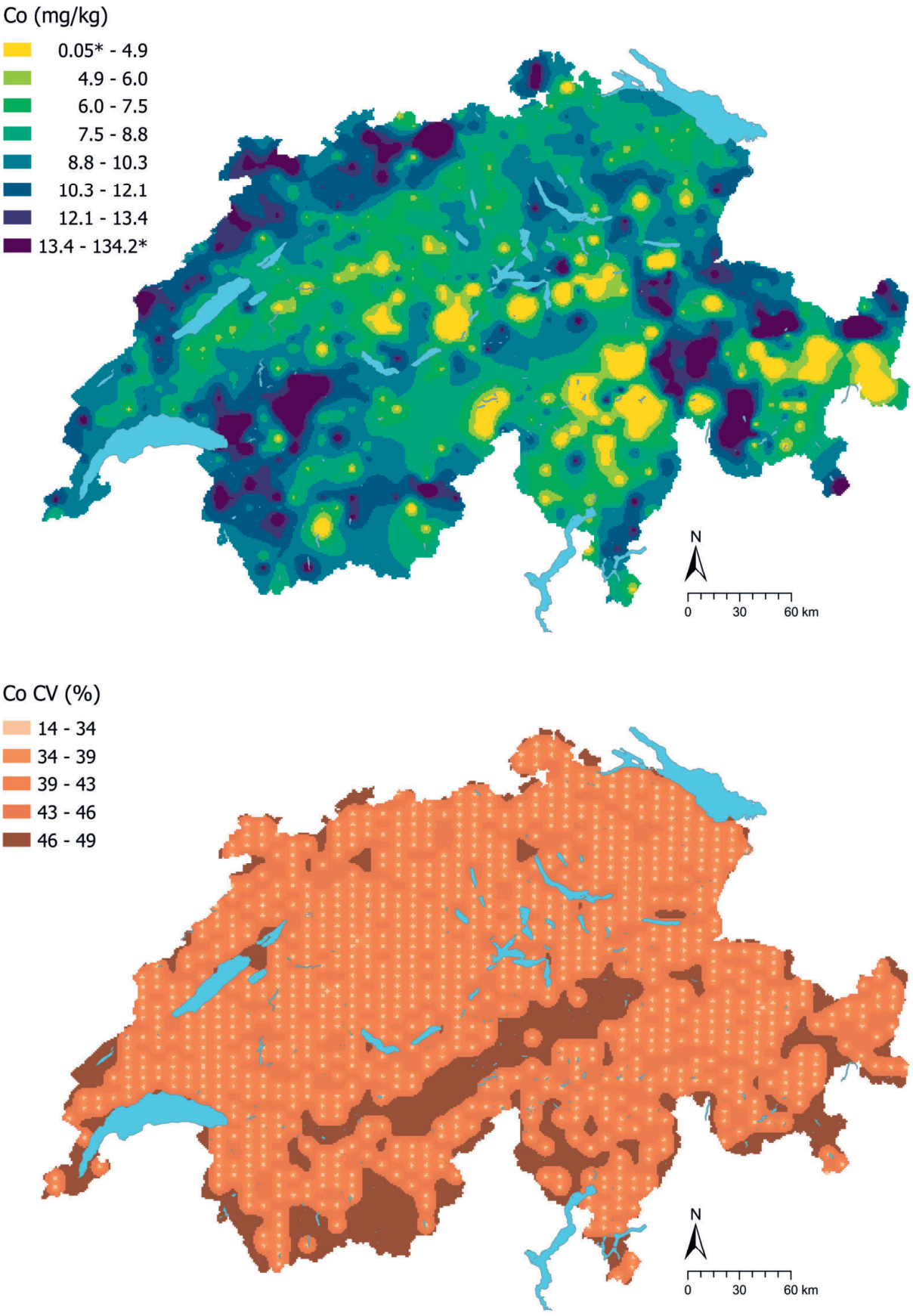

Figure 34 | Interpolated cobalt concentrations (mg/kg soil) at the BDM, NABO and GEMAS sites (top) and coefficient of variation (%) of the interpolated concentrations (bottom). The concentrations were divided into eight classes corresponding to the 5 %, 10 %, 25 %, 50 %, 75 %, 90 % and 95 % percentiles. The coefficients of variation were divided into five classes corresponding to the Jenks Natural Breaks algorithm. The interpolation was performed using the ordinary Kriging method (1 km × 1 km grid). In the classes of interpolated values, * denotes the minimum and maximum value of the point data calculated from the limit of detection.

4.8 Iron (Fe)

Iron is an essential metal in group 8 of the periodic table. The two cations Fe^{2+} and Fe^{3+} constitute approximately 5.1 % by mass of the Earth's crust, making iron the fourth most abundant element after aluminium (Amelung *et al.*, 2018a). The main minerals of Fe are iron oxides such as magnetite (Fe_3O_4), haematite (Fe_2O_3) and goethite (FeO[OH]), and pyrite (FeS_2). Iron also occurs in minerals such as olivine, pyroxene, amphibole and mica (Reimann *et al.*, 2014). Mafic and ultramafic rocks contain the highest concentrations of iron: 70–90 g/kg (Reimann *et al.*, 2014). Bole clays, mainly non-calcareous kaolinitic clays produced by weathering of Jurassic strata, contain 4–18 % iron oxide (FGS, 2023b). These embedded iron ore concretions (bean ores) were formerly mined to extract iron. In Switzerland, iron ore mining is documented mainly in the north and at various sites in the cantons of Grisons and Ticino (FGS, 2023b). Comparatively high concentrations of iron were measured in the topsoils in these areas (Figure 37). In contrast, iron concentrations in the topsoils of the Swiss Plateau tend to be low.

The use of iron dates back to the Iron Age, beginning in the Middle East around 1200 BC with its extraction and processing. Iron production in Switzerland started in the 8th century BC (Drack, 1968). In 2022, 1.6 billion tonnes of iron were mined worldwide, predominantly destined for the iron and steel industry (USGS, 2023).

The iron concentration and its form in the soil are largely determined by pH and prevailing redox conditions. During weathering of iron-bearing minerals, Fe^{2+} is oxidised to Fe^{3+} and then hydrolysed to reddish brown iron oxides (e.g. goethite, haematite and ferrihydrite) (Amelung *et al.*, 2018a). Oxyanions, e.g. phosphate or selenite, and cations of heavy metals and trace elements (e.g. Cr^{3+}, Hg^{2+}, Pb^{2+}) can form complexes at the surfaces of iron oxides, reducing their mobility in the soil (Amelung *et al.*, 2018c). Although iron oxides are not readily soluble, if soil conditions become anaerobic, for example due to waterlogging, iron oxides are reduced to Fe^{2+} by microbial oxidation of soil organic matter. This process releases complexed elements and other chemical compounds in addition to Fe^{2+}. In soil science, the reduction of iron oxides to Fe^{2+} under the influence of waterlogging, which causes the colour of the soil to change from reddish brown to grey, is known as gleying. When dissolved Fe^{2+} encounters aerobic conditions, it precipitates back to iron oxide, giving rise to the typical rust spots.

Iron is an important micronutrient for plants as well as humans and animals. The measured concentrations, with a median of 21.8 g/kg (Table 2), lie within the range of documented concentrations in the soil (2–50 g/kg; Amelung *et al.*, 2018). However, it is worth noting that iron deficiency in plants can also occur on calcium carbonate-containing soils with high iron oxide contents due to immobilisation processes (Amelung *et al.*, 2018a). Grassland sites were found to have significantly higher iron concentrations than forest sites (Figure 36). This could indicate increased solubility and thus depletion of iron in forests compared with grasslands, although iron concentrations do not correlate with pH (Chapters 5.1 and 6.1).

Element	Symbol	Atomic number	Median	5 %	95 %
Iron	Fe	26	21.8 g/kg	11.4 g/kg	38.3 g/kg

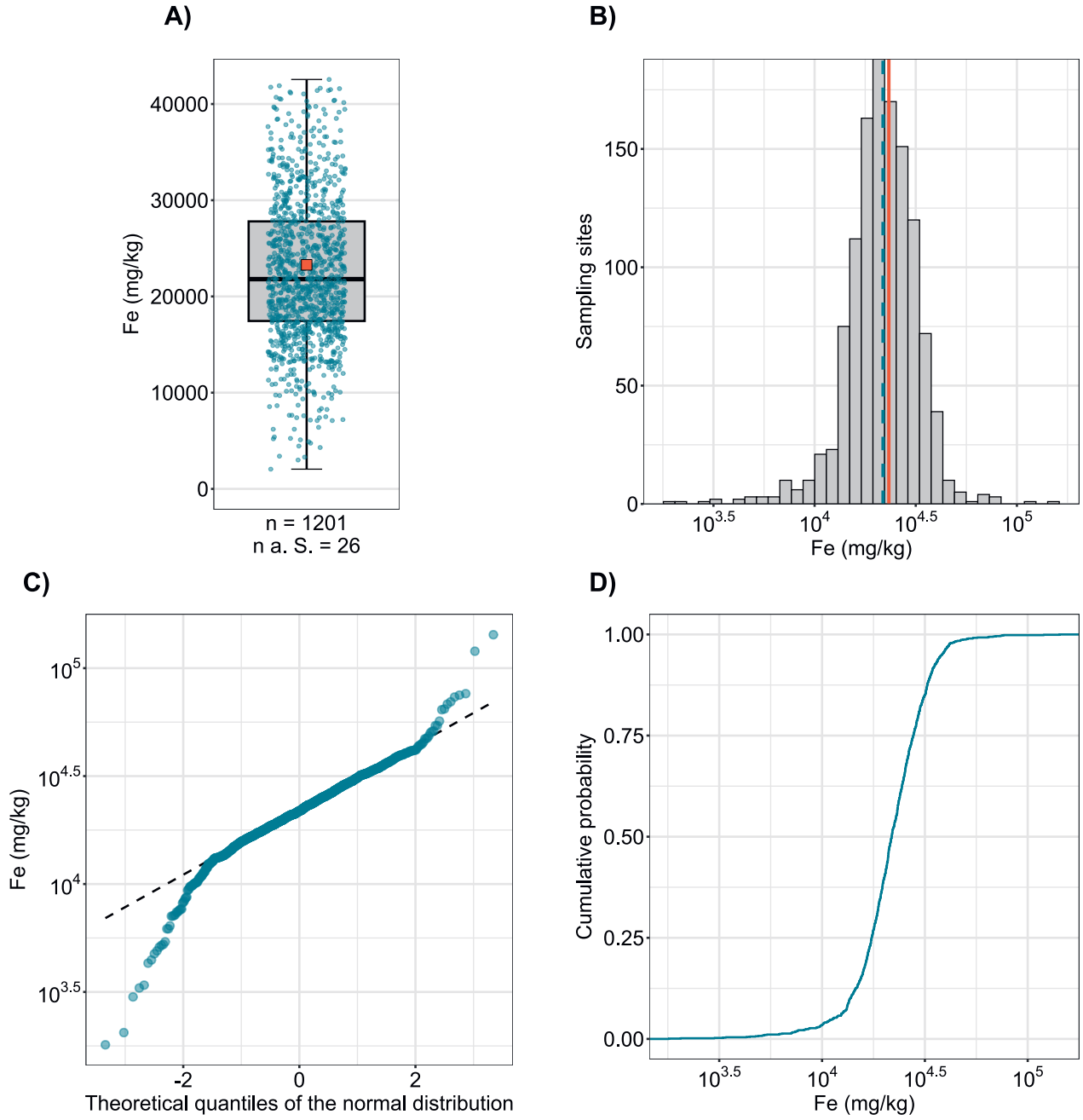

Figure 35 | Distribution of iron concentrations (mg/kg soil). The allocated value is the median of individual samples per site. Measured values below the limit of detection were disregarded. The dataset presented comprises the BDM, NABO and GEMAS sampling sites. n = total number of sites, n a. S. = sites lying outside the axis range or whisker.

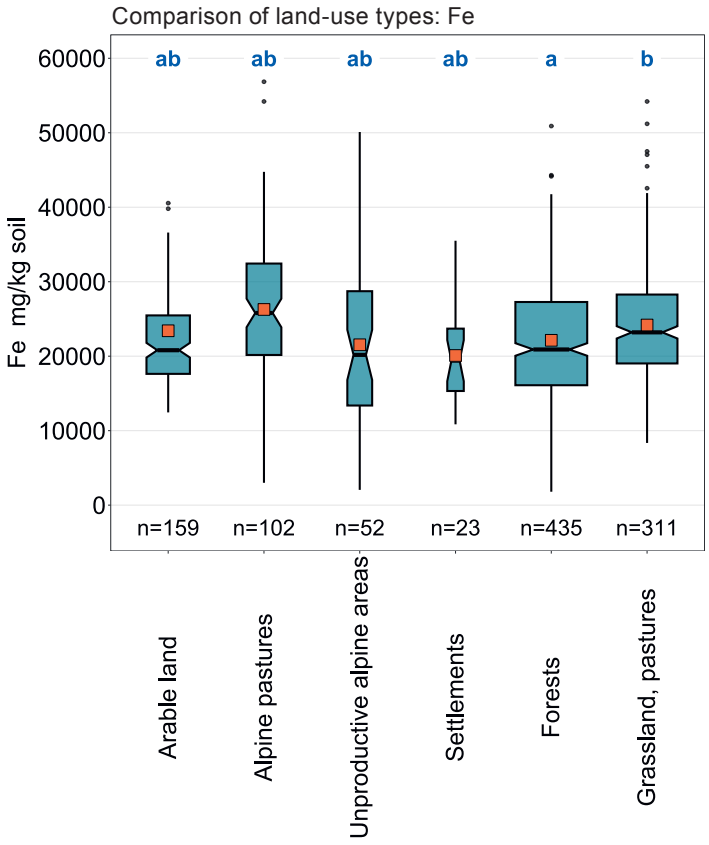

Figure 36 | Comparison of iron concentrations (mg/kg soil) in relation to the Z9 land-use types of the BDM sampling sites (top) and the lithological and petrographic groups in the simplified map of near-surface mineral raw materials of Switzerland (1 : 500 000, swisstopo, bottom). The median of all individual samples per site was included in the data analysis (BDM, NABO and GEMAS datasets). The number of sites per group is indicated beneath the boxes. Letters in blue: significant differences between groups ($p < 0.001$) based on a Wilcoxon rank sum test with P-adjustment using the Benjamini and Hochberg method. Not all outliers are shown. Orange square: arithmetic mean of the data.

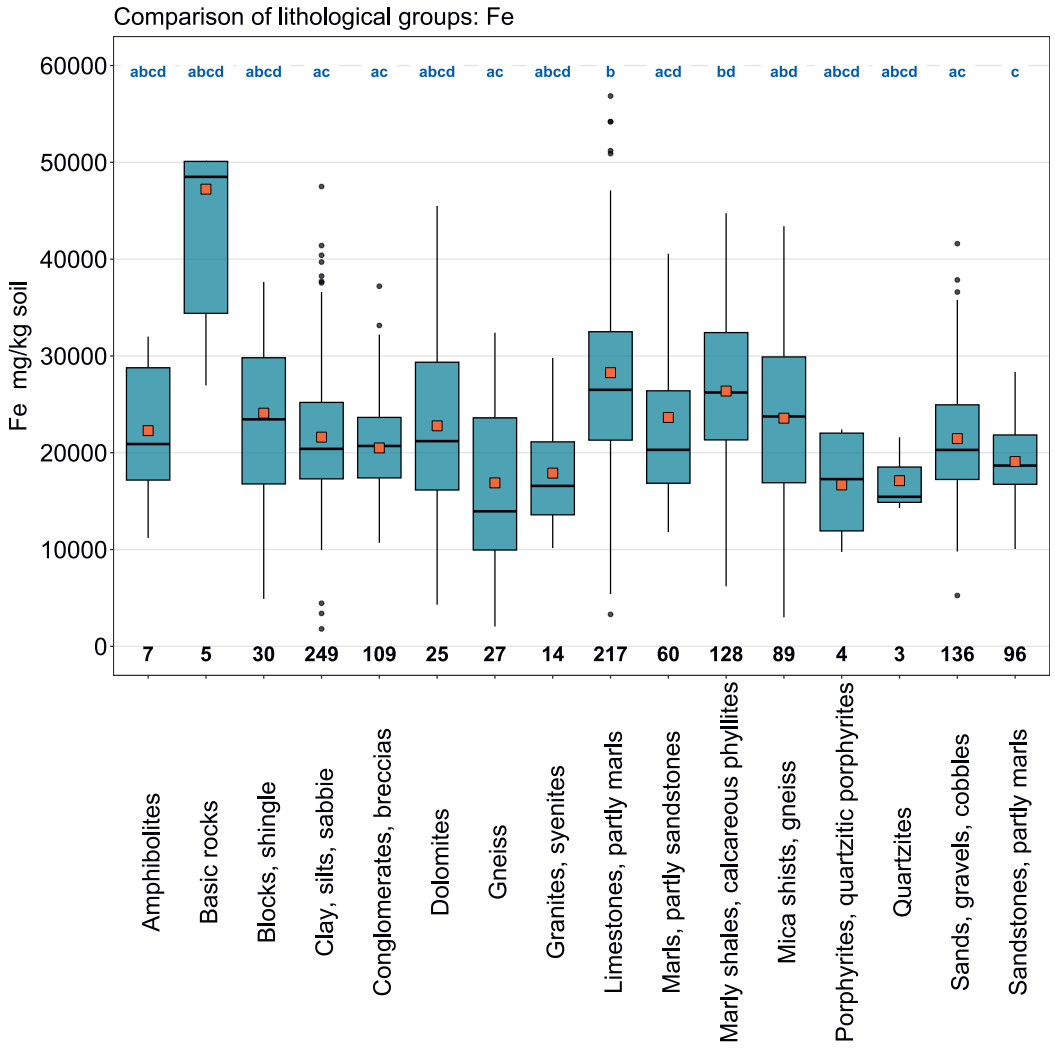

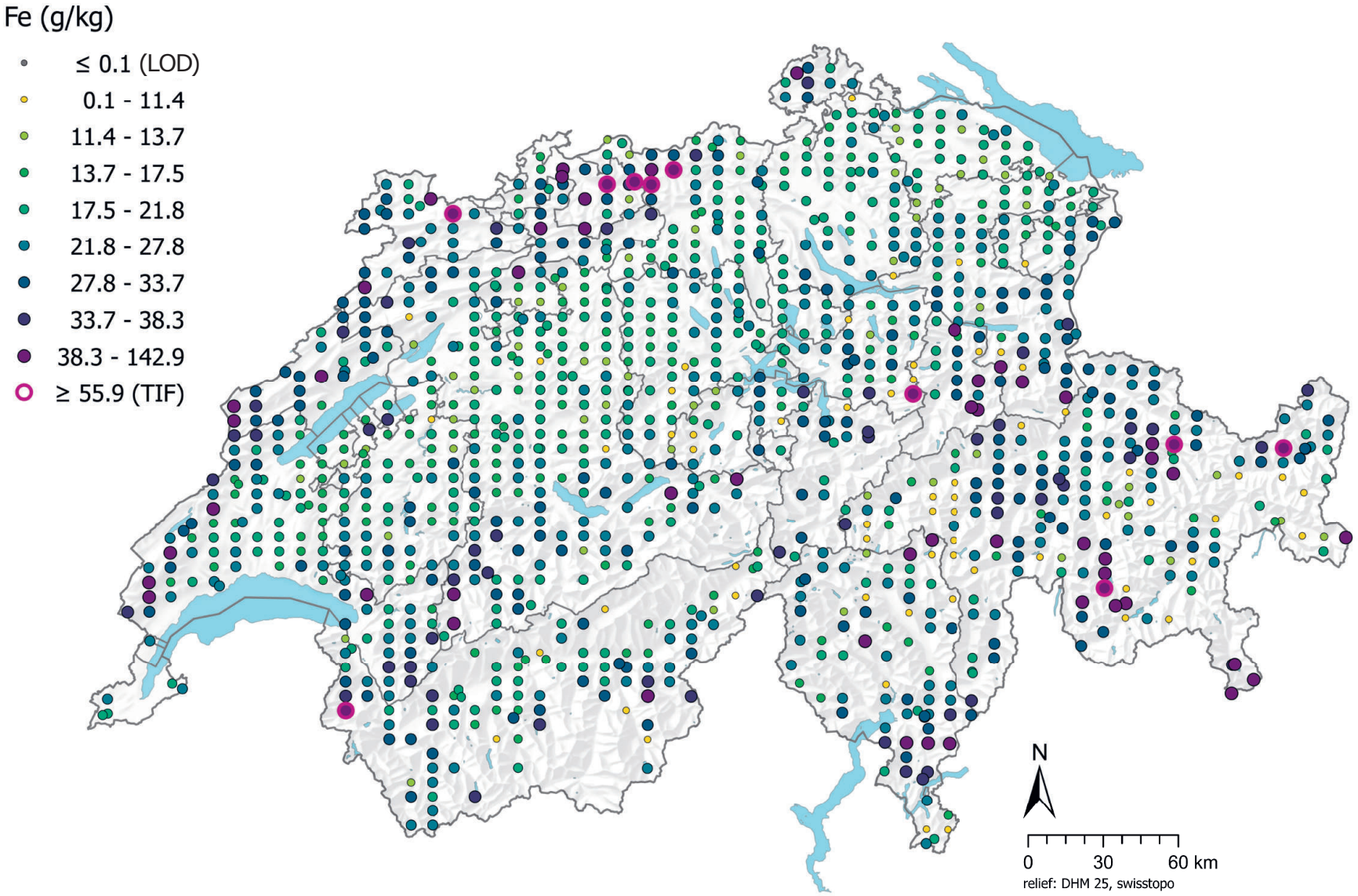

Figure 37 | **Spatial distribution of iron concentrations (mg/kg soil) measured at the BDM, NABO and GEMAS sites. The data points show the median of several individual samples per site. 0.5 times the limit of detection (LOD) was assigned to measured values below the LOD. The classes correspond to the 5 %, 10 %, 25 %, 50 %, 75 %, 90 % and 95 % percentiles. TIF: Tukey Inner Fence, outlier as per Reimann *et al.* (2018). LOD: limit of detection**

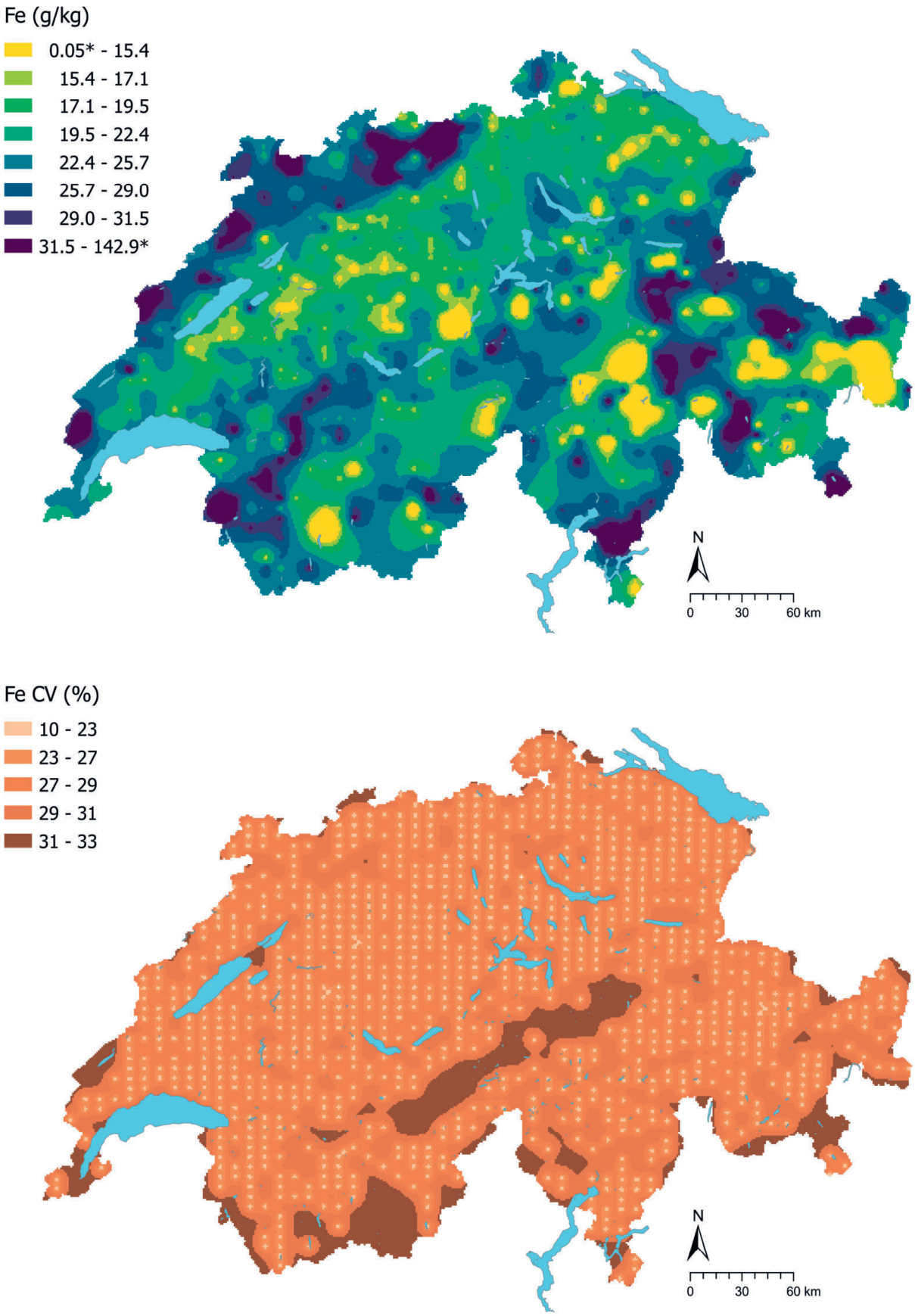

Figure 38 | Interpolated iron concentrations (mg/kg soil) at the BDM, NABO and GEMAS sites (top) and coefficient of variation (%) of the interpolated concentrations (bottom). The concentrations were divided into eight classes corresponding to the 5 %, 10 %, 25 %, 50 %, 75 %, 90 % and 95 % percentiles. The coefficients of variation were divided into five classes corresponding to the Jenks Natural Breaks algorithm. The interpolation was performed using the ordinary Kriging method (1 km × 1 km grid). In the classes of interpolated values, * denotes the minimum and maximum value of the point data calculated from the limit of detection.

4.9 Copper (Cu)

Copper is a metal in group 11 of the periodic table. Like nickel and zinc, it comprises 0.01 % by mass of the geosphere (Earth's crust + atmosphere + hydrosphere) (Fluck & Heumann, 2017). Its main minerals are malachite (copper carbonate), chalcopyrite ($CuFeS_2$) and bornite (Cu_5FeS_4) (Reimann *et al.*, 2014). Due to its strong affinity with sulphur, copper is also found in minerals such as sulphides and sulphosalts, and in arsenides. In addition, traces of copper can occur in iron oxides and iron-magnesium minerals (e.g. olivine, pyroxene, amphibole and biotite) (Tuchschmid, 1995). Tuchschmid (1995) documented elevated copper concentrations in basic rock and claystone in the flysch, Bündner schist and greenschist of the Alps. Geogenic copper deposits have been documented in the Valais and Eastern Swiss Alps (FGS, 2023b; Simoni *et al.*, 2014). In contrast to the other elements, areas with high or low copper concentrations are not as clearly defined by the spatial distribution of the point data (Figure 41). Some sites in the Alpine region defined as TIF outliers could be mainly due to geogenic copper deposits.

Copper was one of the first metals to be mined and processed by humans over 5000 years ago (Reimann *et al.*, 2014). Its electrical conductivity, thermal conductivity and corrosion resistance make the metal an important raw material for the electronics and construction industry (Bader *et al.*, 2011). Due to its toxicity to microorganisms, copper is also used in the agricultural sector in pesticides and fertilisers (Bader *et al.*, 2011). In Switzerland, the modelled copper emissions in soil and aquatic systems in 2000 amounted to 800 t, with agriculture accounting for 70 % and corrosion of building materials (gutters etc.) 20 % (Bader *et al.*, 2011; Simoni *et al.*, 2014). Copper concentrations in the topsoil samples from arable sites and sites in settlements are significantly higher than those from other land-use types (Figure 40). Increased copper concentrations in the topsoil observed at both intensively managed grassland sites and some arable sites in the NABO sampling network between 1985 and 2009 can be attributed to contamination with farmyard manure (Gross *et al.*, 2021; Gubler *et al.*, 2015).

In soil, copper adsorbs strongly to clay minerals, iron and manganese oxide, and soil organic matter (Hough, 2010). The observed correlation of measured copper concentrations with nickel concentrations ($R^2 = 0.65$) could be attributed to a geogenic origin (sulphidic nickel-copper mineralisations; Tuchschmid, 1995). The correlation with zinc ($R^2 = 0.68$) is possibly due to agricultural inputs, especially farmyard manure (Gubler *et al.*, 2015). However, the bivalent cations of all three elements show strong pH-dependent sorption, e.g. to oxide surfaces (Amelung *et al.*, 2018c); correlations between the three elements might also be explained by similar behaviour in the soil under equivalent conditions.

Although copper is an essential element for all living organisms, it can be harmful to plants and some animals in high concentrations (Amelung *et al.*, 2018a). Eikmann *et al.* (1993) define 50 mg/kg as the tolerance/trigger value for agricultural land and non-agricultural ecosystems. These values were exceeded at 27 sites, six of which are in vineyards, probably due to historic inputs of copper-containing pesticides. In contrast, when copper concentrations are lower than 5 mg/kg, there is a risk of copper deficiency in plants. Reimann *et al.* (2014) hypothesised that copper deficiency poses a greater problem than copper toxicity in Europe. In Switzerland, concentrations measured at around 4 % of sites are below this theoretical threshold for copper deficiency.

Element	Symbol	Atomic number	Median	5 %	95 %
Copper	Cu	29	18.1 mg/kg	5.8 mg/kg	40.8 mg/kg

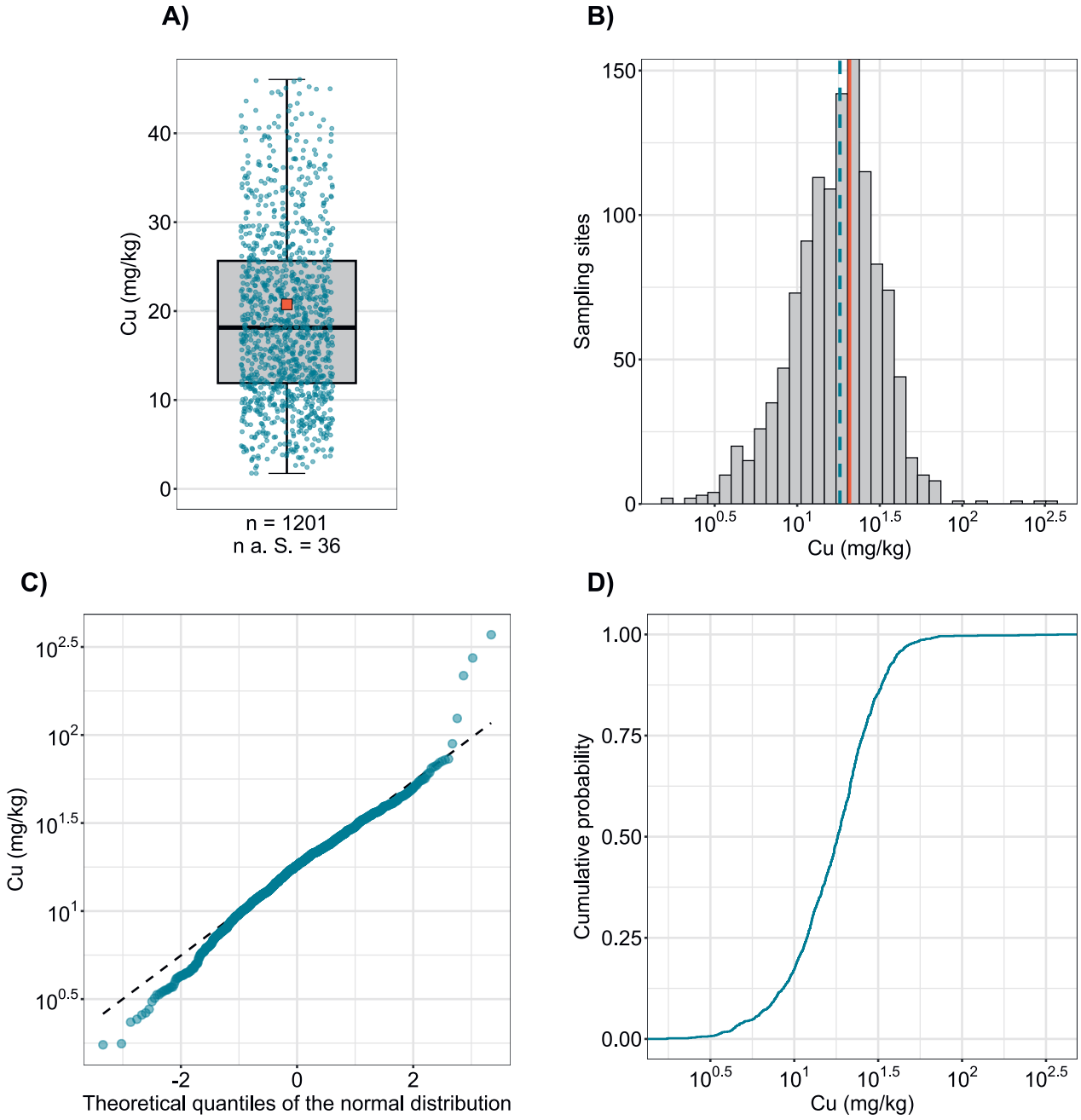

Figure 39 | Distribution of copper concentrations (mg/kg soil). The allocated value is the median of individual samples per site. The dataset presented comprises the BDM, NABO and GEMAS sampling sites. n = total number of sites, n a. S. = sites lying outside the axis range or whisker.

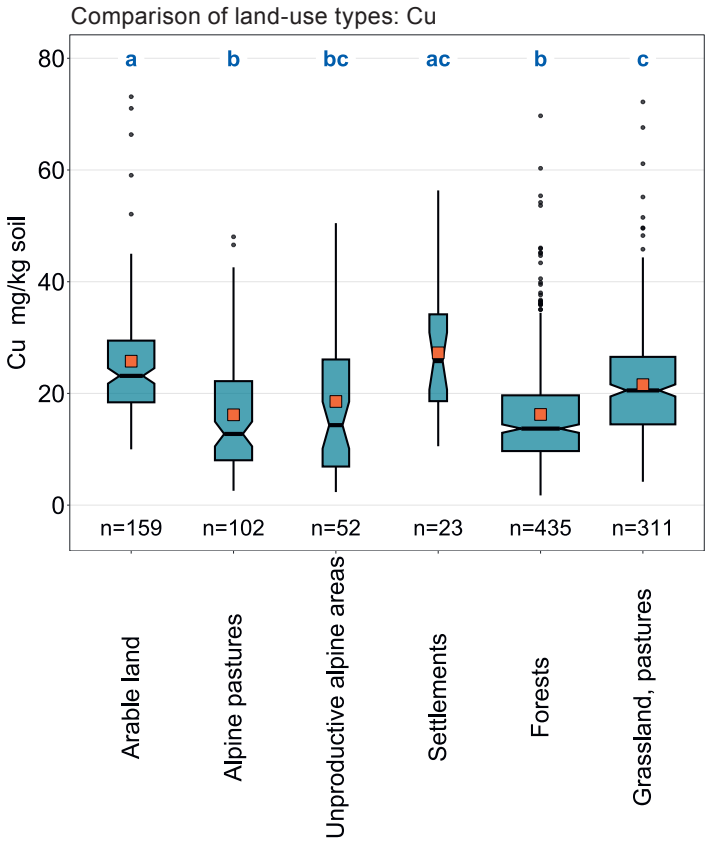

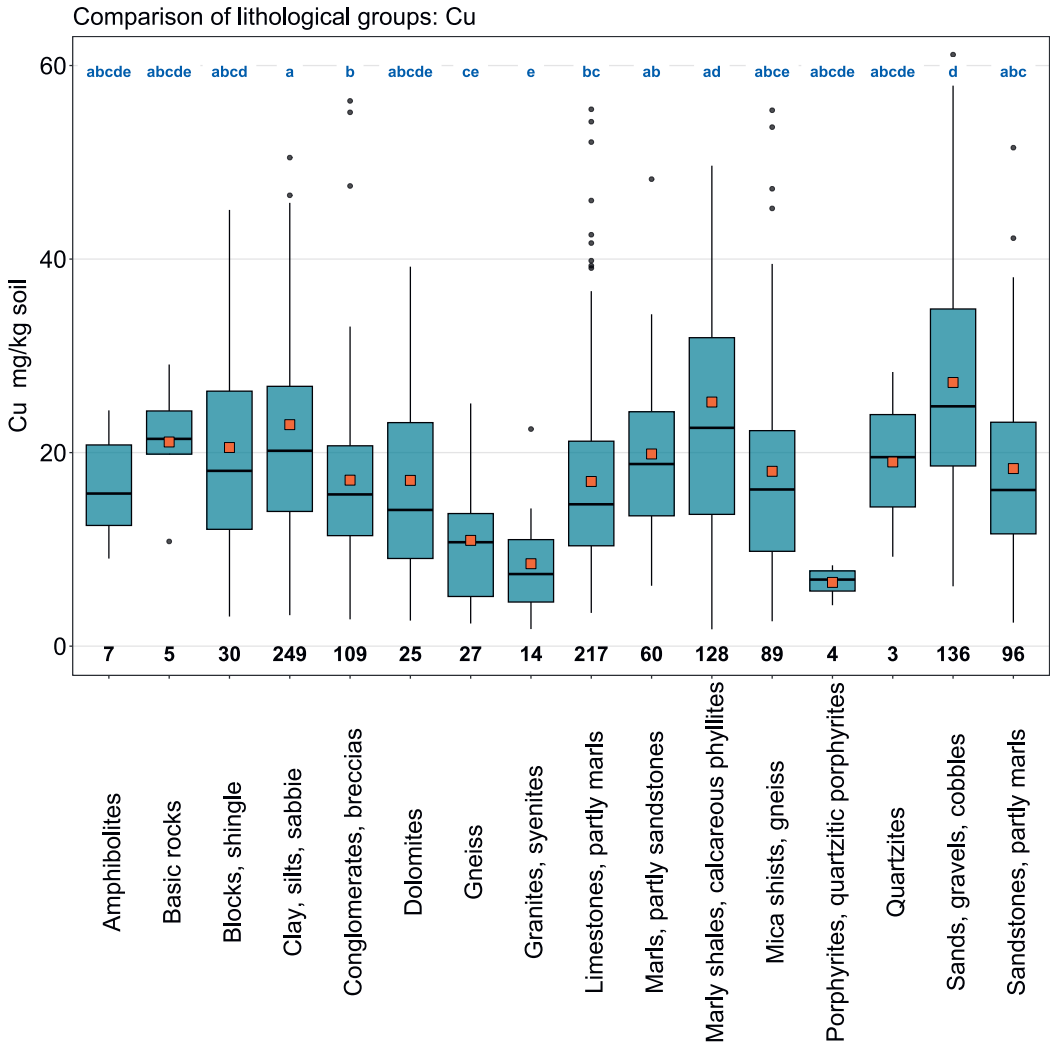

Figure 40 | **Comparison of copper concentrations (mg/kg soil) in relation to the Z9 land-use types of the BDM sampling sites (top) and the lithological and petrographic groups in the simplified map of near-surface mineral raw materials of Switzerland (1 : 500 000, swisstopo, bottom). The median of all individual samples per site was included in the data analysis (BDM, NABO and GEMAS datasets). The number of sites per group is indicated beneath the boxes. Letters in blue: significant differences between groups ($p < 0.001$) based on a Wilcoxon rank sum test with P-adjustment using the Benjamini and Hochberg method. Not all outliers are shown. Orange square: arithmetic mean of the data.**

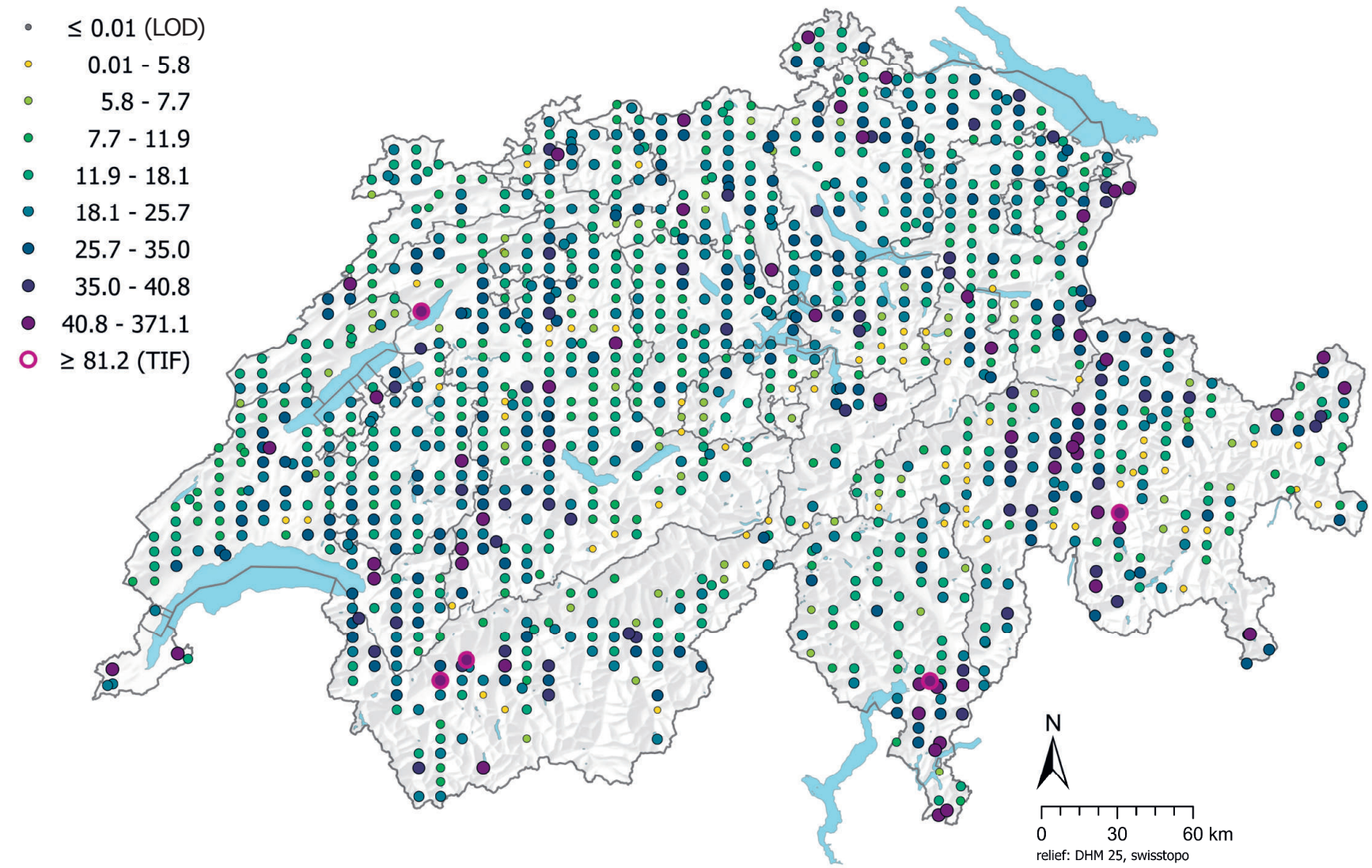

Figure 41 | **Spatial distribution of copper concentrations (mg/kg soil) measured at the BDM, NABO and GEMAS sites. The data points show the median of several individual samples per site. The classes correspond to the 5 %, 10 %, 25 %, 50 %, 75 %, 90 % and 95 % percentiles. TIF: Tukey Inner Fence, outlier as per Reimann *et al.* (2018). LOD: limit of detection**

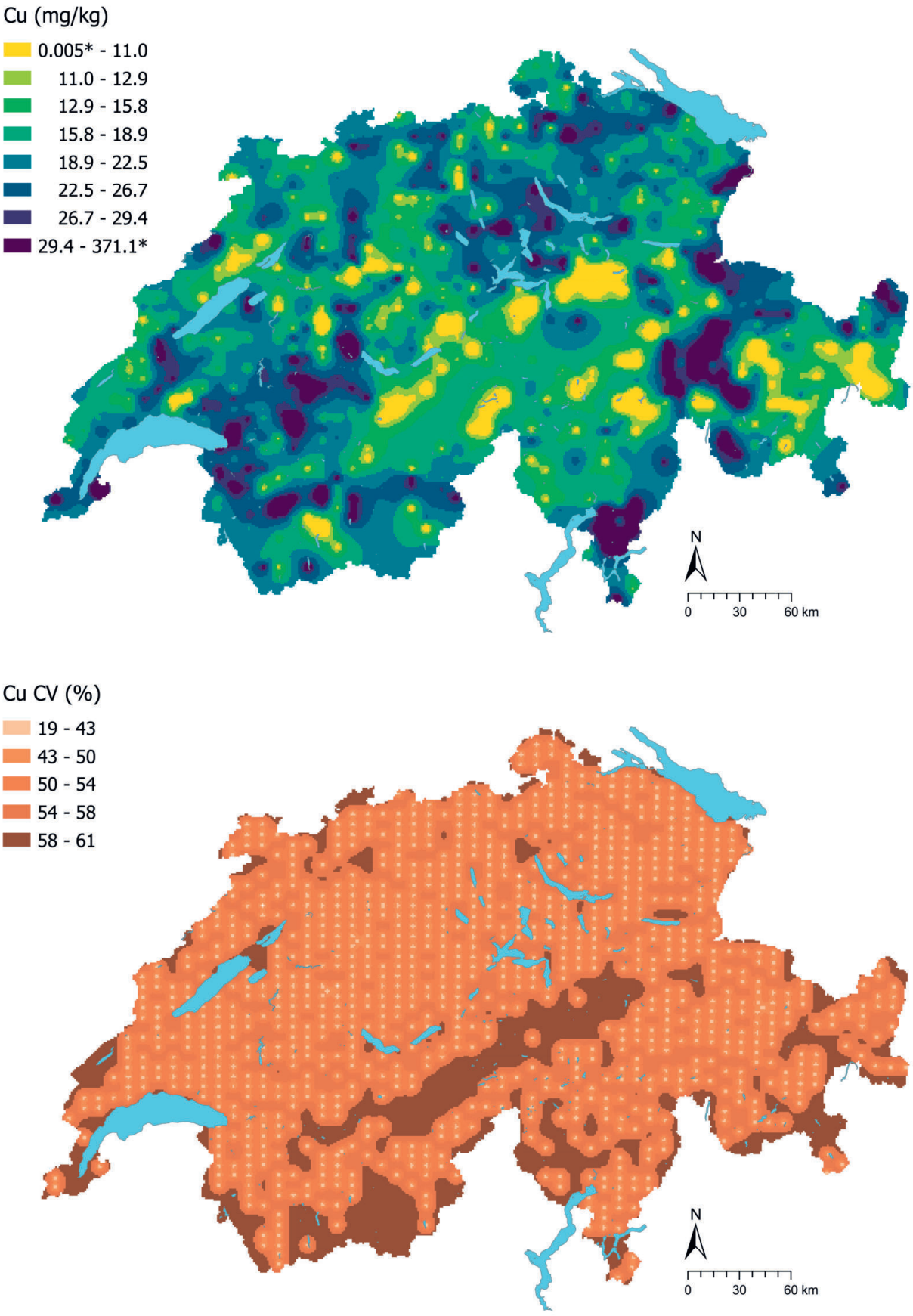

Figure 42 | Interpolated copper concentrations (mg/kg soil) at the BDM, NABO and GEMAS sites (top) and coefficient of variation (%) of the interpolated concentrations (bottom). The concentrations were divided into eight classes corresponding to the 5 %, 10 %, 25 %, 50 %, 75 %, 90 % and 95 % percentiles. The coefficients of variation were divided into five classes corresponding to the Jenks Natural Breaks algorithm. The interpolation was performed using the ordinary Kriging method (1 km × 1 km grid). In the classes of interpolated values, * denotes the minimum and maximum value of the point data calculated from the limit of detection.

4.10 Magnesium (Mg)

Magnesium is an alkaline earth metal in group 2 of the periodic table. It is the eighth most abundant element, comprising 2.3 % by mass of the Earth's crust (Amelung *et al.*, 2018a). As the main component of ferromagnesian silicates, e.g. olivine, amphibole, pyroxene and biotite, magnesium is most commonly found in ultramafic and mafic rocks (Reimann *et al.*, 2014). Apart from occurring in silicates, magnesium is also found in carbonates, e.g. dolomite ($CaMg[CO_3]_2$) and calcite ($CaCO_3$), where it can replace calcium (Reimann *et al.*, 2014). Comparatively high magnesium concentrations in topsoils were recorded at sites in the dolomite and basic rock lithological groups (Figure 44). This could indicate a predominantly geogenic origin in these areas, analogous to the findings of the iron, nickel, cobalt and chromium measurements. However, the concentration differences between these lithological groups are not statistically significant.

Magnesium is an essential element and, as a component of chlorophyll, plays an integral part in photosynthesis. In plants, magnesium deficiency manifests as chlorosis (yellowing of the leaf tips) and in humans and animals it can cause muscle cramps, e.g. grass tetany (staggers) in ruminants (Amelung *et al.*, 2018b). To prevent this issue, farmers apply magnesium to the soil as a fertiliser or in the form of lime in which some of the calcium in the carbonate has been replaced with magnesium (Amelung *et al.*, 2018b). Apart from in agriculture, magnesium is used in numerous alloys and metallurgical processes and is a constituent of food supplements and pharmaceuticals (Reimann *et al.*, 2014).

Mg^{2+} released due to weathering of minerals is readily exchangeable in the soil; Mg^{2+} saturation of the exchange surfaces of slightly acid to slightly alkaline soils is approximately 5 to 15 % (calcium: > 80 %) (Amelung *et al.*, 2018c). According to Amelung *et al.* (2018), silicate-rich clay soils are generally rich in magnesium, while quartz-rich sandy soils tend to have low levels. However, no correlation was found between measured magnesium concentrations and soil texture (Chapter 6.1).

In terms of spatial distribution, soils with comparatively high magnesium concentrations are found in the eastern Central Alps and north-eastern Switzerland (Figure 45). Areas with particularly low magnesium concentrations in topsoil are located in Central Switzerland. There are no significant differences in magnesium concentrations between land-use types (Figure 44).

The median of measured total magnesium concentrations is 4.2 g/kg, which is significantly higher than the median of 2.9 g/kg for European arable soils (Reimann *et al.*, 2014). The median for European arable soils is also based on aqua regia digestion; the magnesium concentrations measured with x-ray fluorescence spectrometry (XRF) in the same soils were significantly higher (median: 5.9 g/kg). The likeliest explanation is that magnesium bound in minerals cannot be fully digested with aqua regia. However, it is the concentration of exchangeable Mg^{2+} rather than the total content that determines plant availability. The concentration of exchangeable Mg^{2+} in salt- and carbonate-poor soils in temperate latitudes is 0.5 to 5 g/kg (Amelung *et al.*, 2018a).

Element	Symbol	Atomic number	Median	5 %	95 %
Magnesium	Mg	12	4.2 g/kg	1.4 g/kg	14.8 g/kg

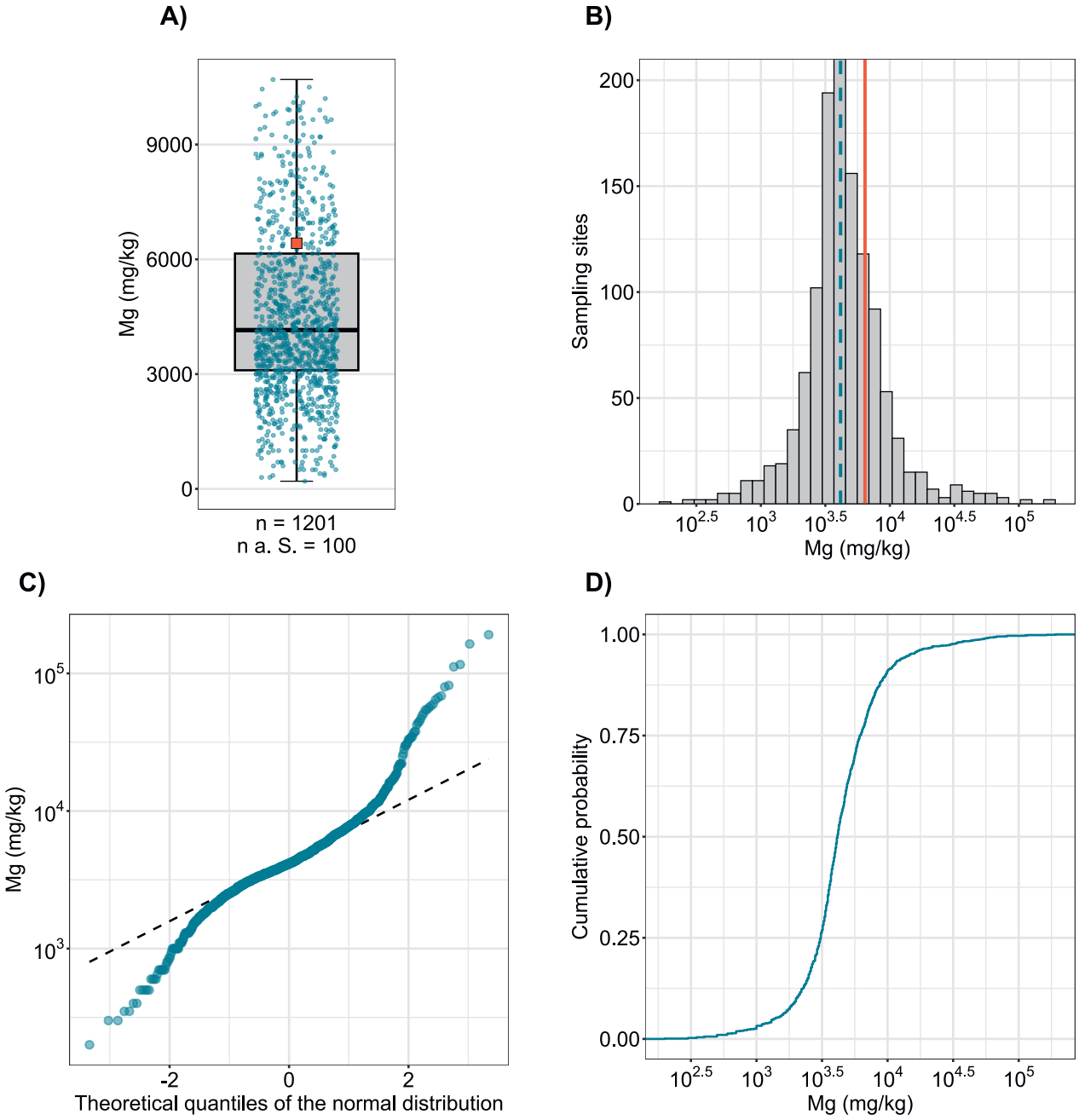

Figure 43 | Distribution of magnesium concentrations (mg/kg soil). The allocated value is the median of individual samples per site. Measured values below the limit of detection were disregarded. The dataset presented comprises the BDM, NABO and GEMAS sampling sites. n = total number of sites, n a. S. = sites lying outside the axis range or whisker.

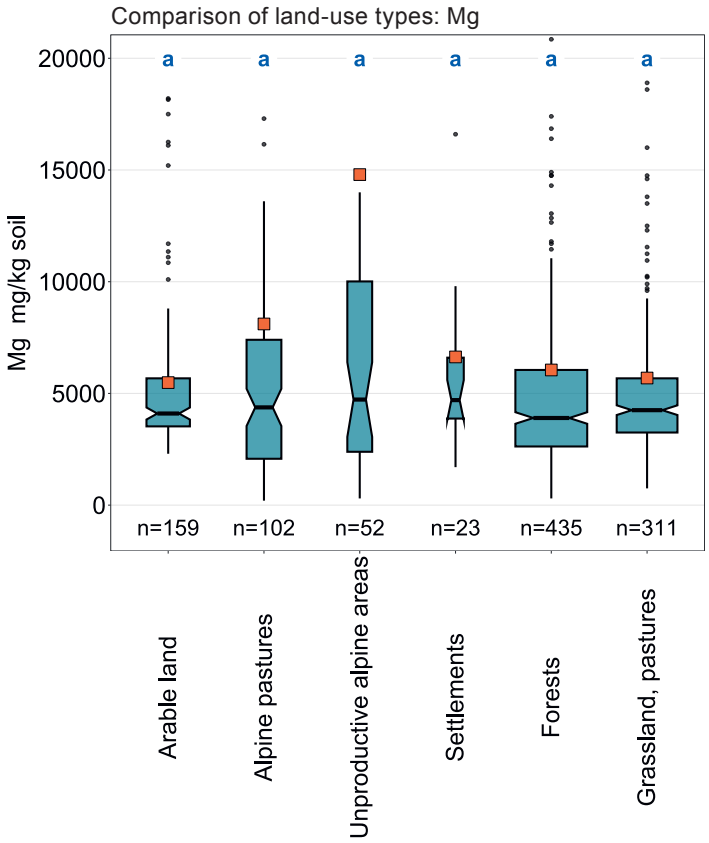

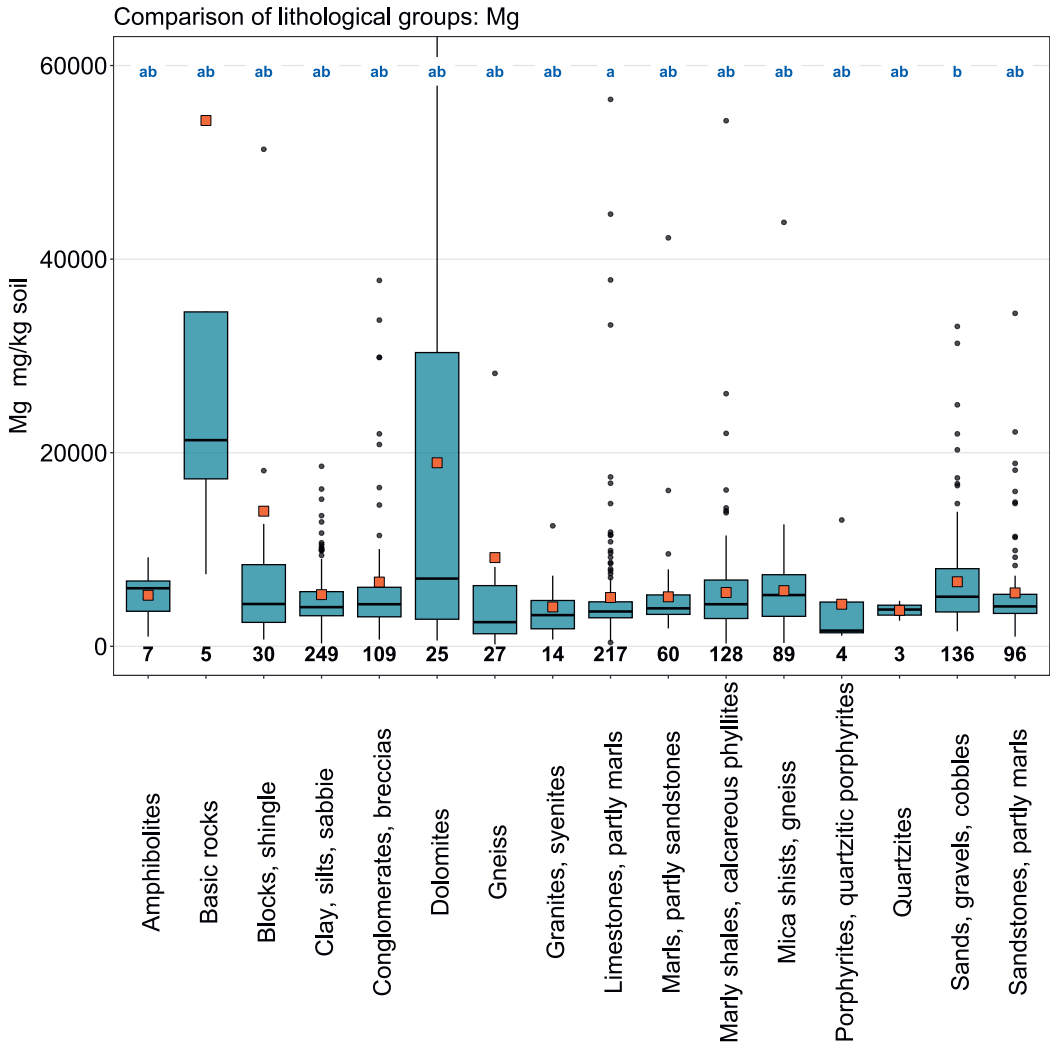

Figure 44 | Comparison of magnesium concentrations (mg/kg soil) in relation to the Z9 land-use types of the BDM sampling sites (top) and the lithological and petrographic groups in the simplified map of near-surface mineral raw materials of Switzerland (1 : 500 000, swisstopo, bottom). The median of all individual samples per site was included in the data analysis (BDM, NABO and GEMAS datasets). The number of sites per group is indicated beneath the boxes. Letters in blue: significant differences between groups ($p < 0.001$) based on a Wilcoxon rank sum test with P-adjustment using the Benjamini and Hochberg method. Not all outliers are shown. Orange square: arithmetic mean of the data.

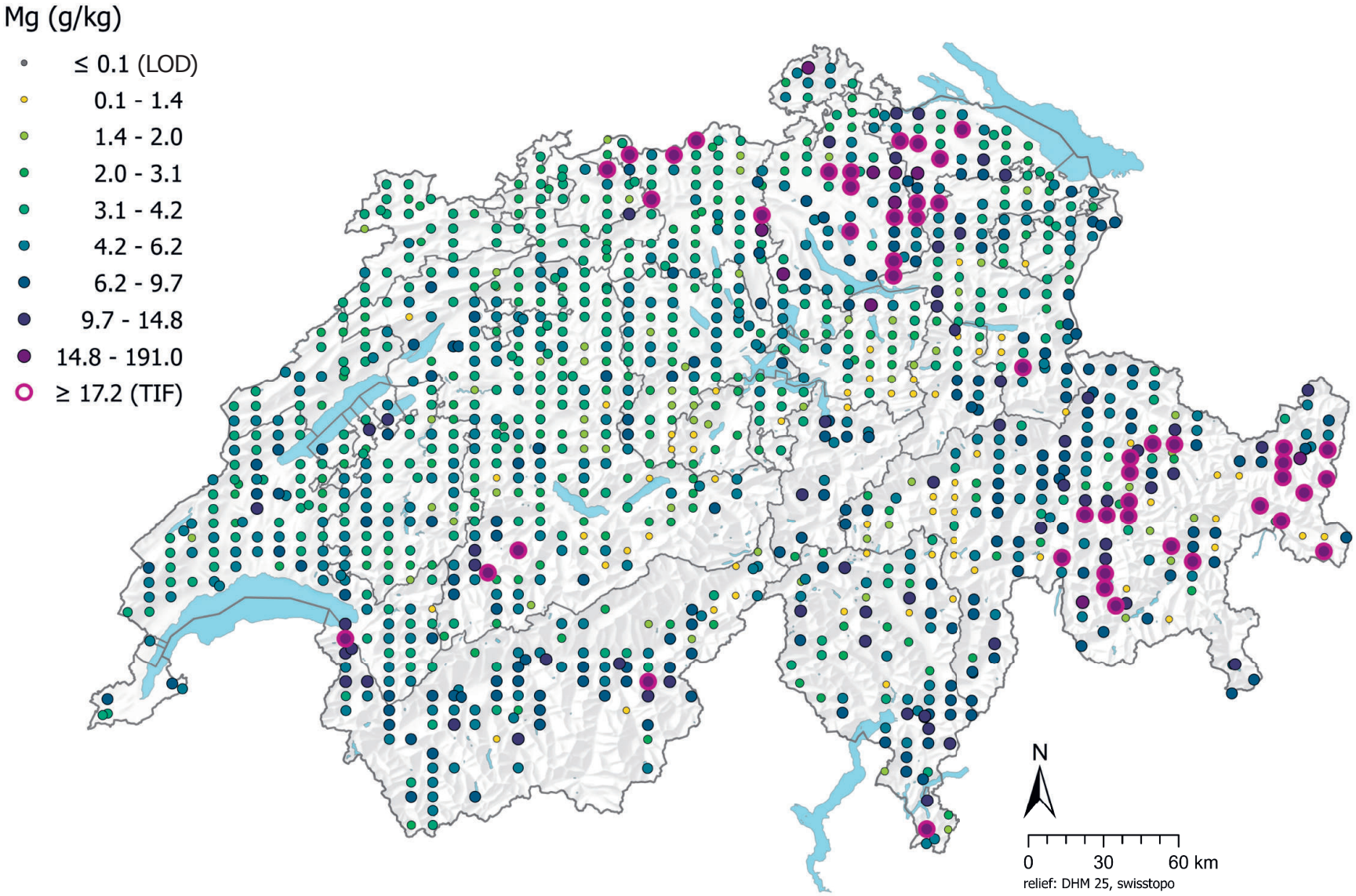

Figure 45 | **Spatial distribution of magnesium concentrations (mg/kg soil) measured at the BDM, NABO and GEMAS sites. The data points show the median of several individual samples per site. 0.5 times the limit of detection (LOD) was assigned to measured values below the LOD. The classes correspond to the 5 %, 10 %, 25 %, 50 %, 75 %, 90 % and 95 % percentiles. TIF: Tukey Inner Fence, outlier as per Reimann *et al.* (2018). LOD: limit of detection**

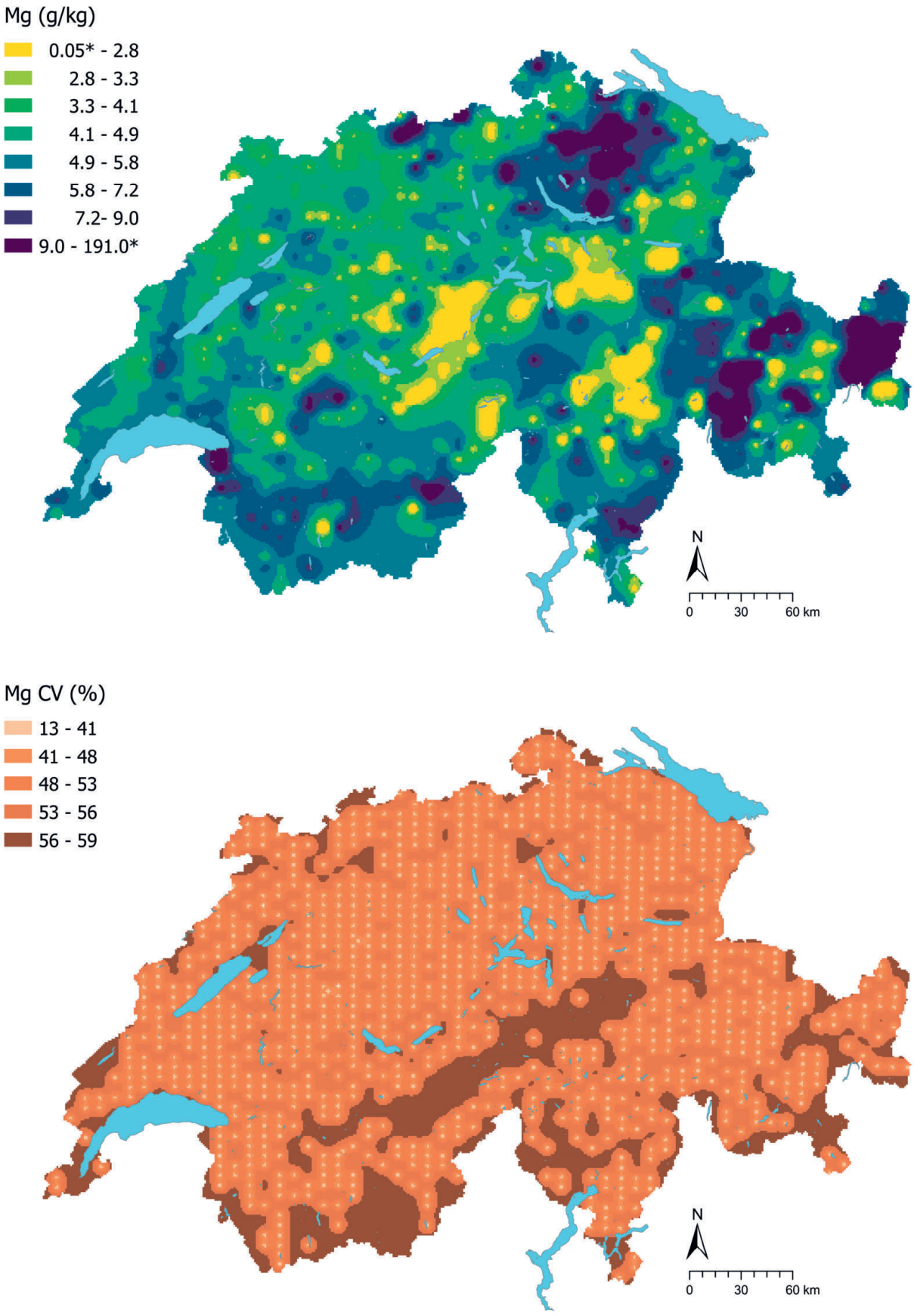

Figure 46 | Interpolated magnesium concentrations (mg/kg soil) at the BDM, NABO and GEMAS sites (top) and coefficient of variation (%) of the interpolated concentrations (bottom). The concentrations were divided into eight classes corresponding to the 5 %, 10 %, 25 %, 50 %, 75 %, 90 % and 95 % percentiles. The coefficients of variation were divided into five classes corresponding to the Jenks Natural Breaks algorithm. The interpolation was performed using the ordinary Kriging method (1 km × 1 km grid). In the classes of interpolated values, * denotes the minimum and maximum value of the point data calculated from the limit of detection.

4.11 Manganese (Mn)

Manganese is a metal in group 7 of the periodic table and one of the most abundant trace elements in the lithosphere (He *et al.*, 2010). Its minerals include the pink-coloured rhodonite ($MnSiO_3$), and the black ore mineral pyrolusite (MnO_2) (Reimann *et al.*, 2014). In addition, the Mn^{2+} cation can replace iron and magnesium in silicates and oxides (He *et al.*, 2010). Thus the element is commonly found in silicate minerals such as chlorite, olivine, biotite, pyroxene and amphibole. Mafic rocks generally contain the highest levels of manganese, with concentrations ranging from 1400 to 1500 mg/kg (Reimann *et al.*, 2014). Major manganese deposits in Switzerland are documented in the oolitic iron ore of the Herznach strata in the Frick Valley (FGS, 2023b).

Manganese is used mainly in metal processing, as well as in batteries, catalysts, pigments, pharmaceuticals, fertilisers, and in the chemical industry in general (Reimann *et al.*, 2014).

In soil, manganese is released mainly in the form of Mn^{2+} during weathering of silicates, oxides and carbonates (He *et al.*, 2010). As with iron, under oxidising conditions the cation is rapidly precipitated as poorly soluble oxides and hydroxides, which can accumulate in the soil as black manganese concretions (He *et al.*, 2010). Under reducing conditions, manganese is either released back to the soil solution, where it is bioavailable, or leached out. Manganese can also adsorb to the surfaces of other oxides (e.g. iron, aluminium and titanium) and to clay minerals, and form complexes with soil organic matter. Some of these complexes, as well as inorganic complexes such as $MnCO_3$ and $MnSO_4$, are labile and thus provide a source of manganese for plants and microorganisms (He *et al.*, 2010). According to He *et al.* (2010), most manganese in soil is derived from the parent material. The weak correlations of manganese concentrations in the topsoil with those of cobalt, nickel and chromium (Chapter 6.1) could indicate either a shared geogenic origin or cobalt precipitation, or sorption of ions to surfaces of secondary manganese (hydro)oxides. Secondary manganese (hydro)oxides often accumulate heavy metals such as cadmium, nickel, lead and zinc (Amelung *et al.*, 2018a).

Manganese is a micronutrient for all living organisms but can be toxic at high concentrations (Amelung *et al.*, 2018a). The authors cite typical manganese concentrations in A horizons of 40 to 1000 mg/kg. With a median of 655 mg/kg, measured manganese concentrations in Swiss topsoils are within this range (Table 2). In the Europe-wide comparison (arable land: 445 mg/kg, grassland sites: 435 mg/kg), this median is slightly elevated, but still below the 75 % quartile of the European data (Reimann *et al.*, 2014). The highest manganese concentrations in topsoil are found in the Jura, the western foothills of the Alps and Grisons (Figure 49). Low manganese levels were measured on the south side of the Alps.

Measured manganese concentrations in arable and grassland areas are significantly higher than in forests, alpine pastures and unproductive alpine areas (Figure 48). These differences between land-use types are also evident in pH (Chapter 5.1), although measured manganese concentrations correlate only very weakly with pH (Chapter 6.1), and data on redox conditions were not available. In addition to inputs from atmospheric deposition, irrigation and effluent from sewage sludge (banned in Switzerland since 2006), manganese can also enter the soil via fertiliser (e.g. farmyard manure) and liming (He *et al.*, 2010), which could result in increased manganese levels in soil.

Element	Symbol	Atomic number	Median	5 %	95 %
Manganese	Mn	25	655 mg/kg	145 mg/kg	1390 mg/kg

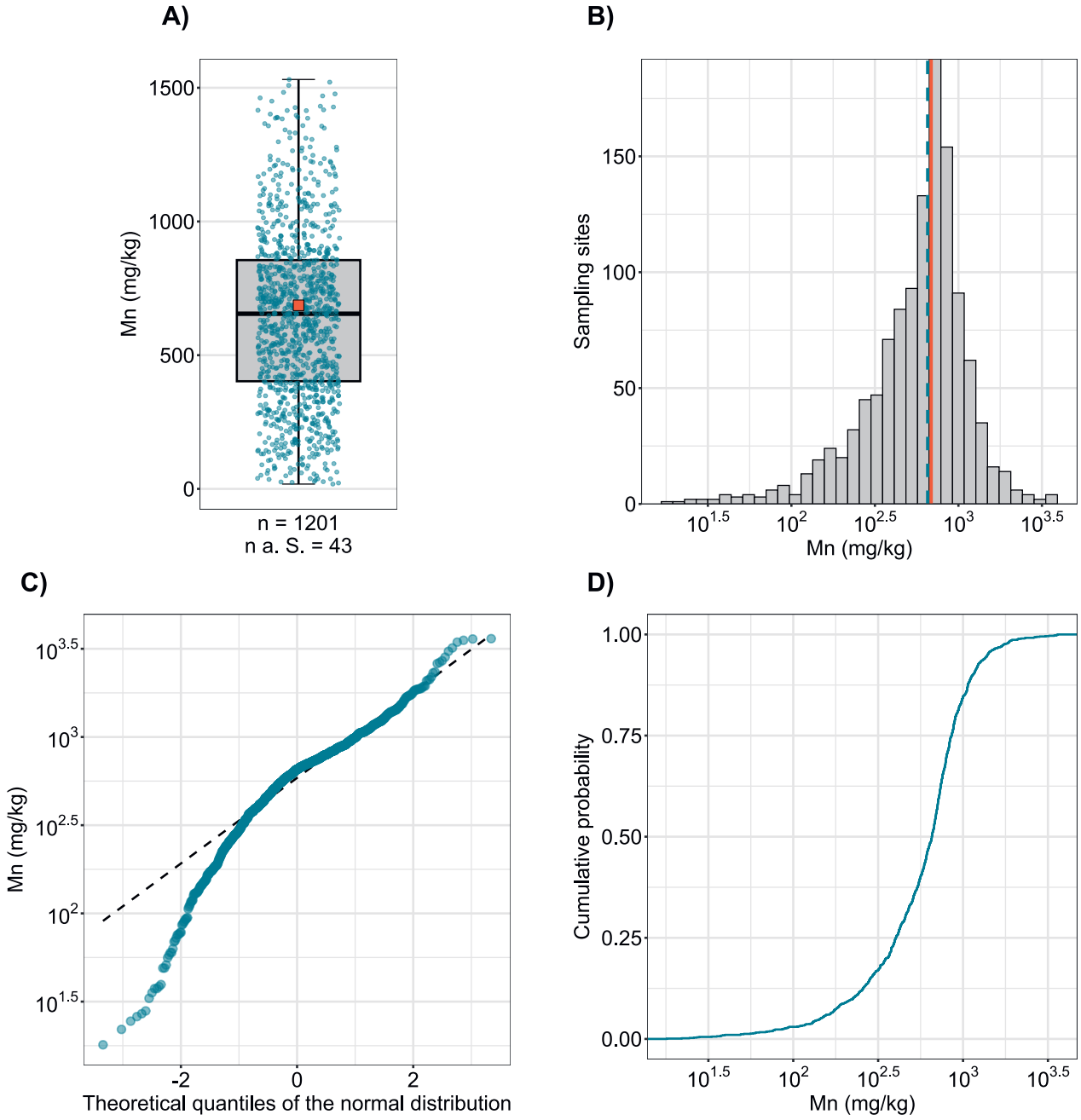

Figure 47 | **Distribution of manganese concentrations (mg/kg soil). The allocated value is the median of individual samples per site. The dataset presented comprises the BDM, NABO and GEMAS sampling sites. n = total number of sites, n a. S. = sites lying outside the axis range or whisker.**

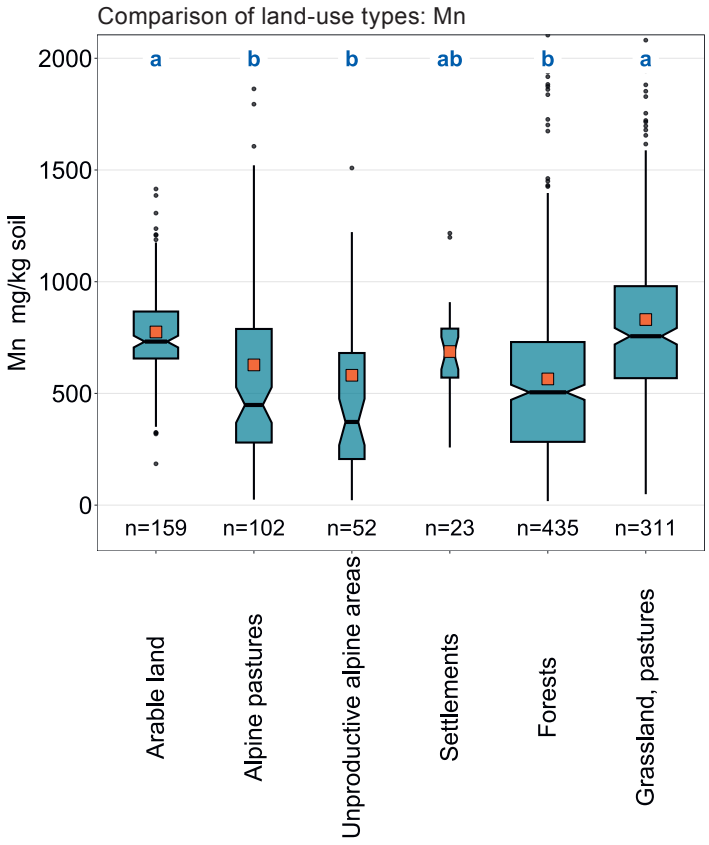

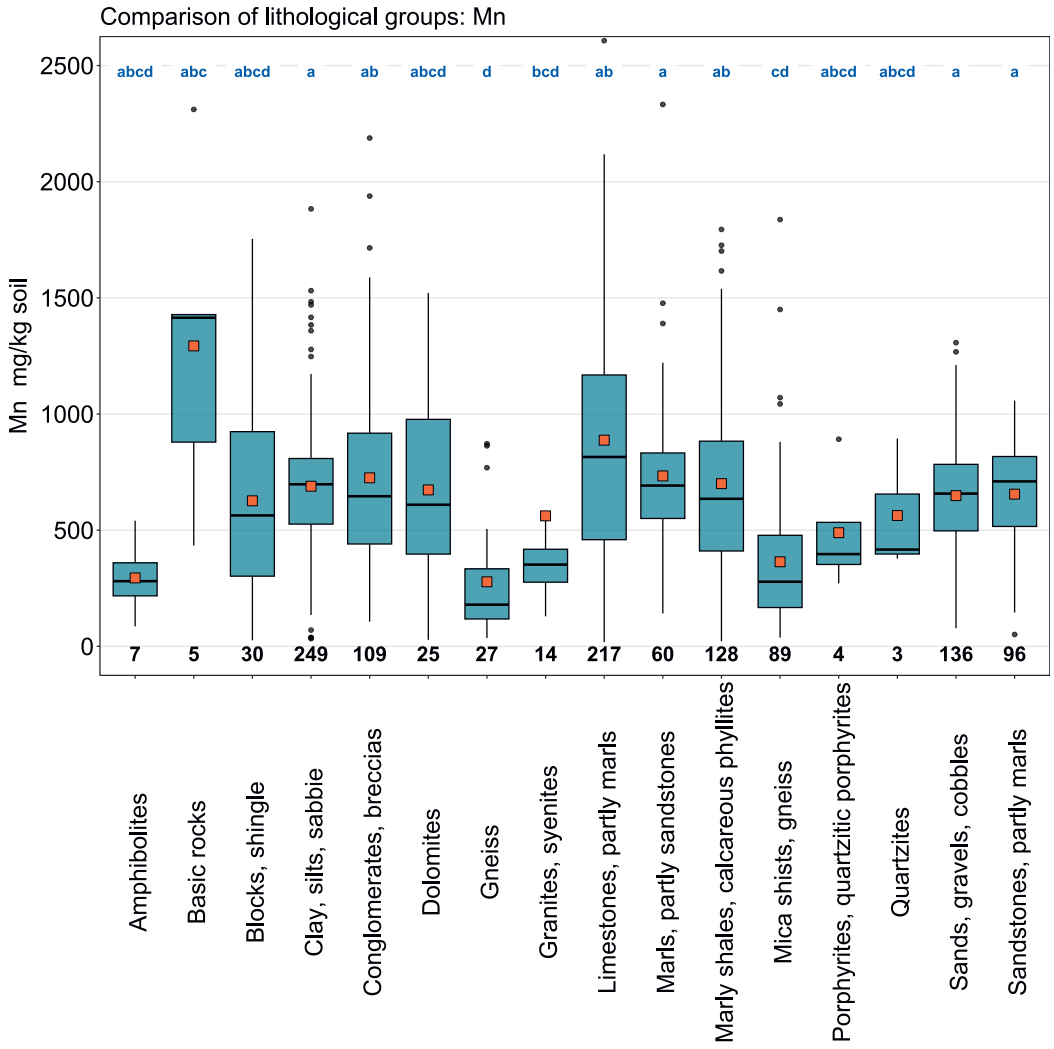

Figure 48 | Comparison of manganese concentrations (mg/kg soil) in relation to the Z9 land-use types of the BDM sampling sites (top) and the lithological and petrographic groups in the simplified map of near-surface mineral raw materials of Switzerland (1 : 500 000, swisstopo, bottom). The median of all individual samples per site was included in the data analysis (BDM, NABO and GEMAS datasets). The number of sites per group is indicated beneath the boxes. Letters in blue: significant differences between groups ($p < 0.001$) based on a Wilcoxon rank sum test with P-adjustment using the Benjamini and Hochberg method. Not all outliers are shown. Orange square: arithmetic mean of the data.

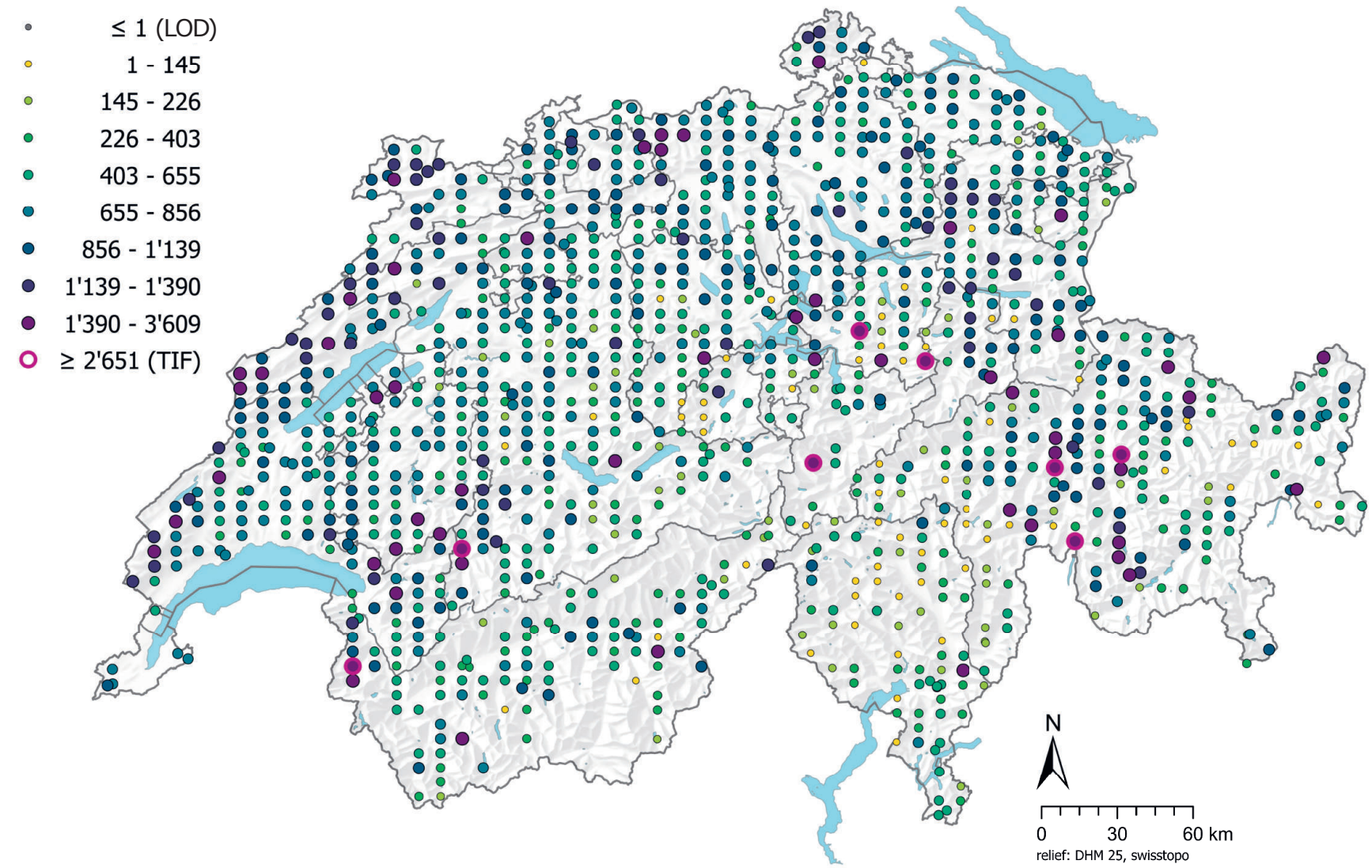

Figure 49 | **Spatial distribution of manganese concentrations (mg/kg soil) measured at the BDM, NABO and GEMAS sites. The data points show the median of several individual samples per site. The classes correspond to the 5 %, 10 %, 25 %, 50 %, 75 %, 90 % and 95 % percentiles. TIF: Tukey Inner Fence, outlier as per Reimann *et al.* (2018). LOD: limit of detection**

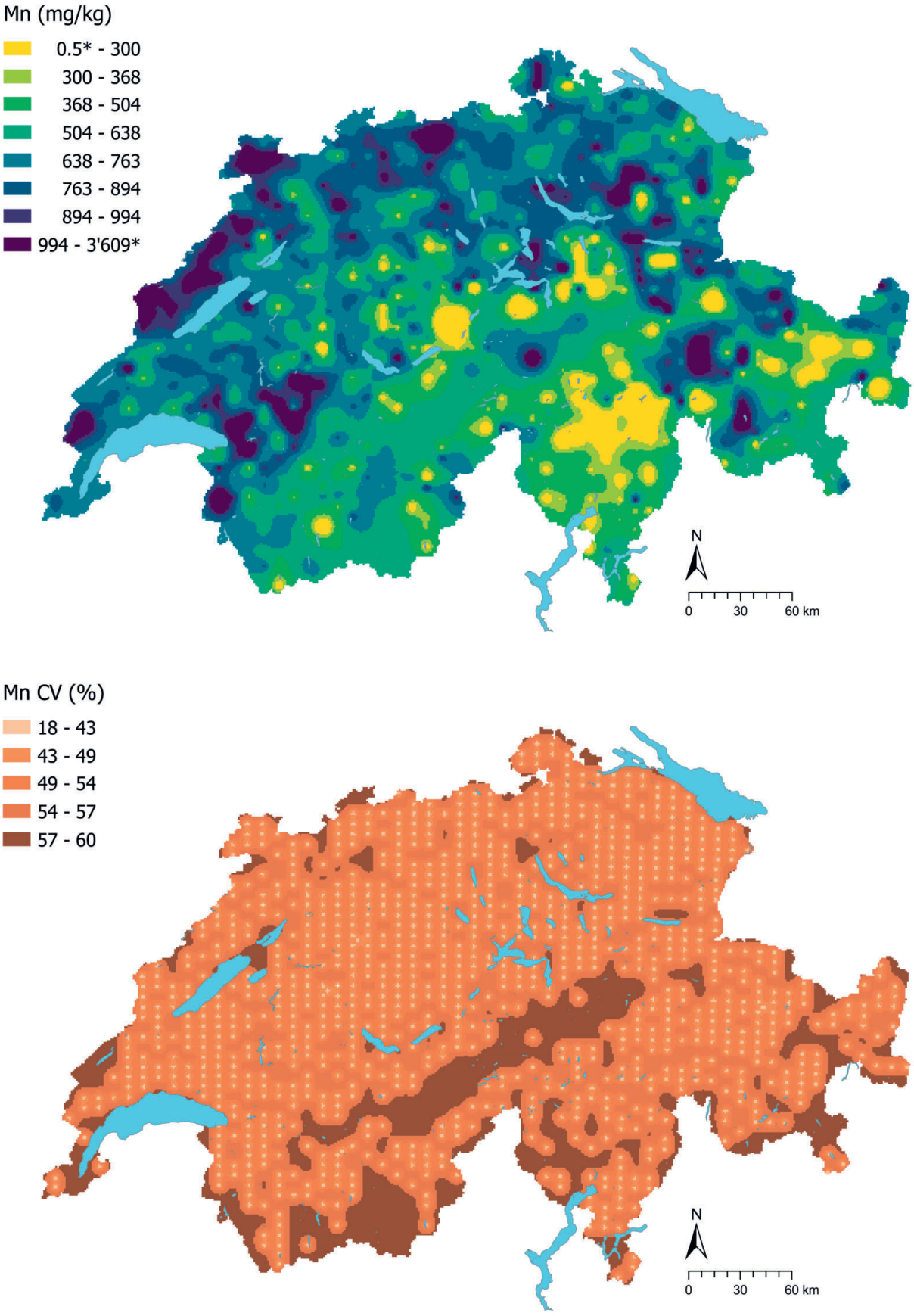

Figure 50 | Interpolated manganese concentrations (mg/kg soil) at the BDM, NABO and GEMAS sites (top) and coefficient of variation (%) of the interpolated concentrations (bottom). The concentrations were divided into eight classes corresponding to the 5 %, 10 %, 25 %, 50 %, 75 %, 90 % and 95 % percentiles. The coefficients of variation were divided into five classes corresponding to the Jenks Natural Breaks algorithm. The interpolation was performed using the ordinary Kriging method (1 km × 1 km grid). In the classes of interpolated values, * denotes the minimum and maximum value of the point data calculated from the limit of detection.

4.12 Molybdenum (Mo)

Molybdenum is a metal in group 6 of the periodic table and is essential for most living organisms. Its main ore is the sulphide molybdenite (MoS_2), but it can also replace other elements (e.g. iron, titanium and aluminium) in minerals and occurs in manganese oxides and sulphides, for example, as well as in biotite, feldspar and amphibole (Evans & Barabash, 2010; Reimann *et al.*, 2014; Tuchschmid, 1995). Molybdenum concentrations in rocks are frequently linked to concentrations of manganese, sulphur and organic carbon (Tuchschmid, 1995). According to Tuchschmid (1995), molybdenum concentrations in typical rocks in Switzerland vary only slightly from around 0.1 mg/kg in limestone to 3 mg/kg in granitic magmatite. Very high molybdenum concentrations can occur in bituminous claystone and coal (up to 200 mg/kg), with relatively high concentrations of 5.4 mg/kg also recorded in an iron oolitic limestone in the Jura (Tuchschmid, 1995).

The steel industry accounts for around 75 % of total molybdenum consumption, although it is also used in catalysts, pigments, corrosion inhibitors, lubricants and fertilisers (Evans & Barabash, 2010). Molybdenum can enter the soil via atmospheric deposition and farmyard manure, as well as through fertilisers.

Under acid conditions, molybdenum adsorbs to the surfaces of iron (hydro)oxides and clay minerals as an anion, unlike many other metals. However, at soil pH values above 5, molybdenum rapidly dissolves and becomes mobile (Evans & Barabash, 2010). In soil solution, molybdenum oxyanions can complex and precipitate with different cations (e.g. Ca^{2+}) as well as with components of soil organic matter (Evans & Barabash, 2010).

Molybdenum concentrations at 42 sites were classified as outliers based on the TIF method. The right-skewed distribution is also evident in the clear deviation of the mean from the median (Figure 51), which at 0.81 mg/kg lies within the typical range of molybdenum concentrations in soil (0.2–5 mg/kg) (Amelung *et al.*, 2018a). Molybdenum levels in topsoils of the western Swiss Plateau are particularly low (Figure 53). In contrast, high concentrations occur in the western Jura. According to the Geological Atlas of Switzerland, micrite, oolitic limestone, marlstone, dolomite, calcareous breccia and bioclastic limestone can be found in these regions (swisstopo, 2022). Some sites in these groups have high concentrations of molybdenum in topsoil, although the concentration differences are not significant (Figure 52).

Although molybdenum is a micronutrient, concentrations as low as 5 to 10 mg/kg in fodder can be toxic to ruminants (Amelung *et al.*, 2018a). No significant differences between land-use types were detected; the highest mean occurs in unproductive alpine areas, mainly located in the Alpine region (Figure 4). The tolerance value for agricultural land of 20 mg/kg (Lühr *et al.*, 1996) is exceeded only at one of the sites.

Element	Symbol	Atomic number	Median	5 %	95 %
Molybdenum	Mo	42	0.81 mg/kg	0.39 mg/kg	2.51 mg/kg

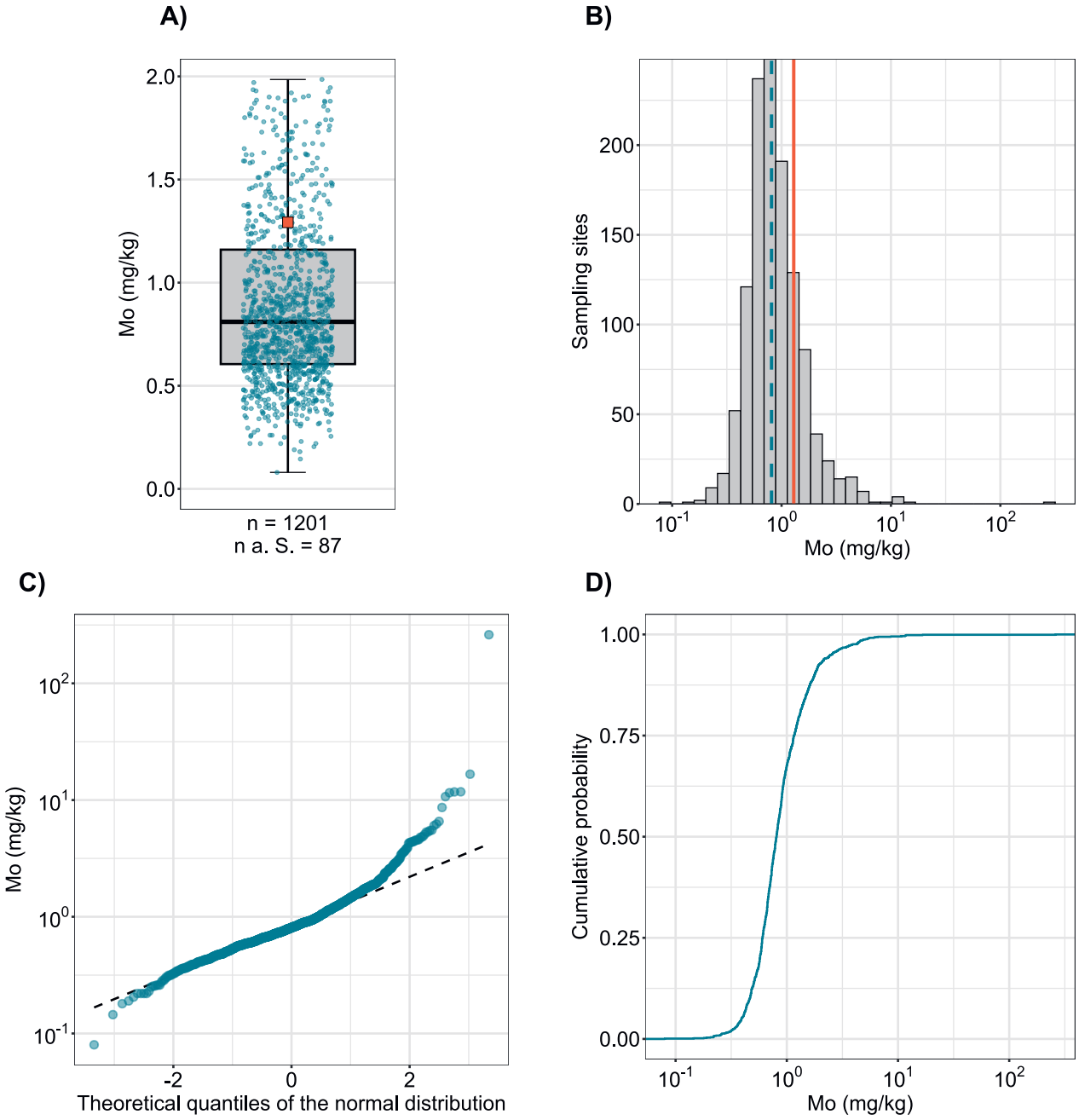

Figure 51 | Distribution of molybdenum concentrations (mg/kg soil). The allocated value is the median of individual samples per site. The dataset presented comprises the BDM, NABO and GEMAS sampling sites. n = total number of sites, n a. S. = sites lying outside the axis range or whisker.

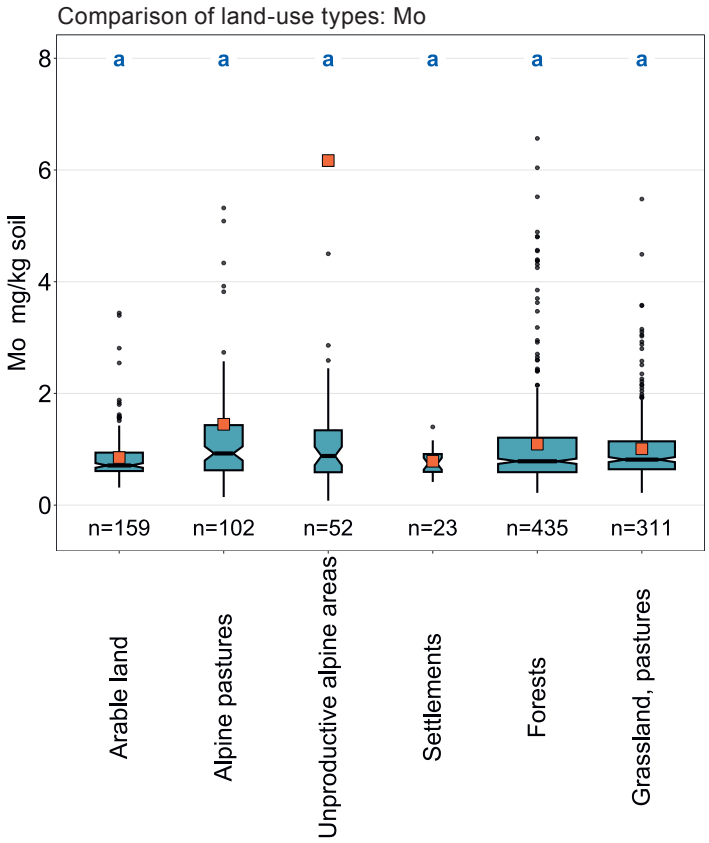

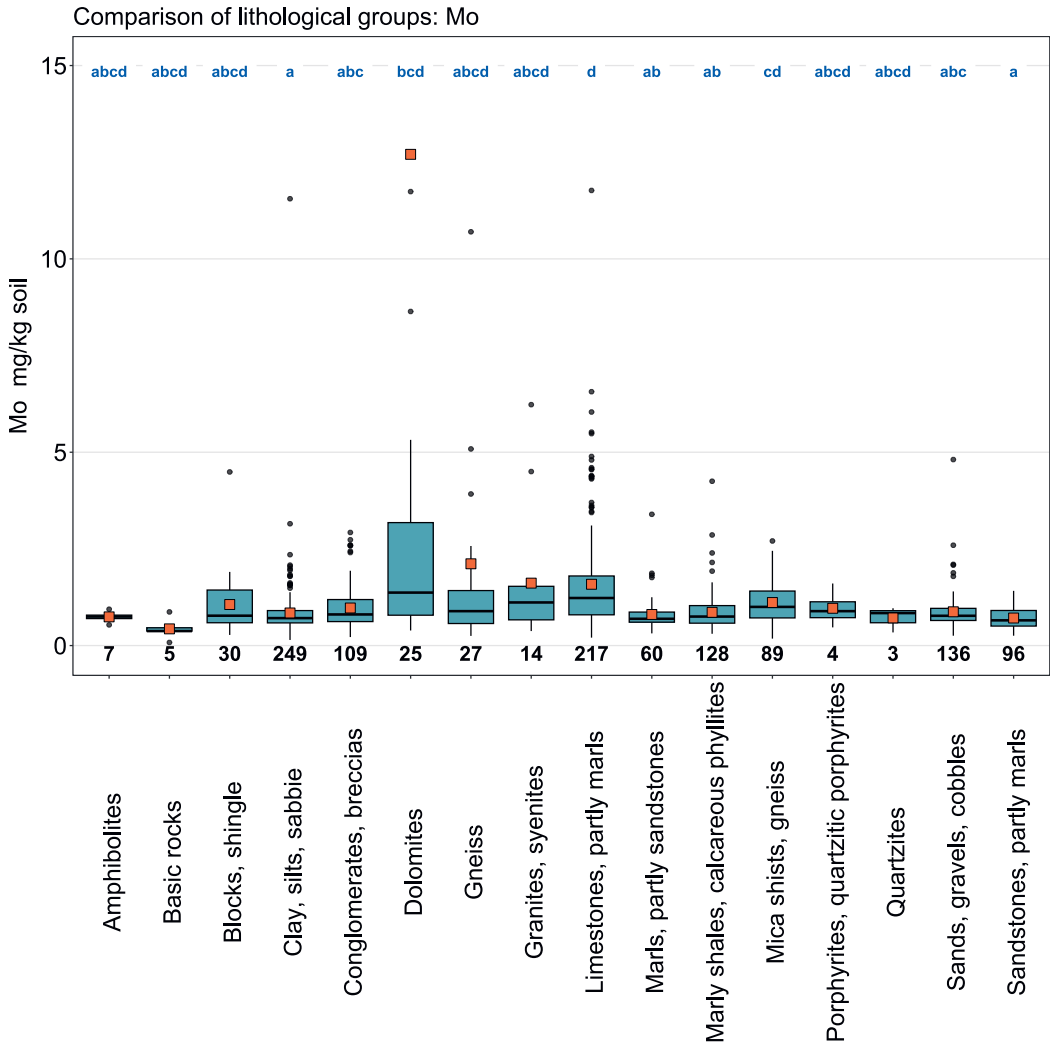

Figure 52 | Comparison of molybdenum concentrations (mg/kg soil) in relation to the Z9 land-use types of the BDM sampling sites (top) and the lithological and petrographic groups in the simplified map of near-surface mineral raw materials of Switzerland (1 : 500 000, swisstopo, bottom). The median of all individual samples per site was included in the data analysis (BDM, NABO and GEMAS datasets). The number of sites per group is indicated beneath the boxes. Letters in blue: significant differences between groups ($p < 0.001$) based on a Wilcoxon rank sum test with P-adjustment using the Benjamini and Hochberg method. Not all outliers are shown. Orange square: arithmetic mean of the data.

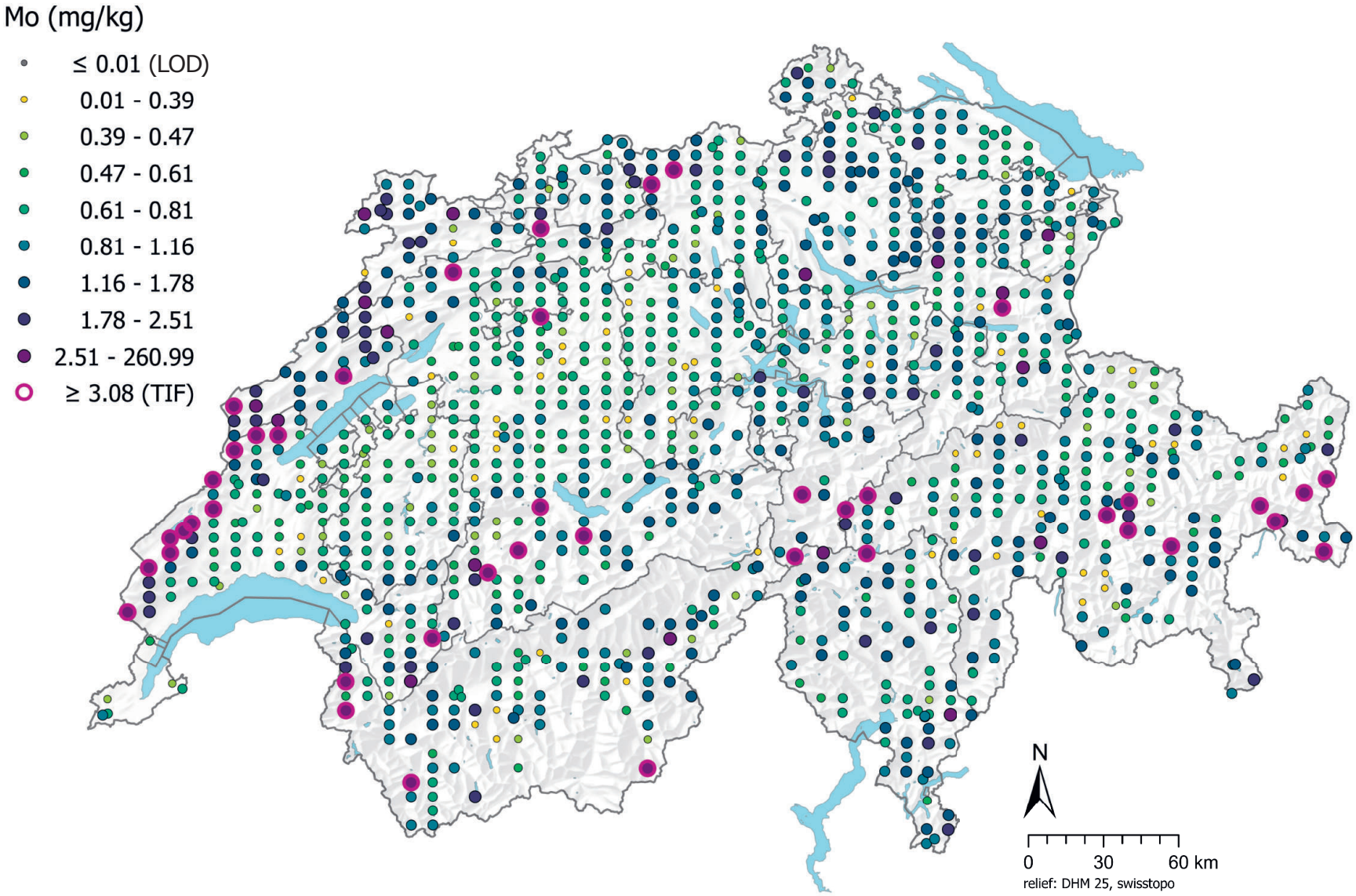

Figure 53 | **Spatial distribution of molybdenum concentrations (mg/kg soil) measured at the BDM, NABO and GEMAS sites. The data points show the median of several individual samples per site. The classes correspond to the 5 %, 10 %, 25 %, 50 %, 75 %, 90 % and 95 % percentiles. TIF: Tukey Inner Fence, outlier as per Reimann *et al.* (2018). LOD: limit of detection**

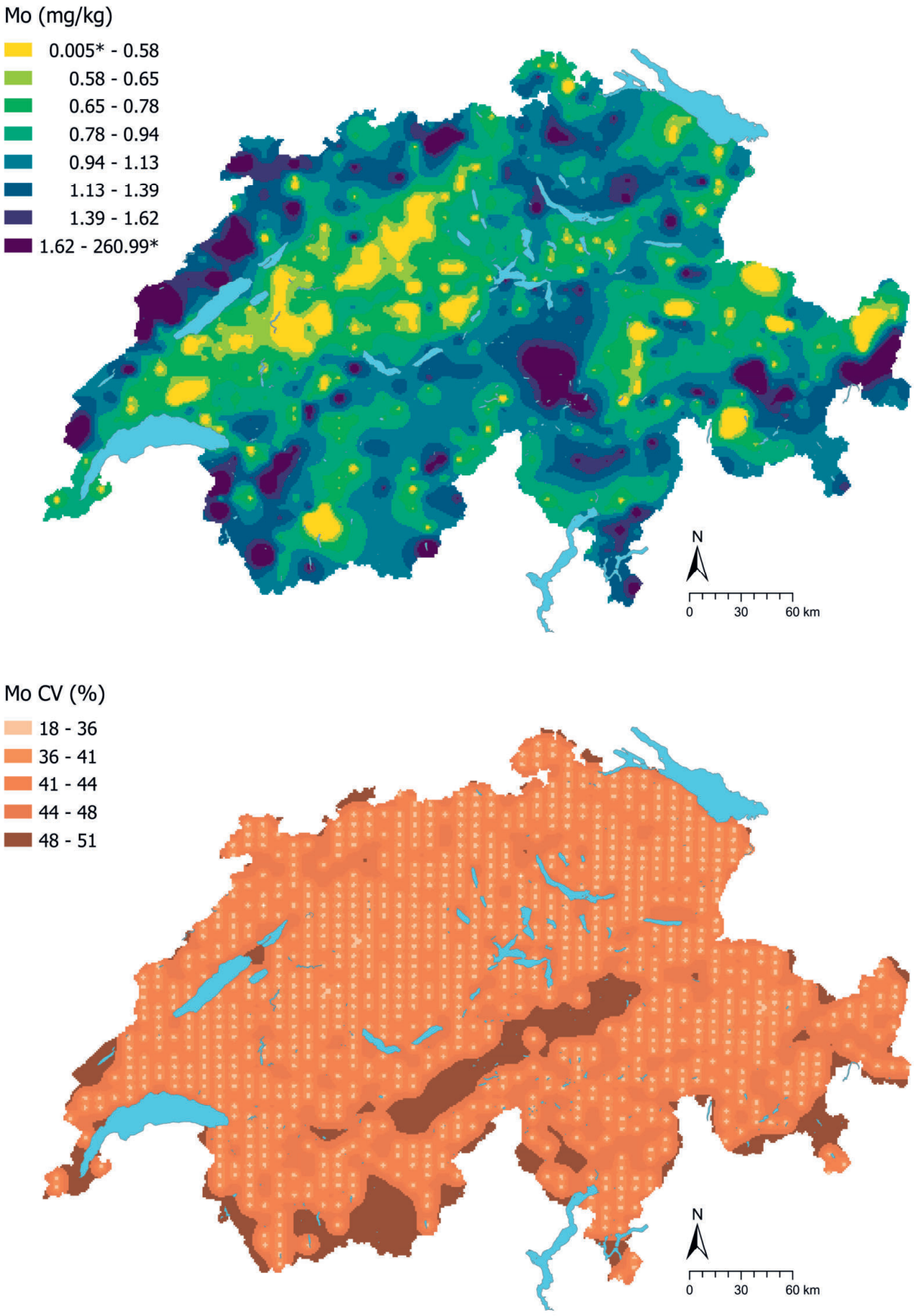

Figure 54 | Interpolated molybdenum concentrations (mg/kg soil) at the BDM, NABO and GEMAS sites (top) and coefficient of variation (%) of the interpolated concentrations (bottom). The concentrations were divided into eight classes corresponding to the 5 %, 10 %, 25 %, 50 %, 75 %, 90 % and 95 % percentiles. The coefficients of variation were divided into five classes corresponding to the Jenks Natural Breaks algorithm. The interpolation was performed using the ordinary Kriging method (1 km × 1 km grid). In the classes of interpolated values, * denotes the minimum and maximum value of the point data calculated from the limit of detection.

4.13 Sodium (Na)

Sodium is an alkali metal in group 1 of the periodic table. It is the sixth most abundant element, comprising 2.1 % by mass of the Earth's crust (Amelung *et al.*, 2018a; Amelung *et al.*, 2018b). Typical minerals of sodium include albite ($NaAlSi_3O_8$) and cryolite (Na_3AlF_6) (Reimann *et al.*, 2014). Bound sodium in the form of a salt, e.g. halite (NaCl), sodium carbonate (Na_2CO_3) and sodium nitrate ($NaNO_3$), is readily soluble and weathers rapidly under humid conditions (Amelung *et al.*, 2018a). Rock salt deposits in Switzerland are documented mainly in the north and in the Valais (Bex salt mines) (FGS, 2023b). Sodium oxide (Na_2O) is found in plagioclase, orthoclase, muscovite and, in smaller amounts, in amphibole. Alkaline syenites contain high sodium concentrations (up to 25 000 mg/kg). In contrast, ultramafic rock and limestone contain relatively small amounts of sodium (1500 mg/kg and 6000 mg/kg respectively) (Reimann *et al.*, 2014). This could be one reason why comparatively low sodium concentrations were measured at sites assigned to the 'limestone (with some marl)' group (Figure 56).

Sodium is widely used in industry, for example in paper and textiles, chemicals and metal processing. Furthermore, sodium compounds have replaced lead as an antiknock agent in petrol (Reimann *et al.*, 2014).

Since sodium is predominantly bound in feldspar, in soil the element occurs mainly in the silt fraction (Amelung *et al.*, 2018b). Sodium chloride (NaCl) enters soil through irrigation, fertilisers and application of road salt, although under humid climate conditions it rapidly leaches out – except when cation exchange causes the Na^+ cation to bind to clay minerals (Amelung *et al.*, 2018a). However, sodium chloride inputs mainly resulting from irrigation can accumulate in arid and semiarid soils and adversely affect plant growth (Amelung *et al.*, 2018b). Sodium can also enter soil via biowaste, seepage water from landfill sites and other wastewater sources (Reimann *et al.*, 2014).

The box plot for sodium concentrations shows that measurement data for the BDM soil samples have a limit of detection of 10 mg/kg (Figure 55). As a result of the low measurement resolution, the distribution of sodium concentrations is highly stepped. Although the median of 80 mg/kg is considerably higher than the median for European topsoils (arable sites: 48 mg/kg, grassland: 49.5 mg/kg), it nonetheless lies within the range of the 75 % quartile (Reimann *et al.*, 2014). In the Swiss-wide comparison, increased sodium concentrations were measured in the Central Alps, the Valais and on the south side of the Alps (Figure 57). In contrast, low concentrations were found in the foothills of the Alps. In north-western Switzerland, where numerous rock salt deposits have been documented, no elevated sodium concentrations were found in the topsoil.

Sodium is a micronutrient for animals, humans and many plants and has similar functions to potassium. However, high concentrations of the element in the form of salt can lead to osmotic stress and cause kidney damage and high blood pressure in humans (Amelung *et al.*, 2018a; Reimann *et al.*, 2014). Sugar beet and spinach are classified as natrophilic and contain more than ten times as much sodium in the dry matter as natrophobic plants such as maize, wheat and potatoes (Amelung *et al.*, 2018b). Topsoils at arable sites have significantly higher sodium concentrations than at grassland and forest sites (Figure 56). This difference between arable and grassland sites is not evident in the Europe-wide comparison (Reimann *et al.*, 2014).

Element	Symbol	Atomic number	Median	5 %	95 %
Sodium	Na	11	80 mg/kg	40 mg/kg	195 mg/kg

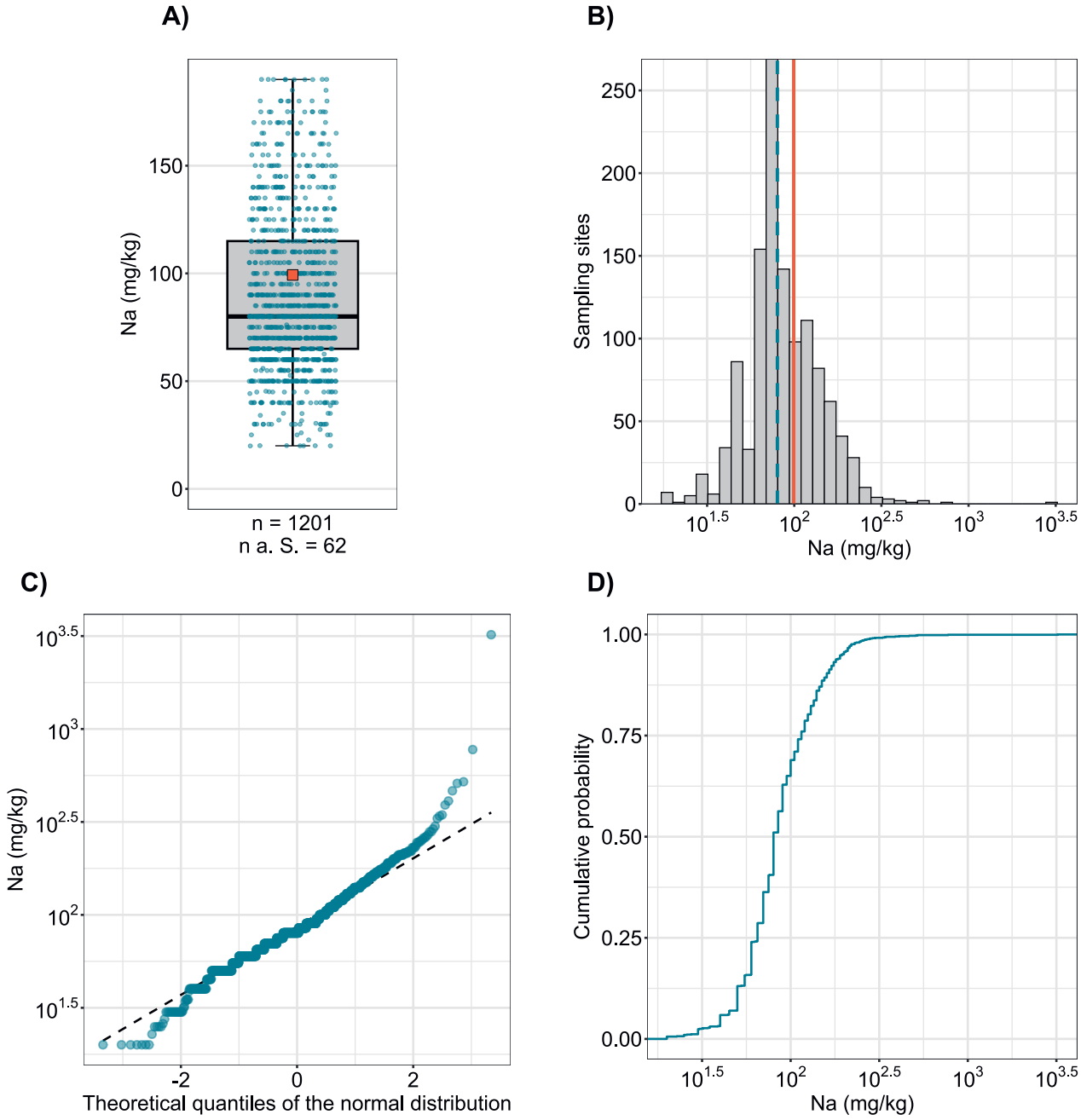

Figure 55 | Distribution of sodium concentrations (mg/kg soil). The allocated value is the median of individual samples per site. Measured values below the limit of detection were disregarded. The dataset presented comprises the BDM, NABO and GEMAS sampling sites. n = total number of sites, n a. S. = sites lying outside the axis range or whisker.

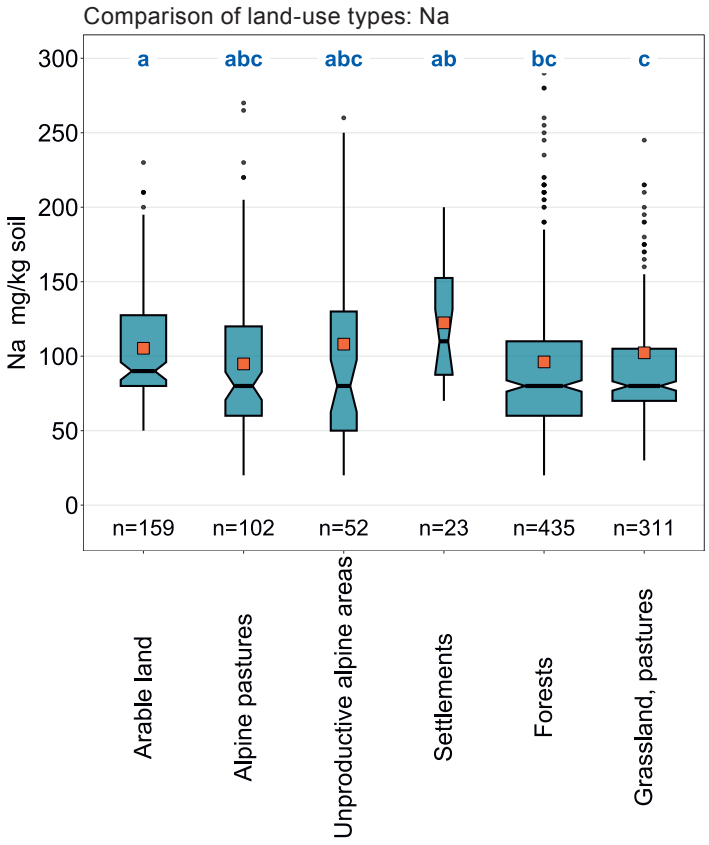

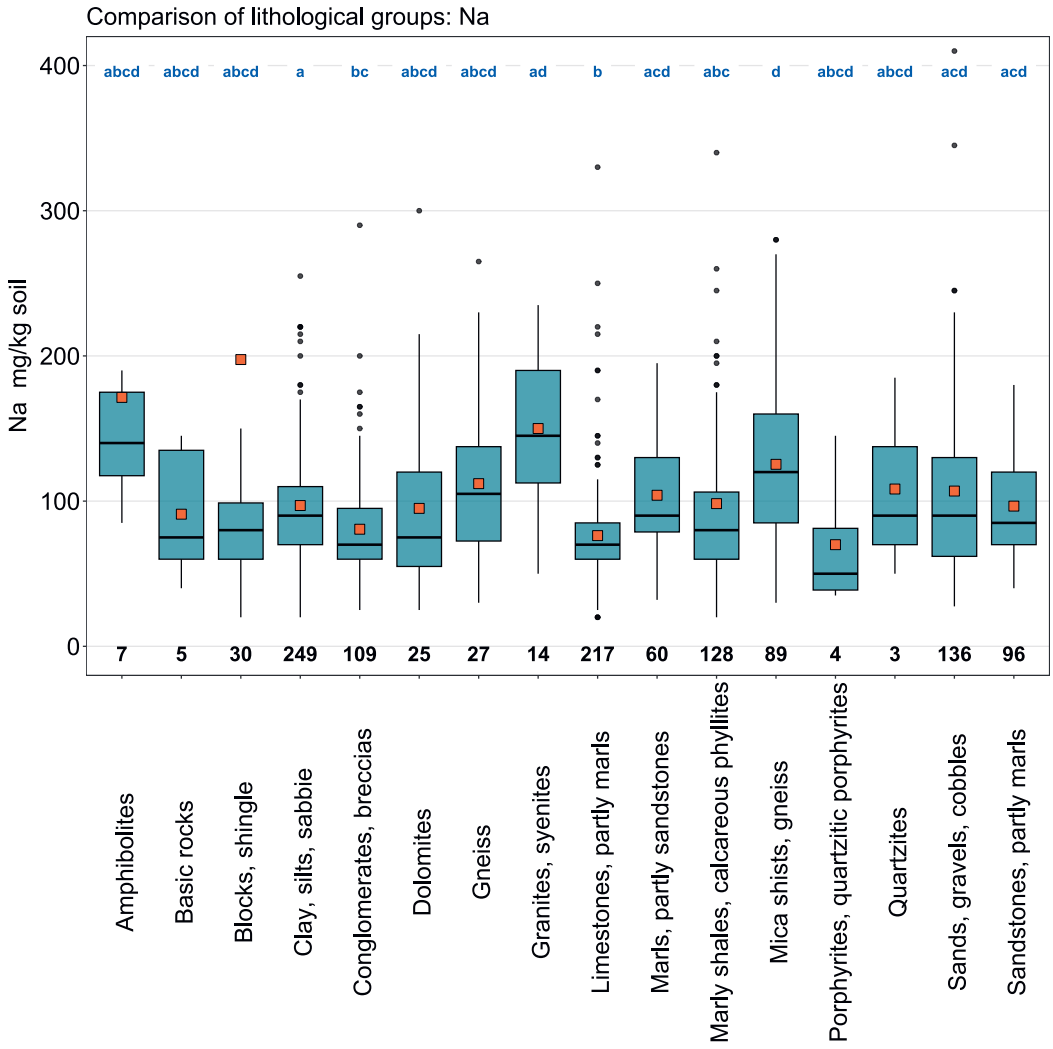

Figure 56 | **Comparison of sodium concentrations (mg/kg soil) in relation to the Z9 land-use types of the BDM sampling sites (top) and the lithological and petrographic groups in the simplified map of near-surface mineral raw materials of Switzerland (1 : 500 000, swisstopo, bottom). The median of all individual samples per site was included in the data analysis (BDM, NABO and GEMAS datasets). The number of sites per group is indicated beneath the boxes. Letters in blue: significant differences between groups ($p < 0.001$) based on a Wilcoxon rank sum test with P-adjustment using the Benjamini and Hochberg method. Not all outliers are shown. Orange square: arithmetic mean of the data.**

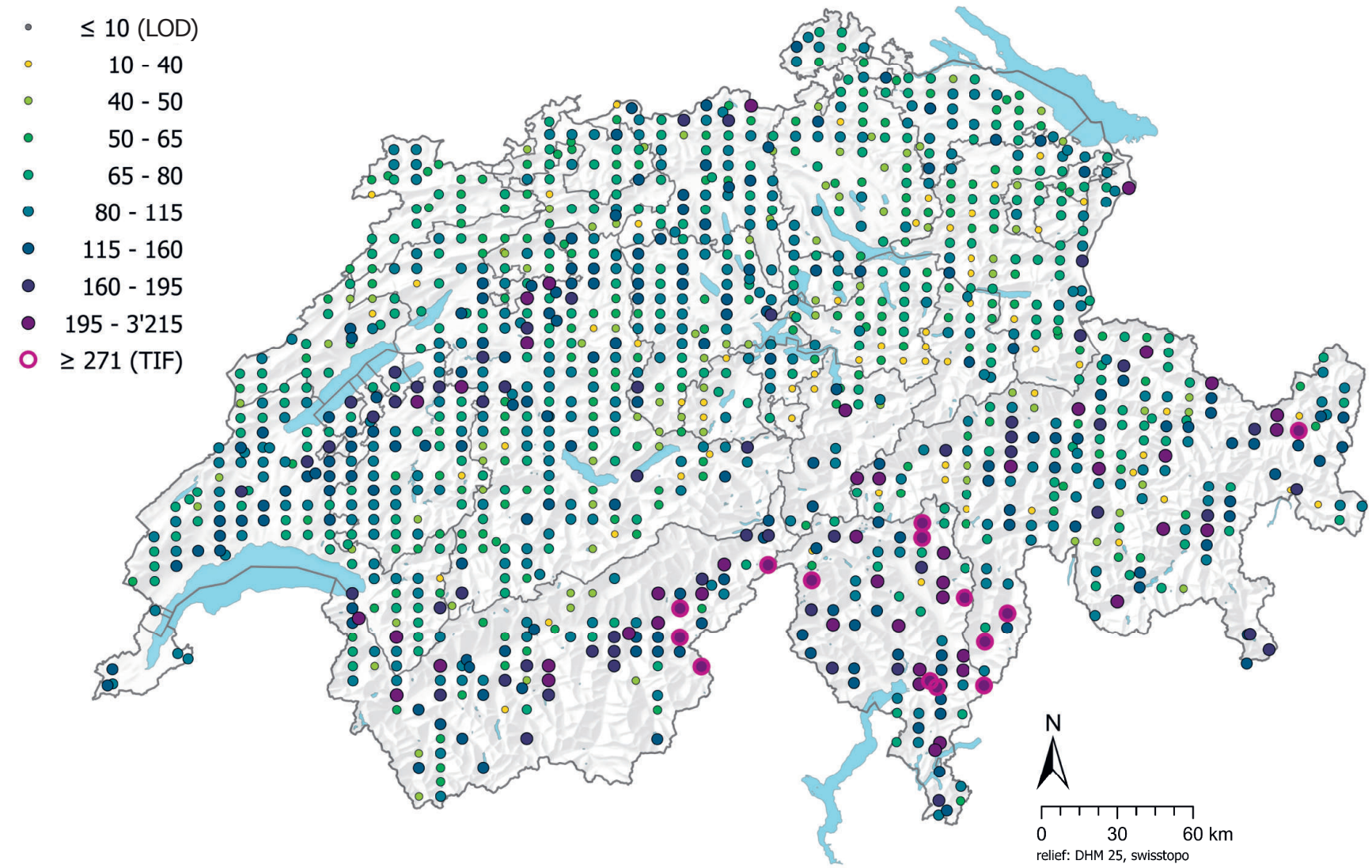

Figure 57 | **Spatial distribution of sodium concentrations (mg/kg soil) measured at the BDM, NABO and GEMAS sites. The data points show the median of several individual samples per site. 0.5 times the limit of detection (LOD) was assigned to measured values below the LOD. The classes correspond to the 5 %, 10 %, 25 %, 50 %, 75 %, 90 % and 95 % percentiles. TIF: Tukey Inner Fence, outlier as per Reimann *et al.* (2018). LOD: limit of detection**

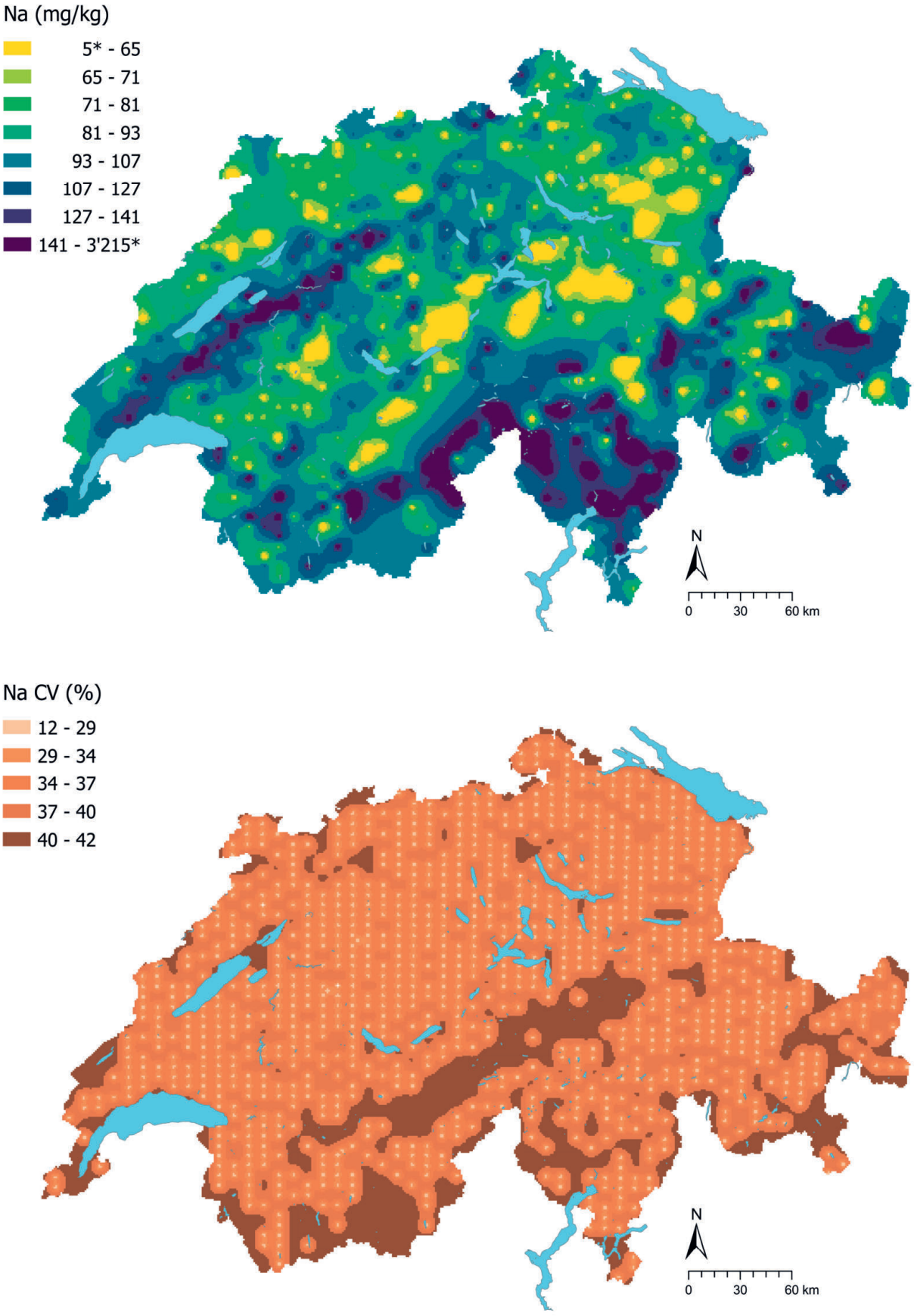

Figure 58 | Interpolated sodium concentrations (mg/kg soil) at the BDM, NABO and GEMAS sites (top) and coefficient of variation (%) of the interpolated concentrations (bottom). The concentrations were divided into eight classes corresponding to the 5 %, 10 %, 25 %, 50 %, 75 %, 90 % and 95 % percentiles. The coefficients of variation were divided into five classes corresponding to the Jenks Natural Breaks algorithm. The interpolation was performed using the ordinary Kriging method (1 km × 1 km grid). In the classes of interpolated values, * denotes the minimum and maximum value of the point data calculated from the limit of detection.

4.14 Nickel (Ni)

Nickel is a metal in group 10 of the periodic table. Minerals containing nickel as the main element include nickeline (NiAs), ullmannite (NiSbS) and kullerudite ($NiSe_2$) (Reimann *et al.*, 2014). Nickel exists in different types of bonds and frequently occurs as a trace element in iron- and magnesium-rich silicates such as olivine, pyroxene, biotite and amphibole (Tuchschmid, 1995). The strong accumulation of nickel in ultrabasic and basic rock could also explain elevated nickel concentrations at sites assigned to the basic rock lithological group (Figure 60). Nickel concentrations in soil-forming rocks in Switzerland typically range from 9.9 to 47.7 mg/kg (Tuchschmid, 1995). In geochemical terms, the element is closely related to cobalt (Tuchschmid, 1995), as seen from the correlations of measured concentrations (Chapter 6.1), the grouping of the two elements in the factor analysis (Chapter 6.2) and their similar spatial distribution (Figure 61). Measured concentrations tend to be higher in the Jura, the Randen Mountains and some regions of Grisons than in the Central and Southern Alps.

Nickel is used mainly in the steel industry (65 %) and in alloys (21 %) (Ma & Hooda, 2010). Nickel inputs to soil result from emissions from metal processing, coal- and oil-fired power plants, and sewage sludge effluent and mineral fertilisers (Gonnelli & Renella, 2013).

Nickel mobility in soil depends on pH, cation exchange capacity and redox conditions (Ma & Hooda, 2010). The element has the highest mobility under acid and oxidising conditions (Reimann *et al.*, 2014). The cation Ni^{2+} can adsorb to iron- and manganese (hydro)oxides, soil organic matter and clay minerals, although it has a lower affinity for sorption than Pb^{2+}, Cu^{2+} and Zn^{2+} (Ma & Hooda, 2010; Uren, 1992).

At 27.3 mg/kg, the median of the measured nickel concentrations (Table 2) lies within the range of typical soil concentrations (40 mg/kg) (Uren, 1992). As with chromium (Chapter 4.6), arable and grassland sites have significantly higher nickel levels in topsoil than alpine pastures, unproductive alpine areas and forests (Figure 60). This difference between arable and grassland areas compared with forest areas was also noted by Gubler *et al.* (2015) at the NABO sites. Mineral phosphate fertilisers contain nickel and chromium as impurities; average concentrations are 14.8 mg/kg and 89.5 mg/kg respectively (Nziguheba & Smolders, 2008). However, like chromium and cobalt, no changes to soil nickel concentrations were reported for the NABO sampling sites between 1985 and 2009 (Gubler *et al.*, 2015). The authors attributed the relatively constant concentrations to the mainly geological origin of the three elements.

Nickel is an essential element for many living organisms, although it can be highly toxic, depending on the speciation and oxidation state (Reimann *et al.*, 2014). The tolerance value for nickel concentrations in agricultural land is 100 mg/kg (Eikmann *et al.*, 1993). This value is exceeded at 17 sites. The toxicity of nickel largely depends on its solubility in soil (Ma & Hooda, 2010; Rooney *et al.*, 2007). In most cases, only 0.001 % of nickel in soil is present in soluble form, although nickel concentrations in the soil solution of serpentinite soils can be extremely high (Johnston & Proctor, 1981; Ma & Hooda, 2010; Uren, 1992).

Element	Symbol	Atomic number	Median	5 %	95 %
Nickel	Ni	28	27.3 mg/kg	6.2 mg/kg	63.9 mg/kg

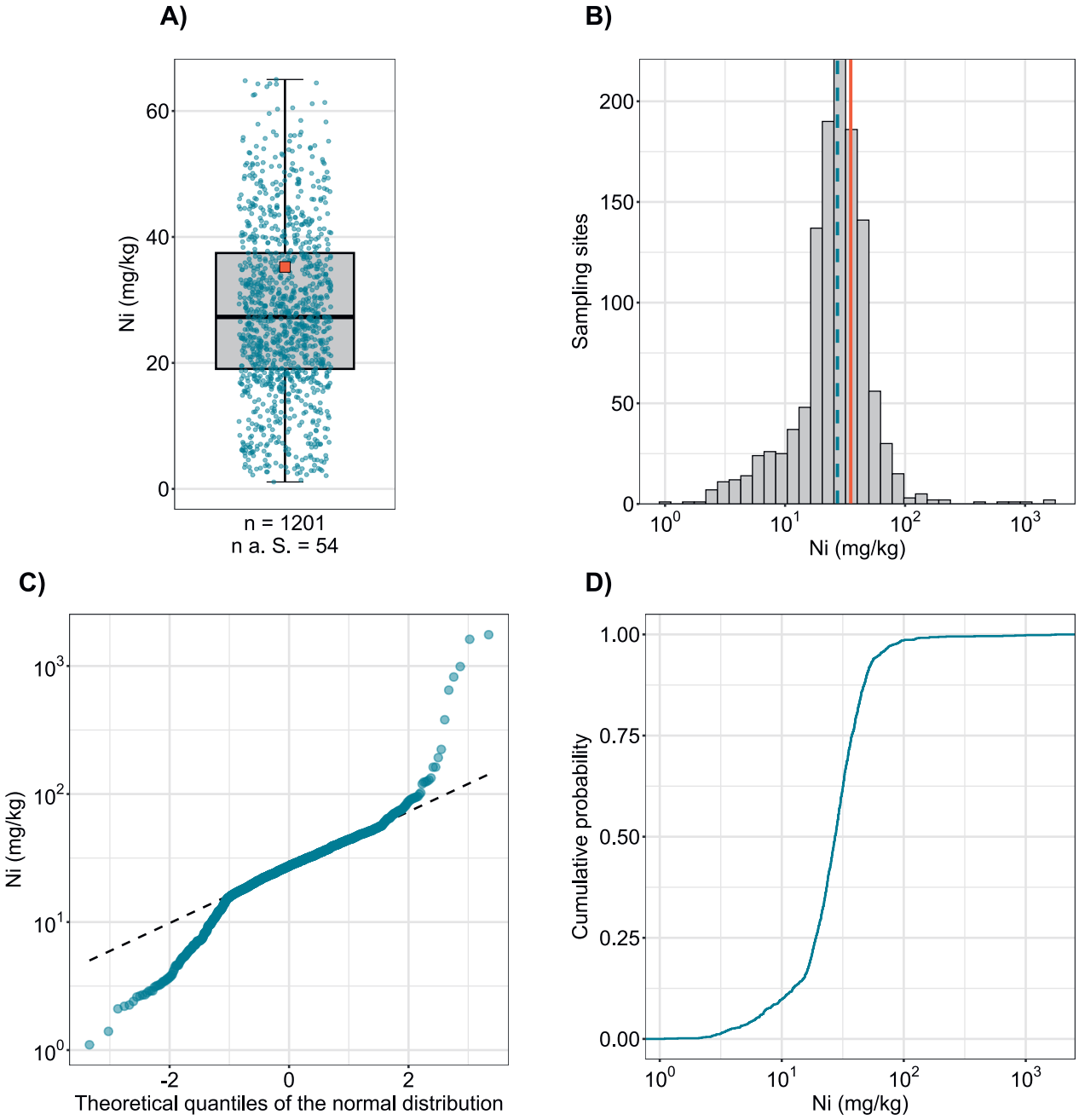

Figure 59 | **Distribution of nickel concentrations (mg/kg soil). The allocated value is the median of individual samples per site. The dataset presented comprises the BDM, NABO and GEMAS sampling sites. n = total number of sites, n a. S. = sites lying outside the axis range or whisker.**

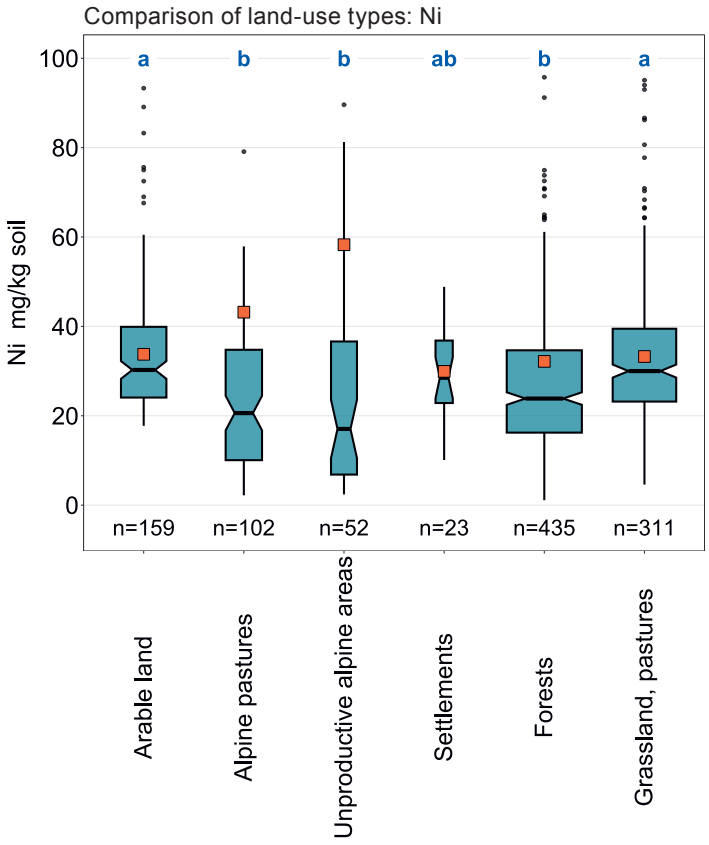

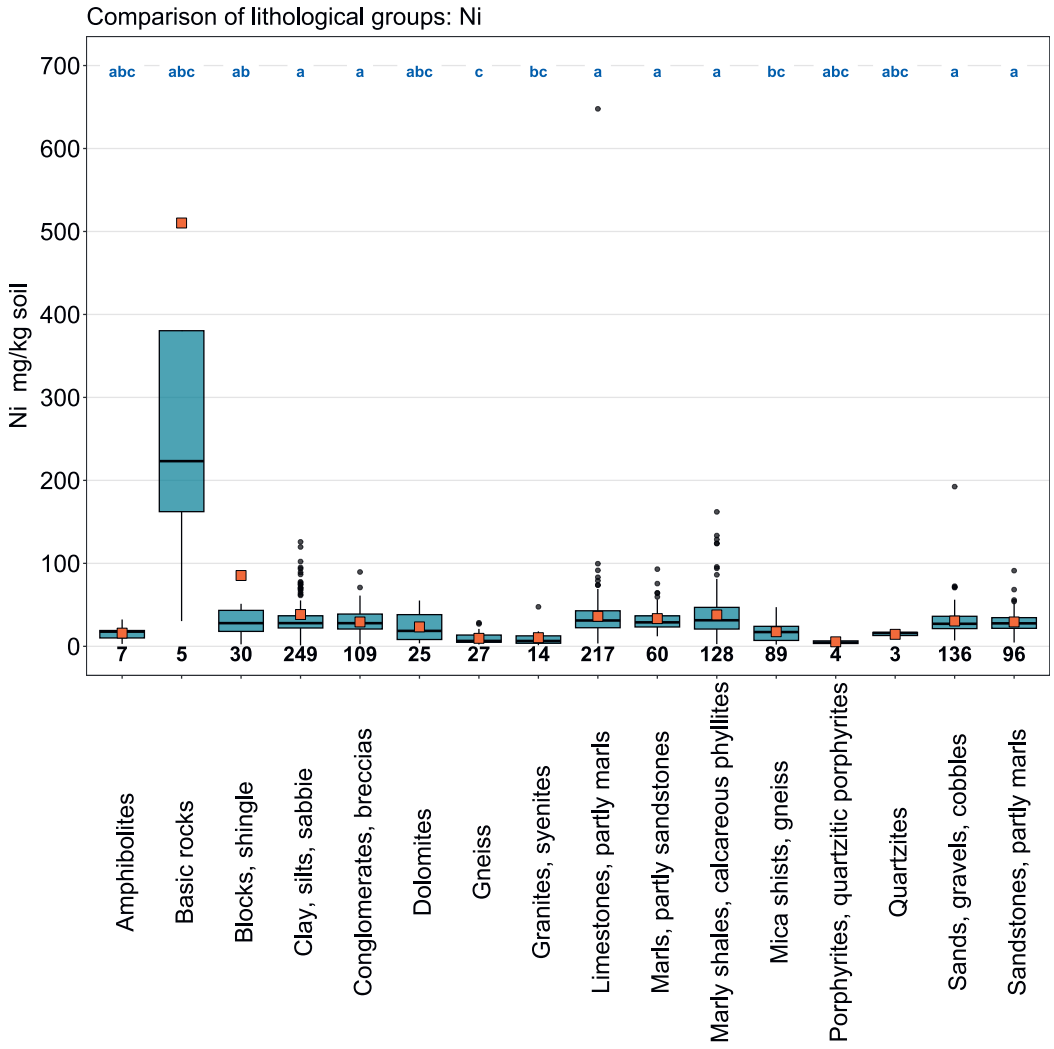

Figure 60 | Comparison of nickel concentrations (mg/kg soil) in relation to the Z9 land-use types of the BDM sampling sites (top) and the lithological and petrographic groups in the simplified map of near-surface mineral raw materials of Switzerland (1 : 500 000, swisstopo, bottom). The median of all individual samples per site was included in the data analysis (BDM, NABO and GEMAS datasets). The number of sites per group is indicated beneath the boxes. Letters in blue: significant differences between groups ($p < 0.001$) based on a Wilcoxon rank sum test with P-adjustment using the Benjamini and Hochberg method. Not all outliers are shown. Orange square: arithmetic mean of the data.

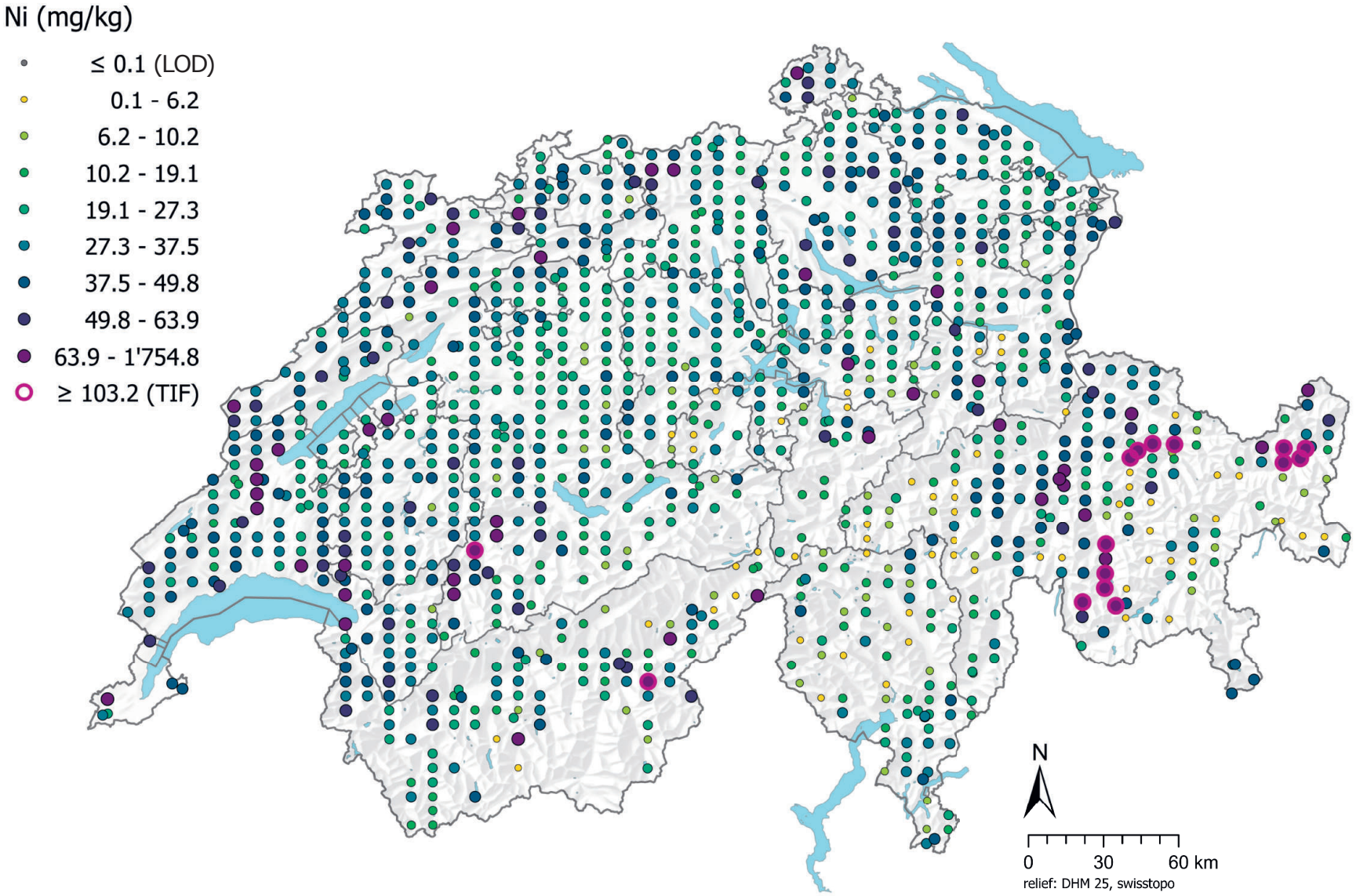

Figure 61 | **Spatial distribution of nickel concentrations (mg/kg soil) measured at the BDM, NABO and GEMAS sites. The data points show the median of several individual samples per site. The classes correspond to the 5 %, 10 %, 25 %, 50 %, 75 %, 90 % and 95 % percentiles. TIF: Tukey Inner Fence, outlier as per Reimann *et al.* (2018). LOD: limit of detection**

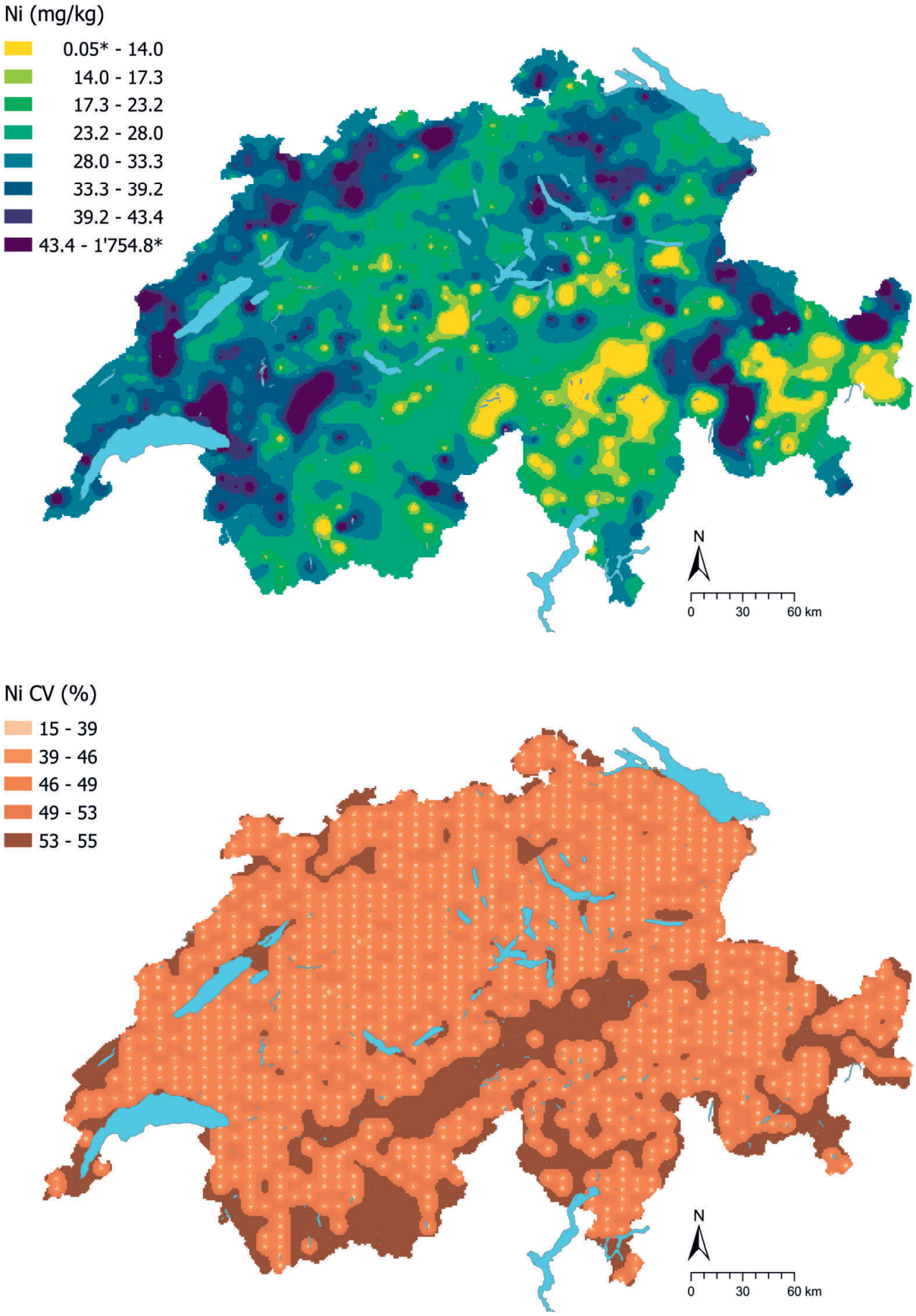

Figure 62 | Interpolated nickel concentrations (mg/kg soil) at the BDM, NABO and GEMAS sites (top) and coefficient of variation (%) of the interpolated concentrations (bottom). The concentrations were divided into eight classes corresponding to the 5 %, 10 %, 25 %, 50 %, 75 %, 90 % and 95 % percentiles. The coefficients of variation were divided into five classes corresponding to the Jenks Natural Breaks algorithm. The interpolation was performed using the ordinary Kriging method (1 km × 1 km grid). In the classes of interpolated values, * denotes the minimum and maximum value of the point data calculated from the limit of detection.

4.15 Mercury (Hg)

Mercury is a highly volatile metal in group 12 of the periodic table. Its main mineral is poorly soluble cinnabarite (HgS), also known as cinnabar (Clifford *et al.*, 2010). Along with this sulphide, mercury occurs as an auxiliary element in the mineral ores of copper, zinc, cadmium and lead, although only in small quantities in oxides and silicates. According to Tuchschmid (1995), rocks containing high levels of mercury (> 0.5 mg/kg) are confined to a few areas of Switzerland with bituminous claystone and coal deposits. Typical mercury concentrations in Swiss rocks range from 0.01 mg/kg (e.g. basic magmatite) to 0.5 mg/kg (claystone).

Humanity has used mercury for 3000 years, for example in goldmining, and more recently in incandescent lightbulbs, batteries and the chemical industry (Reimann *et al.*, 2014). In Europe, airborne mercury emissions mainly stem from combustion processes (including fossil fuels), cement works, metal processing and caustic soda production (Clifford *et al.*, 2010; Pacyna *et al.*, 2006). Atmospheric deposition of these emissions can play a major role in mercury accumulation in soil and its re-release (Fitzgerald *et al.*, 2007). However, this deposition has declined significantly in Switzerland in recent years (BAFU, 2018). Application of sewage sludge, slag and pesticides is another possible (historical) source of mercury inputs to soil (Reimann *et al.*, 2014; Suess *et al.*, 2020).

The mobility of mercury in soil largely depends on pH, redox conditions and soil organic matter content (Clifford *et al.*, 2010). Sorption of Hg^{2+} to soil organic matter, especially under acid conditions, is the main mechanism for immobilising mercury; sorption to clay minerals and iron oxides becomes more significant with increasing pH (Clifford *et al.*, 2010; Gilli *et al.*, 2018). Mercury in soil can also form complexes with chlorine, precipitate with sulphide as HgS under reducing conditions, or occur in organic form (Clifford *et al.*, 2010; Gilli *et al.*, 2018).

The approximated log-normal distribution of mercury concentrations in topsoil shows two outliers in the upper concentration range with mercury levels above 2 mg/kg (Figure 63). Comparatively high mercury concentrations are found in the western Jura and on the south side of the Alps, with hotspots in the eastern foothills of the Alps and the Swiss Plateau (Figure 65). The highest statistically significant mercury concentrations in topsoil were recorded at forest sites (Figure 64). This could be due to mercury accumulation through sorption to soil organic matter, as forest sites contain higher concentrations of organic carbon than other land-use types and also have a lower pH (Chapters 5.2 and 5.1). Furthermore, the 'vegetation pump' (Jiskra *et al.*, 2018) – the mechanism where atmospheric mercury is absorbed by trees, then incorporated into the biomass from where it enters the soil through fallen leaves – could lead to an accumulation of mercury in forest soils.

The non-essential element mercury is toxic even in small quantities, with the chemical speciation being the determining factor: the body effectively absorbs less than 0.01 % of ingested elemental mercury as opposed to around 95 % of its organic form, methylmercury (Clifford *et al.*, 2010). Measured total concentrations in Swiss topsoils are significantly below the tolerance value for agricultural land of 10 mg/kg (Eikmann *et al.*, 1993).

Element	Symbol	Atomic number	Median	5 %	95 %
Mercury	Hg	80	0.066 mg/kg	0.027 mg/kg	0.180 mg/kg

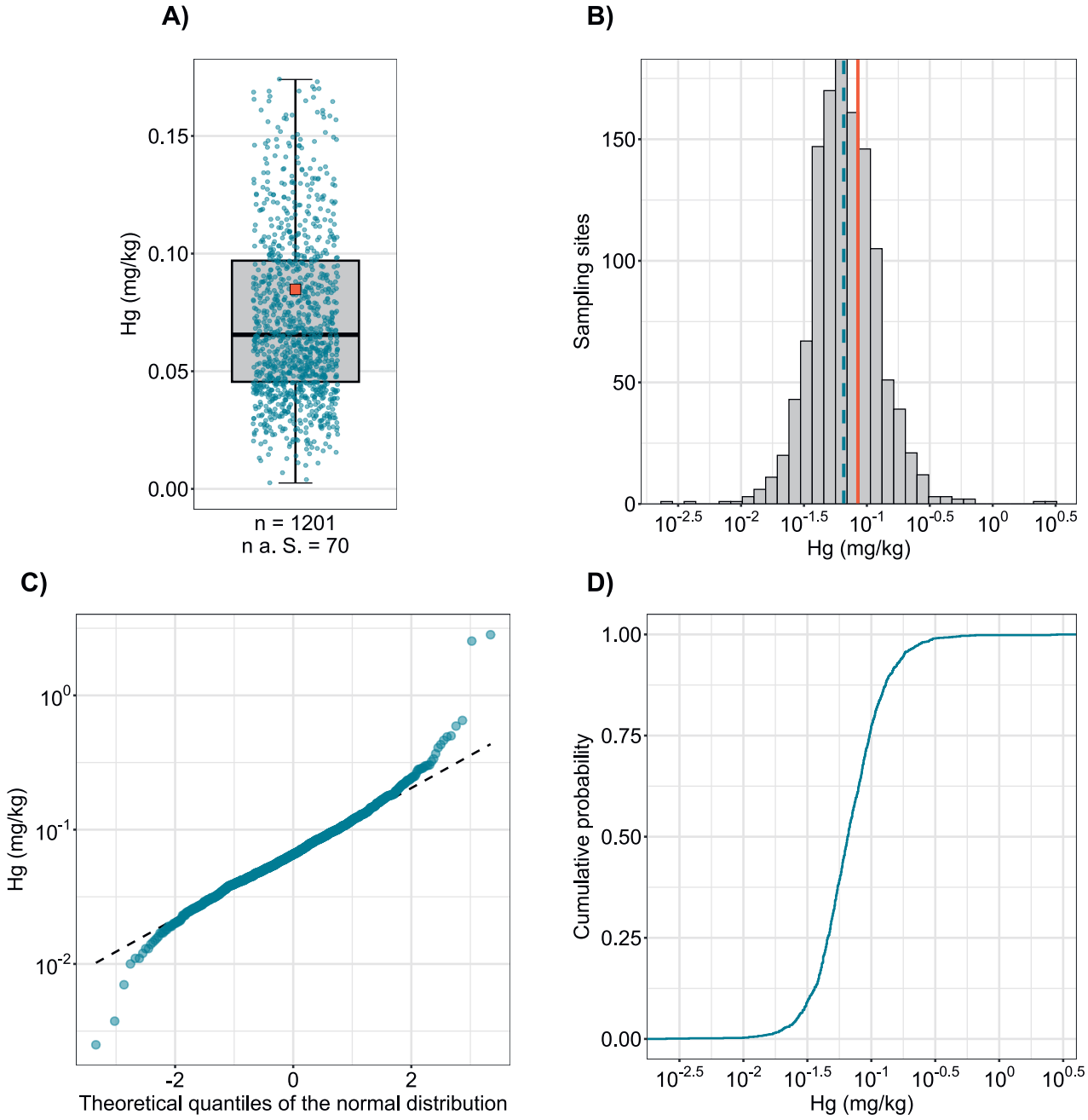

Figure 63 | Distribution of mercury concentrations (mg/kg soil). The allocated value is the median of individual samples per site. Measured values below the limit of detection were disregarded. The dataset presented comprises the BDM, NABO and GEMAS sampling sites. n = total number of sites, n a. S. = sites lying outside the axis range or whisker.

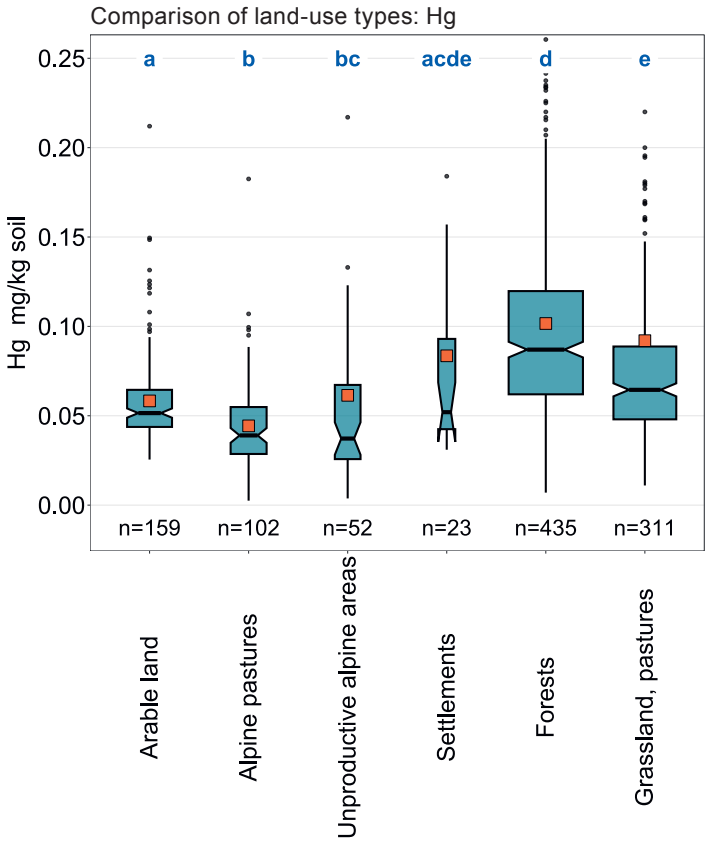

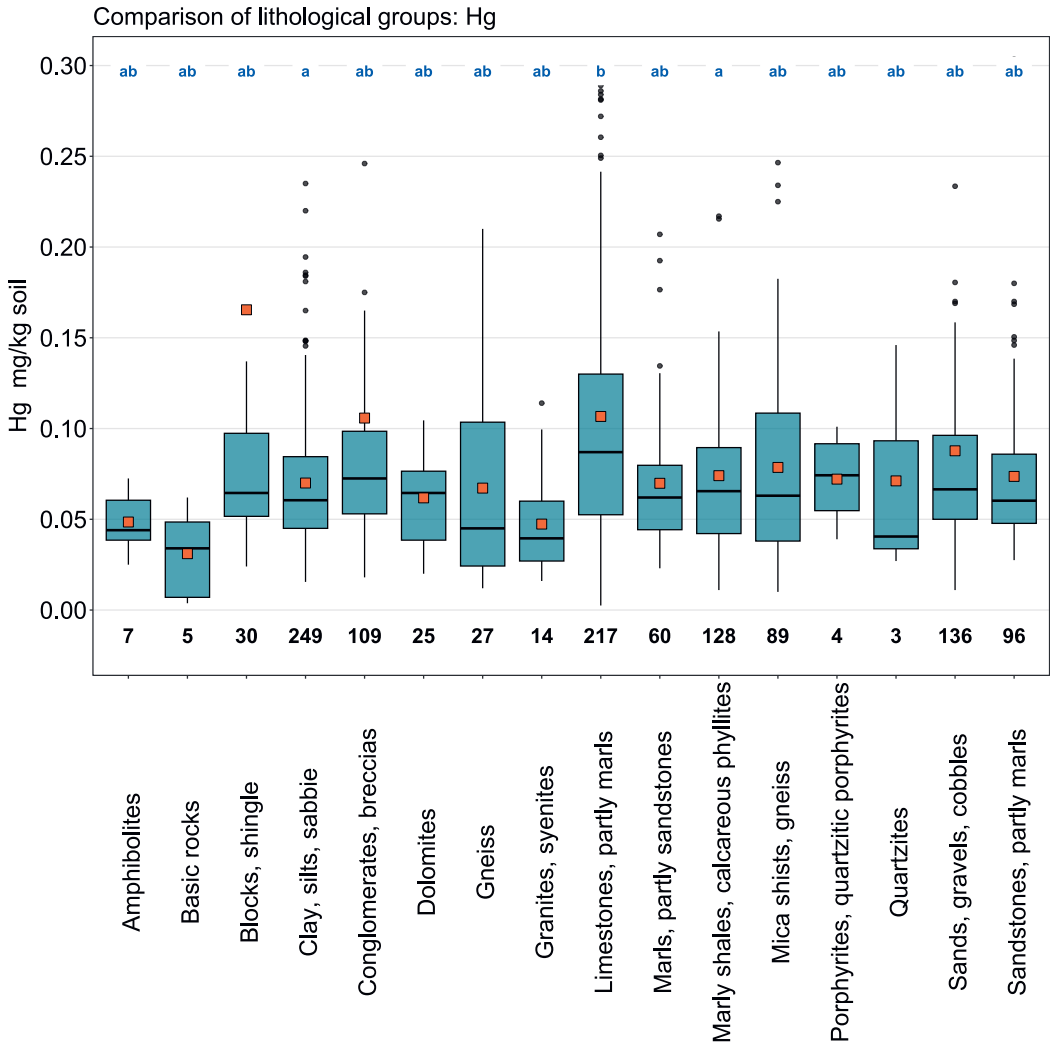

Figure 64 | **Comparison of mercury concentrations (mg/kg soil) in relation to the Z9 land-use types of the BDM sampling sites (top)and the lithological and petrographic groups in the simplified map of near-surface mineral raw materials of Switzerland (1 : 500 000, swisstopo, bottom). The median of all individual samples per site was included in the data analysis (BDM, NABO and GEMAS datasets). The number of sites per group is indicated beneath the boxes. Letters in blue: significant differences between groups ($p < 0.001$) based on a Wilcoxon rank sum test with P-adjustment using the Benjamini and Hochberg method. Not all outliers are shown. Orange square: arithmetic mean of the data.**

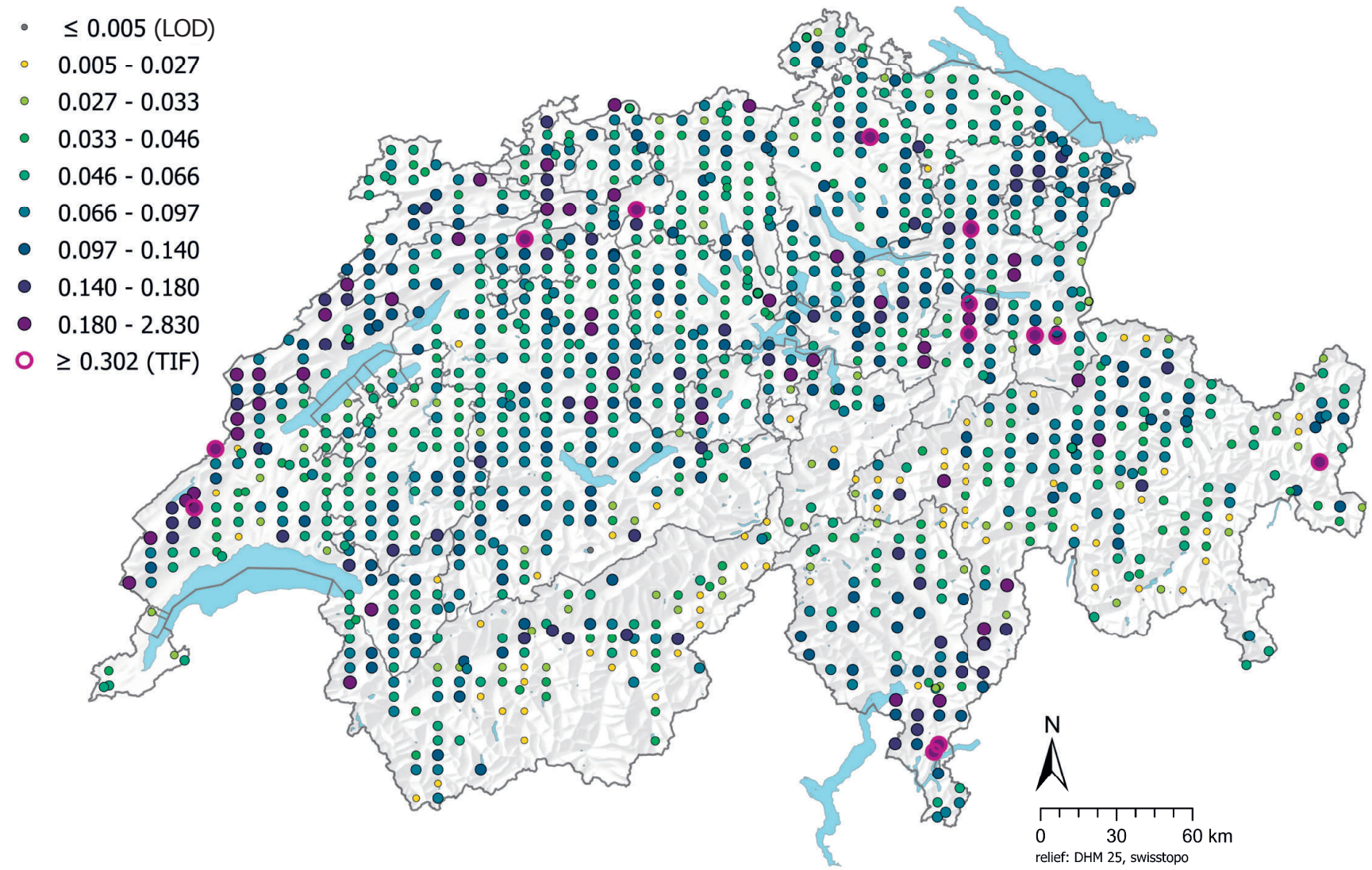

Figure 65 | **Spatial distribution of mercury concentrations (mg/kg soil) measured at the BDM, NABO and GEMAS sites. The data points show the median of several individual samples per site. 0.5 times the limit of detection (LOD) was assigned to measured values below the LOD. The classes correspond to the 5 %, 10 %, 25 %, 50 %, 75 %, 90 % and 95 % percentiles. TIF: Tukey Inner Fence, outlier as per Reimann *et al.* (2018). LOD: limit of detection**

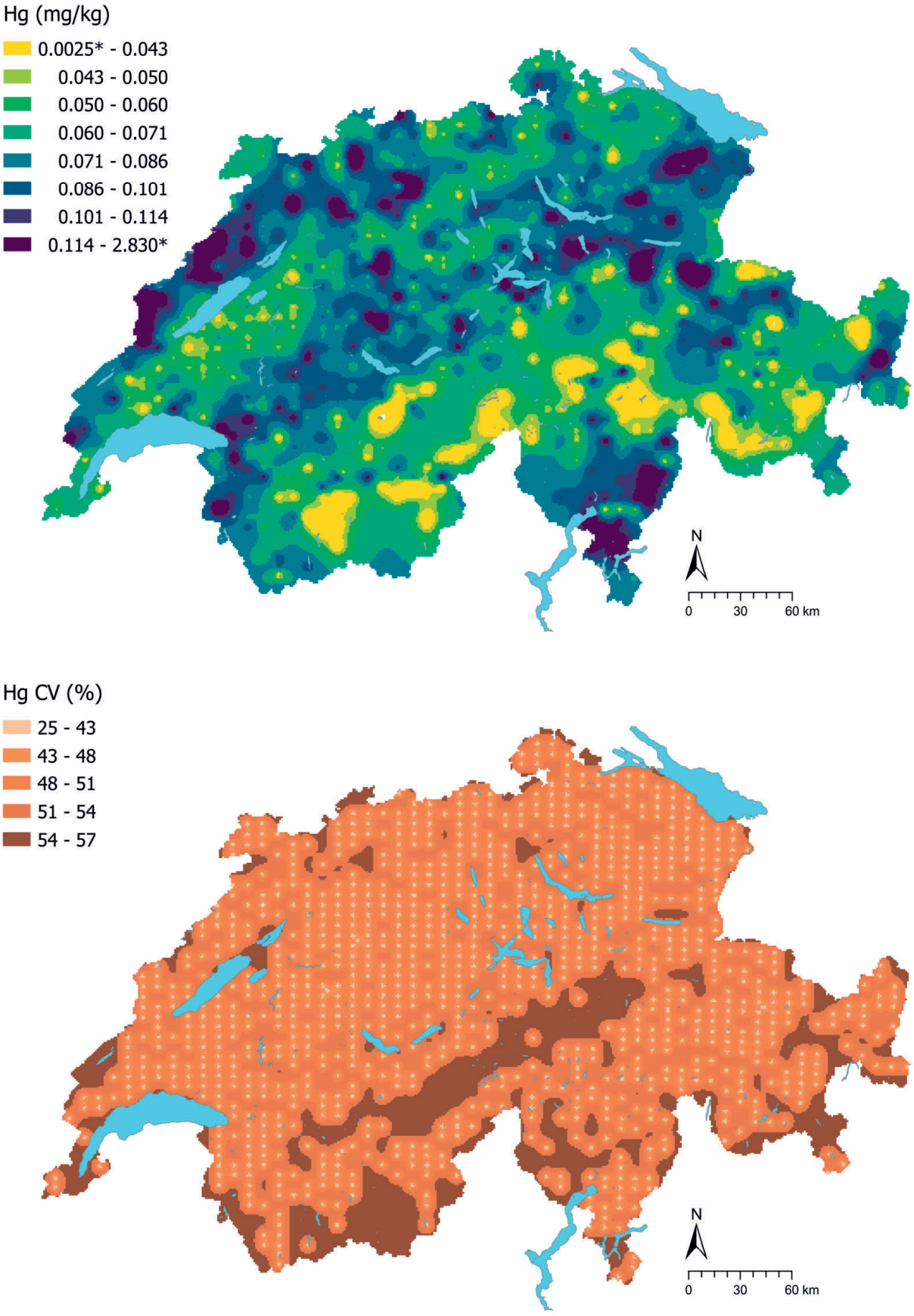

Figure 66 | Interpolated mercury concentrations (mg/kg soil) at the BDM, NABO and GEMAS sites (top) and coefficient of variation (%) of the interpolated concentrations (bottom). The concentrations were divided into eight classes corresponding to the 5 %, 10 %, 25 %, 50 %, 75 %, 90 % and 95 % percentiles. The coefficients of variation were divided into five classes corresponding to the Jenks Natural Breaks algorithm. The interpolation was performed using the ordinary Kriging method (1 km × 1 km grid). In the classes of interpolated values, * denotes the minimum and maximum value of the point data calculated from the limit of detection.

4.16 Sulphur (S)

Sulphur is an essential non-metal in group 16 of the periodic table. Sulphur-bearing minerals include sulphates, e.g. gypsum ($CaSO_4 \cdot 2H_2O$) and anhydrite ($CaSO_4$), and sulphides, e.g. pyrite (FeS_2) and galena (PbS) (Reimann *et al.*, 2014). Sulphur also occurs in silicates such as feldspar, mica, amphibole and pyroxene, but the highest concentrations are found in black shale and coal due to the element's association with soil organic matter (Reimann *et al.*, 2014).

Sulphur is released during combustion of coal and oil, metal extraction and refining processes, cellulose production, chemical processes to produce sulphuric acid, tanning processes and the use of sulphurous pesticides (Brown, 1982; Reimann *et al.*, 2014). Before the introduction of desulphurisation plants, sulphur emissions led to respiratory problems, acid rain and excess sulphur in the soil (Amelung *et al.*, 2018b).

The sulphur content in soil is generally 100 to 1200 mg/kg (Amelung *et al.*, 2018a). Sulphur in topsoils is mainly organically bound (80–98 %; Amelung *et al.*, 2018; Eriksen, 2009). This is evident from the correlation of measured sulphur concentrations with organic carbon ($R^2 = 0.73$) and total nitrogen ($R^2 = 0.86$), and also the grouping of these parameters in the factor analysis (Chapters 6.1 and 6.2). The remaining fraction of sulphur in soil occurs in inorganic form, mainly as sulphates or, under reducing conditions, as sulphides, which can precipitate with trace elements, e.g. with iron to form insoluble pyrite (Brown, 1982; Tack, 2010). Sulphates can be adsorbed to soil constituents, e.g. iron and aluminium (hydro)oxides, or precipitate with calcium carbonate. Around 1 to 10 % of total sulphur in the soil is present in the form of readily soluble sulphate, which can be leached out or taken up by plants; sulphur-deficient soils generally contain less than 10 mg/kg of soluble sulphate (Brown, 1982).

The median sulphur concentration in Swiss topsoils lies within a range that has been previously reported for soils (350 mg/kg, Table 2). In the Europe-wide comparison, measured sulphur concentrations are slightly elevated; the median is above the 75 % quartile for arable sites (322 mg/kg) (Reimann *et al.*, 2014). Sites with the lowest sulphur concentrations are found mainly in the Swiss Plateau in regions important for agricultural production (Figure 69). Arable sites were also found to have significantly lower sulphur concentrations than grassland and alpine pastures (Figure 68). A difference between grassland and arable sites was also observed in the European geochemical soil atlas (median 295 mg/kg and 207 mg/kg respectively) (Reimann *et al.*, 2014). Since sulphur is strongly associated with soil organic matter, the fact that arable sites have lower concentrations of organic carbon is assumed to be the main reason for the difference in concentration (Chapter 5.2) (Bhupinderpal *et al.*, 2004).

Sulphur is an important micronutrient. Sulphur deficiency can make plants more susceptible to fungal diseases (Amelung *et al.*, 2018b). However, some sulphur compounds can be toxic to plants and animals, either directly or through the formation of sulphuric acid (Brown, 1982). Due to the low plant-available sulphur concentrations in combination with a significant decline in sulphur dioxide emissions in recent decades in Switzerland (BAFU, 2022), sulphur deficiency can be assumed to be more prevalent than toxicity in Swiss soils, as also observed at global level (Eriksen, 2009).

Element	Symbol	Atomic number	Median	5 %	95 %
Sulphur	S	16	350 mg/kg	129 mg/kg	900 mg/kg

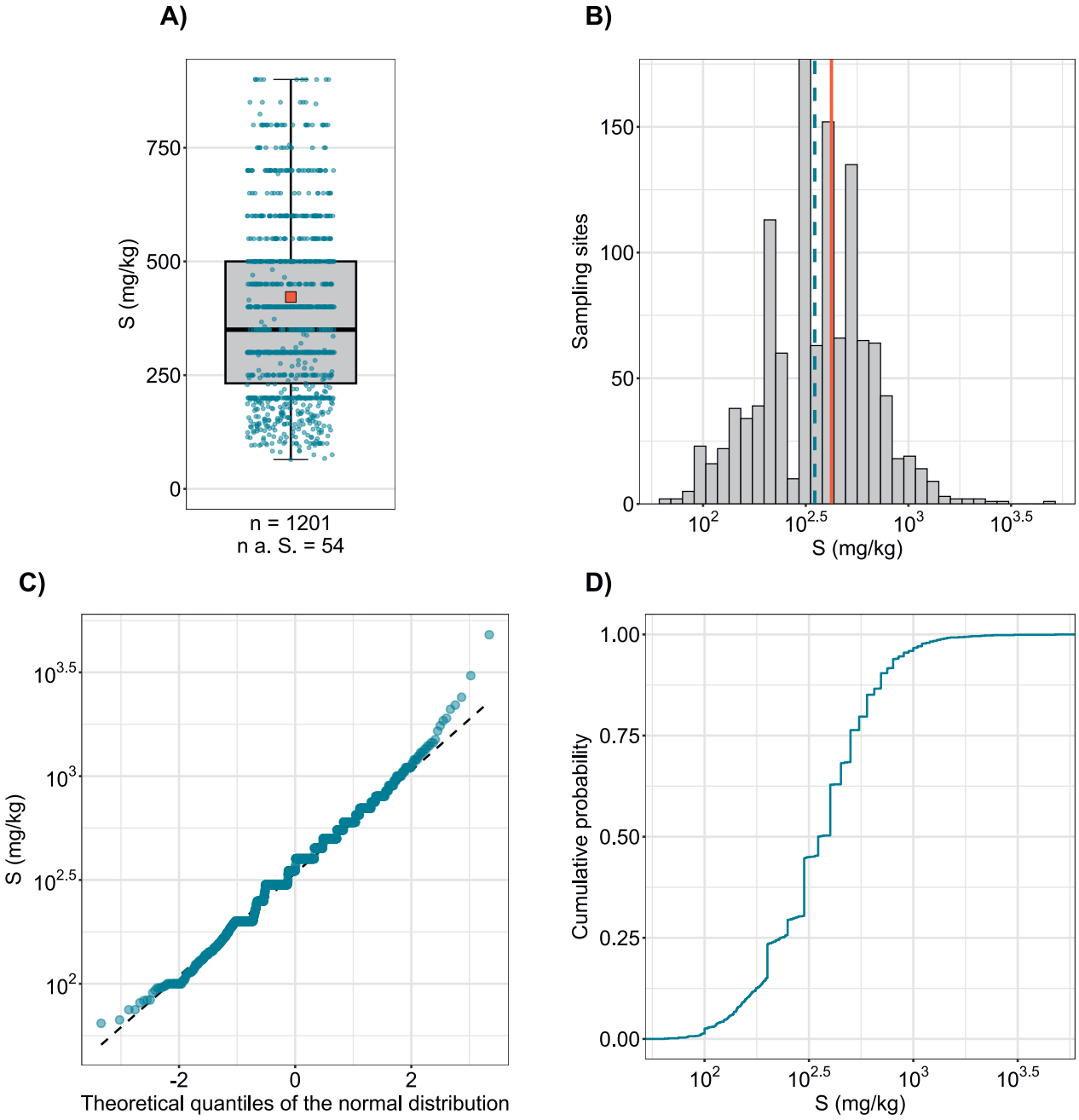

Figure 67 | **Distribution of sulphur concentrations (mg/kg soil). The allocated value is the median of individual samples per site. The dataset presented comprises the BDM, NABO and GEMAS sampling sites. n = total number of sites, n a. S. = sites lying outside the axis range or whisker.**

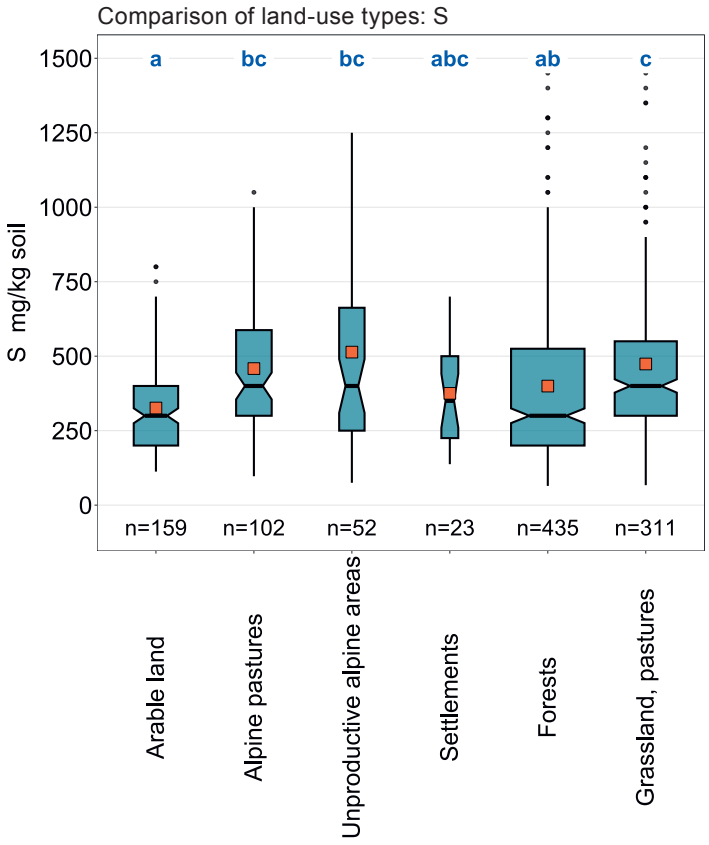

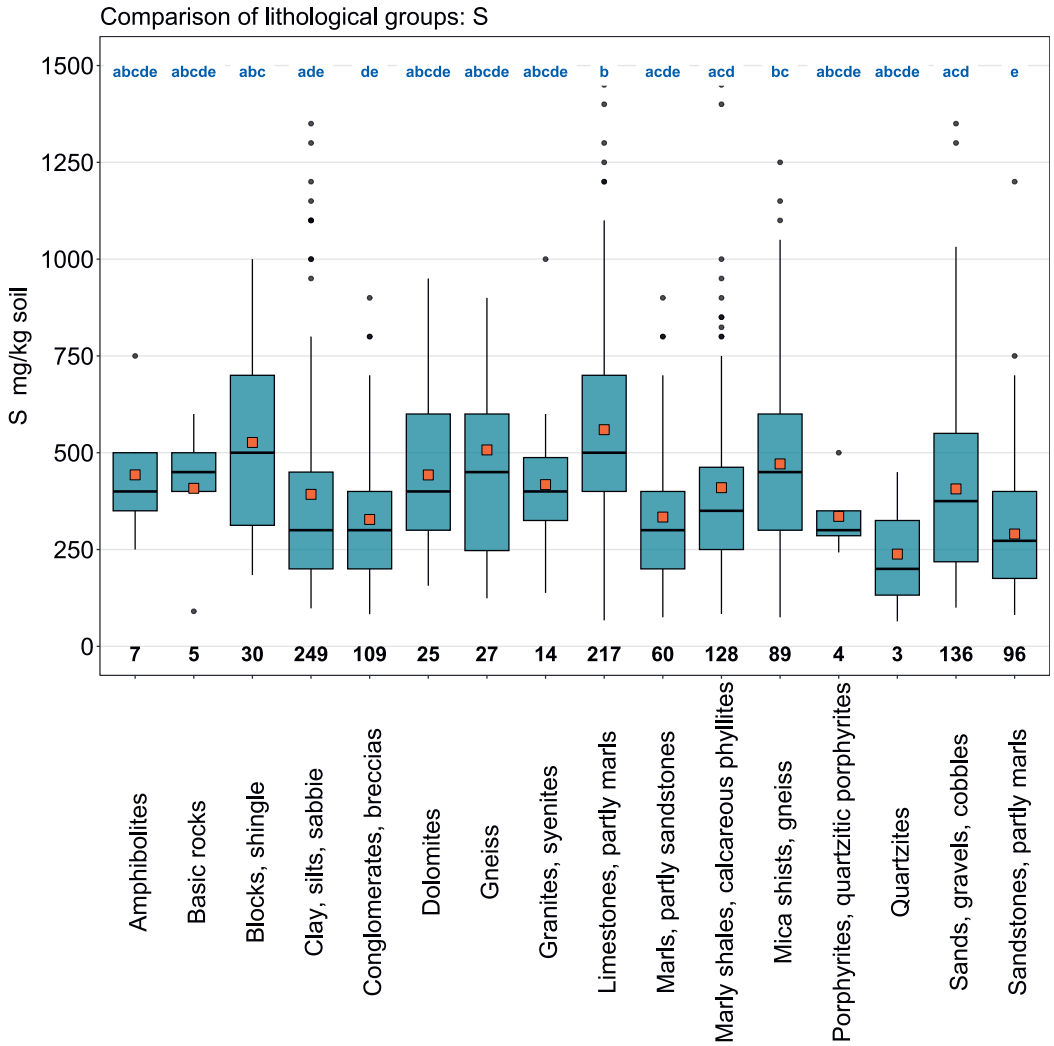

Figure 68 | **Comparison of sulphur concentrations (mg/kg soil) in relation to the Z9 land-use types of the BDM sampling sites (top) and the lithological and petrographic groups in the simplified map of near-surface mineral raw materials of Switzerland (1 : 500 000, swisstopo, bottom). The median of all individual samples per site was included in the data analysis (BDM, NABO and GEMAS datasets). The number of sites per group is indicated beneath the boxes. Letters in blue: significant differences between groups ($p < 0.001$) based on a Wilcoxon rank sum test with P-adjustment using the Benjamini and Hochberg method. Not all outliers are shown. Orange square: arithmetic mean of the data.**

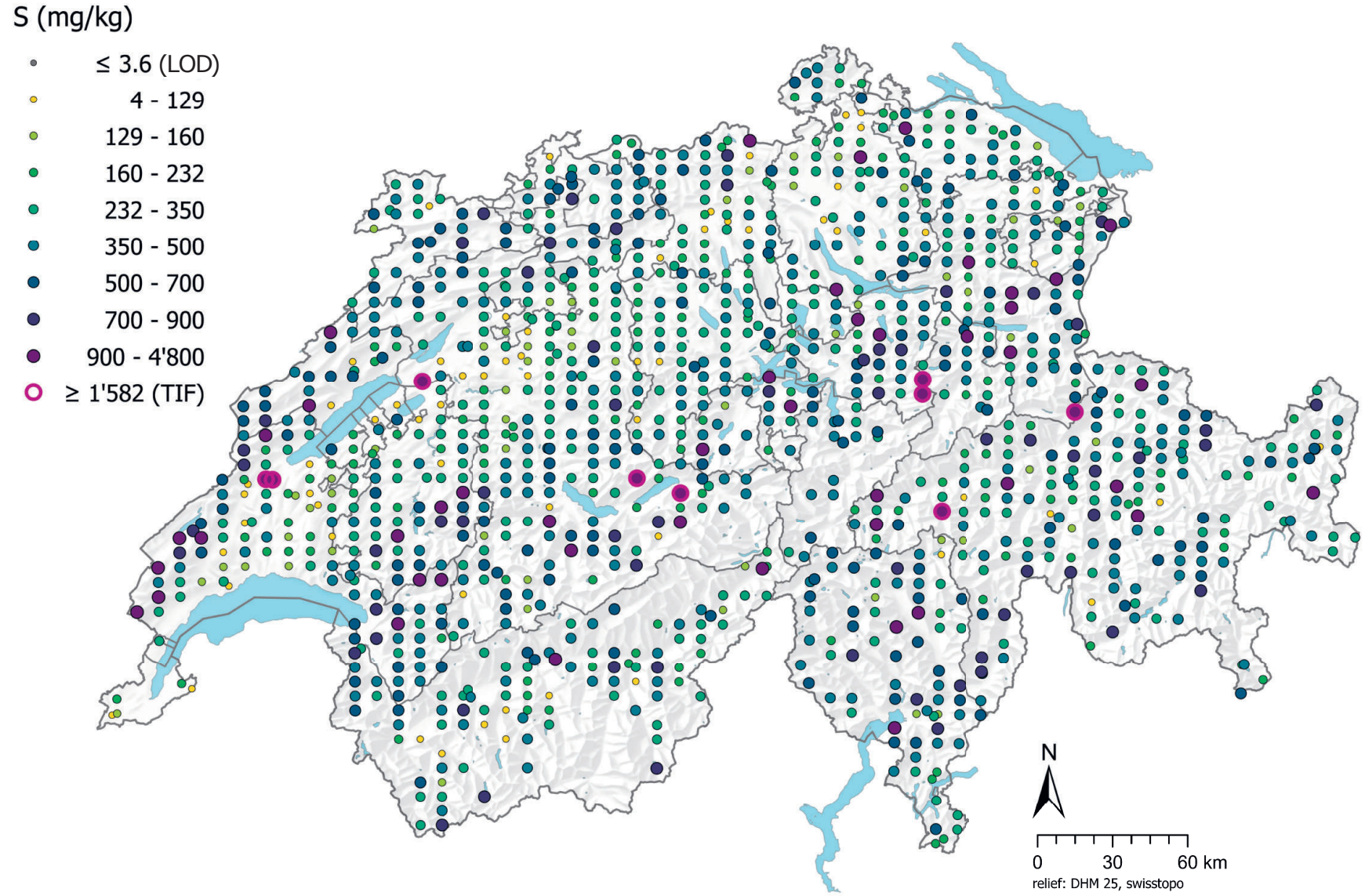

Figure 69 | **Spatial distribution of sulphur concentrations (mg/kg soil) measured at the BDM, NABO and GEMAS sites. The data points show the median of several individual samples per site. The classes correspond to the 5 %, 10 %, 25 %, 50 %, 75 %, 90 % and 95 % percentiles. TIF: Tukey Inner Fence, outlier as per Reimann *et al.* (2018). LOD: limit of detection**

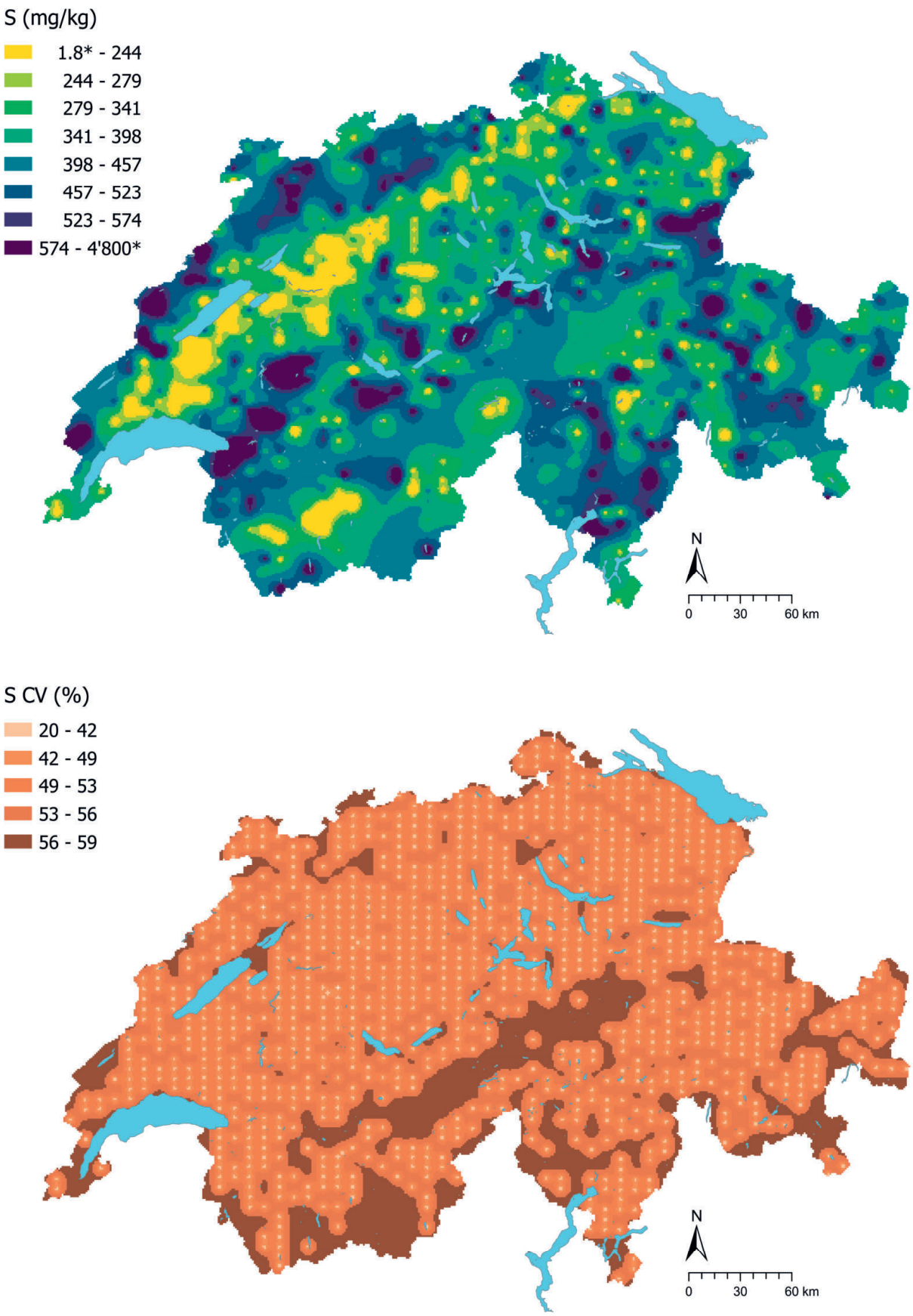

Figure 70 | Interpolated sulphur concentrations (mg/kg soil) at the BDM, NABO and GEMAS sites (top) and coefficient of variation (%) of the interpolated concentrations (bottom). The concentrations were divided into eight classes corresponding to the 5 %, 10 %, 25 %, 50 %, 75 %, 90 % and 95 % percentiles. The coefficients of variation were divided into five classes corresponding to the Jenks Natural Breaks algorithm. The interpolation was performed using the ordinary Kriging method (1 km × 1 km grid). In the classes of interpolated values, * denotes the minimum and maximum value of the point data calculated from the limit of detection.

4.17 Thallium (Tl)

Thallium is a non-essential metal in group 13 of the periodic table (Fluck & Heumann, 2017). The ore mineral lorandite ($TlAsS_2$) often occurs together with sphalerite (ZnS) and galena (PbS) (Evans & Barabash, 2010). Thallium is also found in potassium-rich silicates and various sulphides and sulphates (Tuchschmid, 1995). In Switzerland, lorandite deposits are documented in the Binn Valley in the Valais, where it occurs in mineralised Triassic dolomites (Graeser, 1967). Thallium concentrations in soil-forming rocks are typically between 0.17 and 0.82 mg/kg, with particularly highly concentrations found in granitoid magmatic and metamorphic rock, metapelite, and claystone in the flysch and Bündner schist in the Alps and in the molasse and glacial loam in the Swiss Plateau (Tuchschmid, 1995). In soils in Basel-Landschaft, locally increased thallium concentrations are potentially related to the presence of Trigonodus dolomite (Pfirter, 2020). Indeed, at sites in the dolomite lithological group, thallium is present in higher concentrations, although the difference is not statistically significant (Figure 72). In contrast, limestone was found to have significantly elevated thallium levels in comparison with all other lithological groups. Thallium was once deployed as rat and ant poison, but today is used mainly in the electronics industry (Reimann *et al.*, 2014).

Thallium has been shown to occur in two oxidation states in soils; Tl(III) and Tl(I). Both forms can precipitate with sulphur or chlorine (Evans & Barabash, 2010). Thallium can also adsorb to the surfaces of clay minerals, oxides and soil organic matter, and undergo cation exchange (Evans & Barabash, 2010; Voegelin *et al.*, 2015). In the environment, thallium behaves similarly to lead, which explains the weak correlation between thallium and lead concentrations measured in topsoils ($R^2 = 0.56$) (Chapter 6.1).

Comparatively low thallium concentrations were recorded in topsoils in the central and western Swiss Plateau and in parts of the Valais and Grisons. High thallium levels were measured in some areas in the Jura and the Southern Alps (Figure 73). Sites classified as outliers according to the TIF method are found mainly in the northern and western Jura and a few locations in the Central Alps and Grisons. In the canton of Basel-Landschaft, increased thallium concentrations in soils in Erzmatt (near Buus) and Bretzwil are attributed to weathering of local brown iron ore deposits and other ore minerals (AUE & Schmutz, 2016; Pfirter, 2020; Voegelin *et al.*, 2015). Speciation analysis conducted by Voegelin *et al.* (2015) on these soils shows that thallium is present as Tl(III) in association with manganese oxides and as Tl(I) incorporated in illite. These forms can be derived from weathering of sulphide minerals, or from emissions, e.g. from the cement industry (Voegelin *et al.*, 2015). Interestingly, measured thallium concentrations throughout Switzerland correlate very weakly with proxies for the atmospheric deposition of heavy metals (Chapter 6.1), possibly indicating an additional diffuse atmospheric input of thallium.

Thallium is highly toxic to humans, animals and plants, partly due to its ability to replace potassium in biological systems (Evans & Barabash, 2010). None of the sampling sites exceed the tolerance value for agricultural land of 2 mg/kg (Eikmann *et al.*, 1993). Arable sites have significantly lower thallium concentrations than forest and grassland sites (Figure 72).

Element	Symbol	Atomic number	Median	5 %	95 %
Thallium	Tl	81	0.15 mg/kg	0.07 mg/kg	0.38 mg/kg

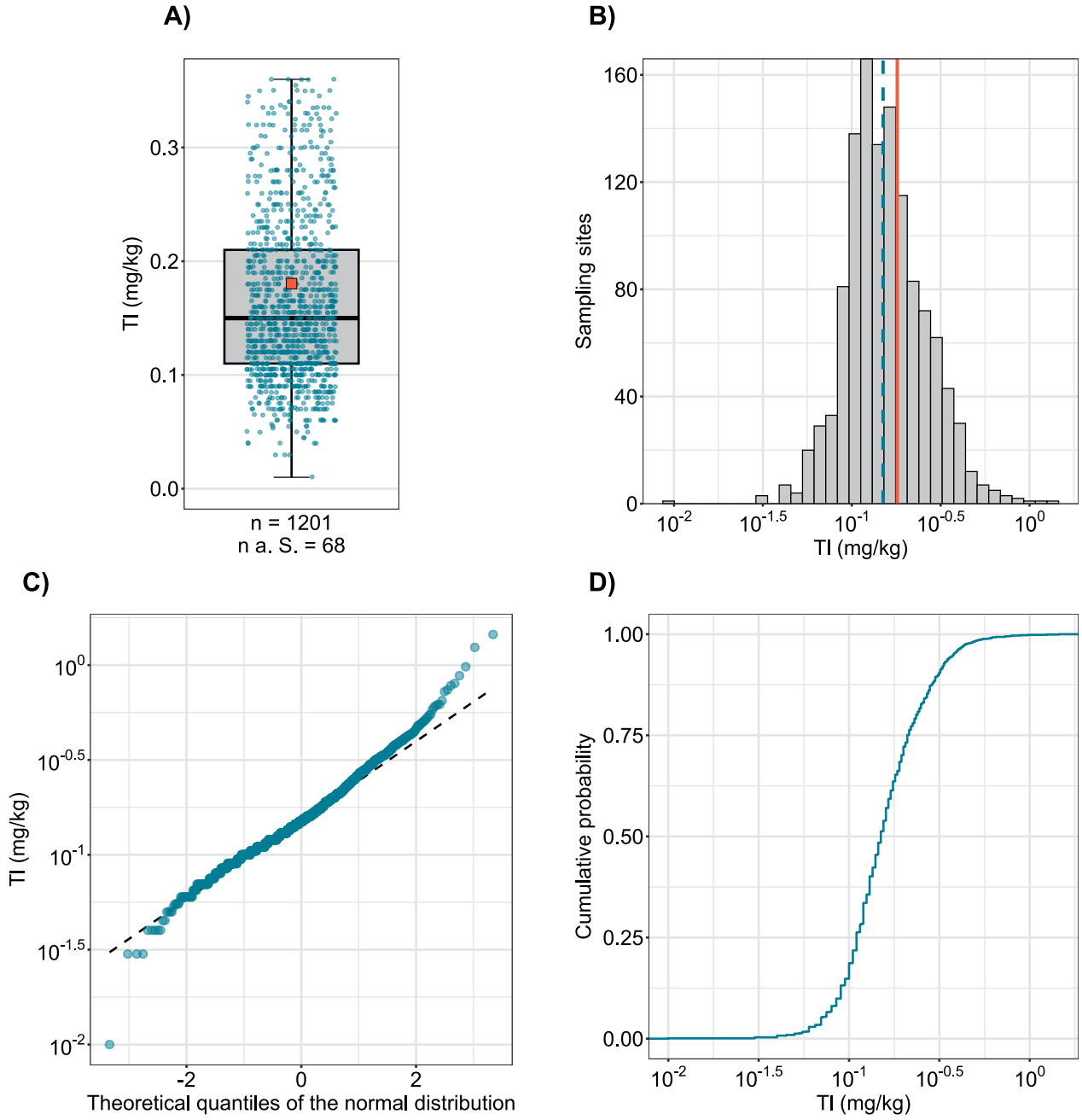

Figure 71 | **Distribution of thallium concentrations (mg/kg soil). The allocated value is the median of individual samples per site. Measured values below the limit of detection were disregarded. The dataset presented comprises the BDM, NABO and GEMAS sampling sites. n = total number of sites, n a. S. = sites lying outside the axis range or whisker.**

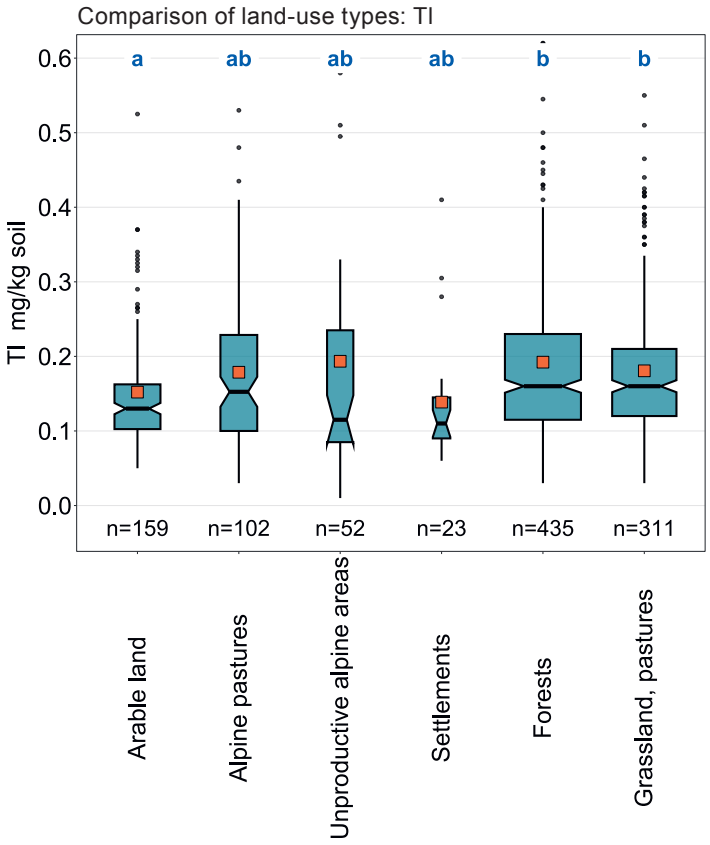

Figure 72 | **Comparison of thallium concentrations (mg/kg soil) in relation to the Z9 land-use types of the BDM sampling sites (top) and the lithological and petrographic groups in the simplified map of near-surface mineral raw materials of Switzerland (1 : 500 000, swisstopo, bottom). The median of all individual samples per site was included in the data analysis (BDM, NABO and GEMAS datasets). The number of sites per group is indicated beneath the boxes. Letters in blue: significant differences between groups ($p < 0.001$) based on a Wilcoxon rank sum test with P-adjustment using the Benjamini and Hochberg method. Not all outliers are shown. Orange square: arithmetic mean of the data.**

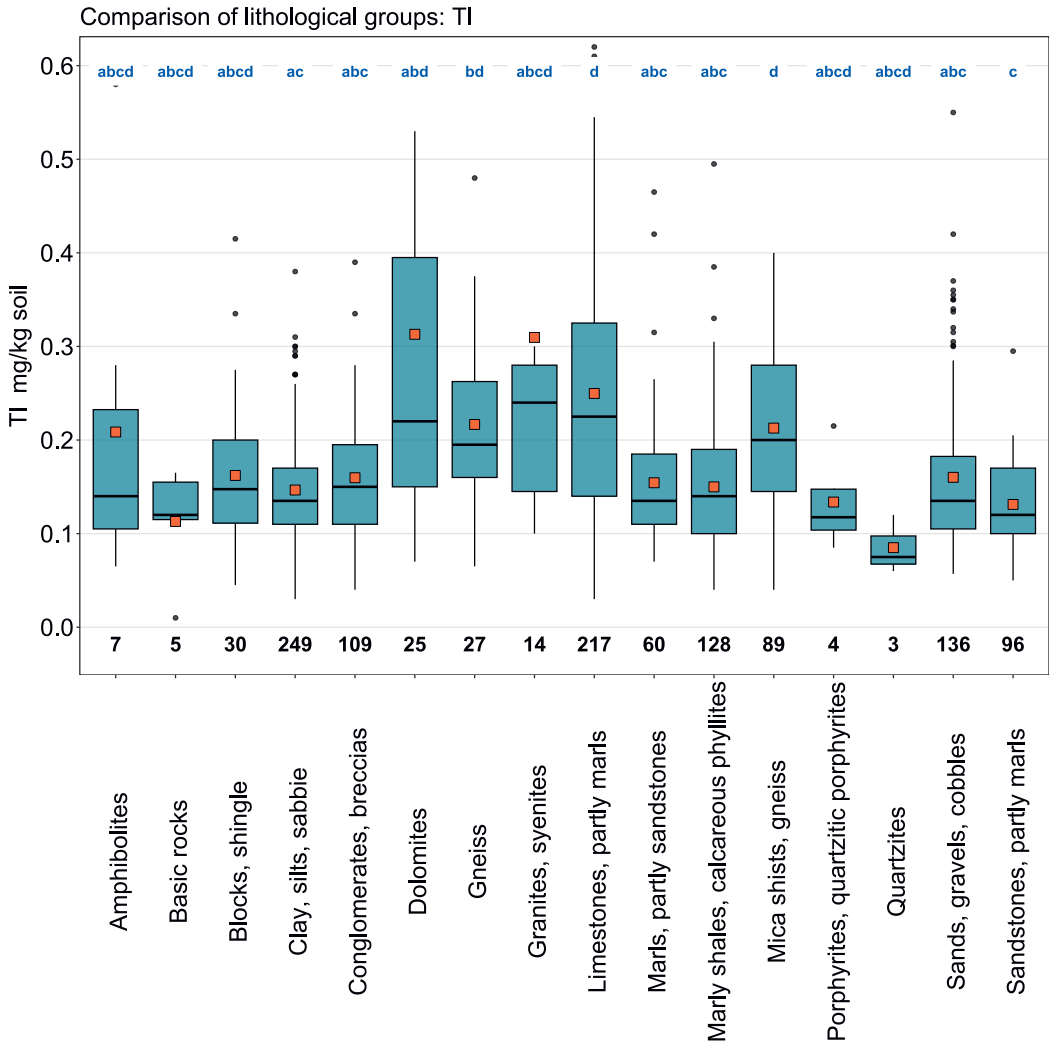

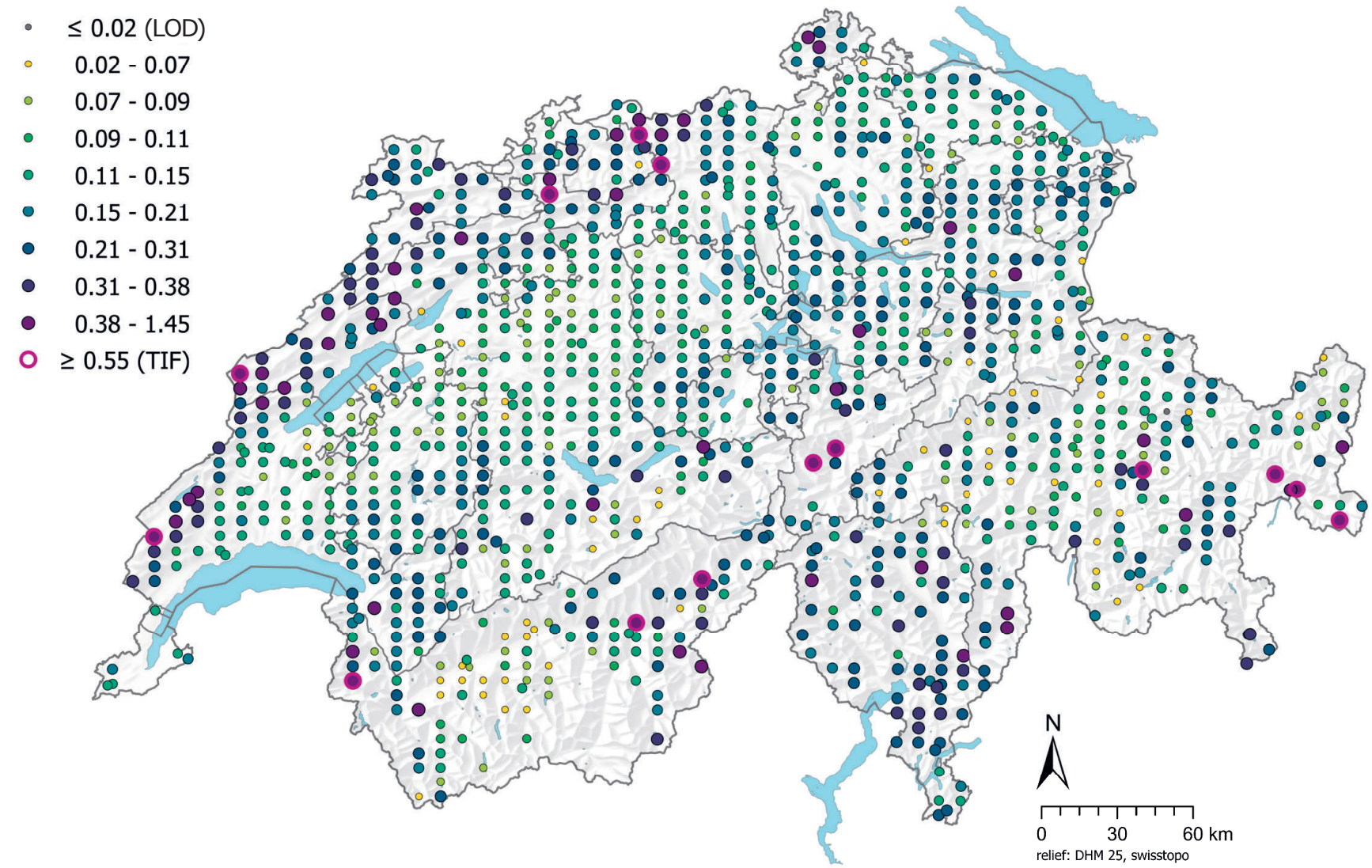

Figure 73 | **Spatial distribution of thallium concentrations (mg/kg soil) measured at the BDM, NABO and GEMAS sites. The data points show the median of several individual samples per site. 0.5 times the limit of detection (LOD) was assigned to measured values below the LOD. The classes correspond to the 5 %, 10 %, 25 %, 50 %, 75 %, 90 % and 95 % percentiles. TIF: Tukey Inner Fence, outlier as per Reimann *et al.* (2018). LOD: limit of detection**

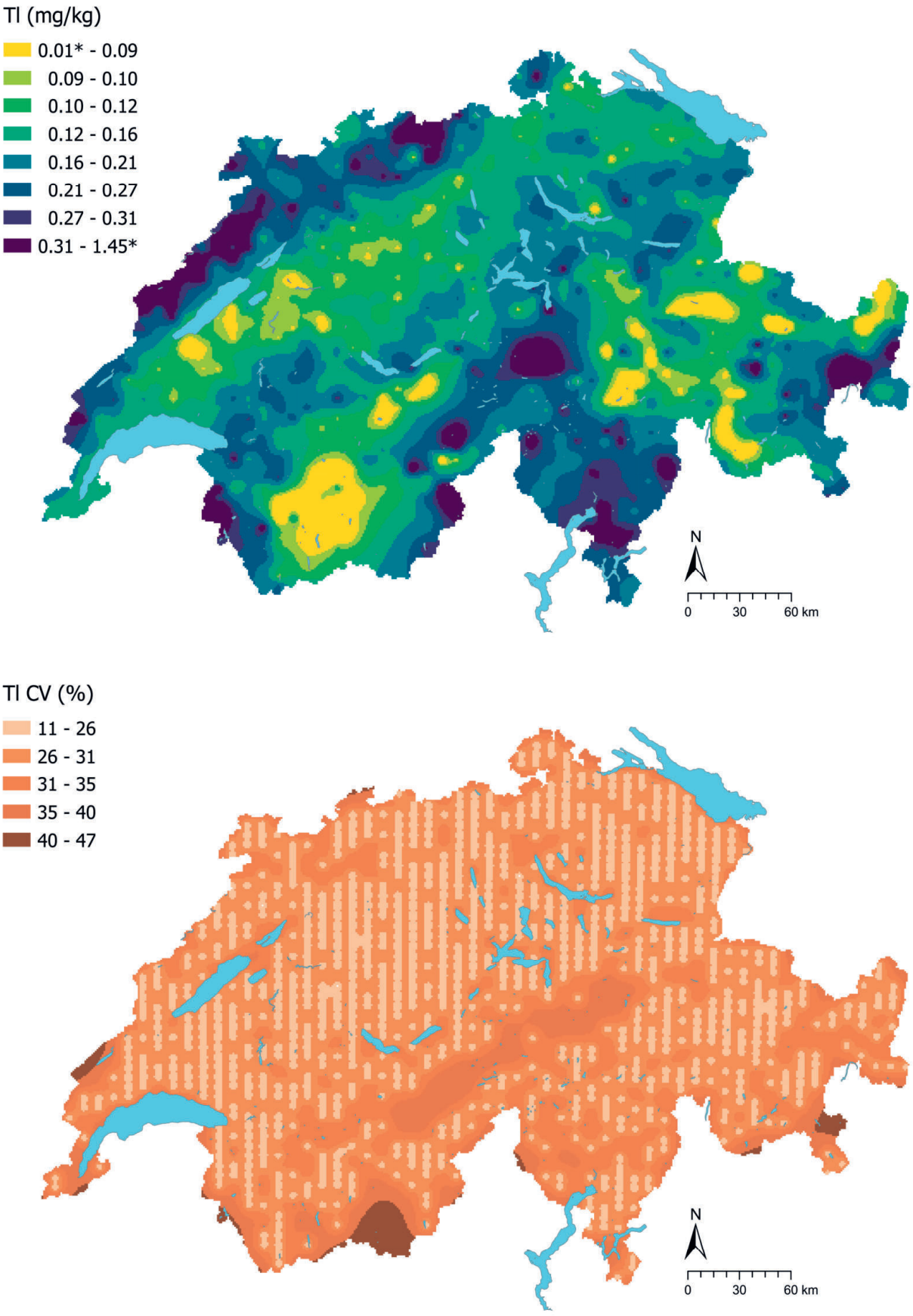

Figure 74 | Interpolated thallium concentrations (mg/kg soil) at the BDM, NABO and GEMAS sites (top) and coefficient of variation (%) of the interpolated concentrations (bottom). The concentrations were divided into eight classes corresponding to the 5 %, 10 %, 25 %, 50 %, 75 %, 90 % and 95 % percentiles. The coefficients of variation were divided into five classes corresponding to the Jenks Natural Breaks algorithm. The interpolation was performed using the ordinary Kriging method (1 km × 1 km grid). In the classes of interpolated values, * denotes the minimum and maximum value of the point data calculated from the limit of detection.

4.18 Uranium (U)

Uranium is a radioactive metal in the actinoid group. It forms stable lead isotopes at the end of its decay series (MacKenzie, 2000). Ore minerals of uranium include the oxides uraninite (UO_2) and brannerite (UTi_2O_6) (Pulford, 2010). The highest concentrations of uranium occur in acidic rocks such as granite, although sedimentary rocks with a high organic matter content (e.g. schist) and phosphate deposits (e.g. apatite) can also contain high levels of uranium due to precipitation of insoluble U(IV) (Pulford, 2010). The concentration distribution of uranium within the lithological groups shows a distinct pattern compared to the other elements, with the highest concentrations recorded at sites belonging to the gneiss, granite and syenite groups (Figure 76). This pattern is also evident from the comparison of bedrock lithologies (swisstopo, 2022), with sites in the two-mica gneiss, augen gneiss, orthogneiss and mica schist classes having the highest uranium contents. These results could indicate a partial geogenic origin. In Switzerland, uranium deposits are known to exist in the Aiguilles Rouges Massif of the Western Alps (Meissner, 2012) and from the Lower Valais along the Rhone Valley, the Vorderrhein Valley, Illanz up to the upper Weisstannen Valley, and the Murg Valley (Gilliéron, 1988; NEROS, 2019). Geogenic hotspots have also been documented in Davos, Poschiavo and Bergün (NEROS, 2019). In topsoils, high uranium concentrations were measured at sites in the Engadin, the Surselva and the Upper Valais, as well as in the western Jura and on the south side of the Alps (Figure 77). Comparatively low concentrations in topsoils were recorded on the western northern slope of the Alps and some parts of the eastern Central Alps.

Since the 20th century uranium has been used to generate electricity and in weapons production, making it one of the most valuable elements (Pulford, 2010).

Uranium in soil occurs in the U(IV) and U(VI) oxidation states (Pulford, 2010). According to Amelung *et al.* (2018d), U^{4+} released during weathering of minerals rapidly oxidises to U^{6+}, which in turn forms uranyl complexes that can adsorb to clay minerals, soil organic matter and oxides (Mikutta *et al.*, 2016). The cation U^{4+}, which is stable under anaerobic conditions, can form poorly soluble compounds such as UO_2, phosphate or sulphide compounds (Amelung *et al.*, 2018d). Uranium is considered to be relatively immobile in soil, resulting in a reduced translocation of the element within the soil profile (Amelung *et al.*, 2018d). Phosphate fertilisers are a primary contributor to uranium accumulation in topsoil (Bigalke *et al.*, 2017). These diffuse inputs from agriculture could partly explain why topsoils at arable sites have significantly higher uranium concentrations than forest soils (Figure 76). However, compared to other land-use types, these differences are not statistically significant.

The median uranium concentration in Swiss topsoils (0.7 mg/kg, Table 2) lies within the range of the European median of 0.77 mg/kg for arable sites and 0.74 mg/kg for grassland sites (Reimann *et al.*, 2014).

Radiation released during the radioactive decay of uranium can pose a risk to living organisms. In soils however, the chemical toxicity of uranium is likely to pose a greater threat than released radiation (Sheppard *et al.*, 2005). The predicted no-effect concentration (PNEC) for uranium – i.e. the concentration below which no adverse effect on organisms is expected – is estimated to be 100 mg/kg for soil organisms and 250 mg/kg for plants (Sheppard *et al.*, 2005). The Eikmann-Kloke tolerance value for agricultural areas (10 mg/kg, Herklotz *et al.*, 1996) is exceeded at four sampling sites.

Element	Symbol	Atomic number	Median	5 %	95 %
Uranium	U	92	0.7 mg/kg	0.3 mg/kg	2.0 mg/kg

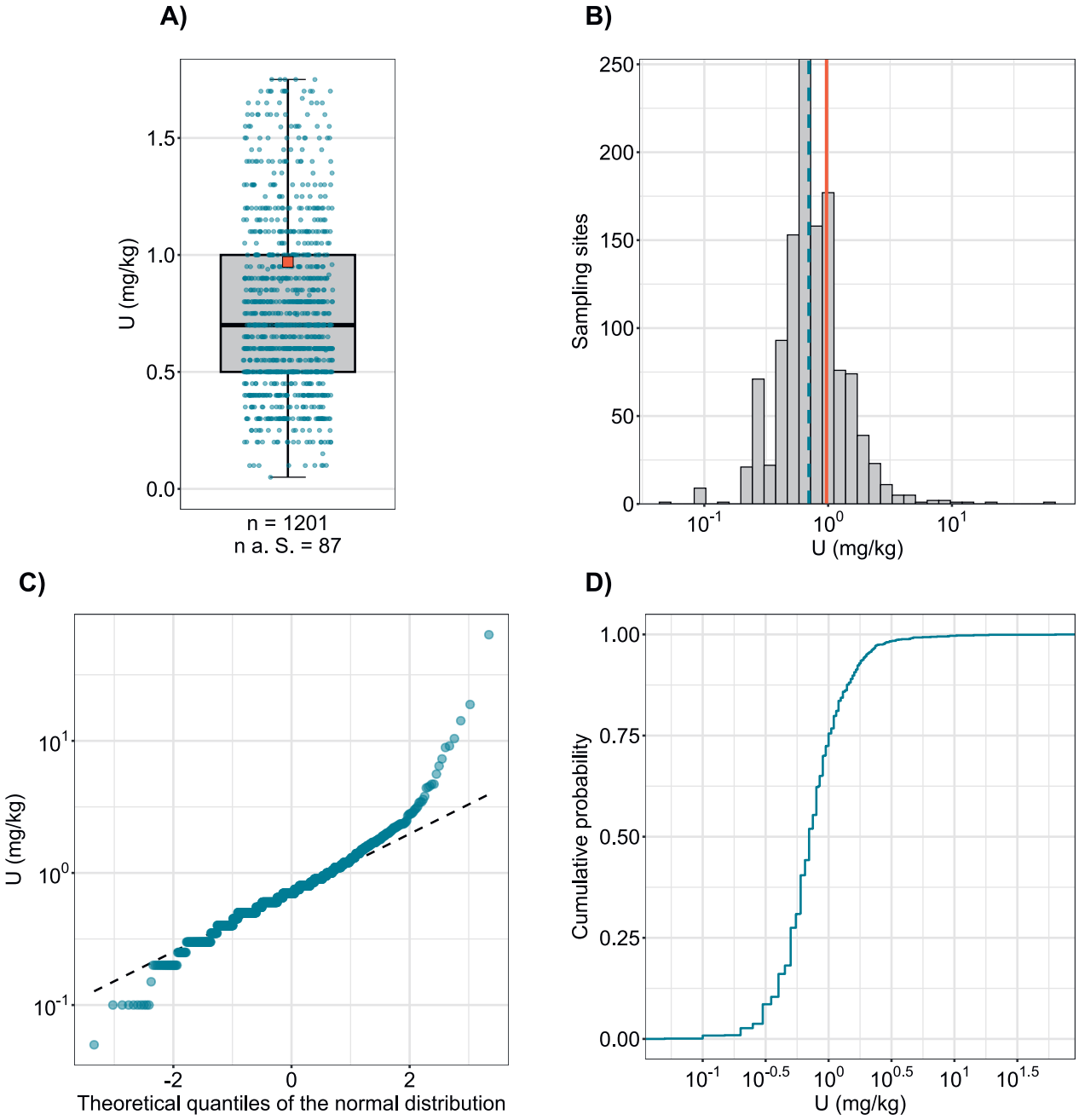

Figure 75 | **Distribution of uranium concentrations (mg/kg soil). The allocated value is the median of individual samples per site. Measured values below the limit of detection were disregarded. The dataset presented comprises the BDM, NABO and GEMAS sampling sites. n = total number of sites, n a. S. = sites lying outside the axis range or whisker.**

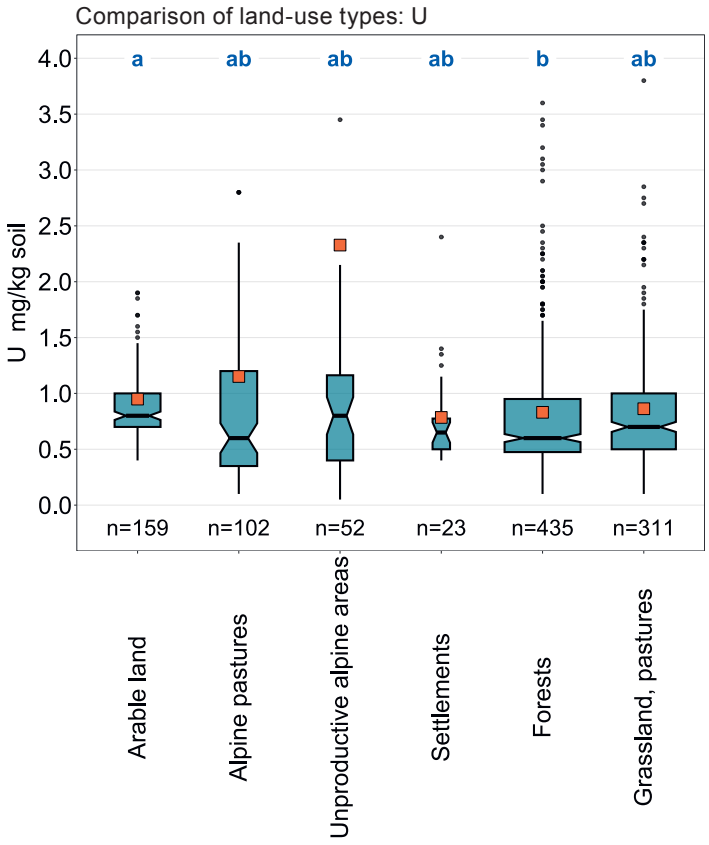

Figure 76 | Comparison of uranium concentrations (mg/kg soil) in relation to the Z9 land-use types of the BDM sampling sites (top) and the lithological and petrographic groups in the simplified map of near-surface mineral raw materials of Switzerland (1 : 500 000, swisstopo, bottom). The median of all individual samples per site was included in the data analysis (BDM, NABO and GEMAS datasets). The number of sites per group is indicated beneath the boxes. Letters in blue: significant differences between groups ($p < 0.001$) based on a Wilcoxon rank sum test with P-adjustment using the Benjamini and Hochberg method. Not all outliers are shown. Orange square: arithmetic mean of the data.

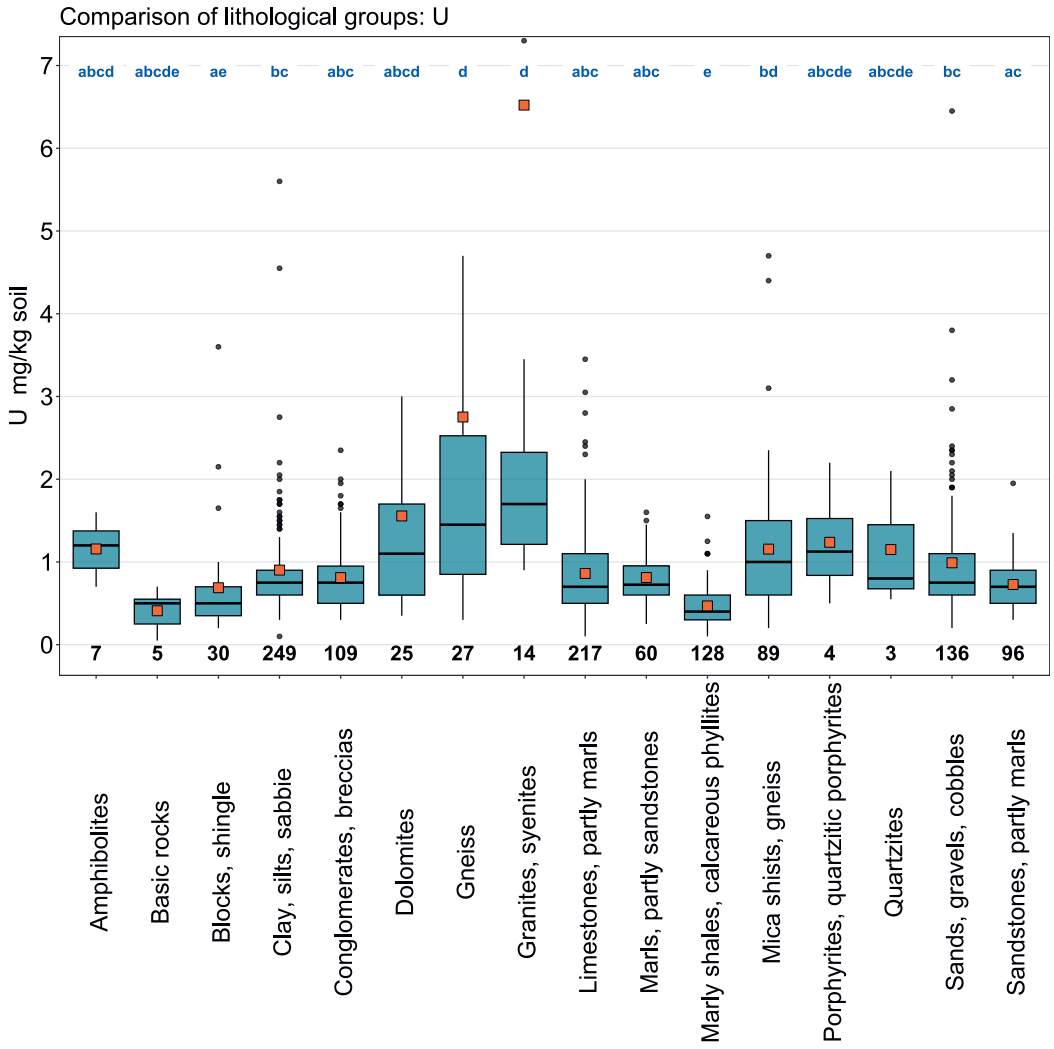

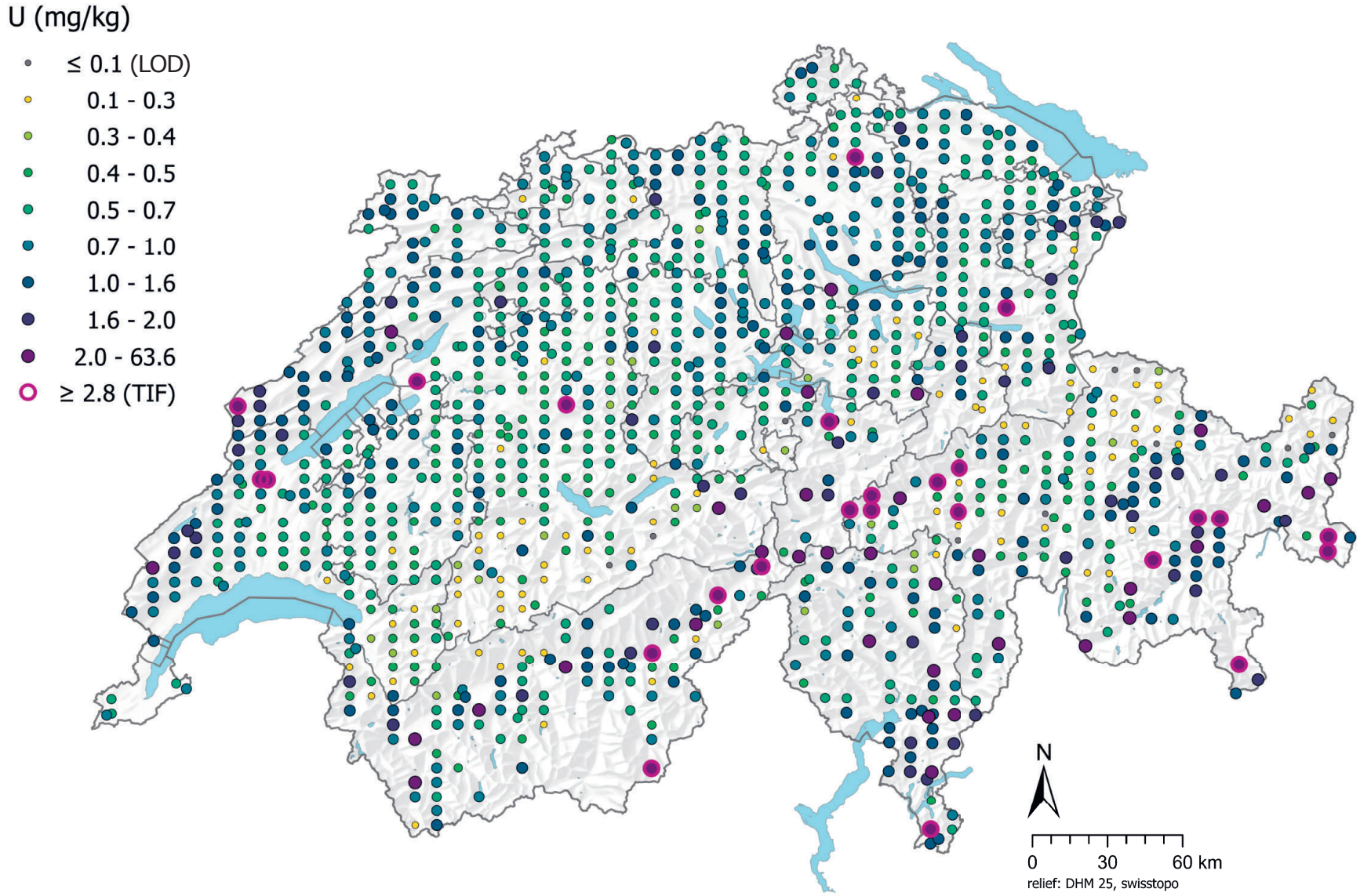

Figure 77 | **Spatial distribution of uranium concentrations (mg/kg soil) measured at the BDM, NABO and GEMAS sites. The data points show the median of several individual samples per site. 0.5 times the limit of detection (LOD) was assigned to measured values below the LOD. The classes correspond to the 5 %, 10 %, 25 %, 50 %, 75 %, 90 % and 95 % percentiles. TIF: Tukey Inner Fence, outlier as per Reimann *et al.* (2018). LOD: limit of detection**

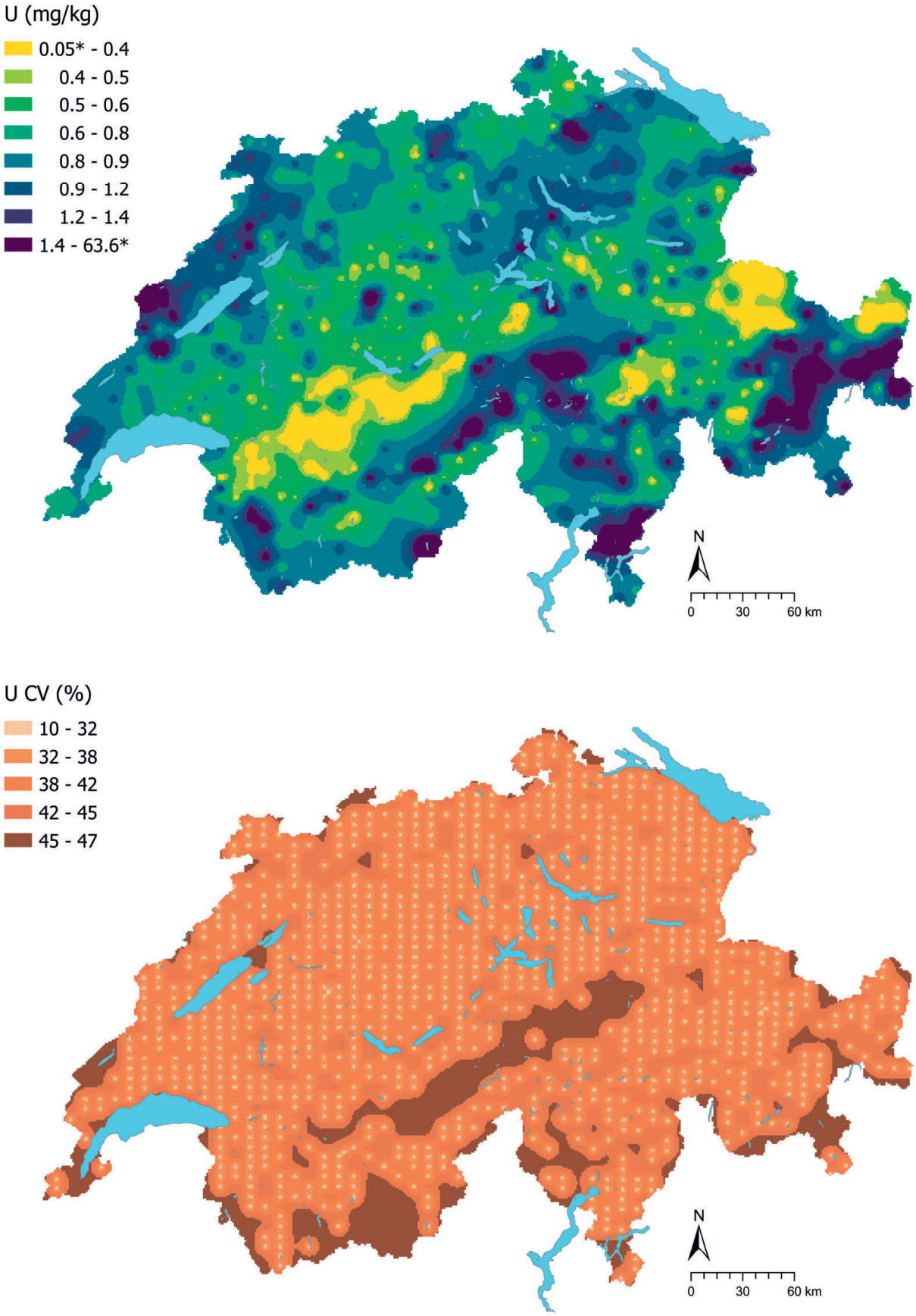

Figure 78 | Interpolated uranium concentrations (mg/kg soil) at the BDM, NABO and GEMAS sites (top) and coefficient of variation (%) of the interpolated concentrations (bottom). The concentrations were divided into eight classes corresponding to the 5 %, 10 %, 25 %, 50 %, 75 %, 90 % and 95 % percentiles. The coefficients of variation were divided into five classes corresponding to the Jenks Natural Breaks algorithm. The interpolation was performed using the ordinary Kriging method (1 km × 1 km grid). In the classes of interpolated values, * denotes the minimum and maximum value of the point data calculated from the limit of detection.

4.19 Vanadium (V)

Vanadium is a metal in group 5 of the periodic table (Mukherjee *et al.*, 2004). It is essential for some living organisms and presumed to be so for humans. Vanadium is present in the minerals vanadinite ($Pb_5[VO_4]_3Cl$) and patronite (VS_4), and in traces in pyroxene, amphibole, mica and apatite (Pilbeam & Drihem, 2007; Reimann *et al.*, 2014). High concentrations of vanadium occur in mafic rocks (e.g. basalt, 250 mg/kg) and black shale (120 mg/kg). Vanadium can also accumulate in carboniferous sedimentary rocks such as petroleum and coal due to its correlation with organic carbon (Breit & Wanty, 1991; Evans & Barabash, 2010; Reimann *et al.*, 2014).

Vanadium is mainly used in steel alloys, in glass and ceramics production, as a chemical catalyst and as a constituent of pharmaceuticals (Evans & Barabash, 2010; Mukherjee *et al.*, 2004).

In soil, vanadium exists in three oxidation states: V(V), V(IV) and V(II) (Evans & Barabash, 2010). During weathering of the parent material, vanadium oxidises to vanadates, which behave similarly to phosphates (Evans & Barabash, 2010; Pilbeam & Drihem, 2007). Since vanadium adsorbs to iron and aluminium oxides, clay minerals and soil organic matter, the element is thought to be relatively immobile in soil (Evans & Barabash, 2010; Pilbeam & Drihem, 2007).

The median of the measured vanadium concentrations in Swiss topsoils is 32 mg/kg and thus above the European median of 25 mg/kg (Reimann *et al.*, 2014). Two regions can be clearly differentiated: above-average concentrations in the Jura and the Randen and low concentrations in the Central Alps (Figure 81). Studies of a peat bed more than 6 m thick in the Étang de la Gruère in the Jura suggested that atmospheric deposition rather than chemical weathering of the underlying sediments led to an accumulation of vanadium and chromium in the soil (Krachler *et al.*, 2003). In the topsoil samples of the geochemical soil atlas, measured vanadium concentrations correlate only weakly with proxies for atmospheric deposition. This is also the case for the measured chromium concentrations ($R^2 = 0.34$, Chapter 6.1). In addition, accumulation of clay minerals due to carbonate weathering could have caused immobilisation and subsequent accumulation through sorption processes, as with cadmium and zinc (correlation with clay content: $R^2 = 0.53$, Chapter 6.1). Measured vanadium concentrations also correlate with measured chromium concentrations ($R^2 = 0.77$) and show a similar distribution across land-use types, with arable and grassland sites having significantly higher vanadium levels in the topsoil than other land uses (Figure 80). This correlation can be attributed to various factors: similar inputs (e.g. atmospheric deposition), incorporation into iron oxides in the soil and increased geogenic occurrence in iron-bearing minerals (Chapter 6.1). In agriculture, the use of mineral phosphorus fertilisers may result in further inputs of vanadium into the topsoil (Evans & Barabash, 2010).

The tolerance value for agricultural areas of 100 mg/kg is exceeded at 19 sites and the corresponding toxicity value of 200 mg/kg at three sites (Herklotz *et al.*, 1996). According to Eikmann & Kloke (1993), a vanadium concentration of 50 mg/kg can be interpreted as a possible upper geogenic and pedogenic background value with no major anthropogenic inputs, (Herklotz *et al.*, 1996). This threshold value is exceeded at 204 sites (17 % of all sites).

Element	Symbol	Atomic number	Median	5 %	95 %
Vanadium	V	92	32 mg/kg	12 mg/kg	75 mg/kg

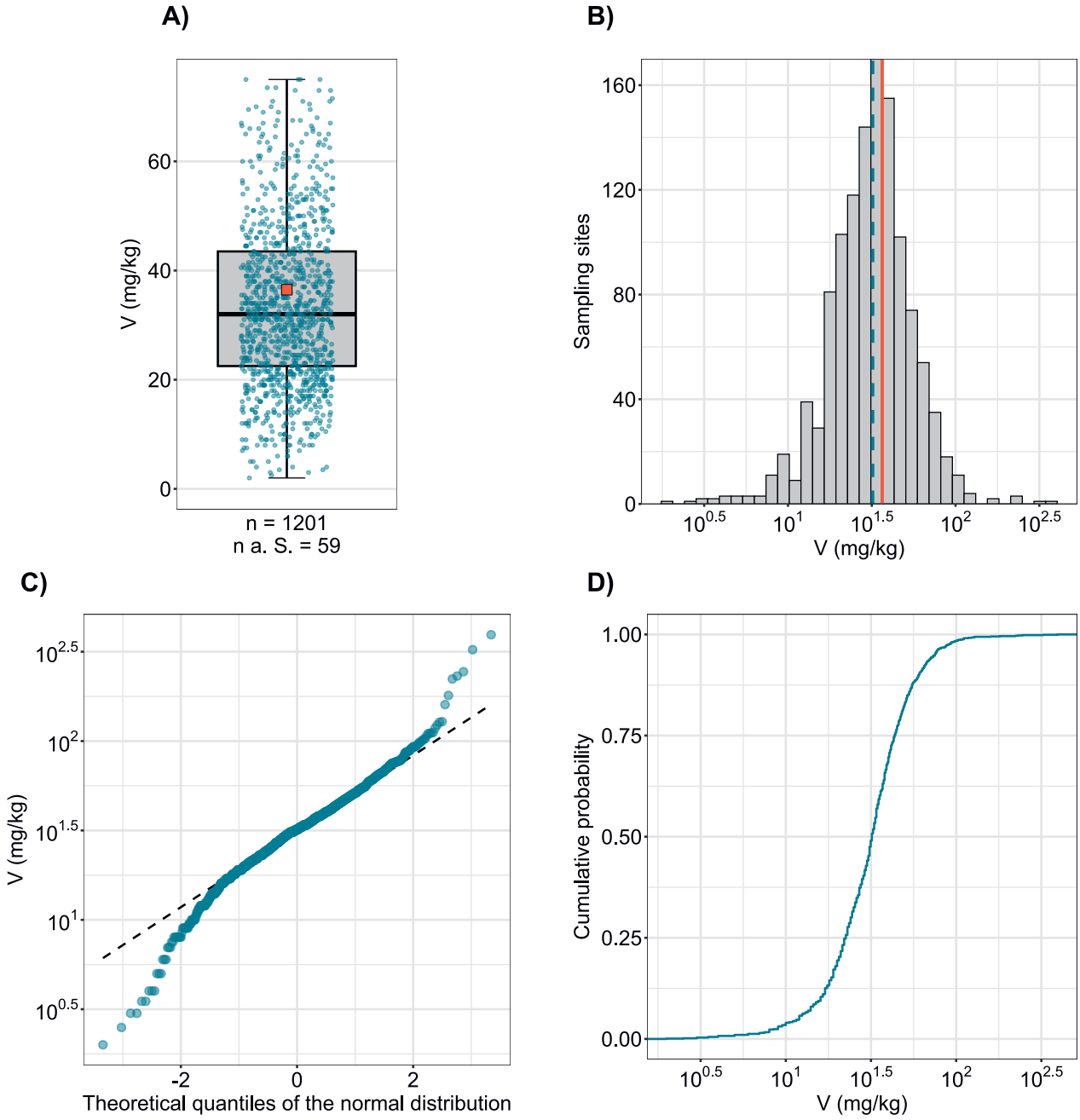

Figure 79 | Distribution of vanadium concentrations (mg/kg soil). The allocated value is the median of individual samples per site. Measured values below the limit of detection were disregarded. The dataset presented comprises the BDM, NABO and GEMAS sampling sites. n = total number of sites, n a. S. = sites lying outside the axis range or whisker.

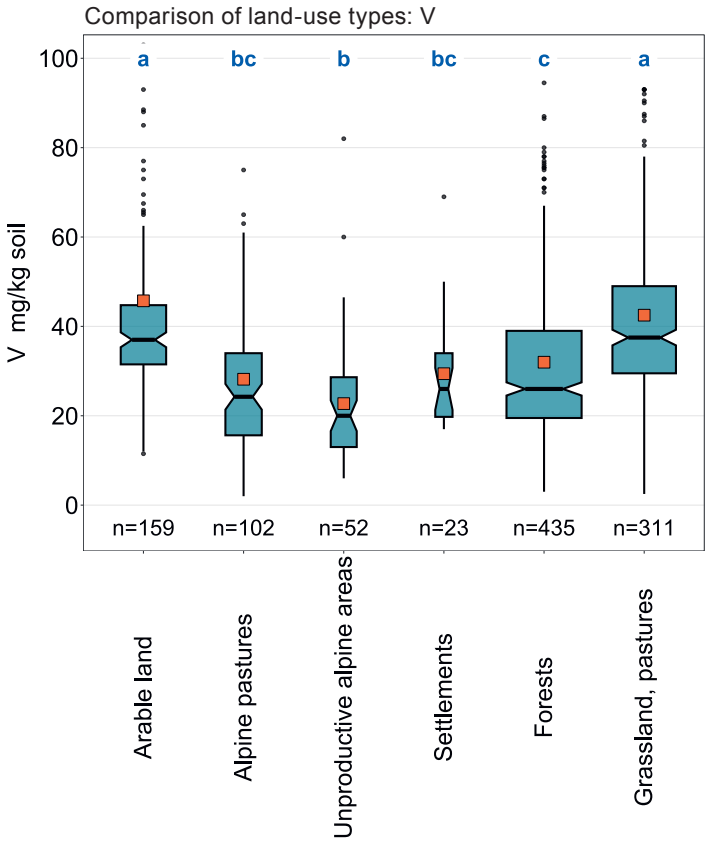

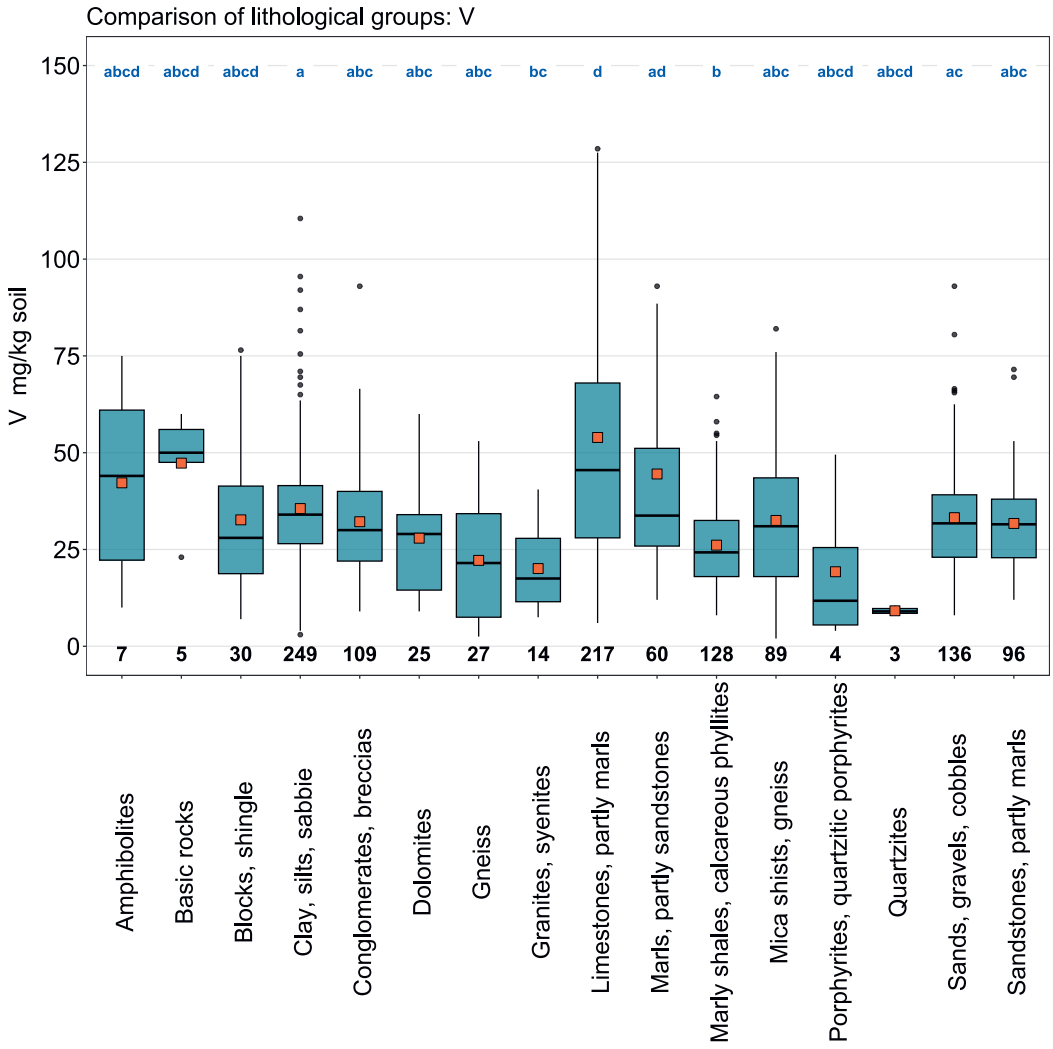

Figure 80 | **Comparison of vanadium concentrations (mg/kg soil) in relation to the Z9 land-use types of the BDM sampling sites (top) and the lithological and petrographic groups in the simplified map of near-surface mineral raw materials of Switzerland (1 : 500 000, swisstopo, bottom). The median of all individual samples per site was included in the data analysis (BDM, NABO and GEMAS datasets). The number of sites per group is indicated beneath the boxes. Letters in blue: significant differences between groups ($p < 0.001$) based on a Wilcoxon rank sum test with P-adjustment using the Benjamini and Hochberg method. Not all outliers are shown. Orange square: arithmetic mean of the data.**

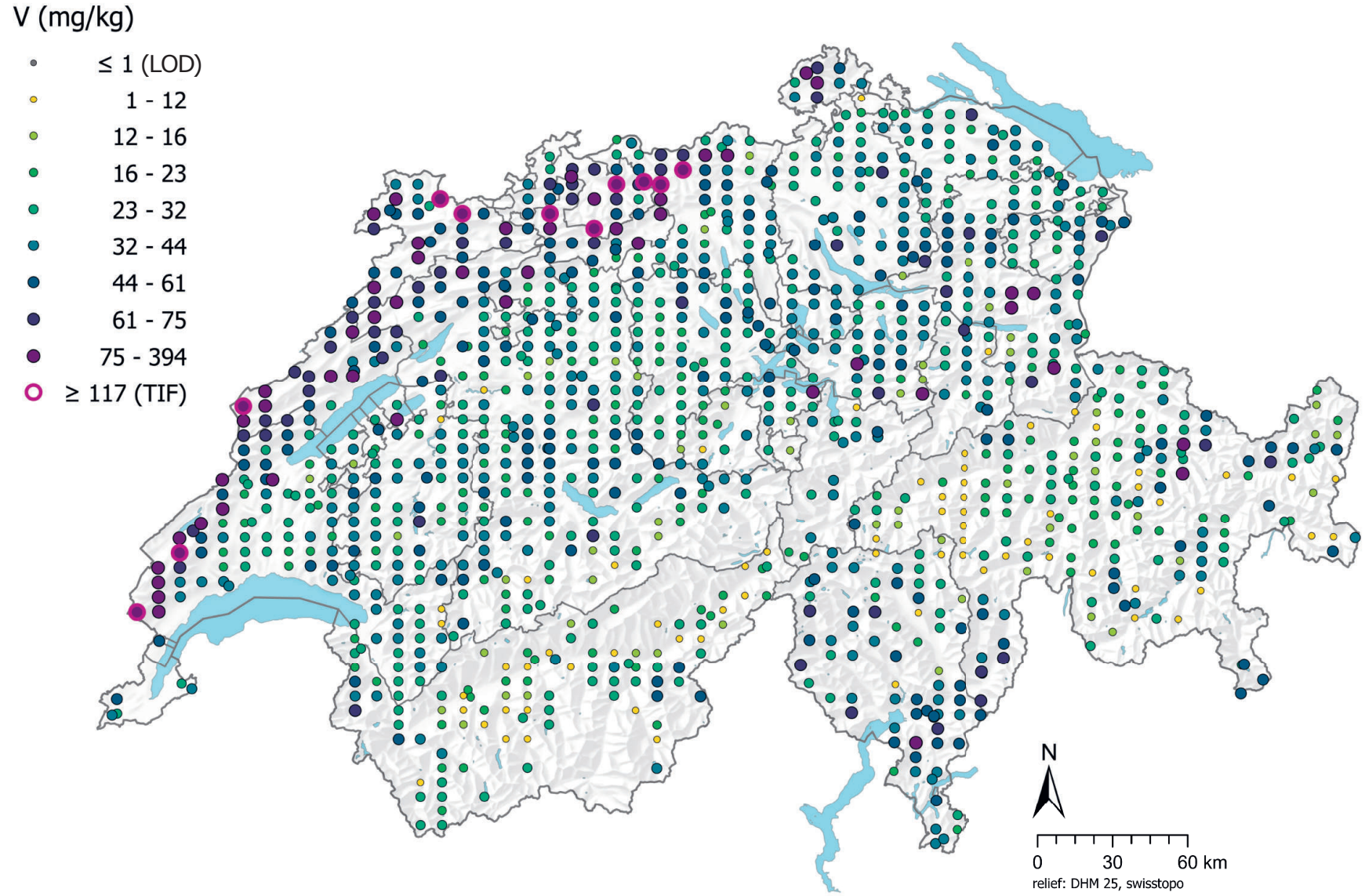

Figure 81 | **Spatial distribution of vanadium concentrations (mg/kg soil) measured at the BDM, NABO and GEMAS sites. The data points show the median of several individual samples per site. 0.5 times the limit of detection (LOD) was assigned to measured values below the LOD. The classes correspond to the 5 %, 10 %, 25 %, 50 %, 75 %, 90 % and 95 % percentiles. TIF: Tukey Inner Fence, outlier as per Reimann *et al.* (2018). LOD: limit of detection**

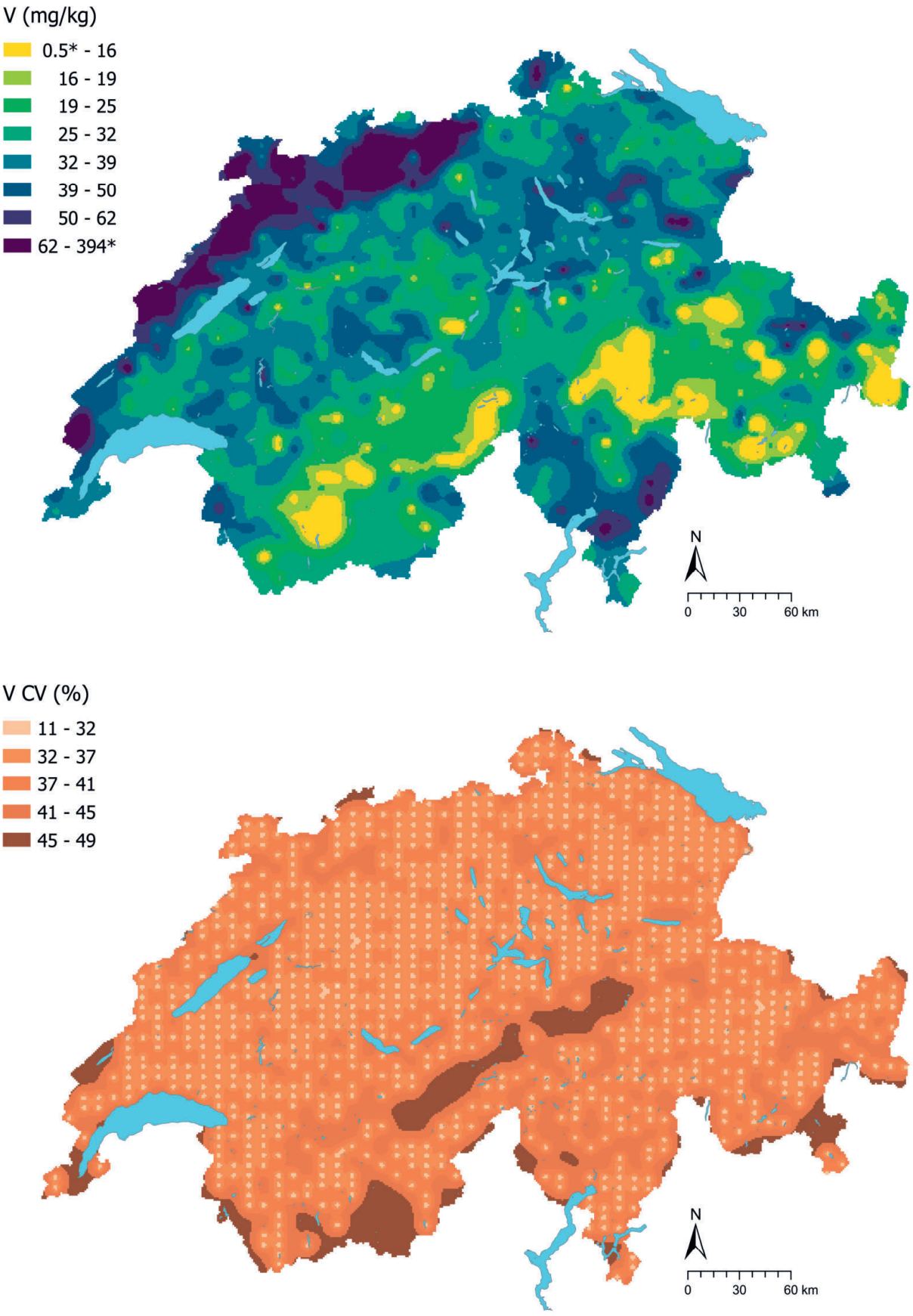

Figure 82 | Interpolated vanadium concentrations (mg/kg soil) at the BDM, NABO and GEMAS sites (top) and coefficient of variation (%) of the interpolated concentrations (bottom). The concentrations were divided into eight classes corresponding to the 5 %, 10 %, 25 %, 50 %, 75 %, 90 % and 95 % percentiles. The coefficients of variation were divided into five classes corresponding to the Jenks Natural Breaks algorithm. The interpolation was performed using the ordinary Kriging method (1 km × 1 km grid). In the classes of interpolated values, * denotes the minimum and maximum value of the point data calculated from the limit of detection.

4.20 Zinc (Zn)

Zinc is an essential metal in group 12 of the periodic table with a concentration in the Earth's crust estimated at roughly 70 mg/kg (SGTK *et al.*, 2013). The main minerals of zinc include sphalerite (zinc blende, ZnS), smithsonite ($ZnCO_3$) and zincite (ZnO) (Reimann *et al.*, 2014). Zinc also occurs in several other ore minerals (e.g. phosphates), in iron-magnesium silicates (e.g. garnet and pyroxene), and in iron oxides (e.g. magnetite) (Tuchschmid, 1995). High concentrations are found in basic to intermediary rocks (basic magmatic rock 150 mg/kg), bituminous claystone (200 mg/kg) and coal (50 mg/kg). In contrast, limestone and dolomite typically exhibit considerably lower concentrations of around 5 mg/kg (Tuchschmid, 1995). Measured zinc concentrations in the topsoil correlate with concentrations of lead, iron, nickel and cobalt (Chapter 6.1), which could indicate a partially geogenic origin as these elements co-occur in certain rocks (Tuchschmid, 1995). In Switzerland, lead- and zinc-bearing ore deposits are mainly found in the Alps, for example in the Middle Triassic limestones and dolomites in Grisons (Kündig *et al.*, 1997; SGTK *et al.*, 2013).

Zinc is used for corrosion protection (galvanising), in alloys, diecasting, piping, etc. (SGTK *et al.*, 2013). In urban areas, zinc emissions result mainly from tyre and brake pad wear (Reimann *et al.*, 2014).

Zinc can be present in soil in various forms: dissolved in soil solution, where its concentration largely depends on pH; adsorbed (e.g. to clay minerals); bound to soil organic matter; associated with carbonates; or incorporated into oxides (Amelung *et al.*, 2018b; Jacquat *et al.*, 2009; Jacquat *et al.*, 2011).

The average zinc concentration in Swiss topsoils ranges from 48 to 83 mg/kg (25–50 %, Table 2) and thus lies within the range of uncontaminated or only slightly contaminated soils (10–80 mg/kg; Amelung *et al.*, 2018a). High concentrations of zinc were measured in the topsoils of the Jura (Figure 85). In a comparison of the lithological groups, the highest statistically significant zinc concentrations were observed at sampling sites belonging to the limestone group (Figure 84). As with cadmium and vanadium, zinc accumulation can be caused not only by geogenic and anthropogenic sources, but also by an accumulation of clay minerals resulting from weathering of carbonate rocks. This clay accumulation can lead to the immobilisation of zinc through sorption processes (correlation with clay content: $R^2 = 0.50$, Chapter 6.1). Sites with comparatively low zinc levels are located in Grisons.

Measured zinc concentrations at grassland sites are significantly higher than for other land-use types (Figure 84). This difference may be attributed to the use of farmyard manure, which led to an increase in zinc levels on arable land and intensively managed grassland at the NABO sites between 1985 and 2009 (Gubler *et al.*, 2015). In addition to the application of farmyard manure, atmospheric deposition may serve as a zinc source for soils, as observed in England and Wales (Nicholson *et al.*, 2003), for example.

Zinc is a micronutrient whose low concentrations in soil cause global dietary deficiencies. At high concentrations, however, zinc can be toxic to plants and microorganisms (Amelung *et al.*, 2018a). According to Amelung *et al.* (2018a), zinc may have a phytotoxic effect at a threshold of 150 mg/kg in sandy soils and soils with a pH of 5 to 6, although this effect strongly depends on the plant availability. The authors report that there is no known chronic zinc toxicity in humans as a result of dietary intake. According to Eikmann & Kloke (1993), the tolerance value for agricultural land is 300 mg/kg, which is exceeded at three sampling sites.

Element	Symbol	Atomic number	Median	5 %	95 %
Zinc	Zn	30	64 mg/kg	27 mg/kg	128 mg/kg

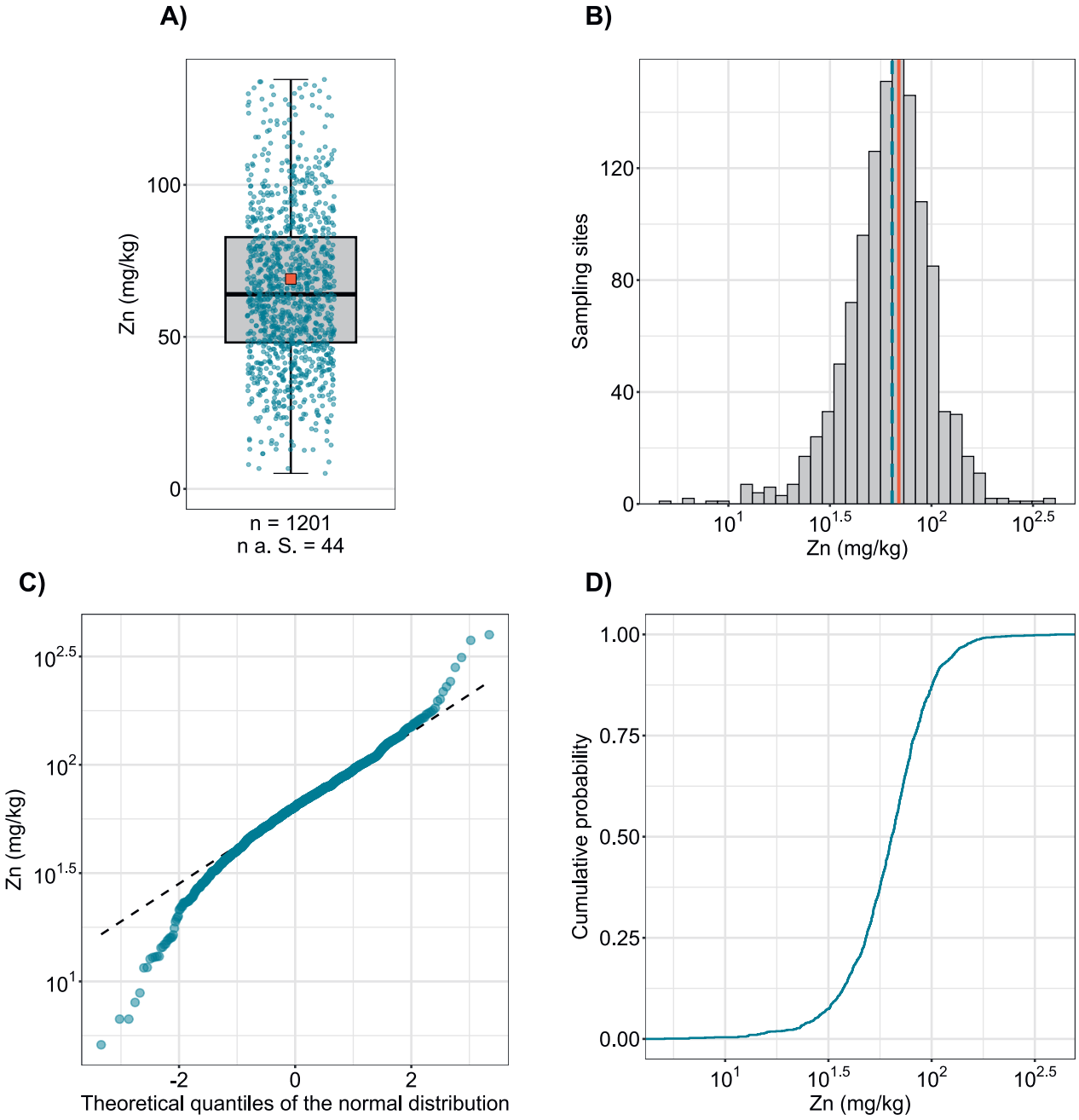

Figure 83 | Distribution of zinc concentrations (mg/kg soil). The allocated value is the median of individual samples per site. The dataset presented comprises the BDM, NABO and GEMAS sampling sites. n = total number of sites, n a. S. = sites lying outside the axis range or whisker.

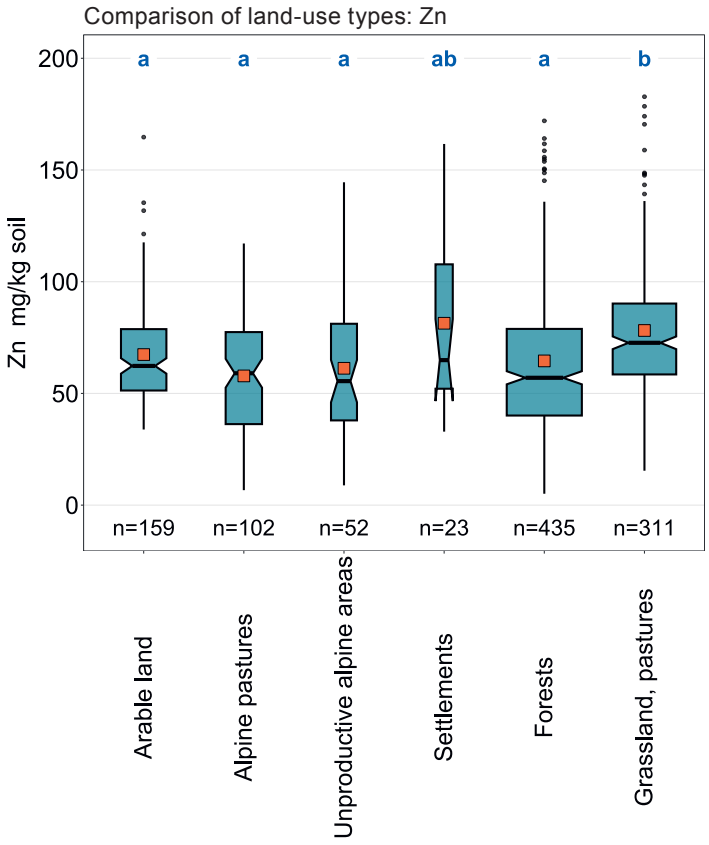

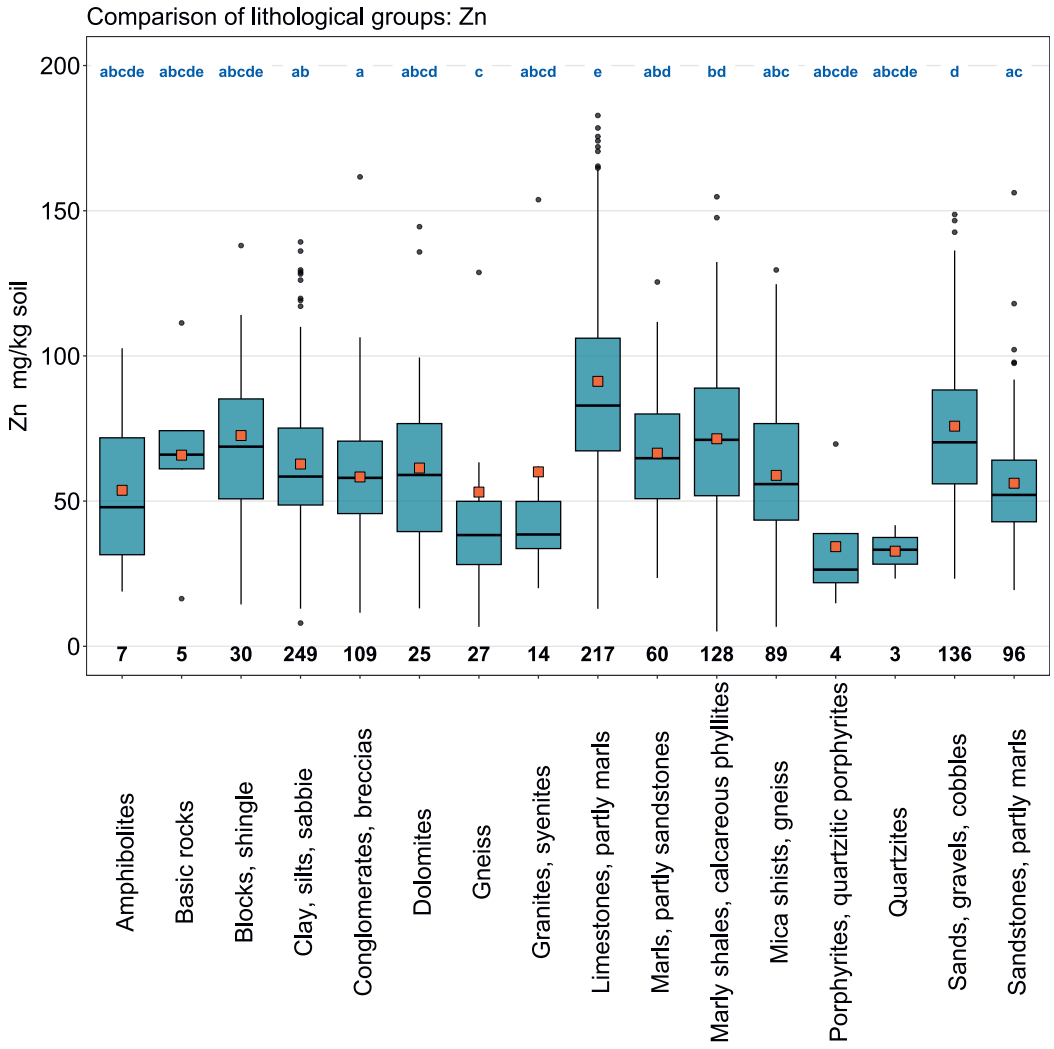

Figure 84 | Comparison of zinc concentrations (mg/kg soil) in relation to the Z9 land-use types of the BDM sampling sites (top) and the lithological and petrographic groups in the simplified map of near-surface mineral raw materials of Switzerland (1 : 500 000, swisstopo, bottom). The median of all individual samples per site was included in the data analysis (BDM, NABO and GEMAS datasets). The number of sites per group is indicated beneath the boxes. Letters in blue: significant differences between groups ($p < 0.001$) based on a Wilcoxon rank sum test with P-adjustment using the Benjamini and Hochberg method. Not all outliers are shown. Orange square: arithmetic mean of the data.

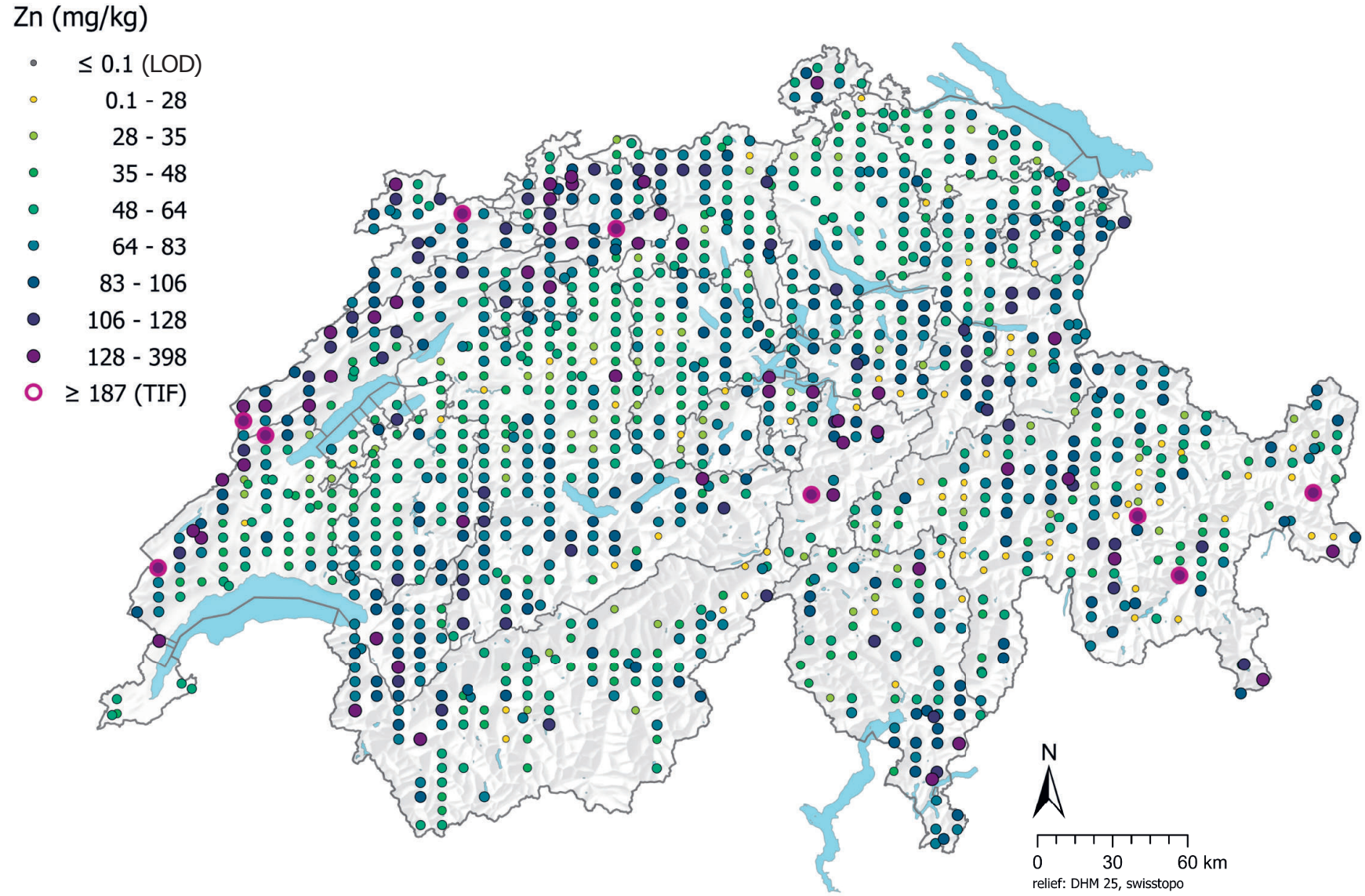

Figure 85 | **Spatial distribution of zinc concentrations (mg/kg soil) measured at the BDM, NABO and GEMAS sites. The data points show the median of several individual samples per site. The classes correspond to the 5 %, 10 %, 25 %, 50 %, 75 %, 90 % and 95 % percentiles. TIF: Tukey Inner Fence, outlier as per Reimann *et al.* (2018). LOD: limit of detection**

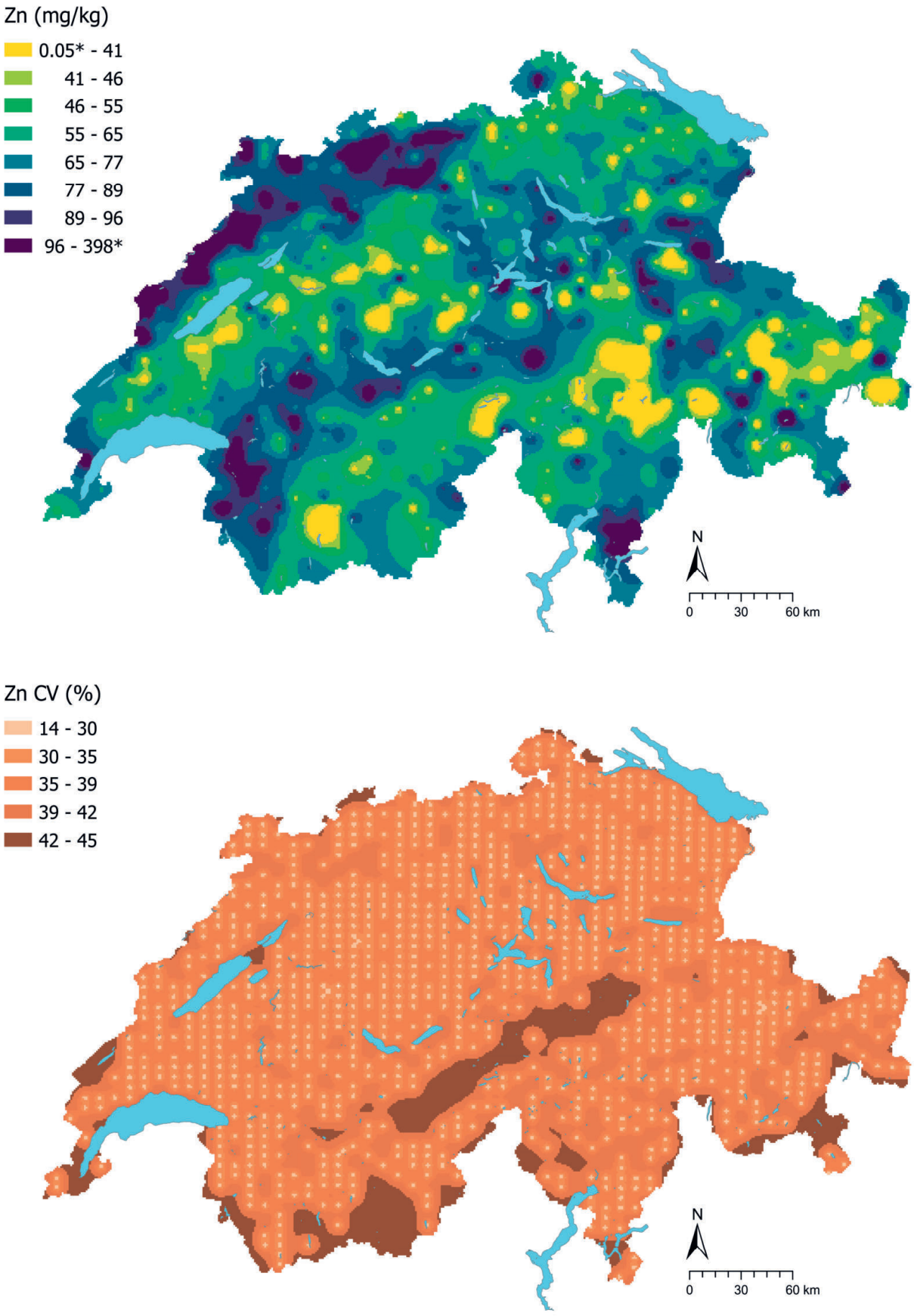

Figure 86 | Interpolated zinc concentrations (mg/kg soil) at the BDM, NABO and GEMAS sites (top) and coefficient of variation (%) of the interpolated concentrations (bottom). The concentrations were divided into eight classes corresponding to the 5 %, 10 %, 25 %, 50 %, 75 %, 90 % and 95 % percentiles. The coefficients of variation were divided into five classes corresponding to the Jenks Natural Breaks algorithm. The interpolation was performed using the ordinary Kriging method (1 km × 1 km grid). In the classes of interpolated values, * denotes the minimum and maximum value of the point data calculated from the limit of detection.

5 Soil properties of Swiss topsoils

In addition to element concentrations, other soil properties such as total organic carbon (TOC), total nitrogen (TN), pH and grain size (Chapter 2) were analysed in the soil samples from the BDM, NABO, GEMAS and UB datasets. The results of these analyses are summarised in Table 3 and in the following chapters.

Since maps of Switzerland modelling pH, total nitrogen, total organic carbon and C:N ratio based on the BDM dataset (Descombes *et al.*, 2020) are already available, no interpolation was undertaken.

Table 3 | Medians, percentiles, maxima, minima and mean absolute deviations from the median (MAD) of soil properties measured in the topsoil (0–20 cm). Results from the combined dataset and from the BDM, NABO and GEMAS sites are listed. The median of all individual samples per site was included in the data analysis. Column n indicates the number of data points on which the analysis is based. TOC: total organic carbon, CEC: cation exchange capacity, TC: total carbon, TN: total nitrogen. Base saturation (Agroscope, 2020c), calcium carbonate (Agroscope, 2020b), potential CEC (Agroscope, 2020c, d, e) and KOF (soil texture) (Agroscope, 2020a): Swiss reference methods of Agroscope research institutes.

	Measurement method	Unit	All sites		BDM, NABO, GEMAS								
			Median	n	Median	n	5 %	25 %	75 %	95 %	Min	Max	MAD
Base saturation	Calculated value as per Agroscope (2020c)	%	65	210	65	210	4	30	87	100	1	100	38
Calcium carbonate $CaCO_3$	As per Agroscope (2020b), incl. $MgCO_3$	% by weight	3.2	496	3	496	0.1	0.4	16.4	39.2	0.0	90.8	4.6
C:N ratio	Calculated value	–	11	1173	11	1173	8	10	15	21	3	68	3
Humus content	Humus content from KOF	% by weight	5.45	2137	6	1078	2.4	4.4	9.9	20.5	0.2	102.1	3.6
Effective CEC	Ca + Mg + K + Na, to ISO/DIS 11260:2017	cmol/kg	17	421	17	421	7	12	24	35	2	47	8
Potential CEC	Ca + Mg + K + Na, as per Agroscope (2020c, d, e)	cmol/kg	22	520	22	520	10	17	30	43	0	104	9
Grain-size class	Grain-size class CH 1 to 13	–	6	933	6	933	3	4	6	9	1	13	1
pH	2 h extraction in 0.01 M $CaCl_2$	–	6.2	3729	5.6	1183	3.5	4.5	6.8	7.4	2.7	8.0	1.7
Volumetric weight of fine soil	KOF (Agroscope, 2020a)	kg/dm^3	0.82	1183	0.82	1183	0.33	0.60	1.02	1.27	0.08	3.77	0.32
Sand content	In the mineral soil fraction; as per KOF	%	48	969	48	969	21	36	59	72	7	86	17
Silt content	As per KOF	%	31	976	31	976	18	25	36	47	11	74	8
TC	Dry combustion	%	4.2	1172	4.2	1172	1.5	2.8	6.4	12.4	0.2	51.8	2.5
TC pool 20 cm	TC reserves in 0–20 cm soil layer	t/ha	67	513	67	513	34	52	89	124	18	268	27
TN	Dry combustion		0.32	1172	0.32	1172	0.14	0.23	0.45	0.77	0.02	2.34	0.17
TN pool 20 cm	TN reserves in 0–20 cm soil layer	t/ha	5.0	1171	5.0	1171	2.2	3.7	6.5	9.1	0.2	54.4	2.1
TOC	TC; pH > 6.5: TOC = TC – $CaCO_3$ * 0.12	%	3.8	1173	3.8	1173	1.4	2.5	5.5	11.7	0.1	51.8	2.0
TOC pool 20 cm	TOC reserves in 0–20 cm soil layer	t/ha	61	1172	61	1172	29	47	76	104	2	780	21
Clay content	AS per KOF	%	19.5	976	19.5	976	7.5	14.0	27.7	41.0	0.5	60.2	9.6
Dry matter	Residual water content at 40 °C dried sample vs drying at 105 °C	%	98	1078	98	1078	95	97	98	99	90	100	1

5.1 pH

The most widely available data in the topsoil samples are for pH, as this parameter was measured at almost all sampling sites where element concentrations were analysed according to the VBBo method. The median pH across all sites (3729) is 6.2, which corresponds to 'neutral' according to the Swiss soil classification system (BGS, 2010). If only the BDM and NABO datasets are considered (1183), the median pH of topsoils is 5.6, which corresponds to 'slightly acid'.

Unlike element concentrations, pH exhibits a left-skewed distribution which consists of numerous underlying distributions (Figure 88). The distribution of alkaline soils is clearly visible in the histogram.

Sites with a high pH are found mainly in northern Switzerland, isolated areas in the Swiss Plateau, in the Alps and in the Rhine Valley (Figure 89). The pH distribution at these sites is influenced by the presence of calcareous parent material and/or by liming of agricultural soils. However, carbonates have a limited capacity to buffer soil acidification: pH decreases comparatively rapidly as soon as all carbonates are dissolved (Amelung *et al.*, 2018c). This is the case in the north-west Jura, where the pH of topsoils is slightly acidic despite the presence of calcareous parent material.

The highest statistically significant pH levels were measured in the topsoils of arable land and settlements. Conversely, the lowest pH levels were recorded at forest sites and alpine pastures (Figure 87).

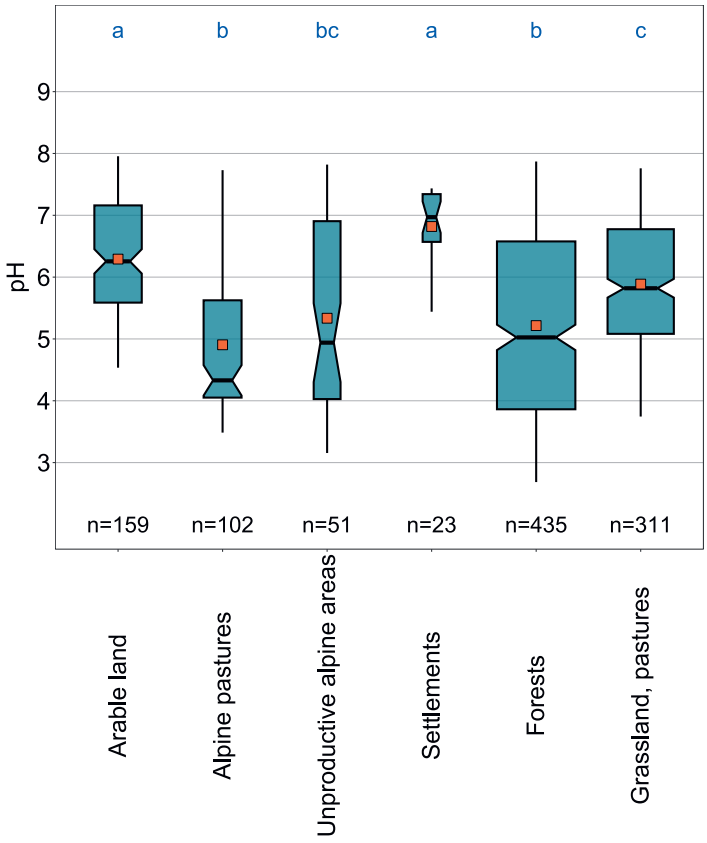

Figure 87 | Comparison of pH between the plotted land-use types of the BDM sites. The median of all individual samples per site was included in the analysis. The number of sites per group is indicated beneath the boxes. Letters in blue: significant differences between groups ($p < 0.001$) based on a Wilcoxon rank sum test with P-adjustment using the Benjamini and Hochberg method.

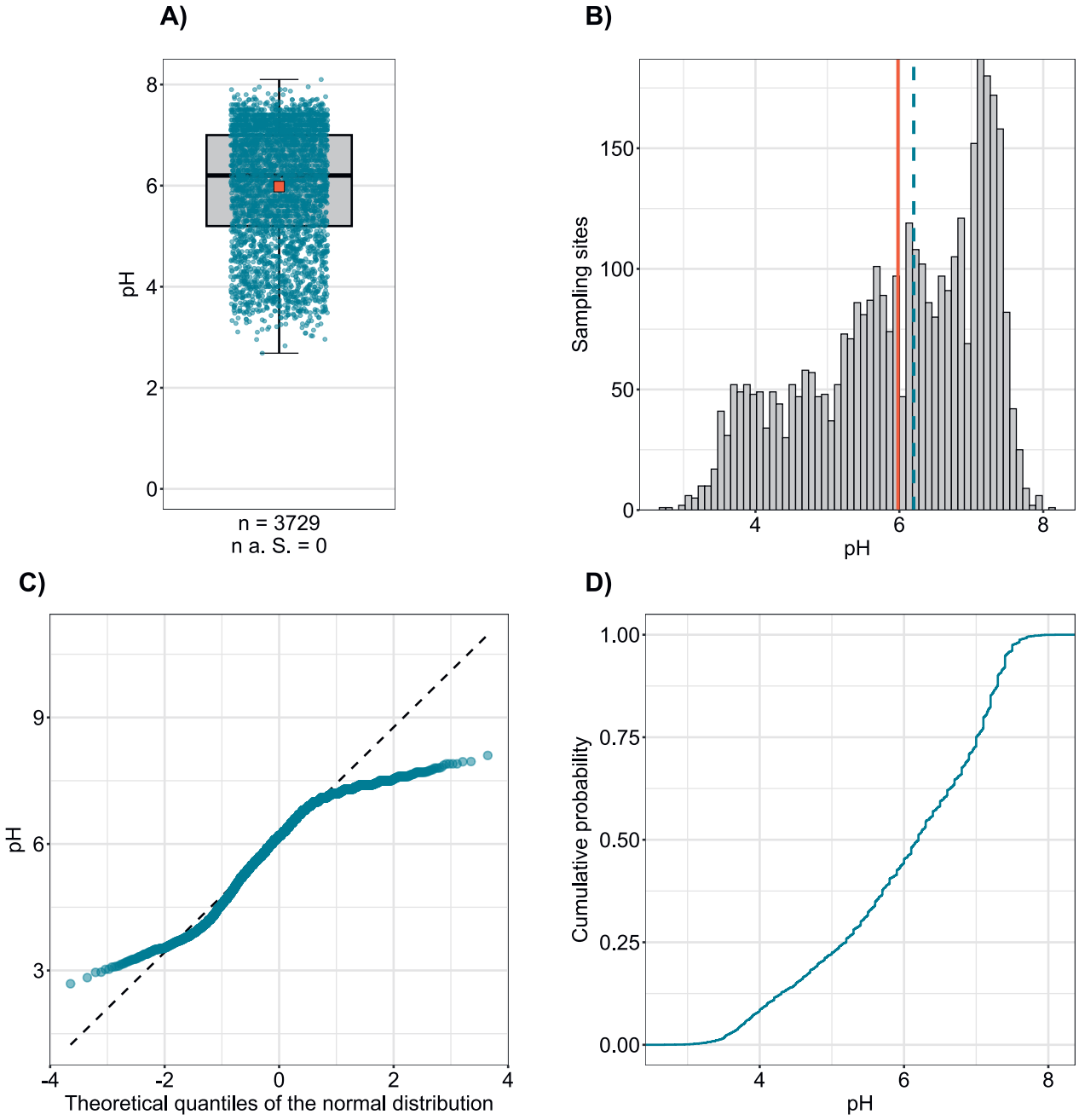

Figure 88 | pH distribution. The allocated value is the median of individual samples per site. The dataset presented comprises the BDM, NABO and UB sampling sites. n = total number of sites, n a. S. = sites lying outside the axis range or whisker.

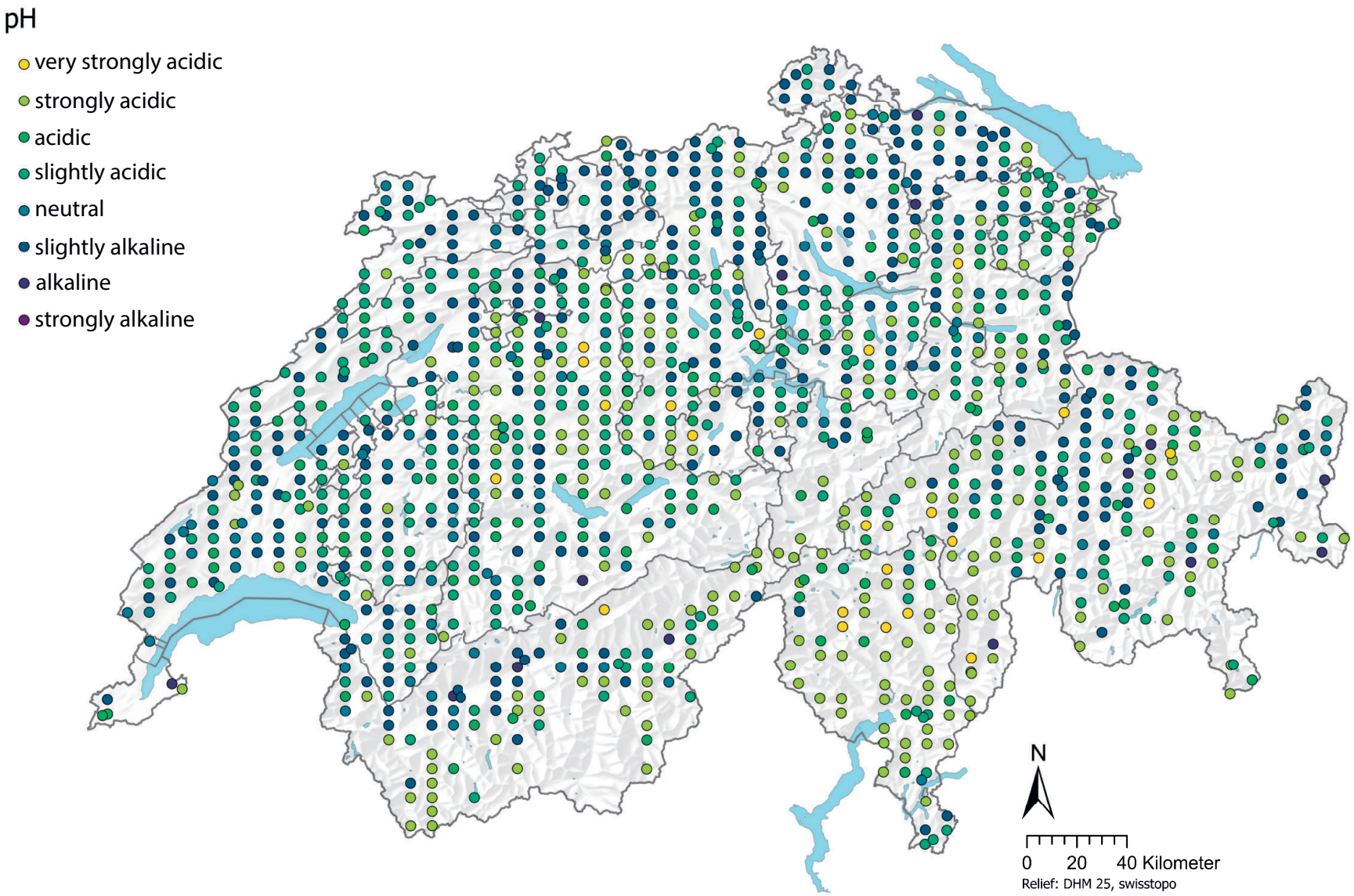

Figure 89 | **Spatial distribution of pH measured in a CaCl2 solution of the BDM and NABO soil samples. The data points show the median of several individual samples per site. The pH was assigned to the following classes in accordance with the Swiss soil classification system (BGS, 2010): very strongly acid < 3.3, strongly acid 3.3–4.3, acid 4.4–5.0, slightly acid 5.1–6.1, neutral 6.2–6.7, slightly alkaline 6.8–7.6, alkaline 7.7–8.2 and strongly alkaline > 8.2.**

5.2 Organic carbon

The median total organic carbon (TOC) content in Swiss topsoils is 3.8 % (Table 3, Figure 91). Assuming that TOC corresponds approximately to soil organic matter (humus) based on the conversion method described by Gubler *et al.* (2018), the median TOC lies within the range classified as 'humus-rich' according to the Swiss soil classification system (BGS, 2010).

TOC concentrations are low in the Swiss Plateau (Figure 92). Arable land exhibits the lowest concentrations when compared with other land-use types (Figure 90). From a pH < 6.5, the calcium carbonate content was not subtracted from the measured total carbon to calculate the TOC. However, since even limed agricultural soils can have a pH below 6.5 (Amelung *et al.*, 2018c), the TOC content at individual arable sites could possibly be even lower. Elevated TOC concentrations were measured at forest sites, although it should be noted that the samples also included the organic layer in the top 0 to 20 cm of soil.

Not only the organic carbon content is of interest, but also the carbon stock in the topsoil, especially regarding carbon sequestration and loss of soil fertility through soil degradation. The distribution of TOC content is similar to that of the TOC stock (Figure 93). Particularly low levels are found in subalpine to alpine regions as well as the Swiss Plateau. The lowest TOC pool was recorded at arable sites and the highest at grassland sites. These findings are consistent with those of previous studies, e.g. Guillaume *et al.* (2022).

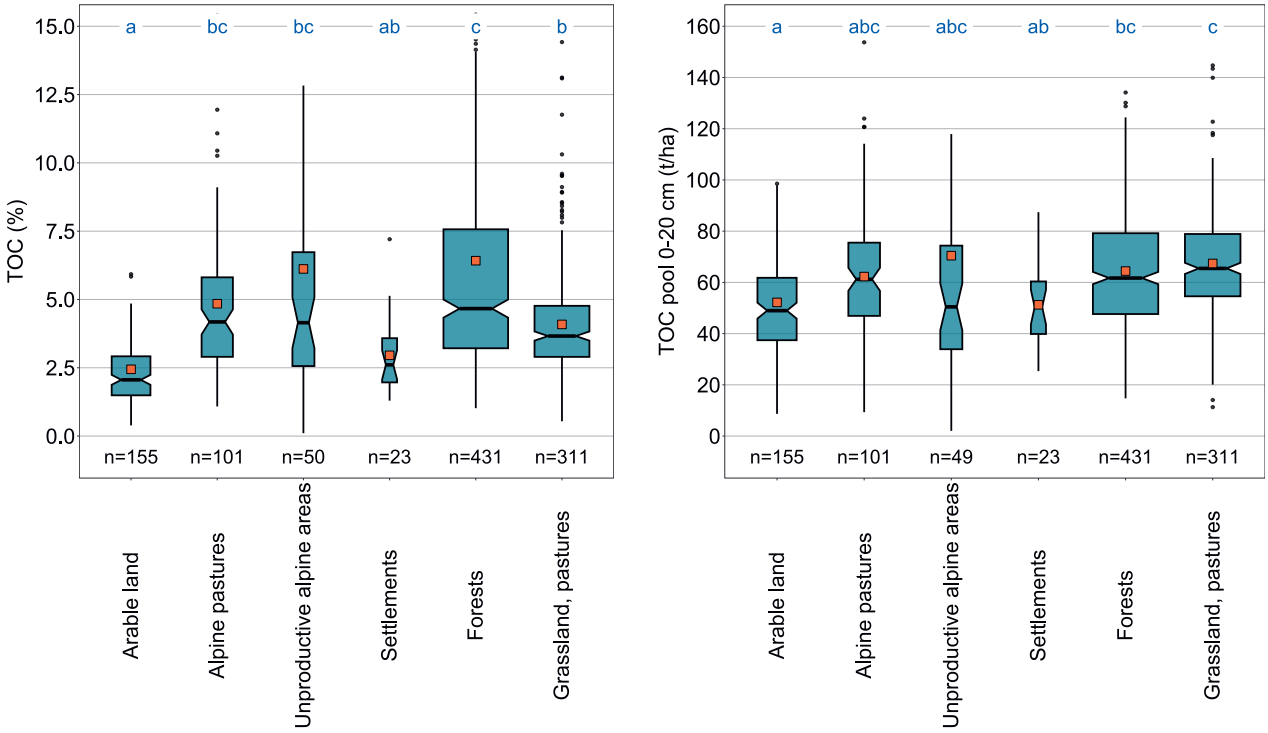

Figure 90 | Comparison of total organic carbon (TOC, %) and TOC stock (t/ha) in topsoil at a depth of 0 to 20 cm between the plotted land-use types of the BDM sites. The median of all individual samples per site was included in the analysis. The number of sites per group is indicated beneath the boxes, although not all outliers are shown. Letters in blue: significant differences between groups (p < 0.001) based on a Wilcoxon rank sum test with P-adjustment using the Benjamini and Hochberg method. 99.5 % of data points are shown. Orange square: arithmetic mean of the data.

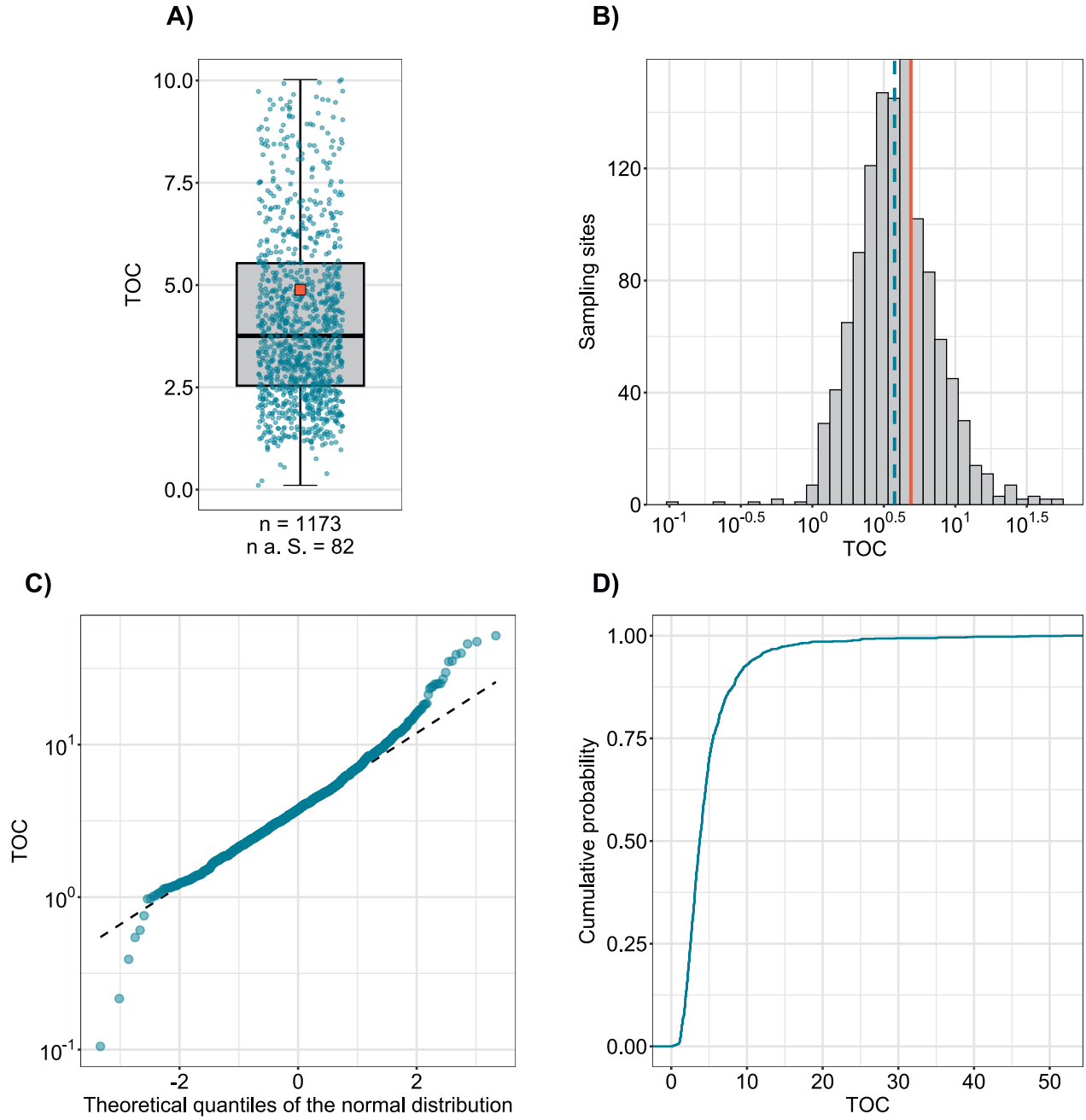

Figure 91 | **Distribution of total organic carbon (TOC, %). The allocated value is the median of individual samples per site. The dataset presented comprises the BDM and NABO sampling sites. n = total number of sites, n a. S. = sites lying outside the axis range or whisker.**

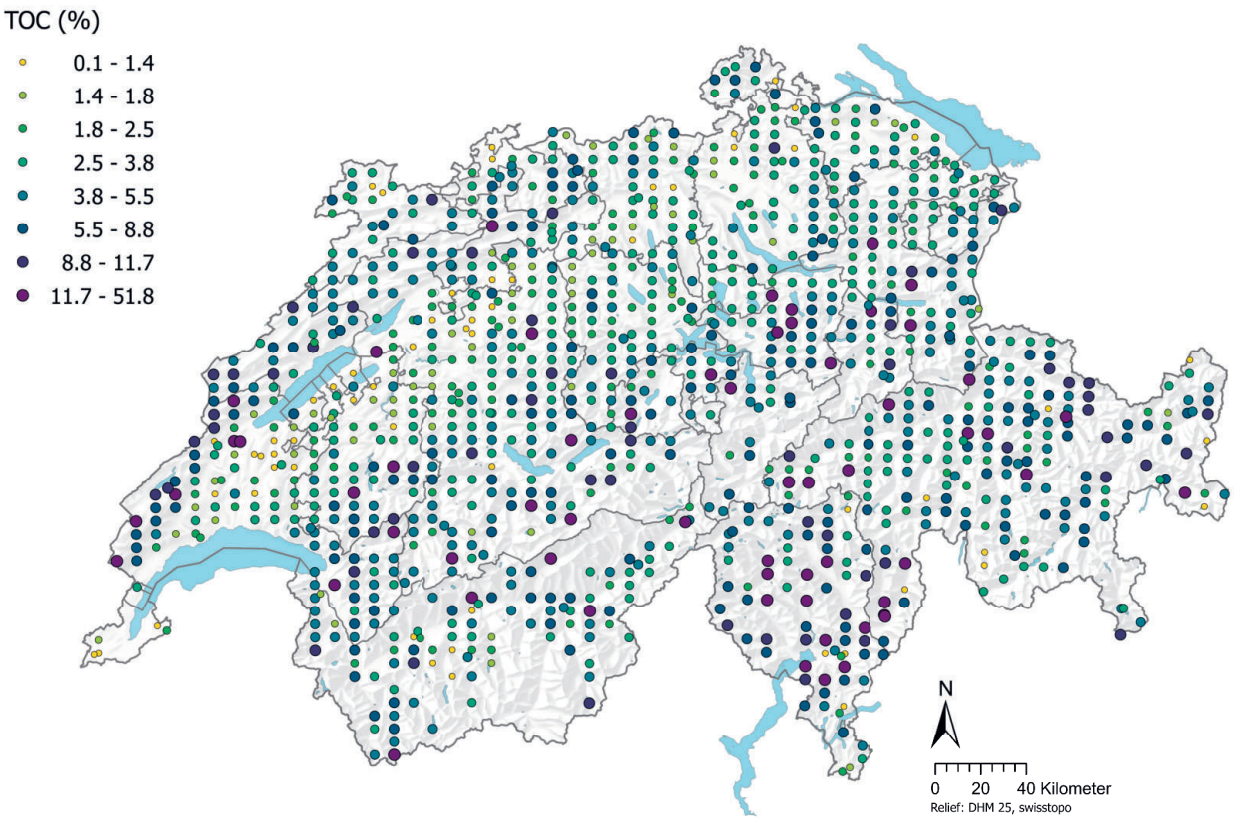

Figure 92 | Spatial distribution of total organic carbon (TOC, %) measured in the BDM and NABO soil samples. The data points show the median of several individual samples per site. The classes correspond to the 5 %, 10 %, 25 %, 50 %, 75 %, 95 % and 95 % percentiles.

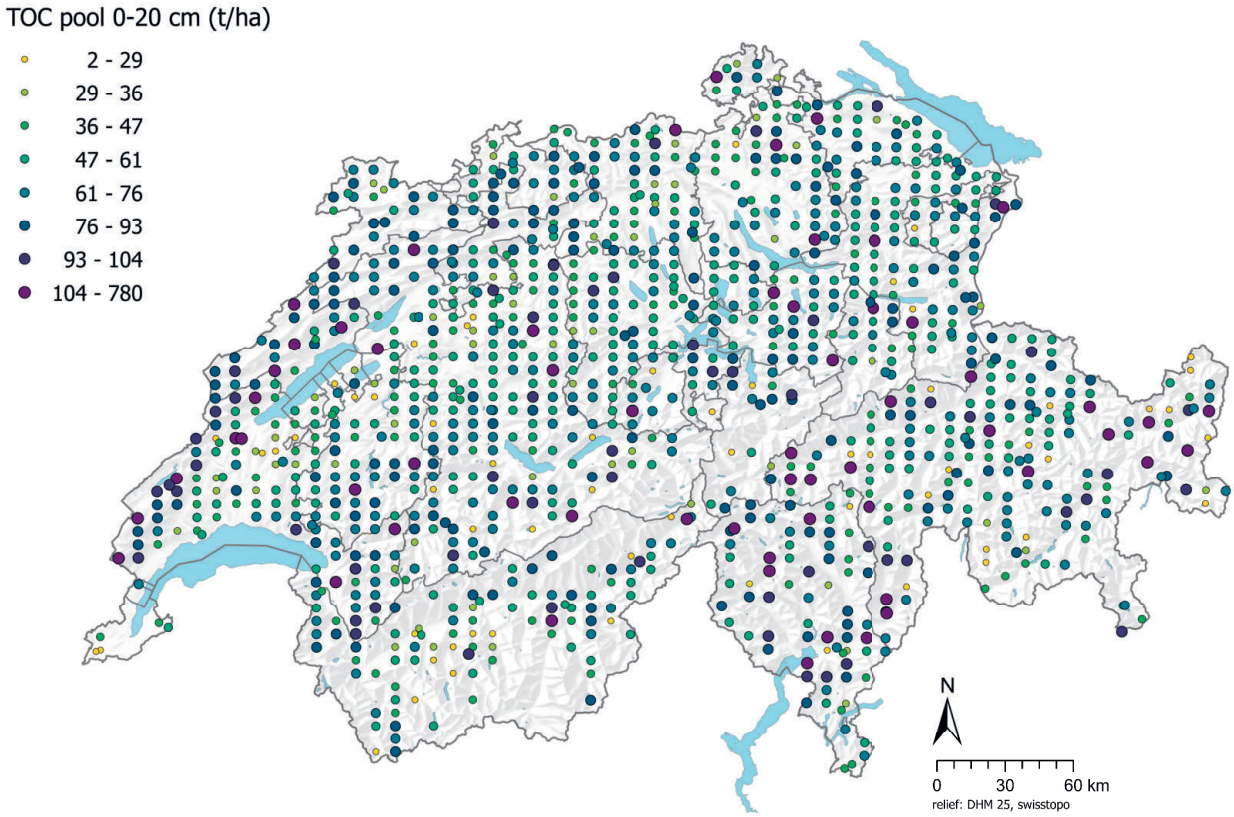

Figure 93 | Spatial distribution of the TOC pool (t/ha) calculated from TOC concentrations at the BDM and NABO sites (0–20 cm depth). The data points show the median of several individual samples per site. The classes correspond to the 5 %, 10 %, 25 %, 50 %, 75 %, 95 % and 95 % percentiles.

5.3 Nitrogen

Although nitrogen is essential for plant growth, excess levels resulting from fertiliser and atmospheric inputs can lead to loss of biodiversity, eutrophication of waterbodies and acidification of the soil (BAFU, 2017). The median total nitrogen (TN) measured in the topsoil across all sites was 0.32 % (Table 3, Figure 94). According to Amelung *et al.* (2018b), TN concentrations in the tillage horizons of temperate soils are equivalent to 0.07–0.2 % and thus somewhat lower than the median in Swiss topsoils. As with TOC, low TN levels are particularly common on arable land in the Swiss Plateau (Figure 95). This is not surprising, since nitrogen is removed with the harvest and replaced by fertilisation on the one hand, and bound in the organic soil matter on the other. Nitrogen concentrations are comparatively high in the north-west Jura, the foothills of the Alps and Ticino, which may be partly due to atmospheric inputs, especially in Ticino.

The ratio of carbon to nitrogen (C:N ratio) serves as a proxy for the degradability of soil organic matter (Amelung *et al.*, 2018c). Arable sites and grassland soils generally have a C:N ratio < 10–15, very acidic forest soils 25–38 and peaty soils 40–60 (Amelung *et al.*, 2018b). A low C:N ratio < 25, e.g. due to the decomposition of microbial biomass (5–8), can result in the release of potentially plant-available nitrogen (Amelung *et al.*, 2018b).

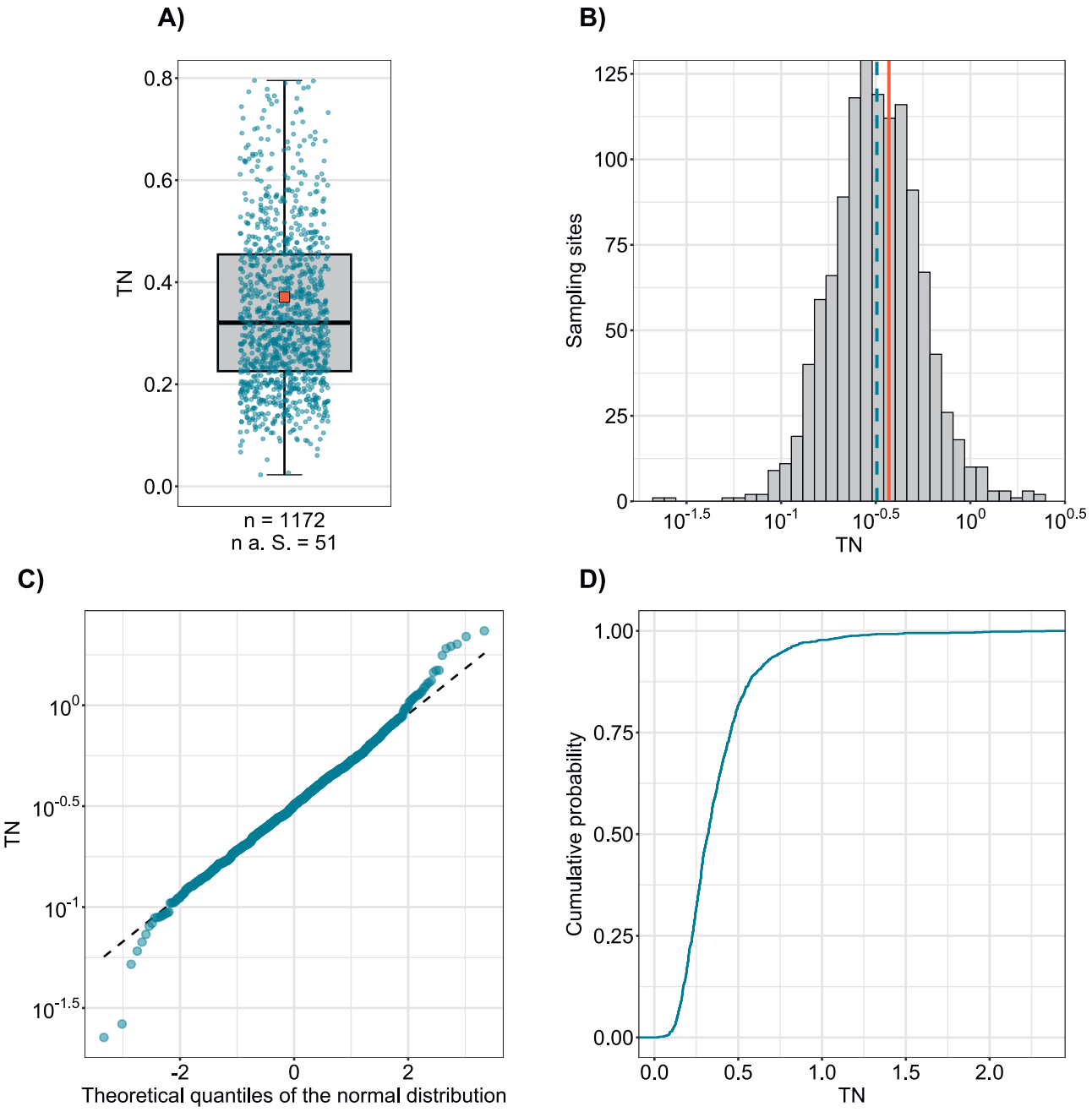

Figure 94 | Distribution of total nitrogen (TN, %). The allocated value is the median of individual samples per site. The dataset presented comprises the BDM and NABO sampling sites. n = total number of sites, n a. S. = sites lying outside the axis range or whisker.

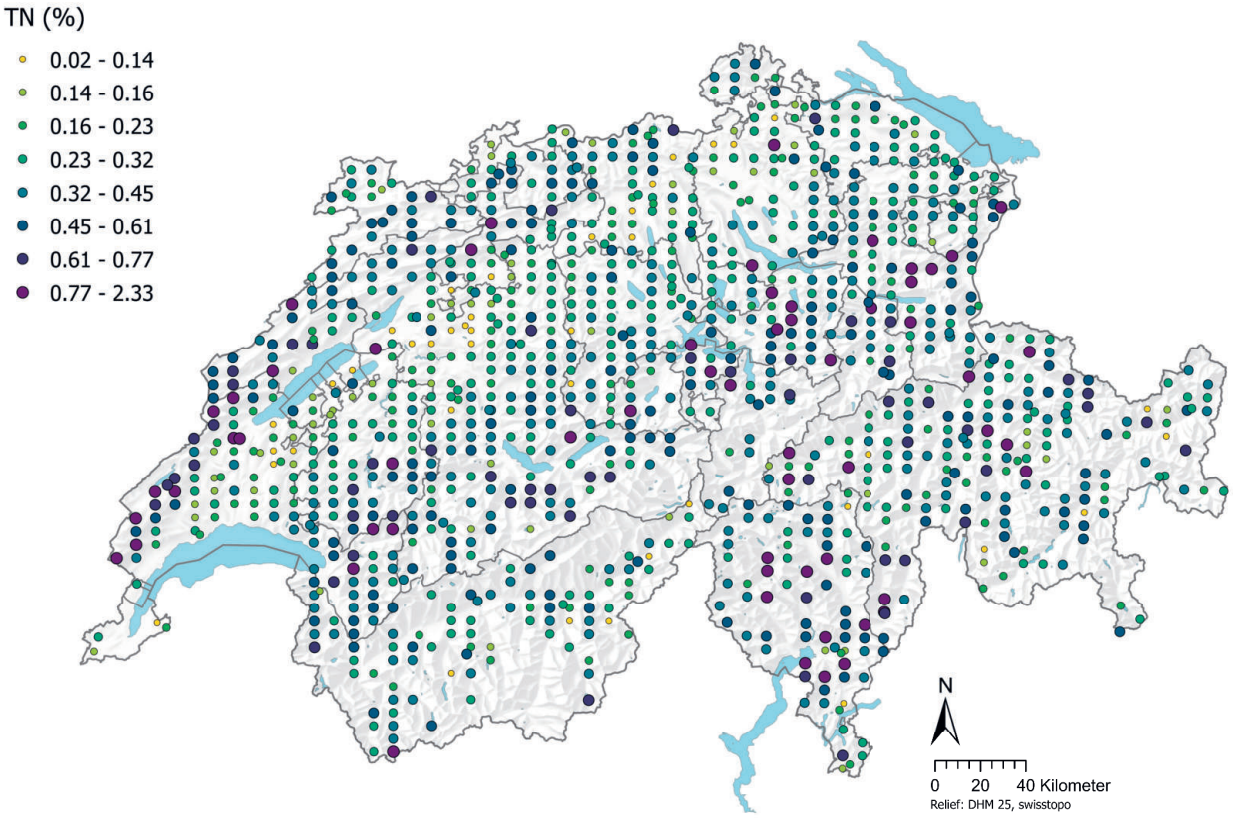

Figure 95 | Spatial distribution of total nitrogen (TN, %) measured in the BDM and NABO soil samples. The data points show the median of several individual samples per site. The classes correspond to the 5 %, 10 %, 25 %, 50 %, 75 %, 95 % and 95 % percentiles.

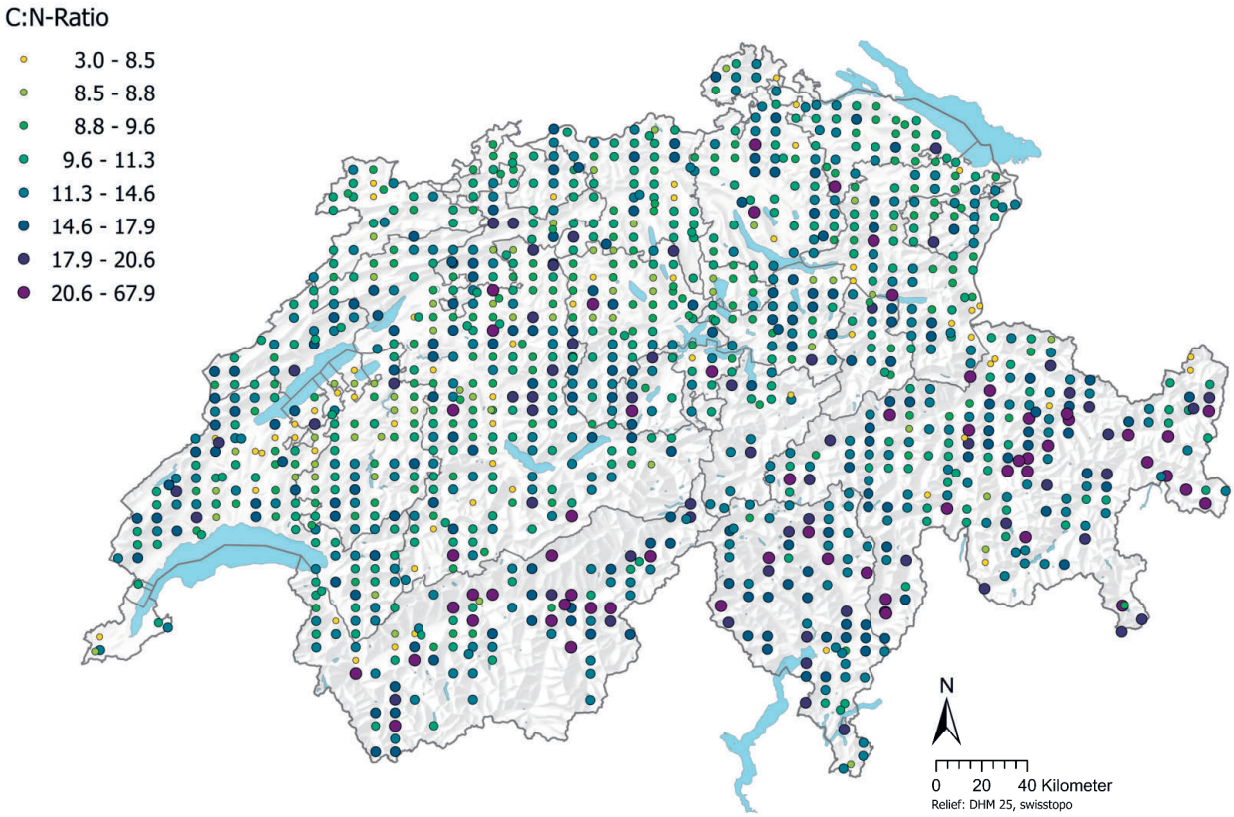

Figure 96 | Spatial distribution of C:N ratio calculated from total carbon and nitrogen concentrations in the BDM and NABO soil samples. The data points show the median of several individual samples per site. The classes correspond to the 5 %, 10 %, 25 %, 50 %, 75 %, 95 % and 95 % percentiles.

5.4 Classification of soil texture

Grain-size classes for mineral soil fractions were derived from the clay, sand and silt content in accordance with the Swiss soil classification system (BGS, 2010) and are illustrated in Figure 100. Sandy soils prevail in the Valais, Ticino and Grisons, while north-western Switzerland and the northern foothills of the Alps are dominated by clayey and silty soils. The Swiss Plateau is characterised by loamy soils.

The measured clay content is indicated separately because clay minerals can strongly influence the immobilisation of heavy metals and other trace elements in the soil through sorption processes. For example, clay minerals can strongly adsorb the cations Ca^{2+}, Mg^{2+}, Na^{+}, K^{+}, Zn^{2+}, Cd^{2+} and Ni^{2+}, depending on pH. In addition to these immobilisation processes, claystone itself can act as a source of trace elements; for example, bituminous claystone contains high to very high cadmium concentrations (Tuchschmid, 1995). The median clay content in the analysed topsoil samples is around 20 % and thus in the loamy range (Table 3, Figure 97). Comparatively high levels of clay were measured in the Jura and the northern foothills of the Alps (Figure 101). Accordingly, the sand content in topsoils in these regions is low (Figure 103).

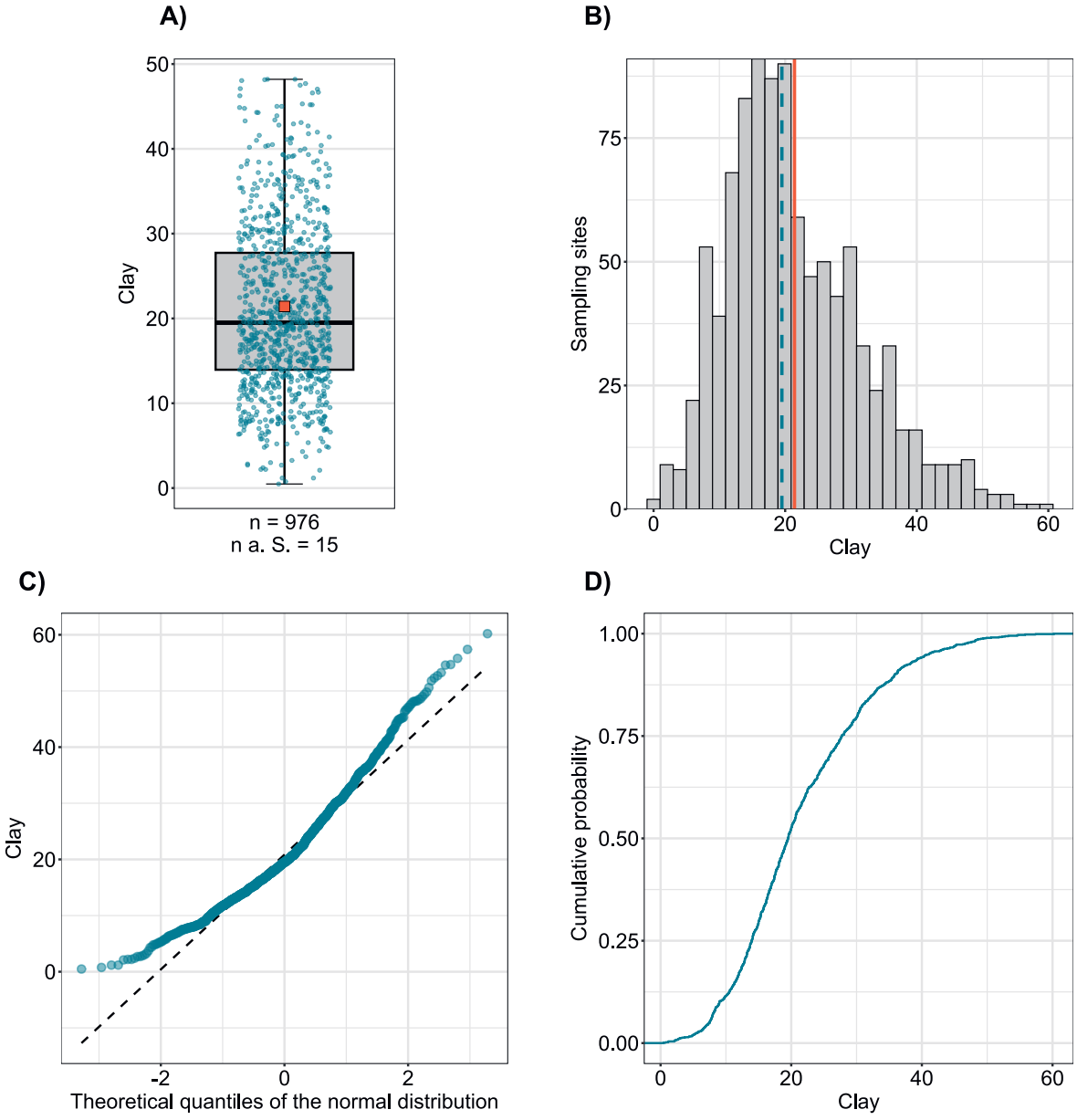

Figure 97 | Distribution of clay content (%). The allocated value is the median of individual samples per site. The dataset presented comprises the BDM and NABO sampling sites. n = total number of sites, n a. S. = sites lying outside the axis range or whisker.

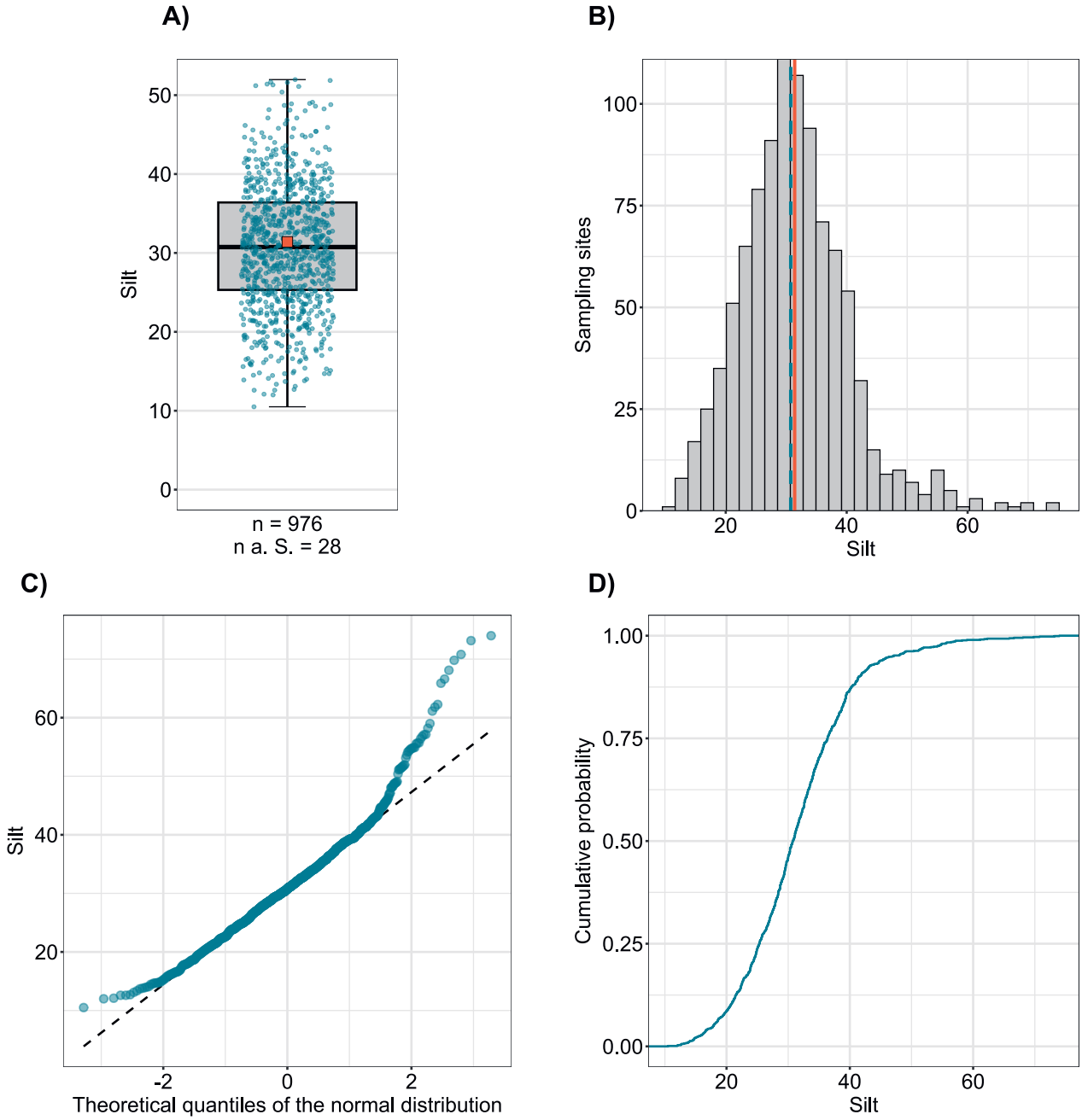

Figure 98 | **Distribution of silt content (%). The allocated value is the median of individual samples per site. The dataset presented comprises the BDM and NABO sampling sites. n = total number of sites, n a. S. = sites lying outside the axis range or whisker.**

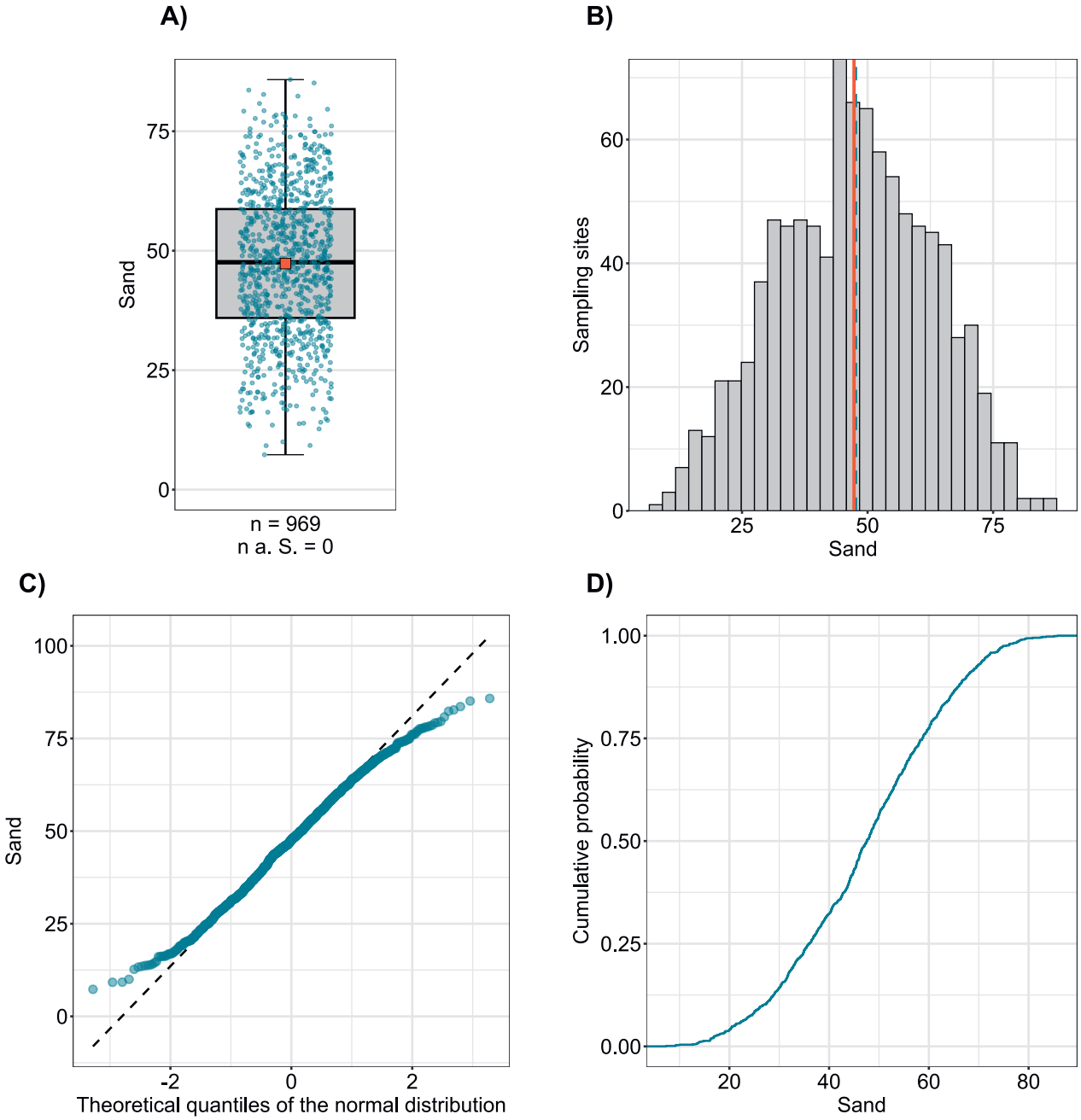

Figure 99 | **Distribution of sand content (%). The allocated value is the median of individual samples per site. The dataset presented comprises the BDM and NABO sampling sites. n = total number of sites, n a. S. = sites lying outside the axis range or whisker.**

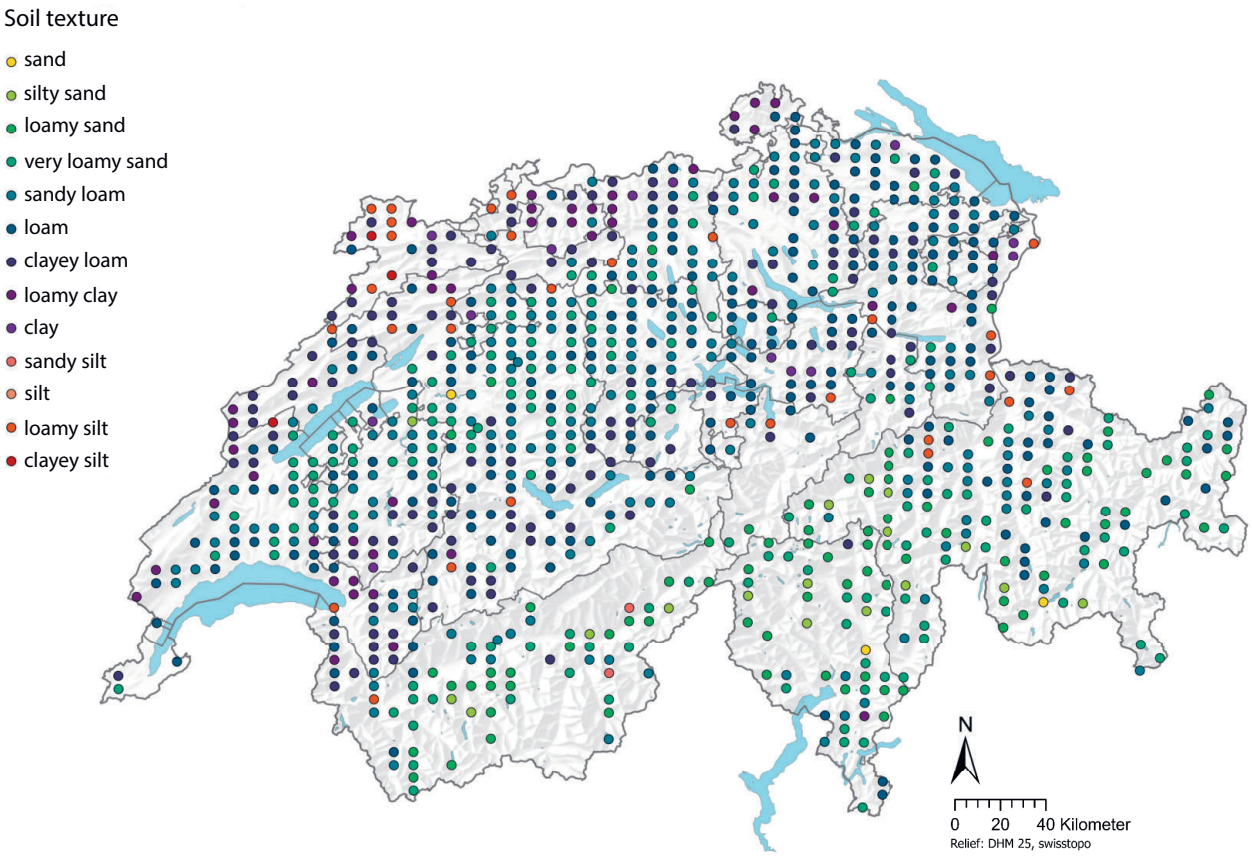

Figure 100 | Spatial distribution of grain-size classes of soil (BDM and NABO sites) The data points show the median of several individual samples per site. The grain-size class was calculated from the measured clay and silt content according to the Swiss soil classification system (BGS, 2010).

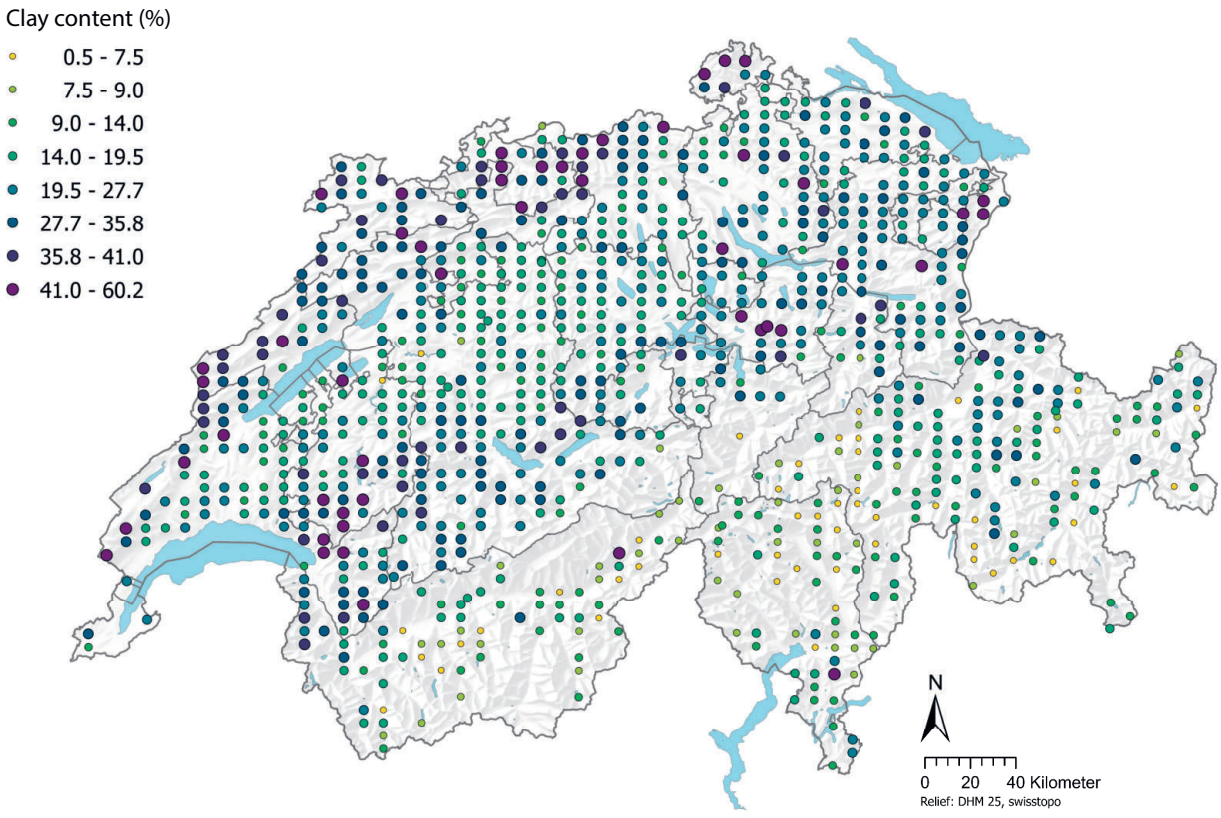

Figure 101 | Spatial distribution of clay content (%) measured in the BDM and NABO soil samples. The data points show the median of several individual samples per site. The classes correspond to the 5 %, 10 %, 25 %, 50 %, 75 %, 95 % and 95 % percentiles.

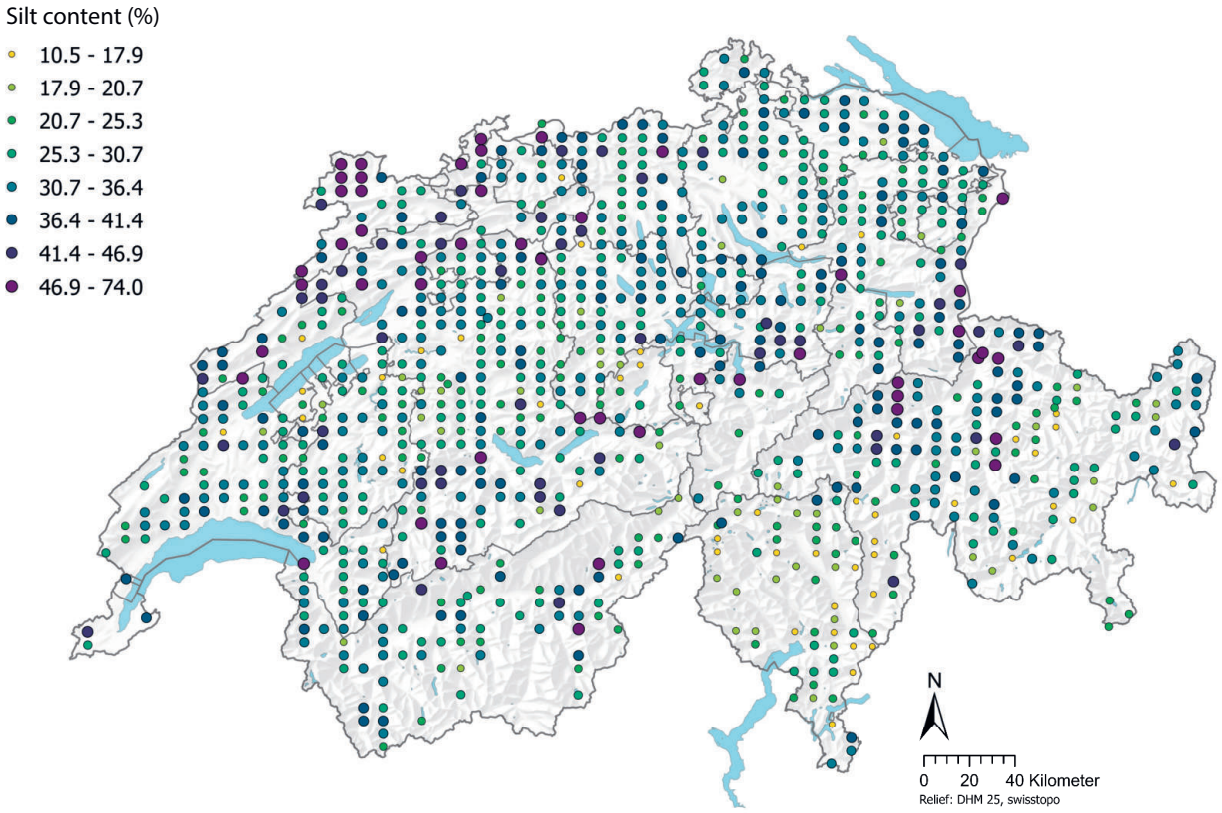

Figure 102 | Spatial distribution of silt content (%) measured in the BDM and NABO soil samples. The data points show the median of several individual samples per site. The classes correspond to the 5 %, 10 %, 25 %, 50 %, 75 %, 95 % and 95 % percentiles.

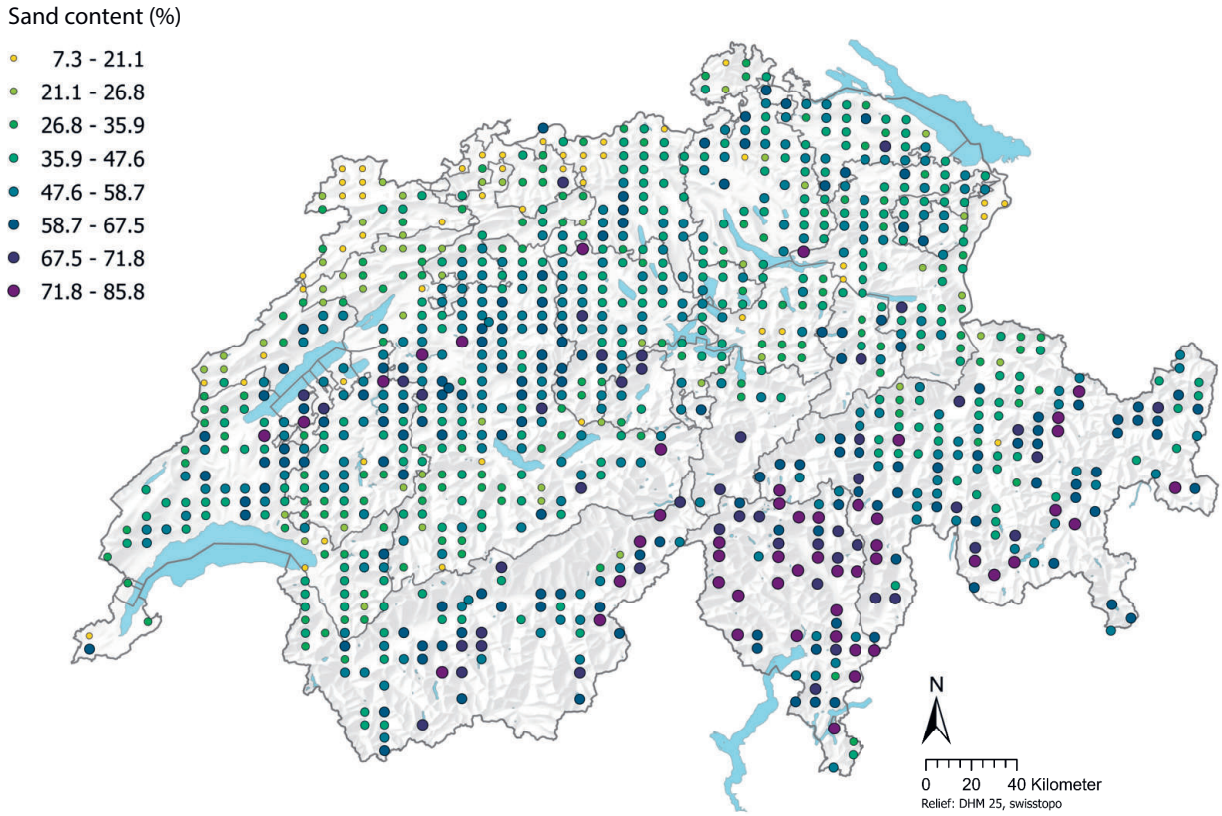

Figure 103 | Spatial distribution of sand content (%) measured in the BDM and NABO soil samples. The data points show the median of several individual samples per site. The classes correspond to the 5 %, 10 %, 25 %, 50 %, 75 %, 95 % and 95 % percentiles.

6 Assessment of potential influencing factors

The results of the multivariate data analysis, including correlations between element concentrations, a selection of the measured soil properties and supplementary data, are summarised in the following chapters. Interpretations of possible geogenic sources of element concentrations and processes influencing concentrations in the soil are also discussed. It should be noted that correlation does not imply causation.

6.1 Correlations

Most elements show a positive correlation with other elements which is significantly different from zero (Table 4). However, only cobalt, iron, nickel, chromium and vanadium concentrations correlate strongly with one another ($R^2 > 0.7$; Matschullat *et al.*, 2018). The close correlation between cobalt, nickel and chromium concentrations is also evident in the factor analysis and the comparison of lithological main groups for the individual elements, suggesting a possible geogenic origin. The positive correlation between cobalt, nickel and chromium is consistent with the findings of Tuchschmid (1995). According to the author, cobalt occurs as a trace element in iron-rich, rock-forming silicates such as olivine and pyroxene and is very closely related to nickel in geochemical terms. The positive correlation between chromium and vanadium may also be explained by the fact that both elements can be incorporated during the formation of iron oxides (Amelung *et al.*, 2018a) and occur mainly in iron-bearing (mafic) minerals (e.g. pyroxene and amphibole) (Coyte & Vengosh, 2020; Tuchschmid, 1995). Similar correlations between chromium and vanadium concentrations in soil were observed in the Advanced Soil Geochemical Atlas of England and Wales (Rawlins *et al.*, 2012).

Calcium concentrations correlate very strongly with pH and calcium carbonate concentrations (Table 5). The pH-dependent chemical weathering of calcium carbonates and resulting mobilisation of Ca^{2+} to the soil solution has been documented (Amelung *et al.*, 2018c) and is reflected in the findings of the correlations, the factor analysis and the comparison of lithological main groups. A similarly strong correlation exists between sulphur concentrations and proxies for soil organic matter (humus content, TN and TC). According to Eriksen (2009), over 95 % of sulphur in soil is organically bound. Likewise, lead, cadmium and mercury concentrations correlate, albeit weakly, with soil parameters describing soil organic matter. These correlations might be explained by incorporation into organic molecules through biochemical processes, as well as through sorption processes. In addition to clay minerals, humic substances are important soil sorbents, especially of cations (Amelung *et al.*, 2018c). According to the authors, the variable negative loading of soil organic matter plays a major role in the cation exchange capacity – especially in topsoil.

Most elements exhibit a slightly negative correlation with sand content and a slightly positive correlation with clay content. This may reflect the importance of clay minerals as sorbents of cations present in the soil solution. In soils with a high sand content, this retention through sorption is significantly lower, and so presumably constitutes the negative correlation. These results indicate that element concentrations in the topsoil are influenced not only by the source and/or inputs, but also by immobilisation processes.

In contrast to the parameters measured in the soil samples, the element concentrations were found to correlate only very weakly, if at all, with the supplementary geodata (Table 6 in the Annex). There is a very slight negative correlation between chromium and the slope and elevation. Thallium and vanadium show a very slight positive correlation with variables reflecting atmospheric deposition. The correlation of thallium concentrations with modelled deposition data for lead, although significant, is only weak.

Table 4 | Spearman's rank correlation coefficient R2 of the measured element concentrations (mg/kg soil) in the aqua regia digests of individual samples in the BDM and NABO data set. The significance levels are indicated by asterisks: * denotes very highly significant (p < 0.001), ** denotes highly significant (0.001 < p < 0.01), * denotes significant (0.01 < p < 0.1) and no asterisk not significant (p > 0.1).**

R^2	As	Ca	Cd	Co	Cr	Cu	Fe	Hg	Mg	Mn	Mo	Na	Ni	Pb	S	Sb	Tl	U	V	Zn
As		***	***	***	***	***	***	***	***	***	***	**	***	***	***	***	***	***	***	***
Ca	0.25		***	***	***	***	*	**	***	***	**		***	**	***	***		**	***	***
Cd	0.41	0.54		***	***	***	***	***	***	***	***	***	***	***	***	***	***	***	***	***
Co	0.50	0.21	0.34		***	***	***	***	***	***	***	*	***	***	***	***	***	**	***	***
Cr	0.28	0.23	0.34	0.61		***	***	***	***	***	***	*	***	***	**	***	***	***	***	***
Cu	0.25	0.29	0.26	0.58	0.42		***		***	***	**	***	***	***	***	***		***	***	***
Fe	0.56	0.06	0.35	0.84	0.58	0.46		***	***	***	***	**	***	***	***	***	***	***	***	***
Hg	0.15	0.07	0.40	0.10	0.17	0.06	0.15		**	***	***	***	***	***	***	***	***		***	***
Mg	0.22	0.35	0.11	0.52	0.42	0.53	0.43	-0.08		***	***	***	***		**	***	***	***	***	***
Mn	0.35	0.25	0.40	0.63	0.51	0.43	0.48	0.15	0.27		***		***	***		***	***	**	***	***
Mo	0.51	0.09	0.41	0.25	0.16	0.12	0.35	0.22	0.11	0.23			***	***	***	***	***	***	***	***
Na	-0.05	0.05	-0.18	0.07	0.06	0.28	0.10	-0.19	0.35	-0.04	0.01		*	***	*	*		***		
Ni	0.37	0.37	0.37	0.84	0.72	0.65	0.65	0.10	0.56	0.62	0.16	0.07		***	**	***	***		***	***
Pb	0.41	0.08	0.57	0.35	0.24	0.23	0.45	0.59	0.06	0.28	0.42	-0.14	0.24		***	***	***	***	***	***
S	0.24	0.36	0.55	0.10	0.09	0.13	0.22	0.36	0.09	0.05	0.29	-0.07	0.08	0.45		***	***	***	***	***
Sb	0.51	0.14	0.38	0.31	0.16	0.31	0.33	0.45	0.22	0.30	0.40	-0.05	0.28	0.58	0.26		***	***	***	***
Tl	0.38	0.01	0.46	0.30	0.31	0.07	0.40	0.34	0.10	0.20	0.49	-0.03	0.16	0.56	0.28	0.25		***	***	***
U	0.32	0.08	0.21	0.09	0.25	0.12	0.11	0.06	0.26	0.09	0.40	0.17	0.06	0.18	0.12	0.19	0.44		***	***
V	0.35	0.18	0.48	0.47	0.77	0.28	0.58	0.24	0.24	0.45	0.30	0.01	0.45	0.37	0.27	0.17	0.51	0.32		***
Zn	0.48	0.32	0.65	0.67	0.48	0.56	0.68	0.29	0.34	0.50	0.35	0.05	0.59	0.60	0.38	0.36	0.45	0.17	0.51	

Table 5 | Spearman's rank correlation coefficient R2 of the measured element concentrations and soil properties in the individual soil samples in the BDM and NABO data set. BasenS: base saturation (%); CaCO3: calcium carbonate content (%); C:N ratio (–); humus content (%), CECeff and CECpot: effective and potential cation exchange capacity (cmol/kg); Swiss soil grain-size class (–); pH (–); sand content (%); silt content (%); TC: total carbon (%); TC 20: total carbon reserves at a depth of 0–20 cm (t/ha); TN: total nitrogen (%); TN 20: total nitrogen stock at a depth of 0–20 cm (t/ha); TOC: total organic carbon (%); TOC 20: total organic carbon reserves at a depth of 0–20 cm (t/ha); and clay content (%).

R^2	BasenS	$CaCO_3$	CN-Ratio	Humus	CECeff	CECpot	Grain-size	pH	Sand	Silt	TC	TC 20	TN	TN 20	TOC	TOC 20	Clay
As	0.10	-0.04	-0.13	0.13	0.35	0.16	0.35	0.22	-0.37	0.22	0.14	0.14	0.24	0.26	0.14	0.17	0.36
Ca	0.89	0.91	-0.19	0.12	0.70	0.20	0.33	0.90	-0.30	0.07	0.37	0.50	0.24	0.29	0.13	0.19	0.37
Cd	0.31	0.06	-0.14	0.37	0.60	0.51	0.55	0.41	-0.47	0.14	0.41	0.44	0.54	0.48	0.39	0.42	0.55
Co	0.13	-0.29	-0.26	-0.00	0.33	0.16	0.44	0.20	-0.44	0.26	-0.04	0.05	0.14	0.25	0.01	0.07	0.40
Cr	0.24	-0.28	-0.33	-0.05	0.37	0.19	0.45	0.20	-0.40	0.13	-0.09	0.11	0.12	0.37	-0.04	0.15	0.45
Cu	0.37	-0.13	-0.40	-0.12	0.19	-0.05	0.24	0.36	-0.19	0.15	-0.10	0.08	0.05	0.27	-0.13	0.02	0.17
Fe	-0.09	-0.35	-0.17	0.15	0.28	0.28	0.40	0.03	-0.41	0.21	0.08	0.08	0.28	0.28	0.17	0.18	0.40
Hg	-0.07	-0.09	0.25	0.47	0.27	0.57	0.32	-0.10	-0.23	0.03	0.42	0.29	0.46	0.22	0.49	0.42	0.31
Mg	0.31	0.25	-0.15	-0.04	0.16	-0.06	0.04	0.35	-0.04	0.03	0.08	0.17	0.02	0.10	-0.04	0.01	0.03
Mn	0.25	-0.23	-0.41	-0.15	0.29	0.04	0.38	0.30	-0.35	0.22	-0.17	-0.02	0.05	0.27	-0.14	-0.01	0.36
Mo	0.00	-0.05	0.04	0.24	0.24	0.28	0.22	0.02	-0.23	0.07	0.23	0.22	0.29	0.20	0.27	0.24	0.26
Na	0.18	0.09	-0.10	-0.16	-0.20	-0.28	-0.24	0.10	0.20	-0.06	-0.12	-0.09	-0.15	-0.06	-0.16	-0.13	-0.27
Ni	0.38	-0.20	-0.34	-0.09	0.43	0.09	0.45	0.39	-0.43	0.22	-0.07	0.10	0.08	0.29	-0.08	0.06	0.44
Pb	-0.05	-0.22	0.08	0.44	0.33	0.52	0.43	-0.06	-0.38	0.16	0.38	0.30	0.53	0.34	0.47	0.42	0.41
S	0.17	0.21	0.01	0.69	0.51	0.62	0.33	0.20	-0.28	0.02	0.74	0.70	0.86	0.61	0.73	0.69	0.37
Sb	-0.01	-0.10	0.04	0.26	0.17	0.23	0.23	0.09	-0.16	0.09	0.24	0.20	0.29	0.18	0.26	0.23	0.18
Tl	-0.12	-0.17	0.11	0.31	0.26	0.46	0.37	-0.11	-0.33	0.05	0.26	0.19	0.35	0.25	0.34	0.32	0.38
U	0.08	-0.11	-0.06	0.04	0.12	0.05	-0.01	0.06	-0.03	-0.04	0.02	0.10	0.06	0.14	0.03	0.10	0.04
V	0.10	-0.24	-0.29	0.11	0.34	0.37	0.51	0.12	-0.45	0.14	0.07	0.20	0.30	0.46	0.13	0.29	0.53
Zn	0.18	-0.20	-0.28	0.20	0.44	0.30	0.49	0.25	-0.50	0.26	0.16	0.21	0.40	0.44	0.21	0.27	0.50

6.2 Factor analysis

The four factors presented account for 43 % of the overall variance (Figure 104). Ten factors were analysed in total, together explaining 76 % of the overall variance. The individual factor loadings for the variables are presented in Figure 104. One way of interpreting the factor analysis is to group variables with similar factor loadings. With Factor 1, most elements form a single group with high loadings, with cobalt and nickel lying particularly close together. This could indicate the geogenic origin of these two elements, as suggested by the correlations.

In addition to the correlation and factor analysis, comparison of the simplified lithological groups also indicates a close, possibly geogenic association between cobalt and nickel concentrations (see chapter on the respective elements). The basic rock class contains very high concentrations of both elements, together with chromium, which is consistent with the findings of Tuchschmid (1995). According to the author, the concentrations of these elements are particularly closely linked to iron and magnesium levels in the different lithofacies; high levels of iron and magnesium are also found in the basic rock group. However, since this class comprises only a few sites, the differences are not statistically significant. Ma & Hooda (2010) reported that high levels of chromium, cobalt and nickel of geogenic origin in soil can be explained by the presence of mafic to ultramafic source rock, with serpentinite-bearing parent material particularly likely to contain high concentrations of chromium and nickel. Other elements such as chromium, copper, iron, aluminium, zinc, manganese and magnesium appear in a similar region of the factor analysis. It is therefore assumed that Factor 1 may represent the mineralogy and/or sorption processes to iron oxides.

Furthermore, cadmium and lead are closely related in Factors 1 and 2, with the clay content having similar loadings here. This could indicate sorption processes to clay minerals and/or claystone as the parent material.

Unlike other elements, sulphur appears in a similar range to total nitrogen and total organic carbon – the parameters which serve as proxies for soil organic matter. Mercury concentrations exhibit comparable loadings to precipitation.

Factors 3 and 4 clearly show the grouping of calcium and calcium carbonate associated with the pH value, as well as a second grouping consisting of the proxies for atmospheric deposition. Atmospheric depositions of cadmium, lead and mercury are grouped in Factor 6 (not shown), although no element appears in this group.

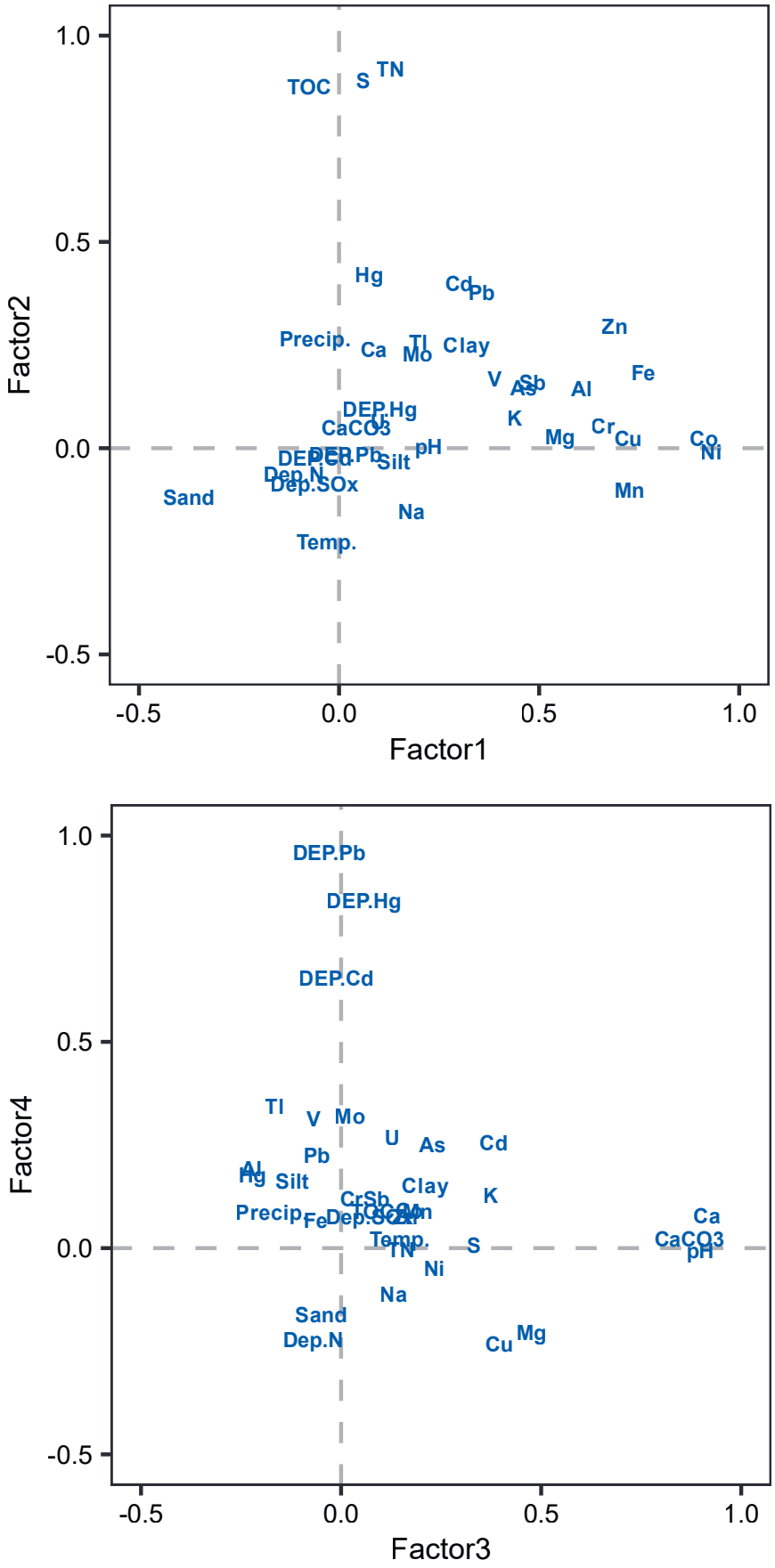

Figure 104 | Maximum likelihood factor analysis of element concentrations and selected soil and environmental parameters (Dep. = atmospheric deposition, Temp = temperature, NS = precipitation, Chapter 2.5). The median values from the BDM and NABO sites were included in the analysis. The loadings of the individual variables per factor (varimax rotation) are shown. Robust scaling based on the minimum covariance determinant. Factor 1 explains 16 % of the variance, Factor 2 a further 9.5 %, Factor 3, 9.1 % and Factor 4, 8.8 %.

7 Conclusions

As a bioreactor for the lithosphere, topsoil plays a vital role in several processes, such as nutrient uptake by plants and soil organisms, or the filtering of pollutants. The Geochemical Soil Atlas is the first comprehensive documentation of 20 essential and/or potentially harmful elements in topsoil to cover the whole of Switzerland. It provides a unique overview of the distribution and total concentrations of elements and thus serves as an important tool for implementing soil protection measures at national level. The data can be used to identify areas where further investigations are needed to gauge the risk of potentially adverse effects on plant, animal and human health due to too-high or too-low element levels, and to adapt resource management accordingly.

Measured element concentrations in Switzerland lie within typical concentration ranges for European soils. However, there are clear regional differences, with comparatively high element concentrations frequently measured in the Jura and the Eastern Central Alps. At some sites, concentrations of toxic elements – especially arsenic, cadmium, chromium, copper, nickel and vanadium – are elevated and exceed threshold values. However, these potentially contaminated areas are mostly restricted to small-scale hotspots. At most of the sites investigated, measured concentrations lie within a range that can be classified as largely non-hazardous. In contrast to the hotspots, topsoils in the Swiss Plateau tend to have medium to low element concentrations, especially in the case of essential elements such as sulphur. Since these areas are important for agricultural production, it is vital to ensure an adequate supply of essential elements. For this reason, further investigations are needed.

The regional distribution of element concentrations is illustrated in the interpolated maps, with a focus on hotspots and areas with low concentrations. These maps form the basis for defining areas requiring further investigation to assess toxicity or potential deficits. However, no precise or plot-level concentrations can be derived from the interpolated maps. Rather, the maps serve to visualise the regional distribution of element concentrations in topsoils and identify areas with potential hotspots (or potential nutrient deficits).

The multivariate data analysis indicates a link between concentrations of some elements and possible parent materials, which differ according to region. In addition to these sources, however, soil processes such as sorption to clay minerals and iron oxides, chemical precipitation processes, and incorporation into soil organic matter etc. are relevant for the immobilisation and thus accumulation of elements in topsoil.

8 Outlook

The maps of the Geochemical Soil Atlas depict background levels of element concentrations in topsoils during the sampling period, including diffuse inputs from agricultural or atmospheric sources, for example. Anthropogenic point sources were excluded as far as possible based on the existing data. The lower soil horizons would have to be sampled and further chemical analysis undertaken (e.g. isotope analysis) to differentiate between geogenic and anthropogenic sources in more detail. In addition to different sources, soil processes play a key role in the accumulation of elements in topsoil. These sources and processes show temporal dynamics reflected in the findings of the National Soil Monitoring Network (NABO) long-term monitoring programme. It would be advisable to re-sample the BDM sites to record possible changes in element concentrations and thus evaluate the dynamics. This would enable the nationwide impact of reduced atmospheric deposition and/or degradation of soil organic matter on sulphur concentrations to be evaluated, for example. In addition, the degradation of soil organic matter adversely affects key soil functions such as the ability to filter pollutants, leading to the mobilisation of potentially toxic elements.

The Geochemical Soil Atlas presents the total concentrations of the analysed elements in Swiss topsoils. However, the effective risk is determined not only by the total concentration of any given element, but also its bioavailability. Further investigations are needed in the relevant areas to estimate the bioavailability of an element. These could include bioavailability modelling (Smolders *et al.*, 2009) combined with analysis of the element species present in the soil (organically bound, inorganically bound, oxidation state), and selective extraction methods. The respective use must also be considered, e.g. tolerance values for children's playgrounds are lower than those for agricultural land due to possible direct uptake of soil material via ingestion. These types of analysis and information are necessary to carry out a detailed risk assessment.

Other elements measured in the BDM samples but not included in the Geochemical Soil Atlas and therefore not analysed in depth also exhibit a spatial distribution pattern featuring relatively high element concentrations in the Jura and the Eastern Central Alps and relatively low concentrations in the Swiss Plateau. For example, like sulphur, the essential element selenium is present in particularly low concentrations at arable sites in the Swiss Plateau. Tolerance, trigger and toxicity values in aqua regia digests are available for selenium and other elements, e.g. barium, beryllium, gallium and zircon, due to their potential toxicity (Eikmann & Kloke, 1993; Herklotz *et al.*, 1996). Concentrations of beryllium, gallium and zircon in particular are elevated in the Jura, suggesting a similar distribution pattern to chromium, cadmium and thallium. Lithium is another element of interest that has yet to be evaluated for the Geochemical Soil Atlas. Due to its use in batteries, the element is considered a key critical raw material (FGS, 2023a). Together with beryllium, gallium, germanium, indium, thallium and the lanthanides (e.g. cerium), lithium is classified as an emerging 'high-tech' critical element (HTCE). Although the use of HTCEs and their potential environmental emissions are rising, little is known about their eco-toxicity and background levels in the soil (Reimann *et al.*, 2018). A detailed evaluation would provide valuable additional information about the current state of potentially critical elements in Swiss topsoils.

9 Acknowledgements

The authors would like to thank the following people and institutions for their support:

- Sulphur remeasurements: Micha Vontobel and Dr Diane Bürge (Soil and Elemental Analysis, Agroscope); Dr Julie Tolu, Caroline Stengel and Björn Studer (Environmental Inorganic Geochemistry Group, Eawag and ETH Zurich)
- Mercury remeasurements: Dr Sylvain Bouchet and Kurt Barmettler (Soil Chemistry Group, ETH Zurich)
- Sampling and underlying data: colleagues from the Z9 indicator programme at Biodiversity Monitoring Switzerland (BDM) 2011–2015, Dr Tobias Roth (Hintermann & Weber AG), Ramon Zimmermann and the NABO team (Agroscope); Lucija Stanisic, Dr Juliet Blum, Prof. Dr Moritz Bigalke, Sabnam Mahat and Prof. Dr Adrien Mestrot (Institute of Geography, University of Bern), Dr Reto Meier (NABEL, BAFU), Peter Hayoz (swisstopo)
- Multivariate data analysis: Dr Andrea Stenke and David Haaf (Environmental Inorganic Geochemistry Group, Eawag and ETH Zurich)
- Colour schemes, preliminary evaluation of soil parameters: Vincent Marmier
- Technical advisory group and initialisation of investigations: the cantonal soil protection agencies' working group on intervention levels and risk assessment (AGIR) and the Federal Office for the Environment (FOEN), Soil and Biotechnology Division
- Technical feedback: Dr Madlene Nussbaum (Department of Agriculture, School of Agricultural, Forest and Food Sciences HAFL) and Dr Felix Stumpf (Competence Centre Soil, HAFL)

10 Authors' contributions

Jolanda E. Reusser
- Geochemical Soil Atlas data: quality control of laboratory analysis, validation, evaluation, interpretation, map creation and visualisation
- Report: compilation of draft report, revision and editing
- Scientific project management and project administration

Maja B. Siegenthaler
- Sulphur remeasurement data: data collection and laboratory analysis, quality control of laboratory analysis, validation and evaluation
- Report: compilation of the chapter on sulphur remeasurement, revision and editing, significant contribution to the conclusion and outlook chapters

Lenny H. E. Winkel
- Conceptualisation
- Supervision of and significant contribution to data evaluation and interpretation
- Report: revision and editing
- Support with the scientific project management

Daniel Wächter
- BDM and NABO data: supervision of sampling and laboratory analysis, preliminary quality control of the laboratory analysis, establishment and curation of data management system, preliminary data analysis, map visualisation
- Report: revision and editing

Ruben Kretzschmar
- Conceptualisation
- Supervision
- Report: revision and editing

Reto G. Meuli
- Conceptualisation
- Lead supervisor
- Report: revision and editing
- Overall project management

Abbreviations

As	Arsenic
FOEN	Federal Office for the Environment
BDM	Biodiversity Monitoring Switzerland
BDM-Z9	Biodiversity Monitoring Switzerland's indicator Z9 'Species diversity in habitats'
Ca	Calcium
Cd	Cadmium
Co	Cobalt
Cr	Chromium
Cu	Copper
CV	Coefficient of variation
Fe	Iron
GEMAS	European geochemical soil atlas
Hg	Mercury
ICP-MS	Inductively coupled plasma mass spectrometry
KbS	Register of contaminated sites
Mg	Magnesium
Mn	Manganese
Mo	Molybdenum
Na	Sodium
NABO	National Soil Monitoring Network
NABODAT	National Soil Information System
Ni	Nickel
LOD	Limit of detection
p-value	Significance value
Pb	Lead
R2	Spearman's rank correlation coefficient
S	Sulphur
Sb	Antimony
swisstopo	Swiss Federal Office of Topography
TC	Total carbon content
TIF	Tukey Inner Fence
Tl	Thallium
TN	Total nitrogen content
TOC	Total organic carbon content
U	Uranium
UB	University of Bern
V	Vanadium
VBBo	Swiss Ordinance on Soil Pollution
XRF	X-ray fluorescence spectrometry
Zn	Zinc

References

DFG, 2020. *Faktenblatt «Bodenbelastungen entlang von Strassen».* Arbeitsgruppe Interventionswerte und Risikobeurteilung (AGIR), Konferenz der Vorsteher der Umweltschutzämter KVU, Bern.

Agroscope, 2020a. KOF: Bestimmung der Körnung in der Feinerde. Schweizerische Referenzmethoden der Forschungsanstalten Agroscope, Zürich-Reckenholz. https://ira.agroscope.ch/en-US/Page/Publikation/Index/45990.

Agroscope, 2020b. $CaCO_3$: Bestimmung des Gesamtkalkgehaltes ($CaCO_3$) in Bodenproben. Schweizerische Referenzmethoden der Forschungsanstalten Agroscope, Zürich-Reckenholz. Version 3.1. https://ira.agroscope.ch/de-CH/publication/45887.

Agroscope, 2020c. KAK: Bestimmung der potentiellen Kationenaustauschkapazität und Basensättigung. Schweizerische Referenzmethoden der Forschungsanstalten Agroscope, Zürich-Reckenholz. Version 2.0. https://ira.agroscope.ch/de-CH/publication/46182.

Agroscope, 2020d. KAK-Ex: Extraktion der potentiell austauschbaren Kationen des Bodens mit Bariumchlorid bei pH 8.1. Schweizerische Referenzmethoden der Forschungsanstalten Agroscope, Zürich-Reckenholz. Version 2.0. https://ira.agroscope.ch/de-CH/publication/46183.

Agroscope, 2020e. KAK-H: Austauschbare H+ Ionen für potentielle Kationenaustauschkapazität und Basensättigung. Schweizerische Referenzmethoden der Forschungsanstalten Agroscope, Zürich-Reckenholz. Version 2.0. https://ira.agroscope.ch/de-CH/publication/46184.

Amelung W., Blume H.-P., Fleige H., Horn R., Kandeler E., Kögel-Knabner I., Kretzschmar R., Stahr K., Wilke B.-M., 2018a. *Anorganische Komponenten der Böden – Minerale und Gesteine.* In: W. Amelung *et al.* (eds.), Scheffer/Schachtschabel Lehrbuch der Bodenkunde. Springer Berlin Heidelberg, pp. 11–62.

Amelung W., Blume H.-P., Fleige H., Horn R., Kandeler E., Kögel-Knabner I., Kretzschmar R., Stahr K., Wilke B.-M., 2018b. *Böden als Pflanzenstandorte.* In: W. Amelung *et al.* (eds.), Scheffer/Schachtschabel Lehrbuch der Bodenkunde. Springer Berlin Heidelberg, pp. 491–581.

Amelung W., Blume H.-P., Fleige H., Horn R., Kandeler E., Kögel-Knabner I., Kretzschmar R., Stahr K., Wilke B.-M., 2018c. *Chemische Eigenschaften und Prozesse.* In: W. Amelung *et al.* (eds.), Scheffer/Schachtschabel Lehrbuch der Bodenkunde. Springer Berlin Heidelberg, pp. 151–211.

Amelung W., Blume H.-P., Fleige H., Horn R., Kandeler E., Kögel-Knabner I., Kretzschmar R., Stahr K., Wilke B.-M., 2018d. *Gefährdung der Bodenfunktionen.* In: W. Amelung *et al.* (eds.), Scheffer/Schachtschabel Lehrbuch der Bodenkunde. Springer Berlin Heidelberg, pp. 583–686.

Arai Y., 2010. *Arsenic and Antimony.* In: P.S. Hooda (ed.), Trace Elements in Soils. Wiley, Chichester, pp. 381–407.

AUE, Schmutz D., 2016. *Faktenblatt: Arsen und Thallium in Landwirtschafts- und Waldböden im Gebiet Erzmatt bei Buus und Umgebung.* Amt für Umweltschutz und Energie (AUE), Bau- und Umweltschutzdirektion, Kanton Basel Landschaft, Liestal. https://www.baselland.ch/politik-und-behorden/direktionen/bau-und-umweltschutzdirektion/umweltschutz-energie/boden/publikationen/

Bader H.P., Scheidegger R., Wittmer D., Lichtensteiger T., 2011. *Copper flows in buildings, infrastructure and mobiles: a dynamic model and its application to Switzerland.* Clean Technologies and Environmental Policy 13(1), 87–101.

BAFU (eds.), 2017. *Boden in der Schweiz. Zustand und Entwicklung. Stand 2017.* Bundesamt für Umwelt, Bern, Umwelt-Zustand Nr. 1721: 86 S.

BAFU (eds.), 2018. *Deposition von Luftschadstoffen in der Schweiz. Moosanalysen 1990–2015.* Bundesamt für Umwelt, Bern, Umwelt-Zustand Nr. 1818: 134 S.

BAFU (eds.), 2020. *Monitoring und Wirkungskontrolle Biodiversität. Übersicht zu nationalen Programmen und Anknüpfungspunkte.* Bundesamt für Umwelt, Bern, Umweltwissen Nr. 2005: 57 S.

BAFU (eds.), 2022. *Luftqualität 2021. Messresultate des Nationalen Beobachtungsnetzes für Luftfremdstoffe (NABEL).* Bundesamt für Umwelt, Bern, Umwelt-Zustand Nr. 2227: 29 S.

Benjamini Y., Hochberg Y., 1995. *Controlling the false discovery rate: a practical and powerful approach to multiple testing.* Journal of the Royal Statistical Society Series B 57, 289–300. doi:10.1111/j.2517-6161.1995.tb02031

BGS, 2010. Klassifikation der Böden der Schweiz. 3. Ausgabe. Bodenkundliche Gesellschaft der Schweiz BGS, Luzern. https://www.soil.ch/download/pictures/c3/lbgit58se3ti5d6a7mpzo3cfktdz2o/klass_03_2010.pdf

Bhupinderpal S., Hedley M.J., Saggar S., Francis G.S., 2004. *Chemical fractionation to characterize changes in sulphur and carbon in soil caused by management.* European Journal of Soil Science 55(1), 79–90.

Bigalke M., Ulrich A., Rehmus A., Keller A., 2017. *Accumulation of cadmium and uranium in arable soils in Switzerland.* Environmental Pollution 221, 85–93.

Bivand R.S., Pebesma E.J., Gomez-Rubio V., 2013. *Applied spatial data analysis with R.* Use R, volume 10. Second edition. Springer New York, NY.

Breit G.N., Wanty R.B., 1991. *Vanadium accumulation in carbonaceous rocks: A review of geochemical controls during deposition and diagenesis.* Chemical Geology 91(2), 83–97.

Brown K.A., 1982. *Sulphur in the environment: A review.* Environmental Pollution Series B, Chemical and Physical 3(1), 47–80.

Chaney R.L., 2010. *Cadmium and Zinc.* In: P.S. Hooda (ed.), Trace Elements in Soils. Wiley, Chichester, pp. 409-439.

Christie T., Brathwaite B., 2011. *Mineral Commodity Report 2 – Antimony.* Institute of Geological and Nuclear Services Ltd.

Clifford M.J., Hilson G.M., Hodson M.E., 2010. *Tin and Mercury.* In: P.S. Hooda (ed.), Trace Elements in Soils. Wiley, Chichester, pp. 497–513.

Coyte R.M., Vengosh A., 2020. *Factors Controlling the Risks of Co-occurrence of the Redox-Sensitive Elements of Arsenic, Chromium, Vanadium, and Uranium in Groundwater from the Eastern United States.* Environmental Science & Technology 54(7), 4367–4375.

Cressie N., 1993. *Statistics for Spatial Data.* Wiley Series in Probability and Statistics. 2nd ed. John Wiley & Sons, Incorporated, New York.

De Smith M.J., Goodchild M.F., Longley P.A., 2018. *Geospatial analysis : a comprehensive guide to principles, techniques and software tools.* 6th edition ed. Drumlin Security, London.

Delarze R., Gonseth Y., Galland P., 2008. *Lebensräume der Schweiz : Ökologie - Gefährdung - Kennarten.* 2. vollständig überarb. Aufl. Ott Verlag, Thun.

Descombes P., Walthert L., Baltensweiler A., Meuli R.G., Karger D.N., Ginzler C., Zurell D., Zimmermann N.E., 2020. *Spatial modelling of ecological indicator values improves predictions of plant distributions in complex landscapes.* Ecography 43(10), 1448–1463.

Drack W., 1968. *Ur- und frühgeschichtliche Archäologie der Schweiz: 6 Bände.* Verlag Schweizerische Gesellschaft für Ur- und Frühgeschichte, Basel.

Eikmann T., Kloke A., 1993. *Nutzung- und schutzgutbezogene Orientierungswerte für (Schad-)Stoffe in Böden.* In: D. Rosenkranz, G. Bachmann, W. König, G. Einsele (ed.), Bodenschutz, ergänzbares Handbuch. E. Schmidt Verlag, Berlin.

Eriksen J., 2009. *Chapter 2: Soil Sulfur Cycling in Temperate Agricultural Systems.* In: D.L. Sparks (ed.), Advances in Agronomy. Elsevier Academic Press, Amsterdam, pp. 55–89.

Evans L.J., Barabash S.J., 2010. *Molybdenum, Silver, Thallium and Vanadium.* In: P.S. Hooda (ed.), Trace Elements in Soils. Wiley, Chichester, pp. 515–549.

FGS, 2023a. *Lithium in Schweizer Tiefengewässer.* Fachgruppe Georessourcen Schweiz (FGS), ETH Zürich. https://georessourcen.ethz.ch/lithium-aus-schweizer-tiefenwaessern/

FGS, 2023b. *Rohstoffinformationssystem Schweiz (RIS).* Fachgruppe Georessourcen Schweiz, ETH Zürich. https://map.georessourcen.ethz.ch/

Fitzgerald W.F., Lamborg C.H., Hammerschmidt C.R., 2007. *Marine Biogeochemical Cycling of Mercury.* Chemical Reviews 107(2), 641–662.

Fluck E., Heumann K.G., 2017. *Periodensystem der Elemente.* Wiley-VCH, Weinheim, 6. Auflage, 2 S.

Gilli R.S., Karlen C., Weber M., Rüegg J., Barmettler K., Biester H., Boivin P., Kretzschmar R., 2018. *Speciation and Mobility of Mercury in Soils Contaminated by Legacy Emissions from a Chemical Factory in the Rhône Valley in Canton of Valais, Switzerland.* Soil Systems 2(3), 44. https://doi.org/10.3390/soilsystems2030044

Gilliéron F., 1988. *Zur Geologie der Uranmineralisation in den Schweizer Alpen.* Beiträge zur Geologie der Schweiz, Geotechnische Serie, Lieferung 77, Fachgruppe Georessourcen Schweiz, ETH Zürich. 60 S. https://georessourcen.ethz.ch/publikationen/beitraege-zur-geologie-der-schweiz-geotechnische-serie/

Goldschmidt V.M., Muir A., 1954. *Geochemistry.* The international series of monographs on physics. Clarendon Press, Oxford.

Gonnelli C., Renella G., 2013. *Chromium and Nickel.* In: B.J. Alloway (ed.), Heavy Metals in Soils: Trace Metals and Metalloids in Soils and their Bioavailability. Springer Netherlands, Dordrecht. pp. 313–333.

Graeser S., 1967. *Ein Vorkommen von Lorandit ($TlAsS_2$) in der Schweiz.* Contributions to Mineralogy and Petrology 16(1), 45–50.

Gräler B., Pebesma E.J., Heuvelink G., 2016. *Spatio-Temporal Interpolation using gstat.* The R Journal 8(1), 204–218.

Graves S., Piepho H.-P., Selzer L., Dorai-Jai S., 2019. *multcompView: Visualizations of Paired Comparisons. R Package Version 0.1-8.*

Gross T., Keller A., Müller M., Gubler A., 2021. *Stoffbilanzen für Parzellen der Nationalen Bodenbeobachtung : Nährstoffe und Schwermetalle 1985–2017.* Agroscope Science 123, 1–99. https://doi.org/10.34776/as123g

Gubler A., Gross T., Hug A.-S., Moll-Mielewczik J., Müller M., Rehbein, K., Schwab P., Wächter D., Zimmermann R., Meuli R.G., 2022. *Die Nationale Bodenbeobachtung 2021.* Agroscope Science 128, 1–66. https://doi.org/10.34776/as128g

Gubler A., Schwab P., Wächter D., Meuli R.G., Keller A., 2015. *Ergebnisse der Nationalen Bodenbeobachtung (NABO) 1985-2009: Zustand und Veränderungen der anorganischen Schadstoffe und Bodenbegleitparameter.* Bundesamt für Umwelt (BAFU), Bern, Umwelt-Zustand Nr. 1507: 1–81.

Gubler A., Wächter D., Schwab P., 2018. *Homogenisation of series of soil organic carbon: harmonising results by wet oxidation (Swiss Standard Method) and dry combustion.* Agroscope Science 62, 1–9. https://ira.agroscope.ch/en-US/publication/37689

Guillaume T., Makowski D., Libohova Z., Elfouki S., Fontana M., Leifeld J., Bragazza L., Sinaj S., 2022. *Carbon storage in agricultural topsoils and subsoils is promoted by including temporary grasslands into the crop rotation.* Geoderma 422, 115937.

Gulley A.L., 2022. *One hundred years of cobalt production in the Democratic Republic of the Congo.* Resources Policy 79, 103007.

He Z.L., Shentu J., Yang X.E., 2010. *Manganese and Selenium.* In: P.S. Hooda (ed.), Trace Elements in Soils. Wiley, Chichester, pp. 481–495.

Hengl T., 2009. *A Practical Guide to Geostatistical Mapping.* EUR 22904 EN Scientific and Technical Research. 2 ed. Office for Official Publications of the European Communities, Luxembourg.

Herklotz K., Coldewey W.G., Hoffmann K., Rump H.H., Wagner H., Kloke A., Lühr H.P., Eikmann T., 1996. *Erfassen und Bewerten.* In: H. Neumaier, H.H. Weber (ed.), Altlasten: Erkennen, Bewerten, Sanieren. Springer Berlin Heidelberg, Berlin, Heidelberg, pp. 42-218.

Hooda P.S., 2010. *Introduction.* In: P.S. Hooda (S.), Trace Elements in Soils. Wiley, Chichester, pp. 1–8.

Hough R.L., 2010. *Copper and Lead.* In: P.S. Hooda (ed.), Trace Elements in Soils. Wiley, Chichester, pp. 441–460.

Imseng M., Wiggenhauser M., Keller A., Müller M., Rehkämper M., Murphy K., Kreissig K., Frossard E., Wilcke W., Bigalke M., 2018. *Fate of Cd in Agricultural Soils: A Stable Isotope Approach to Anthropogenic Impact, Soil Formation, and Soil-Plant Cycling.* Environmental Science & Technology 52(4), 1919–1928.

Jacquat O., Voegelin A., Kretzschmar R., 2009. *Soil properties controlling Zn speciation and fractionation in contaminated soils.* Geochimica et Cosmochimica Acta 73(18), 5256–5272.

Jacquat, O., Rambeau, C., Voegelin, A., Efimenko N., Villard A., Föllmi K. B., Kretzschmar R., 20011. *Origin of high Zn contents in Jurassic limestone of the Jura mountain range and the Burgundy: evidence from Zn speciation and distribution.* Swiss Journal of Geosciences 104(3), 409–424.

Jarva J., Tarvainen T., Reinikainen J., Eklund M., 2010. *TAPIR — Finnish national geochemical baseline database.* Science of The Total Environment 408(20), 4385–4395.

Jiskra M., Sonke J.E., Obrist D., Bieser J., Ebinghaus R., Myhre C.L., Pfaffhuber K.A., Wängberg I., Kyllönen K., Worthy D., Martin L.G., Labuschagne C., Mkololo T., Ramonet M., Magand O., Dommergue A., 2018. *A vegetation control on seasonal variations in global atmospheric mercury concentrations.* Nature Geoscience 11(4), 244–250.

Johnson C.A., Moench H., Wersin P., Kugler P., Wenger C., 2005. *Solubility of Antimony and Other Elements in Samples Taken from Shooting Ranges.* Journal of Environmental Quality 34(1), 248–254.

Johnston W.R., Proctor J., 1981. *Growth of Serpentine and Non-Serpentine Races of Festuca Rubra in Solutions Simulating the Chemical Conditions in a Toxic Serpentine Soil.* Journal of Ecology 69(3), 855–869.

Jost B., SGTK, GEO Partner AG, 2014. *Urban Mining: AWEL Factsheet Antimon.* Schweizerische Geotechnische Kommission SGTK, ETH Zürich, GEO Partner AG; Amt für Abfall, Wasser, Energie und Luft (AWEL), Baudirektion Kanton Zürich, available in English at: https://georessourcen.ethz.ch/en/publications/factsheets

Kabata-Pendias A., 2011. *Trace elements in soils and plants.* Fourth edition. CRC Press, Boca Raton, FL.

Kaiser H.F., 1958. *The varimax criterion for analytic rotation in factor analysis.* Psychometrika 23(3), 187–200.

Keller A., Schulin R., 2003. *Modelling regional-scale mass balances of phosphorus, cadmium and zinc fluxes on arable and dairy farms.* European Journal of Agronomy 20(1), 181–198.

Khan M., Castro-Guerrero N., Mendoza-Cozatl D., 2014. *Moving toward a precise nutrition: preferential loading of seeds with essential nutrients over non-essential toxic elements.* Frontiers in Plant Science 5. https://doi.org/10.3389/fpls.2014.00051

Krachler M., Mohl C., Emons H., Shotyk W., 2003. *Atmospheric Deposition of V, Cr, and Ni since the Late Glacial: Effects of Climatic Cycles, Human Impacts, and Comparison with Crustal Abundances.* Environmental Science & Technology 37(12), 2658–2667.

Kündig R., Mumenthaler T., Eckardt P., Keusen H.R., Schindler C., Hofmann F., Vogler F., Guntli P., 1997. *Die mineralischen Rohstoffe der Schweiz.* Schweizerische Geotechnische Kommission.

Lado L.R., Hengl T., Reuter H.I., 2008. *Heavy metals in European soils: A geostatistical analysis of the FOREGS Geochemical database.* Geoderma 148(2), 189–199.

Laurent A.G., 1963. *The Lognormal Distribution and the Translation Method: Description and Estimation Problems.* Journal of the American Statistical Association 58(301), 231–235.

Ma Y., Hooda P.S., 2010. *Chromium, Nickel and Cobalt.* In: John Wiley & Sons, Ltd, Chichester, UK, pp. 461–479.

Mächler M., Rousseeuw P., Croux C., Todorov V., Ruckstuhl A., Salibian-Barrera M., Verbeke T., Koller M., Conceicao E., Anna di Palma M., 2016. *robustbase: Basic Robust Statistics. R package version 0.92-7.*

MacKenzie A.B., 2000. *Environmental radioactivity: experience from the 20th century — trends and issues for the 21st century.* Science of The Total Environment 249(1), 313–329.

MacSween K., Edwards G.C., Howard D.A., 2020. *Up-scaling mercury emissions from terrestrial surfaces as a response to sustained temperature increase.* Atmospheric Environment 223, 117190.

Mailänder R.A., Hämmann M., 2005. *Manual on risk assessment and measures for polluted soils.* Federal Office for the Environment (FOEN), Berne, 99 pp.

Malone B.P., Minasny B., McBratney A.B., 2017. *Using R for Digital Soil Mapping.* Progress in Soil Science. 1st edition. Published by Springer International Publishing, Cham, Switzerland.

Mathys R., Dittmar J., Johnson C.A., 2007. *Antimony in Switzerland: A substance flow analysis.* .Bundesant für Umwelt(BAFU), Bern, Environmental studies 0724: 149 S.

Matschullat J., Ottenstein R., Reimann C., 2000. *Geochemical background – can we calculate it?* Environmental Geology 39(9), 990–1000.

Matschullat J. *et al.*, 2018. *GEMAS: CNS concentrations and C/N ratios in European agricultural soil.* Science of The Total Environment 627, 975–984.

Meissner N., 2012. *La minéralogie de l'uranium dans le massif des Aiguilles Rouges (Alpes occidentales).* Beiträge zur Geologie der Schweiz, Geotechnische Serie, Lieferung 96, 183.

Meuli R.G., Wächter D., Schwab P., Kohli L., Zimmermann R., 2017. *Connecting biodiversity monitoring with soil inventory data - a Swiss case study.* BGS Bulletin 38, 65–69.

Mikutta C., Langner P., Bargar J.R., Kretzschmar R., 2016. *Tetra- and Hexavalent Uranium Forms Bidentate-Mononuclear Complexes with Particulate Organic Matter in a Naturally Uranium-Enriched Peatland.* Environmental Science & Technology 50(19), 10465–10475.

Mukherjee B., Patra B., Mahapatra S., Banerjee P., Tiwari A., Chatterjee M., 2004. *Vanadium—an element of atypical biological significance.* Toxicology Letters 150(2), 135–143.

NEROS, 2019. *Geogene Belastungen in Gesteinseinheiten der Schweiz. Übersicht, Charakterisierung, Handlungspotenzial.* Netzwerk mineralische Rohstoffe Schweiz (NEROS); Bundesamt für Umwelt (BAFU), Bern.

Nicholson F.A., Smith S.R., Alloway B.J., Carlton-Smith C., Chambers B.J., 2003. *An inventory of heavy metals inputs to agricultural soils in England and Wales.* Science of The Total Environment 311(1), 205–219.

Nziguheba G., Smolders E., 2008. *Inputs of trace elements in agricultural soils via phosphate fertilizers in European countries.* Science of The Total Environment 390(1), 53–57.

Pacyna E.G., Pacyna J.M., Steenhuisen F., Wilson S., 2006. *Global anthropogenic mercury emission inventory for 2000.* Atmospheric Environment 40(22), 4048–4063.

Pebesma E.J., 2004. *Multivariable geostatistics in S: the gstat package.* Computers & Geosciences 30(7), 683–691.

Pebesma E.J., Bivand R.S., 2005. *Classes and methods for spatial data in R.* R news 5(2), 9-13.

Pfeifer H.-R., Hassouna M., Plata N., 2010. *Arsenic in the different environmental compartments of Switzerland: an updated inventory.* Kristianstad, Schweden.

Pfirter U., 2020. *Geologischer Kurzbericht zu den Belastungen mit Thallium und Arsen im Kanton BL.* Kanton Basel-Landschaft, Liestal.

Pilbeam D.J., Drihem K., 2007. *Vanadium.* In: A.V. Barker, D.J. Pilbeam (Hrsg.), Handbook of plant nutrition. Books in soils, plants, and the environment. CRC Press, Taylor & Francis, Boca Raton, FL.

Pulford I.D., 2010. *Gold and Uranium.* In: P.S. Hooda (ed.), Trace Elements in Soils. Wiley, Chichester, pp. 551–565.

Quezada-Hinojosa R.P., Föllmi K.B., Verrecchia E., Adatte T., Matera V., 2015. *Speciation and multivariable analyses of geogenic cadmium in soils at Le Gurnigel, Swiss Jura Mountains.* CATENA 125, 10–32.

R Core Team, 2022. *R: A language and environment for statistical computing.* R Foundation for Statistical Computing, Vienna, Austria.

Rawlins B.G., McGrath S.P., Scheib A.J., Breward N., Cave M., Lister T.R., Ingham M., Gowing C., Carter S., 2012. *The advanced soil geochemical atlas of England and Wales.* British Geological Survey, Nottingham, GB: 227 S. http://www.bgs.ac.uk/GBASE/advSoilAtlasEW.html

Reimann C., Birke M., Demetriades A., Filzmoser P., O'Connor P., 2014. *Chemistry of Europe's agricultural soils, Part A: Methodology and Interpretation of the GEMAS Data Set.* Geologisches Jahrbuch. Reihe B, Regionale Geologie Ausland Heft 102-103. Schweizerbart'sche Verlagsbuchhandlung, Hannover.

Reimann C. *et al.*, 2018. *GEMAS: Establishing geochemical background and threshold for 53 chemical elements in European agricultural soil.* Applied Geochemistry 88, 302–318.

Reimann C., Filzmoser P., Garrett R., Dutter R., 2011. *Statistical data analysis explained: applied environmental statistics with R.* John Wiley & Sons.

Revelle W., 2022. *psych: Procedures for Psychological, Psychometric, and Personality Research. R Package Version 2.2.5.*, Northwestern University, Evanston, Illinois.

Rooney C.P., Zhao F.-J., McGrath S.P., 2007. *Phytotoxicity of nickel in a range of European soils: Influence of soil properties, Ni solubility and speciation.* Environmental Pollution 145(2), 596–605.

RStudio Team, 2022. *RStudio: Integrated Development for R.* RStudio, PBC, Boston, MA.

Scheinost A.C., Rossberg A., Vantelon D., Xifra I., Kretzschmar R., Leuz A.-K., Funke H., Johnson C.A., 2006. *Quantitative antimony speciation in shooting-range soils by EXAFS spectroscopy.* Geochimica et Cosmochimica Acta 70(13), 3299–3312.

Schulin R., Johnson A., Frossard E., 2010. *Trace Element-Deficient Soils.* In: P.S. Hooda (ed.), Trace Elements in Soils. Wiley, Chichester, pp. 175–197.

SGTK, Simoni M., Jost B., 2013. *Factsheet Zink (NEROS).* Schweizerische Geotechnische Kommission SGTK, ETH Zürich; Netzwerk Mineralische Rohstoffe Schweiz NEROS. https://georessourcen.ethz.ch/publikationen/faktenblaetter/

Sheppard S.C., Grant C.A., Sheppard M.I., de Jong R., Long J., 2009. *Risk Indicator for Agricultural Inputs of Trace Elements to Canadian Soils.* Journal of Environmental Quality 38(3), 919–932.

Sheppard S.C., Sheppard M.I., Gallerand M.-O., Sanipelli B., 2005. *Derivation of ecotoxicity thresholds for uranium.* Journal of Environmental Radioactivity 79(1), 55–83.

Simoni M., Jost B., SGTK, GEO Partner AG, 2014. *Urban Mining: AWEL Factsheet Kupfer.* Schweizerische Geotechnische Kommission SGTK, ETH Zürich, GEO Partner AG; Amt für Abfall, Wasser, Energie und Luft (AWEL), Baudirektion Kanton Zürich, https://georessourcen.ethz.ch/publikationen/faktenblaetter/ [available in English at https://georessourcen.ethz.ch/en/publications/factsheets/]

Smith D.B., Cannon W.F., Woodruff L.G., Solano F., Ellefsen K.J., 2014. *Geochemical and mineralogical maps for soils of the conterminous United States.* U.S.G. Survey, Reston, VA, Open-File Report: 399. http://pubs.er.usgs.gov/publication/ofr20141082

Smolders E., Oorts K., Van Sprang P., Schoeters I., Janssen C.R., McGrath S.P., McLaughlin M.J., 2009. *Toxicity of Trace Metals in Soil as Affected by Soil Type and Aging After Contamination: Using Calibrated Bioavailability Models to Set Ecological Soil Standards.* Environmental Toxicology and Chemistry 28(8), 1633–1642.

Stanisic L., Blum J., Bigalke M., 2021. *Zusammenfassender Bericht über bestehende Studien und Untersuchungen zu geogenen Schadstoffgehalten in Böden und Gesteinen der Schweiz.* Geographisches Institut Universität Bern; Bundesamt für Umwelt (BAFU). Bern.

Suess E., Berg M., Bouchet S., Cayo L., Hug S.J., Kaegi R., Voegelin A., Winkel L.H.E., Tessier E., Amouroux D., Buser A.M., 2020. *Mercury loads and fluxes from wastewater: A nationwide survey in Switzerland.* Water Research 175, 115708.

swisstopo, 2022. *GeoCover.* Bundesamt für Landestopografie swisstopo, Wabern, Version 3.

Tack F.M.G., 2010. *Trace Elements: General Soil Chemistry, Principles and Processes.* In: P.S. Hooda (ed.), Trace Elements in Soils. Wiley, Chichester, pp. 9-37.

Tamaki S., Frankenberger W.T., 1992. *Environmental Biochemistry of Arsenic.* In: G.W. Ware (ed.), Reviews of Environmental Contamination and Toxicology: Continuation of Residue Reviews. Springer New York, New York, NY, pp. 79–110.

Tuchschmid M.P., 1995. *Quantifizierung und Regionalisierung von Schwermetall- und Fluorgehalten bodenbildender Gesteine der Schweiz.* Institut für Mineralogie und Petrographie, ETH Zürich; Bundesamt für Umwelt, Wald und Landschaft (BUWAL), Bern.

Tukey J.W., 1977. *Exploratory data analysis.* 2nd Reading, MA.

Uren N.C., 1992. *Forms, Reactions, and Availability of Nickel in Soils.* In: D.L. Sparks (ed.), Advances in Agronomy. Academic Press, pp. 141–203.

USGS, 2023. *Mineral Commodity Summaries.* U.S. Geological Survey, Reston, VA

Venables W.N., Ripley B.D., 2002. *Modern Applied Statistics with S. R package version 7.3-45.* Springer, New York.

Voegelin A., Pfenninger N., Petrikis J., Majzlan J., Plötze M., Senn A.-C., Mangold S., Steininger R., Göttlicher J., 2015. *Thallium Speciation and Extractability in a Thallium- and Arsenic-Rich Soil Developed from Mineralized Carbonate Rock.* Environmental Science & Technology 49(9), 5390–5398.

Wickham H., 2016. *ggplot2: Elegant Graphics for Data Analysis. R Package Version 3.3.5.* Springer-Verlag New York.

Wiggenhauser M., Bigalke M., Imseng M., Keller A., Rehkämper M., Wilcke W., Frossard E., 2019. *Using isotopes to trace freshly applied cadmium through mineral phosphorus fertilization in soil-fertilizer-plant systems.* Science of The Total Environment 648, 779–786.

Zayed A.M., Terry N., 2003. *Chromium in the environment: factors affecting biological remediation.* Plant and Soil 249(1), 139–156.

Annex

Correlations with supplementary data

Table 6 | Spearman's rank correlation coefficient R2 of the measured element concentrations and additional geodata at the site level of the BDM and NABO data set. The median of several individual samples per site was included in the data analysis. Temp.: standard temperature 1981–2010; Precip.: standard precipitation 1981–2010; elevation, slope and exposure (Expo.) from the DHM25 elevation model (swisstopo); Dep.: modelled deposition data for sulphur oxides (SOx), nitrogen (N), cadmium, mercury and lead (Chapter 2.5).

R^2	Temp.	Precip.	Elevation	Slope	Expo.	Dep. SOx	Dep. N	DEP.Pb	DEP.Cd	DEP.Hg
As	0.01	−0.06	−0.02	−0.02	0.03	−0.00	−0.12	0.15	0.14	0.21
Ca	0.24	−0.17	−0.28	−0.14	0.02	0.15	0.10	−0.08	0.10	−0.08
Cd	0.06	0.26	−0.09	−0.03	0.02	0.20	0.10	0.20	0.28	0.17
Co	0.01	−0.04	−0.00	−0.03	0.00	−0.02	−0.11	0.07	−0.00	0.09
Cr	0.30	−0.04	−0.32	−0.31	0.02	0.32	0.24	0.09	0.21	−0.04
Cu	0.29	−0.19	−0.29	−0.27	−0.02	0.13	0.11	−0.10	−0.04	−0.15
Fe	−0.12	0.12	0.14	0.09	0.02	−0.10	−0.20	0.19	0.01	0.23
Hg	0.07	0.19	−0.08	0.06	0.04	0.23	0.21	0.04	0.16	−0.01
Mg	0.09	−0.21	−0.08	−0.05	0.01	−0.04	−0.09	−0.11	−0.17	−0.09
Mn	0.14	−0.08	−0.18	−0.22	−0.01	0.17	0.14	−0.02	0.14	−0.05
Mo	−0.14	0.14	0.12	0.12	0.00	−0.05	−0.17	0.25	0.14	0.26
Na	0.13	−0.23	−0.10	−0.04	0.02	−0.10	−0.11	0.01	−0.21	−0.04
Ni	0.20	−0.12	−0.20	−0.18	−0.00	0.14	0.08	−0.03	0.04	−0.07
Pb	−0.04	0.30	0.04	0.08	0.00	0.14	0.02	0.28	0.24	0.25
S	−0.18	0.23	0.17	0.08	0.03	−0.11	−0.15	0.13	0.02	0.19
Sb	0.03	−0.02	−0.02	0.04	−0.00	0.06	−0.02	0.03	0.04	0.05
Tl	−0.09	0.31	0.09	0.10	0.01	0.08	−0.07	0.38	0.24	0.34
U	0.12	−0.06	−0.13	−0.17	−0.00	0.08	0.00	0.22	0.15	0.15
V	0.22	0.15	−0.25	−0.25	0.07	0.34	0.24	0.22	0.31	0.09
Zn	0.06	0.14	−0.08	−0.05	0.02	0.09	0.01	0.16	0.15	0.14

Results of validation interpolation

The ordinary Kriging interpolation was validated at site level (median of individual samples) and at sampling level (Table 7 and Table 8) using the leave-one-out method (Lado *et al.*, 2008; Pebesma & Bivand, 2005). Between 11 % (sulphur) and 37 % (vanadium) of the variance is explained at site level; the root mean square prediction error (RMSE) is between 0.37 (iron) and 1.42 (calcium). The nugget variance is significantly reduced in comparison with the site-level interpolation when the individual samples are included. Since small-scale variability is much lower at individual sites than between sites, the validation results using the leave-one-out method are significantly better at sampling level, where the RMSE lies between 0.17 (thallium) and 0.52 (calcium). Therefore, the interpolated values for cadmium, cobalt, copper and lead were compared with the converted concentrations from the UB dataset sites (Table 9). Since the coefficient of determination of the linear regression is very low, no plot-level information can be gleaned from the interpolated maps.

Table 7 | Model parameters and validation of the ordinary Kriging interpolation at site level (median of individual samples) using the leave-one-out method. MaxDist = maximum distance considered, Varexp = variance explained, MSNE = mean squared normalised error, MSE = mean squared prediction error, RMSE = root mean squared prediction error, calculated according to Hengl (2009).

Element	Range (m)	Nugget	Psill	maxDist (m)	Varexp (%)	MSNE	MSE	RMSE
As	29418	0.143	0.384	98841	34	1.76	0.39	0.63
Ca	3254	0.000	1.903	48693	13	1.37	2.01	1.42
Cd	22219	0.170	0.381	78929	34	1.45	0.39	0.63
Co	3414	0.002	0.209	28865	15	1.93	0.32	0.57
Cr	4886	0.048	0.146	39059	24	1.96	0.30	0.55
Cu	3691	0.011	0.306	39059	17	1.33	0.31	0.56
Fe	5080	0.021	0.083	28865	16	1.75	0.14	0.37
Hg	3938	0.080	0.192	28865	16	1.38	0.32	0.57
Mg	3181	0.000	0.300	28865	13	2.18	0.49	0.70
Mn	3371	0.000	0.301	28865	19	1.88	0.42	0.65
Mo	22108	0.135	0.146	78929	21	1.60	0.29	0.54
Na	1736074	0.196	1.947	148969	18	0.91	0.19	0.44
Ni	3185	0.007	0.261	28865	20	1.90	0.42	0.65
Pb	13244	0.063	0.086	98841	22	1.53	0.15	0.39
S	10266	0.192	0.134	78929	11	1.19	0.32	0.56
Sb	30887	0.122	0.107	89141	25	1.43	0.21	0.46
Tl	28539	0.073	0.186	98841	34	1.55	0.18	0.42
U	31510	0.119	0.219	129029	23	1.83	0.31	0.55
V	14407	0.088	0.159	58937	37	1.42	0.21	0.46
Zn	7489	0.038	0.155	98841	15	1.63	0.20	0.45

Table 8 | Model parameters and validation of the ordinary Kriging interpolation at sampling level (median of individual samples) using the leave-one-out method. MaxDist = maximum distance considered, Varexp = variance explained, MSNE = mean squared normalised error, MSE = mean squared prediction error, RMSE = root mean squared prediction error, calculated according to Hengl (2009).

Element	Range (m)	Nugget	Psill	maxDist (m)	Varexp (%)	MSNE	MSE	RMSE
As	9242	0.012	0.335	39166	92	2.00	0.04	0.21
Ca	4689	0.059	1.848	39167	89	2.14	0.27	0.52
Cd	17423	0.034	0.501	59172	84	1.90	0.10	0.32
Co	4877	0.009	0.203	28970	89	2.34	0.04	0.20
Cr	6216	0.008	0.188	39166	92	2.10	0.03	0.18
Cu	4601	0.019	0.295	39167	86	1.62	0.05	0.23
Fe	6235	0.005	0.100	28970	84	2.91	0.03	0.17
Hg	4550	0.039	0.240	28970	79	1.43	0.09	0.29
Mg	4415	0.004	0.298	28970	92	3.26	0.04	0.21
Mn	4633	0.016	0.295	28969	85	2.54	0.08	0.28
Mo	6110	0.021	0.206	39166	86	1.41	0.05	0.22
Na	4529	0.006	0.155	39166	85	3.11	0.04	0.19
Ni	4217	0.009	0.257	28970	92	2.22	0.04	0.21
Pb	6879	0.015	0.120	39167	76	2.09	0.05	0.22
S	4299	0.022	0.271	39166	68	3.09	0.12	0.34
Sb	4632	0.016	0.164	39167	85	1.75	0.05	0.21
Tl	29052	0.008	0.239	98891	89	2.18	0.03	0.17
U	5224	0.002	0.197	39166	90	5.21	0.04	0.20
V	7931	0.005	0.211	39166	92	2.66	0.03	0.17
Zn	6375	0.010	0.170	39167	85	2.12	0.04	0.20

Table 9 | Comparison of concentration levels interpolated using the ordinary Kriging method with the converted measurement data from the UB dataset. Outliers in accordance with the TIF method were not considered.

Element	Coefficient of determination R^2 interpolated vs observed UB dataset
Cd	0.21
Co	0.14
Cu	0.06
Pb	0.19

Comparison of ordinary Kriging and universal Kriging

The universal Kriging method was additionally used to interpolate element concentrations at sampling level with regard to the lithological groups (Chapter 2.5), the parameters elevation, slope and exposure of the digital elevation model (Chapter 2.5), and the total organic carbon and pH modelled for the whole of Switzerland by Descombes *et al.* (2020). The R package *geostat,* Version 2.1-0 (Gräler *et al.*, 2016; Pebesma, 2004) was also used for modelling. The results are summarised in Table 10. Comparison of the interpolated values with the UB dataset shows that the universal Kriging method improves prediction only marginally (Table 11). Both methods are suitable only for distinguishing areas with high concentrations from areas with low concentrations; they cannot be used to deduce plot-level information.

Table 10 | Model parameters and validation of the universal Kriging interpolation at sampling level (median of individual samples) using the leave-one-out method. MaxDist = maximum distance considered, Varexp = variance explained, MSNE = mean squared normalised error, MSE = mean squared prediction error, RMSE = root mean squared prediction error, calculated according to Hengl (2009).

Element	Range (m)	Nugget	Psill	maxDist (m)	Varexp (%)	MSNE	MSE	RMSE
As	5517	0.012	0.293	39166	92	1.94	0.05	0.21
Ca	2831	0.072	1.106	39167	88	2.01	0.27	0.52
Cd	4440	0.034	0.301	59172	84	1.84	0.10	0.32
Co	3805	0.009	0.191	28970	89	2.32	0.04	0.20
Cr	5423	0.008	0.176	39166	92	2.10	0.03	0.18
Cu	4223	0.020	0.230	39167	86	1.60	0.05	0.23
Fe	4497	0.005	0.092	28970	84	2.90	0.03	0.17
Hg	2430	0.039	0.187	28970	79	1.42	0.09	0.29
Mg	4043	0.005	0.285	28970	92	3.03	0.04	0.21
Mn	3940	0.016	0.292	28969	85	2.50	0.08	0.28
Mo	3681	0.021	0.183	39166	86	1.41	0.05	0.22
Na	2318	0.005	0.151	39166	85	2.95	0.04	0.19
Ni	3903	0.009	0.233	28970	92	2.19	0.04	0.21
Pb	2701	0.015	0.101	39167	76	2.05	0.05	0.22
S	445	0.029	0.231	39166	68	2.89	0.12	0.34
Sb	2770	0.015	0.151	39167	85	1.72	0.04	0.21
Tl	11516	0.008	0.169	98891	89	2.08	0.03	0.17
U	2525	0.002	0.187	39166	90	4.77	0.04	0.20
V	5258	0.005	0.195	39166	92	2.56	0.03	0.17
Zn	3490	0.010	0.137	39167	85	2.09	0.04	0.20

Table 11 | Comparison of concentration levels interpolated using the universal Kriging method with the converted measurement data from the UB dataset. Outliers in accordance with the TIF method were not considered.

Element	Coefficient of determination R^2 interpolated vs observed UB dataset
Cd	0.23
Co	0.12
Cu	0.13
Pb	0.18